The Effects of Three-Dimensional Imposed Disturbances on Bluff Body Near Wake Flows

Nicholas Tombazis
and
Peter Bearman

Department of Aeronautics
Imperial College of Science, Technology and Medicine
Prince Consort Road, London, SW7 2BY

Final Report on ONR contract no. N00014-90-J-4083

April 1994

ABSTRACT

The three-dimensionality of the near wake of bluff bodies at high Reynolds numbers is studied experimentally. Measurements were carried out in a 0.91m× 0.91m wind tunnel (for Re=20000 to 60000) and flow visualisation in a 0.6m× 0.6m water flume (for Re=2500). The main purpose is to identify inherent three-dimensional features that may also arise in nominally two-dimensional flows. In order to fix the three-dimensional effects in both time and space, a mild, periodic, geometrical disturbance was imposed on the otherwise two-dimensional geometry of a model with a blunt trailing edge. The trailing edge thus followed a sinusoidal pattern, but a straight edge model was also studied for comparison purposes.

Quantitative measurements and flow visualisation revealed that a dual shedding frequency characteristic prevails in the wake of the sinusoidal model. Base drag shows a noticeable drop (in comparison to the straight edge model). Most of the activity seems to happen in the region of the peak, where the dual frequency characteristic is more apparent and also the base drag shows its largest variations. Flow visualisation showed different modes of vortex shedding to exist. Vortical structures in the x- and z- directions were observed for both models. ω_z vortices are present in the near wake. It is believed that the observed vortices are responsible for the intense base pressure fluctuations and gradients, and also for thin "wisps" appearing between Kármán vortices in flow visualisation.

A model for the dynamics of the formation region is proposed, by considering the interaction of mean, time-averaged quantities. It is suggested that forming vortices have a tendency to straighten-out. A concept is proposed which links the vortex formation length to other wake parameters, most notably wake width and base pressure. Wake similarity arguments are used in order to explain the shedding frequency variations along the span.

The dynamics of vortex dislocations are also discussed. A mechanism is proposed which explains the significance of a characteristic dislocation frequency, f_d in the near wake dynamics. It is suggested that f_d is a result of the geometrical properties of the vortex filaments and that a link exists between the dislocation frequency and fluctuations in base pressure, vortex strengths and spanwise dislocation position.

CONTENTS

LIST OF SYMBOLS

C_D	coefficient of drag
Cp_b	coefficient of base pressure along the model centre line
D	circular cylinder diameter
f_1	low shedding frequency
f_2	high shedding frequency
f_d	dislocation frequency ($=f_2-f_1$)
f_v	fundamental shedding harmonic
h	model base height
l_f	formation length, measured from model's trailing edge
L	wavelength of sinusoidal model disturbance
L_c	spanwise correlation length
p_{atm}	atmospheric pressure
$r(\Delta)$	correlation coefficient at a time delay Δ
Re	Reynolds number ($=h*U/\nu$ or $D*U/\nu$)
S	Strouhal number (shedding frequency*h/U)
S*	wake Strouhal number (=shedding frequency*w_f/u_s)
u	instantaneous x-velocity
u_s	velocity at the point of separation
U	free stream velocity
U_c	convection velocity of a Kármán vortex
v	instantaneous y-velocity
V	hot-wire cooling velocity
w	instantaneous z-velocity, peak-to-peak amplitude of sinusoidal model disturbance
w_f	wake width at the formation point

w(t)	window function by which data is multiplied prior to Fourier analysis
x	streamwise co-ordinate, measured w.r.t. model's trailing edge
y	spanwise co-ordinate, measured w.r.t. the position of a peak
z	vertical co-ordinate, measured w.r.t. the model's centre line
F_n	indicator function for conditional sampling
q_n	comparison signal for conditional sampling
Q(t)	degree of similarity of signal to indicator functions, at delay t
R	conditional sampling region of interest
S_n	stationary comparison points for conditional sampling
α	fraction of vorticity surviving the formation process
Γ	vortex strength
Γ_v	strength of Kármán vortex just after formation
δ	shear layer deflection ($=(h-w_f)/2l_f$)
θ	phase angle between shedding at two successive valleys
ω	vorticity

1. REVIEW OF PAST LITERATURE

1.1 General remarks

In fluid mechanics, we define as "bluff" a body which exhibits separated flow over a large portion of its surface, when subjected to a fluid stream. Throughout the century bluff bodies have attracted a significant amount of research in very diverse fields, ranging from mathematics to off-shore engineering. The interest shown in this field has primarily two causes: firstly, such flows are present in a variety of engineering applications and therefore their better understanding is of much importance, and secondly, as has been aptly put by other researchers, bluff body flows present a kaleidoscope of mutually interacting and challenging scientific problems worth investigating for their own sake.

There are numerous complicated issues associated with bluff body flows, collectively known as "the bluff body problem". Generally speaking, such bodies generate a wake, in which unsteady phenomena are dominant. Our inability to solve the governing equations (the highly non-linear Navier-Stokes equations) makes it impossible to study all the details of such flows. This work will thus just aim to add to our still very incomplete understanding of bluff body wake flows.

In this chapter, some large, simplifying steps will be taken at first to reduce our problem to a more simple one, and then a review of previous related published literature will gradually take it to more and more complex levels until the purpose of the present investigation is put into proper perspective. The first simplifying step will be the reduction of the number of dimensions from three to two. Furthermore, we will consider a uniform stream in which the two-dimensional body is submerged. We will consider the fluid to be Newtonian and incompressible. We shall start our review from the low Reynolds number regime and move upwards, were complications inevitably arise.

1.2 The (nominally) two-dimensional flow past a bluff body

1.2.1 Circular cylinder flows at different Reynolds number regimes

The shape which has attracted the largest amount of research in bluff body flows is the circular cylinder in cross flow. Although geometrically simple, this problem presents us with a variety of aspects of these flows. At Reynolds numbers

above 5 vorticity generated at the surface can no longer be absorbed by the cylinder, and hence has to be shed downstream. As a result, the flow separates. A stable condition is now reached where we have two standing eddies immediately downstream of the body, forming a re-circulating bubble. At a higher Reynolds number (about 46) this steady flow pattern becomes unstable and the wake starts to oscillate in a periodic fashion.

Although related effects (such as the wind-excited vibration of wires) had been known for quite some time, it was Strouhal in 1878 who first showed that the frequency of vibration could depended on the aerodynamic parameters of the body and not necessarily on the elastic properties, and hence comes the widely used Strouhal number, a non-dimensional measure of the oscillation frequency. In 1911, von Kármán proposed his well known theory of the vortex street, by modelling the periodic wake with two infinite rows of point vortices of opposite signs. By solving for the stability of the vortex street, he predicted a relation between the lateral and the streamwise spacing of the point vortices. For a number of years, not much was added to our understanding of wakes, although alternating, periodic wakes were visualised in numerous studies.

The first systematic and fundamental study in the "modern era" of bluff body wakes is perhaps due to Roshko (1953). In that study, he derived a much-used empirical formula linking the Strouhal number to the Reynolds number. He also observed the existence of another transition range (between Re=150 and Re=300) where the vortices become turbulent. In a further publication (1954), an attempt is made to explain the various physical quantities that interact in the wake, such as drag and shedding frequency. Although the drag prediction methods described are perhaps a bit too ambitious, this work is important because it introduces the concept of wake similarity, whereby wake parameters such as width and base pressure (rather than geometrical parameters) are said to be the directly relevant factors in the selection of the Strouhal number.

An extension to von Kármán's discrete vortex model was proposed by Schaefer and Eskinazi (1959), who assumed that the vortices were viscous with a core of finite size. The size of the core was growing with time (according to the analytic Navier-Stokes solution for an isolated vortex), with time=0 being taken as the moment of vortex formation behind the cylinder. By considering the interaction of the vortices they postulated the existence of three regions in the wake, the formation region (close to the body, where the vortices are formed), the stable region (after the formation region, the region where the viscous vortex core

interactions are small) and the unstable region (further downstream, where vortex cores start to overlap). Comparison with experiments showed that this approach gave a good qualitative explanation for measured velocity patterns in the wake.

The importance of the formation region dynamics to the overall flow pattern was emphasised by Gerrard (1966b). A variety of important concepts were introduced in this paper. It was proposed that a significant parameter in the formation of a vortex street is the interaction between the two separated shear layers of oppositely signed vorticity. Figure 1.1 is a schematic diagram of the various entrainment flows which are said to play an important role in the formation region. Here we see a vortex growing as it is being fed with vorticity from the upper shear layer. At one stage it becomes strong enough to draw the opposing shear layer across the wake. The vorticity carried by the opposing shear layer is then entrained in three possible directions: Most of it (arrow a) gets drawn into the forming vortex and thus reduces its strength, but there is also entrainment into the shear layer (arrow b). The remainder (arrow c) finds its way into the near wake.

The size of the formation region is determined by the balance between these entrainment flows. It is argued that flow (a) remains relatively constant with changes of the Reynolds number. The turbulence level of the shear layer determines the magnitude of entrainment flow (b). For example, if the shear layer becomes turbulent at a point closer to the body, flow (b) will increase, and the forming vortex will be weaker. As a result, the reversed flow will also decrease, and the initial increase in flow (b) will not be balanced by an increased flow into the formation region. Hence the whole formation region will have to shrink in length. Another important parameter highlighted in this paper is the width of the shear layer at the end of the formation region. A thicker (more diffuse) layer will take longer to be entrained, and hence the instant at which vorticity fed into the forming vortex is cut off will be delayed, with a resulting drop in shedding frequency. A further consequence of a more diffuse shear layer will be the increase in strength of the forming vortex.

This qualitative explanation on how some of the very important wake parameters interact does not really solve the problem (and no claim to that effect is made). The number of relevant parameters is too large and too complex as, for example, an increase in the Reynolds number may result in two "competing" phenomena, and no apparent effect on the shedding frequency. Nevertheless, it is

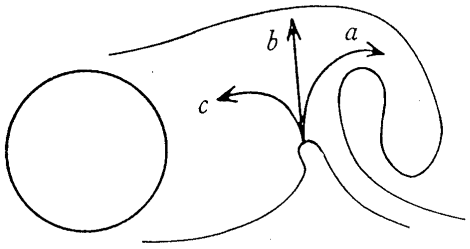

Figure 1.1 Schematic diagram showing Gerrard's entrainment flows (from Gerrard, 1966b).

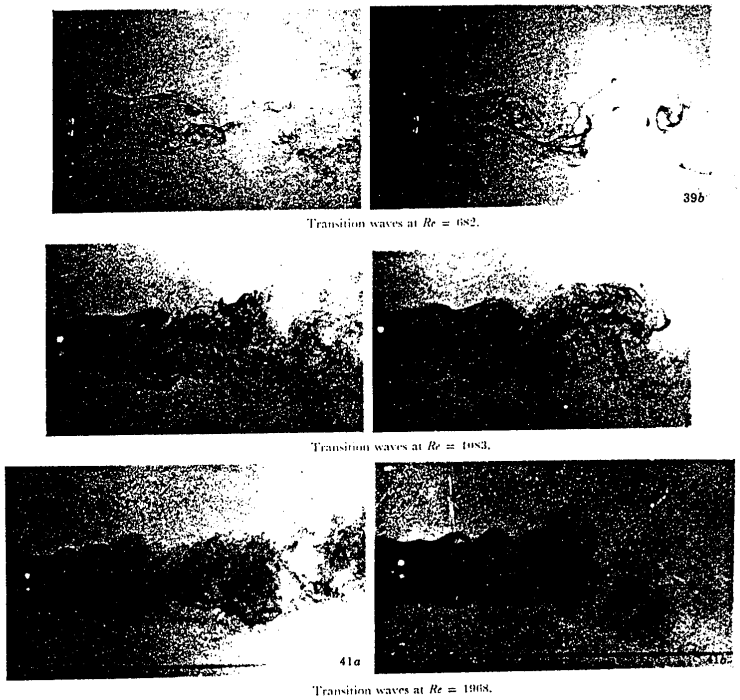

Figure 1.2 Transition waves in the wake of a circular cylinder (from Gerrard, 1978).

important to be able to understand the elementary formation region dynamics which are governed by a balance (and feedback) between many related quantities.

Gerrard (1978) presented a visualisation study of the flow around cylinders of different sections (mostly circular) at a wide range of Reynolds number ($30<Re<2000+$). Smaller scales of fluid motion were observed at $Re>350$, which the author calls transition waves. These are said to be related to the transition to turbulence. As the Reynolds number increases they become stronger and move closer to the cylinder (see figure 1.2). In some cases they interact strongly with the forming vortices and suppress vortex shedding for short periods.

A different aspect was presented by Cantwell and Coles (1983) who used a "flying hot-wire technique" in conjunction with conditional averaging and triple velocity decomposition to obtain the flow field around a circular cylinder for $Re=140000$. The advanced experimental technique used gave them some insight into the topology of material lines and turbulent production in one shedding cycle, shown schematically in figure 1.3. Here we see the evolution of the material lines over half a shedding cycle. The paper mainly concentrated on the production and transport of turbulence. A substantial fraction of the turbulent energy was found to be produced at primarily intermediate or small scales, near flow field saddles. It was then transported to and accumulated at centres (stagnation points at the large-scale vortices).

Circular cylinders, mainly due to the moving point of separation, present a plethora of interesting and complicated wake phenomena. Their wake structure and properties are largely dependent on the Reynolds number, as has been indicated above, and they have attracted a large number of studies. It would not be appropriate in this short review to attempt to go into all the fine details of circular cylinder flows when proper attention is given to them in dedicated reviews, such as that by Coutanceau and Defaye (1991).

1.2.2 Means of two-dimensional flow control

A very useful tool in our understanding of bluff body wakes has been the use of splitter plates in the centre of the formation region. Their positioning is "strategic" as the presence of a splitter plate can reduce or delay the interaction between the two shear layers, which was shown earlier to be the dominant cause of vortex shedding. Bearman (1965) investigated the effect of splitter plates of different lengths attached to a model with a blunt trailing edge. Their effect was

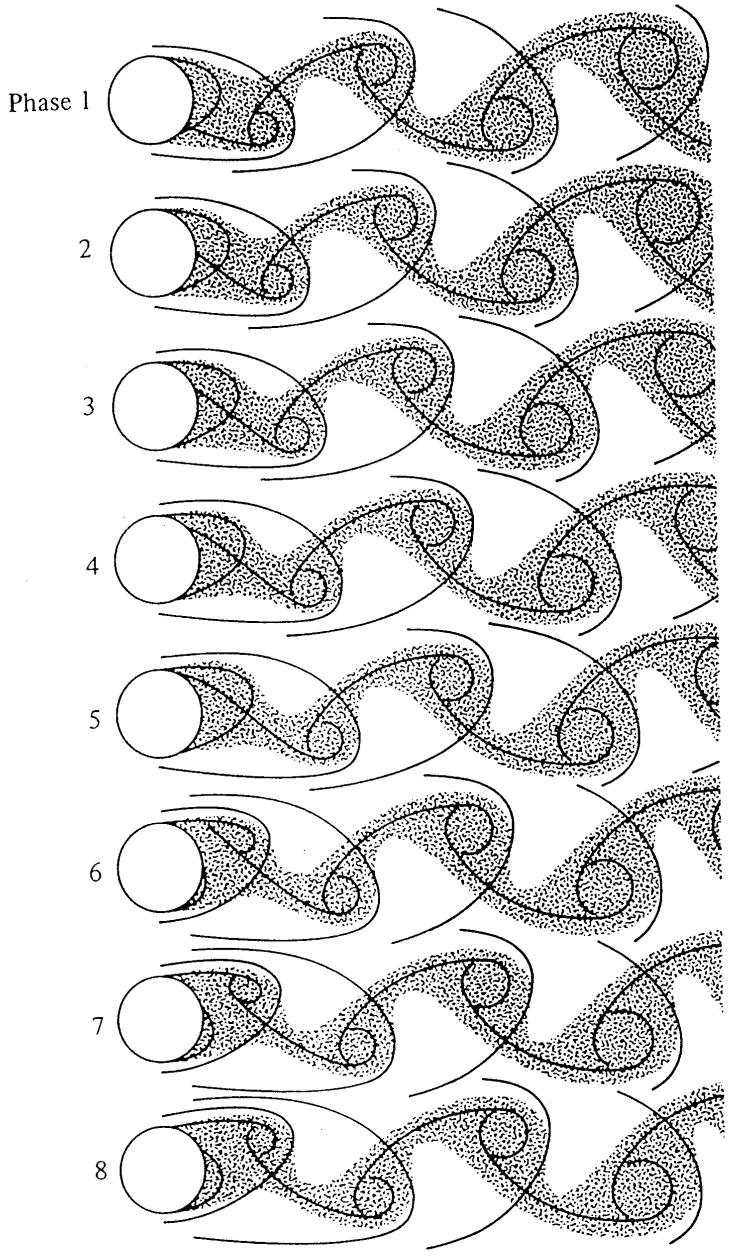

Figure 1.3 Schematic representation for the step-by-step topology of material lines over half a shedding cycle in the turbulent wake of a circular cylinder. Fluid particles that are not allowed to cross a separatrix at the near wake must eventually find their way into a Kármán vortex (from Cantwell and Coles, 1983).

found to be the delay of the shear layer interaction until after the end of the splitter plate with a consequent increase in formation length. Base drag was found to vary in inverse proportion to the formation length (figure 1.4), as an increase in formation length would cause the forming vortices to be weaker and further away from the body. Beyond a certain splitter plate length (but before the necessary length for re-attachment to occur) Bearman observed a complete suppression of vortex shedding. The effect of a splitter plate at a distance from the body has been investigated by Roshko (1954) and, more recently, by Mansingh and Oosthuizen (1990). In both cases, the results were quite similar to those of Bearman, but for sufficient gaps between the splitter plate and the model vortex shedding would resume in a manner similar to that for no splitter plate. The effect of base bleed on bluff body flows was investigated by Bearman (1967a), with similar conclusions regarding the dependence of the base drag on the formation length. Small quantities of bleed were capable of causing a significant reduction in drag, while at larger bleed rates vortex shedding could be suppressed.

Flows around oscillating bodies essentially follow the same basic rules but have the added ingredient of the interaction between the natural shedding frequency and the frequency of oscillation. Three of the reasons they have attracted a lot of attention are (a) their relevance for the study of wind-excited vibrations, (b) their prospects in terms of control of vortex shedding, and (c) under many circumstances the body oscillation acts as a pulse to keep shedding in phase along the span, and the flow hence becomes two-dimensional, which is an attraction for the comparison of two-dimensional CFD codes to experiments. For oscillation amplitudes above a critical threshold value, the frequency of wake oscillation can be forced to follow the forcing frequency (if the forcing frequency is not too different from the natural wake frequency). This is called "lock-in" and can also occur for other kinds of periodic forcing. The relevance of these flows to our problem as a whole is demonstrated in two review papers, by Bearman (1984) and by Griffin and Hall (1991). Further study of these flows is beyond the scope of this investigation.

1.2.3 The stability characteristics of a wake

The concepts of absolute and convective instabilities have been around for about forty years, but were mainly used in plasma physics. The significance of these concepts on bluff body wakes, however, has only emerged recently. Bers (1983) provides the basic theoretical and conceptual framework for the understanding of these principles. Figure 1.5 illustrates the possible evolution of a

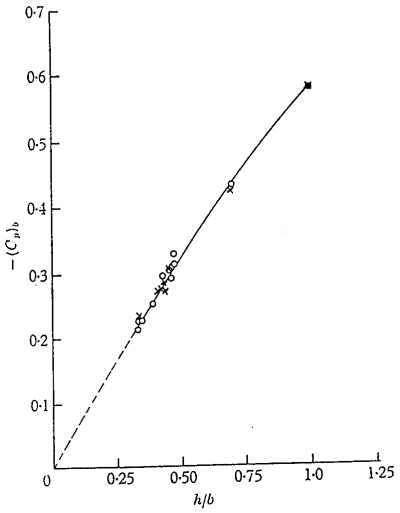

Figure 1.4 Base pressure coefficient as a function of the inverse of the formation length (from Bearman, 1965).

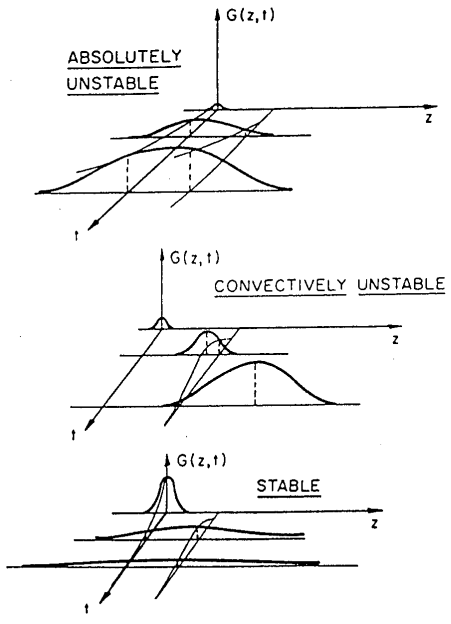

Figure 1.5 Time evolution of a pulse in media of one dimension and different stability characteristics (from Bers, 1983).

pulse in one dimension and time. If the medium is *absolutely unstable*, the disturbance will grow in time and space, so that eventually, at every point in space, it will be growing with time. If the medium is *convectively unstable*, the disturbance will propagate away from its source in such way that although it grows with time, at any given point in space it will eventually die off. Finally if the medium is *stable*, the disturbance will die off in both space and time. We should also make a distinction between *local modes*, where the instability characteristics are confined to a limited region and *global modes*, where the instability characteristics spread over a large portion of the flow. Numerous studies over the last ten years have linked these concepts to wake flows. These principles are surrounded by a considerable mathematical complexity which this study will not enter. Nevertheless, an appreciation of the various kinds of instability can aid our understanding of the fundamental mechanisms governing vortex shedding.

Huerre and Monkewitz (1985) mainly concentrated on applying the stability principles to free shear layers, only mentioning wakes briefly. It has been generally accepted that wake flows have a region of absolute instability in the near wake (loosely associated with the reverse flow region), and that further away from the body the instability is of the convective type. The absolutely unstable region is thought to be of fundamental importance for the self-sustainment of the wake. Monkewitz and Nguyen (1987) investigated various criteria for the selection of the shedding frequency. They postulated the intrinsic wake response to be the resonance between upstream and downstream travelling waves. Triantafyllou, Triantafyllou and Chryssostomidis (1986 and 1987) solved the inviscid Orr-Sommerfeld equation for measured wake velocity profiles to predict the shedding frequency with good accuracy. The stability studies mentioned assumed the mean flow to be parallel. The validity of this simplification was discussed by Hannemann and Oertel (1989), who compared the stability analysis results to those of a Navier-Stokes code and concluded that the assumption is good enough for a qualitative understanding of the wake dynamics. Their work also examined the effects of base bleed from the stability point of view. Similarly, Karniadakis and Triantafyllou (1989) examined the oscillating body problem in conjunction with stability analysis. Finally, the term *global instability* was discussed recently by Chomaz, Huerre and Redekopp (1988). They noted that a local absolute instability was not sufficient always to cause a globally unstable wake, and that it would have to be of large enough size for the instability to become self-sustainable.

The usefulness of the above-described instability concepts is now generally accepted. We should be careful, however, not to treat them as a panacea. The fact

that it is an instability that causes the periodic wake has been appreciated for a long time (e.g. Roshko, 1953). Similarly the need for a feedback mechanism to exist has been emphasised in the past (e.g. Gerrard 1966b). The relatively recent emergence of the absolute-convective instability ideas should be seen as a confirmation of these older hypotheses. We should also be able to see their drawbacks, which include some over-simplifications such as studying the stability of the mean, *parallel* flow, not taking into account the presence of the body (which in reality reflects as well as absorbs instability waves) and the inadequacy in terms of dual frequencies sometimes observed in wake flows (as, for example in cases when both large-scale and small-scale vortical structures are of importance). As is mentioned by Monkewitz and Nguyen (1987), the wake problem has been traditionally approached along three main lines. The first deals with "integral effects", such as drag and shedding frequency and tries to explain their interaction. The second line concentrates on the vortex dynamics of the developed wake. The third approach consists of analysing the stability of the mean velocity profile in the wake. We should not really view these approaches as competing or mutually exclusive. What would seem to be the most promising approach to the wake problem would be a theory that effectively combines all three of these main lines.

Unal and Rockwell (1988a) attempted such a link between experimental observations and the absolute-convective instability concepts. They raised a question over the relative importance of upstream Biot-Savart induction as a feedback mechanism compared to the upstream travelling waves due to the absolute instability (of course there arises another question on whether these two mechanisms are really different from each other). Either way, they suggested that the "upstream influence" mechanism is the main reason why the large-scale vortex formation frequency dominates over the small-scale Bloor-Gerrard vortices that appear in the shear layer. As two further limitations of the instability theory they sited the existence of these two frequencies (the small-scale one of which may be three-dimensional), and also the non-linearity of the disturbance which can not be predicted by a linear theory. In Unal and Rockwell (1988b) they explained the influence of a splitter plate in terms of the stability characteristics of the wake. It was further emphasised that the large-scale vortices are caused by an absolute instability, with their fundamental harmonic (f_V) dominating (as a result) over the other harmonics ($n*f_V$), due to the self-sustaining nature of the absolute instability region. On the other hand, the shear layer instability of Bloor-Gerrard small-scale vortices is of the convective type and hence (a) it does not grow much in the near wake region, and (b) frequency components associated with this small-scale

frequency become quite apparent, as they evolve from secondary instabilities related to the fundamental harmonic.

The wake control methods described so far (base bleed, splitter plates, oscillating body) represent a global forcing of the wake (i.e. the global stability characteristics are changed). A local forcing of the wake was investigated by Williams, Mansy and Amato (1992). They applied a symmetric excitation on the boundary layers of a circular cylinder at small distances upstream of the separation points. It was found that they could control the shedding mode even by this very local form of excitation. This strengthens the view that the separated shear layers play an important part in the feedback mechanism that, in turn, controls the generation of the vortex street, although, it has to be said, no reference is made to the importance of the separation points.

1.2.4 The distinctions between two- and three-dimensionality

We should perhaps make a note here of the significant distinctions between two-dimensionality and three-dimensionality. In the early years it became increasingly obvious to experimentalists that despite efforts to achieve a perfectly two-dimensional flow, this was almost always practically impossible. Perfect two-dimensionality (where along the one axis velocity and derivatives are all zero) could be achieved in very restricted (and seldom realistic) conditions. That the two-dimensional approach has survived even to this date should not surprise us, however. The basic dynamics of the formation of a vortex street are two-dimensional. Clearly for a complete theory on vortex shedding we should have a comprehensive understanding of the two-dimensional phenomena, even if in the real world they never occur in such an isolated form.

The term "nominal two-dimensionality" has also been used. Here, even though there may be either small-scale irregularities (turbulence) or larger-scale irregularities along the span, they do not show any particular spanwise preference and hence all the statistical properties of the flow remain constant over some portion (at least) of the span. Even though many studies that fall in this category totally avoid the subject of three-dimensionality, their importance too should not be underestimated, as the physical significance of some three-dimensional phenomena can sometimes be more clearly highlighted through two-dimensional considerations. For example, although the transition to turbulence by definition implies a transition to three-dimensionality, significant gains in our understanding can also be made if one studies it macroscopically, and simply considers the effect

of turbulent diffusion which (under certain conditions) can be thought of as a nominally two-dimensional phenomenon.

1.3 The three-dimensional flow past a bluff body

The existence of three-dimensional characteristics, even in what one would expect to be two-dimensional flow, has thus been recognised for many years. For example, Tritton (1959) provided flow visualisation evidence on wavy or oblique vortex lines. It is now generally accepted that his transition at $Re \approx 90$ is in fact associated with a three-dimensional effect (actually, an end effect).

It is obvious that any real cylinder has to be of finite length. The question is not whether there will be end effects or not, but how far into the span these effects will be felt, and if there will be any part (perhaps in the region of the mid-span) where the flow can be considered to be two-dimensional. Similarly, it is obvious that at sufficiently high Reynolds numbers the flow will be turbulent and hence three-dimensional. The cause of this turbulence must be some form of an instability. Therefore, the second question that arises is not whether there will be an instability that will cause a transition to three-dimensional turbulence, but whether there will be an inherent instability that can cause larger-scale three-dimensionality (perhaps at the scale of the Kármán vortices) before or after that onset of turbulence. In this section we will briefly go through some of the most important previous work that has been done on the three-dimensionality of wakes.

1.3.1 Oblique vortex shedding and end effects

A relatively simple three-dimensional phenomenon that occurs even at low Reynolds numbers is that of oblique vortex shedding. In this case, if we consider a cylinder, the axes of the vortex filaments will form an oblique angle w.r.t. the cylinder axis. This was observed as early as Tritton (1959), while Gerrard (1966a) observed oblique vortices for low Reynolds numbers (up to 235), but parallel shedding for $Re=20000$. In Gerrard (1978) he observed "bowed" vortices at certain Reynolds numbers, and proposed end effects to be the cause. The importance of such effects has recently been put beyond dispute by Williamson (1988 and 1989). In experiments in a towing tank with large aspect ratio cylinders he observed an initial parallel shedding configuration, while the oblique mode would start from the ends and move progressively inwards, until a chevron-shaped pattern was established (figure 1.6). This proved that there could be various inherent solutions (oblique and parallel) to the flow equations, the choice of which

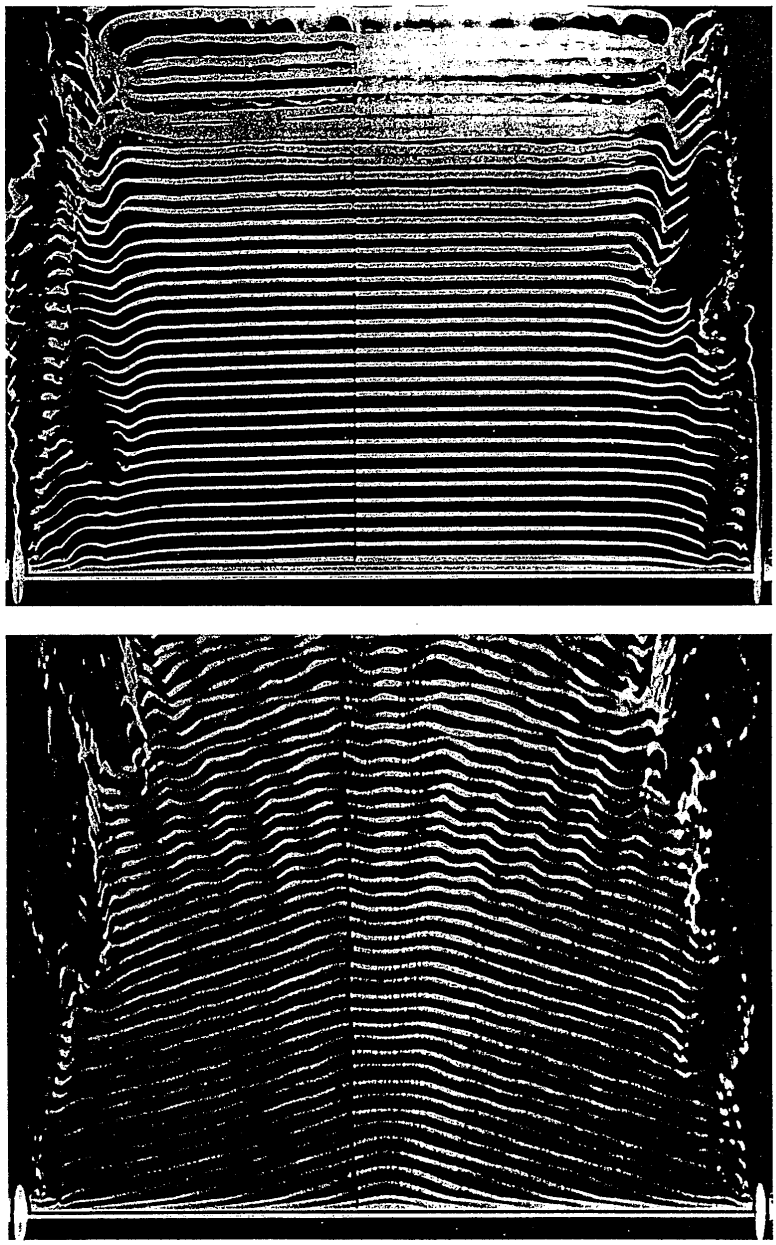

Figure 1.6 Development of an oblique shedding mode in the wake of a circular cylinder at Re=95 (flow is upwards). Photo (a) was shot when the cylinder had travelled a distance x/D=100. Later on, at x/D=600 (photo (b)), the oblique mode has propagated inwards from the ends to form a chevron-shaped pattern (from Williamson, 1989).

solely depended on the end effects. He also proposed the use of the formula $S_0 = S_\theta/\cos(\theta)$ (where θ is the oblique angle, S_θ the measured Strouhal number, and S_0 the universal Strouhal number), in which case all discontinuities are removed from the Strouhal-Reynolds curve for $Re < 180$.

Numerous researchers have found that by manipulating the end conditions one can achieve parallel shedding as the stable solution for the flow. They include Williamson (1989, by angling the end plates and 1992b, by suction in the formation region at the two ends), and Eisenlohr and Eckelmann (1989, by using "end cylinders" with a larger diameter). Gerich and Eckelmann (1982) studied the effect of free ends and that of endplates. The most important conclusion of this work was the existence of what they called the "affected region", for approximately 10D from the cylinder ends, confirmed also in Williamson (1989). This was said to be the region under direct influence from the ends, where a lower shedding frequency was observed. Eisenlohr and Eckelmann (1989) proposed a possible vortex structure close to the end plate (figure 1.7), where Kármán vortices partly loop across the wake to join with their counterparts on the other side of the wake, and partly join the horseshoe vortex generated at the end plate boundary layer. Velocities induced by this structure, it was claimed, oppose the free stream and thus cause the drop in the shedding frequency of the affected region.

1.3.2 Two important three-dimensional mechanisms

The situation thus arises where we have two neighbouring cells (affected region-unaffected region) that shed at different rates. Similar cells shedding at different frequencies have been observed in a wide variety of flows and it was suggested by Gerrard (1966a) that the two possible mechanisms to accommodate this are "vortex splitting" and what one may call "vortex looping". In vortex splitting, as we approach the boundary of a cell, a vortex filament splits and thus gets linked to two vortices of the same sign at the other side of the boundary. In vortex looping a Kármán vortex loops across the wake to get connected with another vortex (with oppositely signed vorticity) on the other side of the wake.

We should see both the above phenomena as topological consequences of a spanwise step-change in a certain quantity as we cross the boundaries of a cell. Vortex splitting can accommodate a spanwise change in the timing of a vortex, either because there is a phase difference across the cell boundary, or because the shedding frequencies across this boundary are different. Vorticity shed per unit

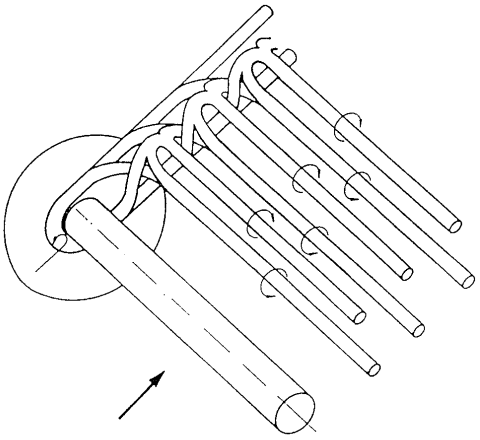

Figure 1.7 A possible vortex structure close to the end-plate of a circular cylinder (from Eisenlohr and Eckelmann, 1989).

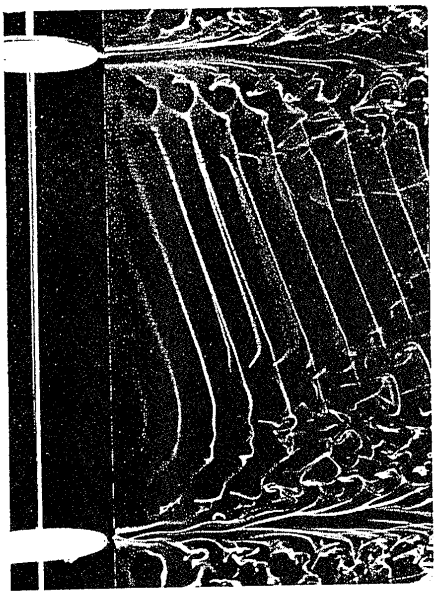

Figure 1.8 Vortex splitting in the wake of a circular cylinder at a low Reynolds number (from Eisenlohr and Eckelmann, 1989).

time on one particular side of the wake remains unchanged across the boundary, but simply gets re-distributed to Kármán vortices in a different way. On the other hand, vortex looping does not accommodate a spanwise change in vortex timing, but does result in different amounts of vorticity shed per unit time on either side of the cell boundary. We should also bear in mind that these two phenomena can also occur simultaneously, as the one does not exclude the other.

Vortex looping is usually observed when there are strongly three-dimensional effects somewhere along the span, such as a free end or an end plate (Eisenlohr and Eckelmann 1989, discussed earlier). It has not been observed, however, when the spanwise disturbance is only mildly three-dimensional. Vortex splitting has been observed by numerous researchers including Gerrard (1966a and 1978),Gaster (1971), Eisenlohr and Eckelmann (1989, figure 1.8), Nuzzi et al (1992) and Williamson (1989,1991 and 1992a). All of them identify it as a key feature to accommodate spanwise shedding frequency variations. Williamson (1992a and earlier papers) uses the term "vortex dislocations" to describe the complex inter-linking across a cell boundary.

1.3.3 Inherent three-dimensional patterns in nominally two-dimensional flows

We have now identified a key three-dimensional feature of bluff body flows (vortex splitting). While with parallel shedding, or oblique shedding, the spanwise correlation of two velocity signals (or any other quantity fluctuating at the Kármán frequency) will be quite high, the occurrence of vortex splitting will drastically reduce that correlation. Evidence from experiments suggests that, especially at high Reynolds numbers, irregularities such as vortex splitting can occur at arbitary positions along the span (for a nominally two-dimensional model) and at random instants in time. Thus the degree of such three-dimensional behaviour could be quantified by measuring the correlation length. Typically, for turbulent wakes the correlation length is of the order of a few diameters, but the exact reason for the irregular three-dimensionalities is not fully understood, and the correlation length can not be predicted.

Graham (1969), investigated the effect of end plates on the correlation length of a D-section bluff body. He found that if the end plates were within one correlation length apart (as measured for a large aspect ratio body), vortex shedding would be in phase along the whole span. Otherwise, irregularities would appear in the flow. Similarly, Szepessy and Bearman (1992) found the fluctuating lift (at the centre-span of a circular cylinder) to increase as the end plate separation

decreased. They suggested that at large apect ratios cross flow was more prominent, which resulted in weaker vortices (and lower lift fluctuations).

Generally speaking, stronger three-dimensionalities in bluff body flows have usually resulted in lower forces (drag or lift). Tanner (1972), for example, achieved significant reductions in drag (up to 64%) for aerofoils with a blunt trailing edge by breaking the separation line. Similarly, Zdravkovich et al (1989) investigated the flow around short cylinders with two free ends. They observed vortex shedding for apect ratios as low as 2, but drag reduction only down to aspect ratios of 6 (the main reason for the drag reduction being the inflow from the free ends). It may not be a coincidence that two-dimensional numerical schemes tend to over-predict lift and drag. There may be some inherent, drag-reducing three-dimensionality even in well set-up "two-dimensional" experiments.

In recent years there has been a large increase in the number of studies concerned with just that point: is there an inherent three-dimensional instability, irrespective of end conditions? Triantafyllou (1990) used linear stability theory to study three-dimensional flow patterns in wakes. He differentiated between two kinds of such patterns. The first one was said to be due to localised inhomogeneities of the flow or the body which generate "guided" three-dimensional waves. Linear resonances can then spread coherent three-dimensional patterns through the entire wake. Though a linear theory, he also explained how end conditions (such as the end cylinders used in Eisenlohr and Eckelmann, 1989) can cause two-dimensionality at the centre of the span. The second kind of three-dimensional pattern was said to be the development in the average flow of steady modulations that cause three-dimensional instability patterns. Triantafyllou identified this pattern as a secondary instability, adding that it would also arise in an infinite body, and that it occurs at Reynolds numbers above 200.

Further important numerical work was reported in Karniadakis and Triantafyllou (1992) who proposed that the main route to chaos is though the "period-doubling scenario". They attributed the period doubling phenomenon to the presence of two three-dimensional absolute instability modes in the near wake. The flow was then said to alternate between these two modes, thus repeating itself only after twice the time it would normally take to do so. It was then proposed that successive period doubling bifurcations are the cause for transition to chaos and turbulence.

The evolution of the flow at high Reynolds numbers as we move towards the far wake has also attracted considerable attention. From a stability point of view, the main characteristic as we move away from the body is that the absolute instability vanishes, and the instability is now of the convective type. It has been observed that in the far wake there tends to be a decay in the main, Kármán frequency component and an appearance of lower frequencies. Browne et al (1989) proposed that this is due to the interaction of large vortical structures at both sides of the wake. Similarly, Ferré and Giralt (1989) observed this rapid destruction of individual vortices with a resulting randomisation of the vortex street, and the appearance of complicated "double roller" vortical structures. Further discussion on the re-organisation of the vortex street in the far wake is included in Bisset et al (1990a and 1990b). Finally, Corke et al (1992) studied the growth of three-dimensional modes in the wake of a two-dimensional body. They concluded that a fundamental mechanism for their growth is the resonance between the fundamental (Kármán) mode and the three-dimensional instabilities. The complicated aspects of far wakes have been touched here in a very superficial way, just to illustrate how important our knowledge of the fundamental three-dimensional dynamics of the near wake may be to the flow further downstream. The present investigation, however, will concentrate on the direct body-flow interaction, and therefore we will concern ourselves predominantly with the near and the intermediate wake.

1.3.4 Imposed three-dimensionality in wakes

So far, in our review of studies aiming to understand inherent three-dimensional flow behaviour, all of them (be they computational of experimental studies) were essentially concerned with the growth of three-dimensional instabilities in a "two-dimensional" wake. Some recent studies have approached this subject from a different angle. Their common aspect is that they investigated three-dimensional patterns imposed by geometrical disturbances on the body. The main reasoning behind this approach is that by doing so, the three-dimensional characteristics that appear irregularly behind a two-dimensional body may now appear more regularly in space and time and thus be more easy to study experimentally (in contrast, studies of effects such as end plates, oncoming shear, etc. do not impose three-dimensionality in such a controlled way, but rather approach it as an inevitable feature of the flow).

In an interesting study, Breidenthal (1980) compared the response of plane shear layers to strong three-dimensional disturbances to that of wakes. Whereas the

shear layer quickly relaxed to a two-dimensional pattern (in terms of the large vortical structures), the wake retained its three-dimensionality far downstream of the body (figure 1.9). A few interesting conclusions can thus be drawn. Breidenthal observed that both the wake and the shear layer behaved as if they "wanted" to minimise the volume of rotational fluid. In the case of the shear layer there is predominantly one sign of vorticity shed from the model. Vortex lines must start from one wall of the test section and end in the other. In that way, their most "economic" (least energetic) arrangement seems to be in two-dimensional large-scale vortical structures. On the other hand, in the case of the wake we have two signs of vorticity shed from the model (and at equal quantities). In that way the least energetic arrangement seems to be in closed loops that show little tendency to grow in the spanwise direction. Topologically, the formation of these loops is only possible because of the presence of the opposite shear layer. Hence, it seems that a hypothesis originally made by Roshko is confirmed: the asymptotic state for the plane shear layer seems to be predominantly two-dimensional, whereas the asymptotic state of the wake (two interacting shear layers) seems to be three-dimensional.

Nuzzi, Magness and Rockwell (1992) reported on the effects of body oscillation on vortex formation from a non-uniform circular cylinder (for Re=145). The cylinder had a smooth neck at mid span with a minimum diameter a bit smaller (by 20%) than the diameter of the uniform part. At a certain oscillation frequency global lock-in was observed and even though the vortices shed were three-dimensional, their structure was repetitive from cycle to cycle (figure 1.10). At slightly lower forcing frequency, however, the flow from the non-uniform part of the cylinder experienced a period-doubled response, while the flow from the uniform part remained locked-in (figure 1.11). In the period-doubled portion, the vortices would alternately be first normal and then split, in terms of their joining with the vortices from the locked-in region. Various other flow patterns were observed for different oscillation frequency regimes.

Two interesting comments can be made about these results. First, they seem to tie in well with the period-doubling scenario predicted in Karniadakis and Triantafyllou (1992) due to two competing, inherently three-dimensional flow modes. Second, they raise a question about the coupling between the flows in adjacent sections of the body. Lock-in has been achieved by a wide variety of possible forcing methods (sound, transverse oscillation, streamwise oscillation, periodic rotation, etc.). The results of Nuzzi et al indicate strongly that some kind of frequency forcing can also be transmitted in the spanwise direction, a fact

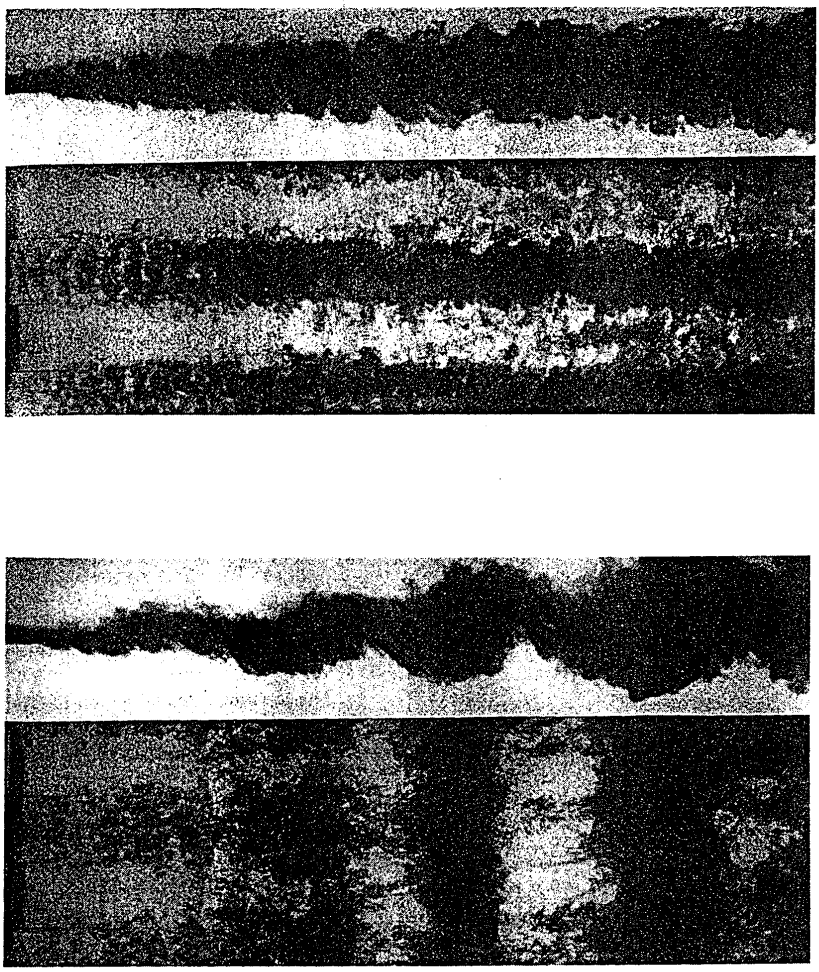

Figure 1.9 Top: side and plan views of a wake responding to a strong three-dimensional disturbance. The flow retains its three-dimensionality far downstream. Bottom: side and plan views of a shear layer responding to a similar disturbance. The shear layer quickly relaxes to a two-dimensional pattern. Hence we can conclude that the asymptotic state of a wake is three-dimensional, while the asymptotic state of a shear layer is two-dimensional (from Breidenthal, 1980).

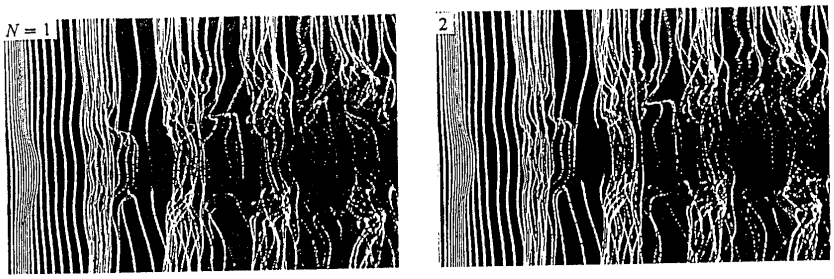

Figure 1.10 Spanwise visualisation of global lock-in achieved in the wake of an oscillating, non-uniform circular cylinder at Re=145 (from Nuzzi, Magness and Rockwell, 1992).

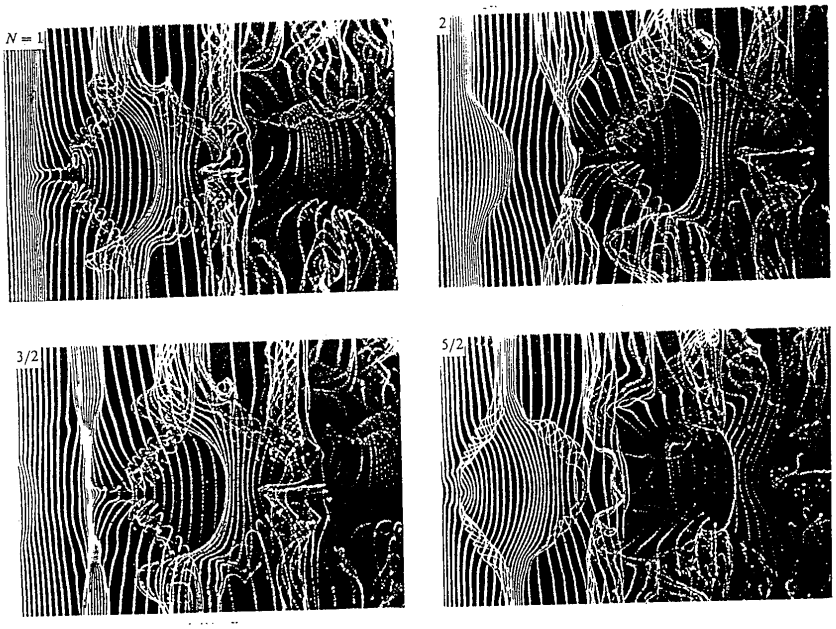

Figure 1.11 Spanwise visualisation of period-doubled vortex formation, achieved in the wake of an oscillating, non-uniform circular cylinder at Re=145. N=1 and N=2 correspond to maximum positive displacement, while N=3/2 and N=5/2 correspond to maximum negative displacement. Comparing N=1 with N=2 (and also N=3/2 with N=5/2) we can see that the same pattern is not repeated at each cycle, but only at every other cycle, i.e. the period has been doubled (from Nuzzi, Magness and Rockwell, 1992).

which may not be surprising as such, but which may explain why non-uniform flows tend to organise themselves in spanwise cells of different frequencies.

In Williamson (1992a) the flow around an otherwise uniform cylinder (of large aspect ratio and at low Reynolds numbers) was perturbed by a ring of slightly larger diameter fastened at mid-span. This disturbance caused two-sided vortex dislocations to appear regularly downstream of the ring, as the ring would shed vortices at a lower frequency than the rest of the cylinder. The predominant dislocation frequency was the beat frequency ($f_{cylinder}$-f_{ring}). Williamson reached several interesting conclusions regarding the fine structure of dislocations at these low Reynolds numbers. He proposed a mechanism whereby the dislocation spreads in the spanwise direction. In figure 1.12a, we can see how the rotation of the main vortex C causes its branches, vortices A and B to helically rotate about each other, thus inducing an axial component of velocity, that would tend to further split vortex C. The induced strain rates form A and B are shown in diagram 1.12b. The further "unravelling" of vortex C will effectively cause the spanwise dislocation spread. Williamson suggested also that the cores out of the dislocation would tend to become thicker and leave behind them thinner, stretched vortex "wisps" within the dislocation, as a result of the induced axial motion (figure 1.13). The vortex wisps within the dislocation were then said to reorganise themselves into "Λ-vortices", the predominant structure observed within the two-sided dislocation (figure 1.14).

Williamson's proposed ideas concerning the detailed structure of dislocations are very useful but should perhaps be treated with some degree of caution, especially for their applicability to higher Reynolds numbers. For example, even though the velocity induced on the particular fluid element at the point where the vortex filament splits (in figure 1.12a) may be in the direction shown in the diagram, it is still possible that the two vortices A and B will merge at that point under the influence of diffusion or turbulence (at higher Reynolds numbers). In that way although the fluid *element* at the vortex "junction" may move in the direction suggested by Williamson, the *junction* may in fact appear to move in the opposite direction. The fact that the low frequency cell appears to spread gives an indication that higher frequency vortices (linked though vortex splitting to a smaller number of lower frequency vortices) may indeed be rolling up and merging, even at the low Reynolds numbers considered by Williamson.

In closing this brief review on three-dimensional wakes, it would be appropriate perhaps to mention attempts that have been made to mathematically

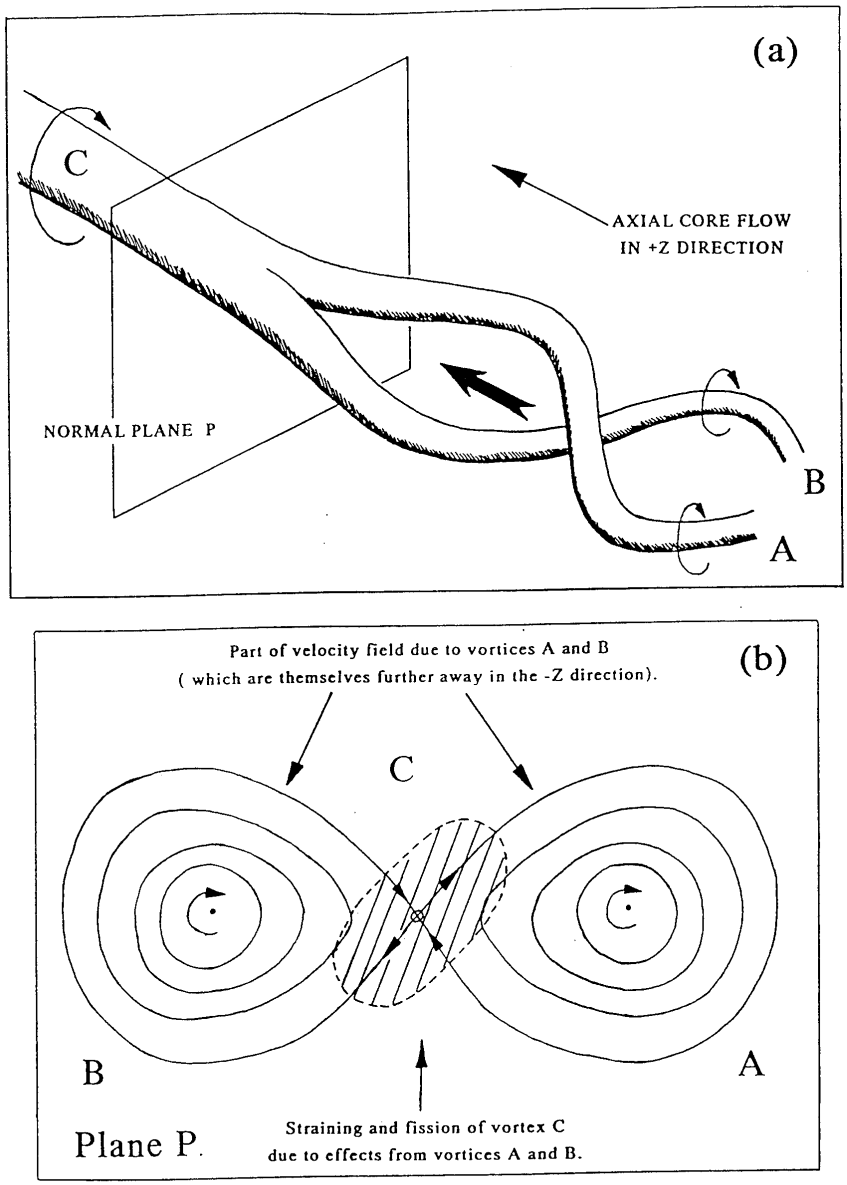

Figure 1.12 Williamson's proposal for the motion of a "vortex junction": In (a) we see two vortices (A and B) of similar sign joining together (into C). The vortices will tend to twist helically and thus induce an axial velocity at the core of the vortex junction. This, in combination with the straining mechanism shown in (b) will cause vortex C to further unravel and the dislocation to spread (from Williamson 1992a).

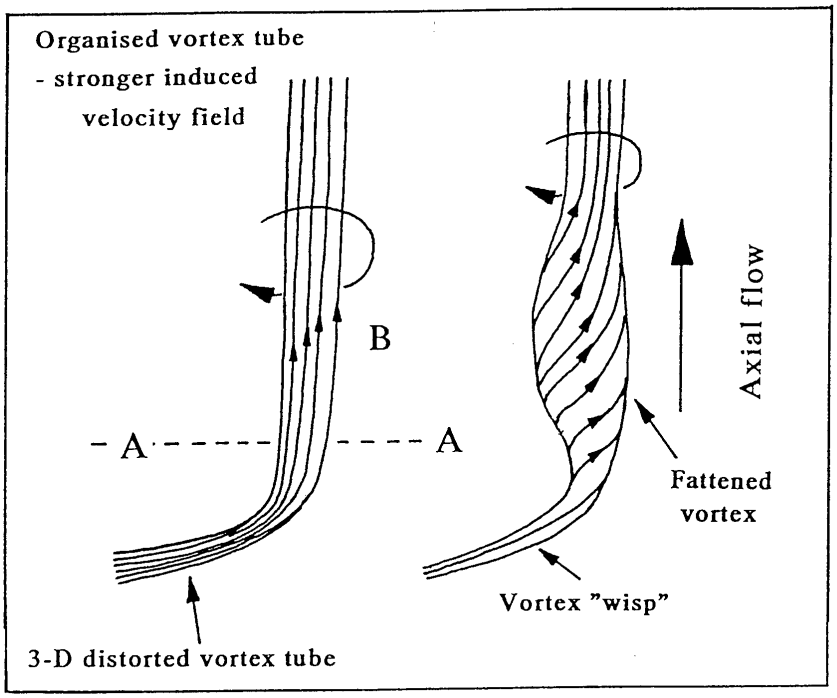

Figure 1.13 Williamson's proposal for the creation of vortex "wisps": A non-uniformity causes the vortex tube to twist. The helical arrangement of vortex lines within the vortex tube will induce an upward axial flow that will tend to "fatten" the vortex tube away from the non-uniformity leaving a thin vortex "wisp" at the region of the non-uniformity (from Williamson 1992a).

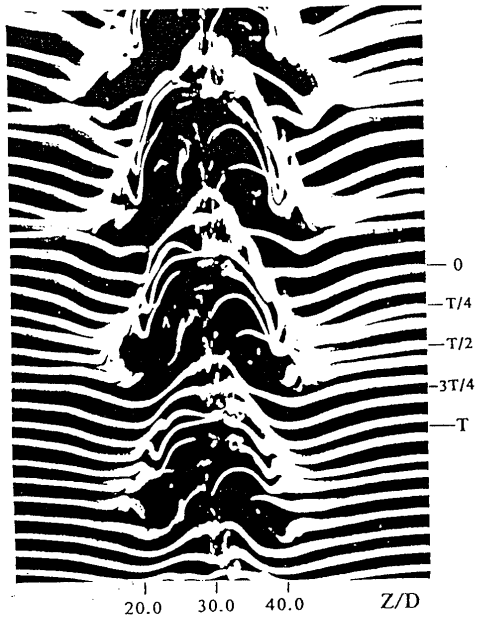

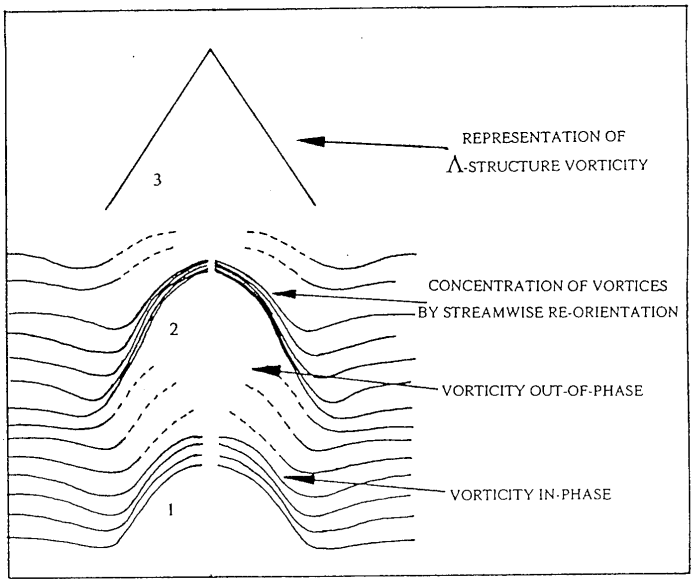

Figure 1.14 (Following from figure 1.13) the resulting structure from a local model non-uniformity: vortex wisps have organised themselves into Λ-structures (from Williamson 1992a).

model three-dimensional wakes. Notable examples here are Gaster (1969) and Noack et al (1991). In both investigations a simple van der Pol oscillator was used to model each cross section of the flow. By selecting appropriate characteristics (according to the spanwise conditions-diameter, free stream velocity, etc.) and coupling parameters between neighbouring cells, the cellular type of flow was predicted quite impressively in both cases. It seems therefore that this method is quite useful to give us a basic understanding of the phase-frequency relationships along the span, although it goes without saying that we should not expect any real insight into the details of vortex dynamics and the transition to turbulence from such a simplistic model.

2. INTRODUCTION TO THE PRESENT INVESTIGATION

2.1 Aims of the project

2.1.1 Areas of importance and interest

There can be no doubt that our understanding of three-dimensionality in wakes has improved considerably over the past few years. There are many reasons which necessitate our better understanding of three-dimensional wakes. In real-life engineering problems flows are never two-dimensional, yet most of our efforts, so far, have been in investigating such flows. A better understanding of the Kármán vortex street dynamics would eventually enable us to have better control over parameters such as the intensity of vortex shedding and consequently, the drag and the fluctuating forces acting on bodies (due to their unsteady wakes) could be controlled to a greater extent.

An experimental investigation into three-dimensionality could also provide a two-fold contribution to computational simulations. First, two-dimensional simulations have traditionally over-predicted quantities like drag or fluctuating lift (e.g. Braza et al, 1986). It is therefore important to be able to understand the reason of this over-prediction and see whether it is due to a general inability of two-dimensional codes to match real-life flow conditions. Second, as computers become more and more powerful, a number of cautious steps have been taken by various C.F.D. investigations in the direction of three dimensions (e.g. Karniadakis and Triantafyllou, 1992). As even the power of modern super computers is still not sufficient to simulate three-dimensional flows down to their smallest scales, it is vital to have sufficient information about the nature of the complex flow patterns (as a means of comparison and code validation).

It is now widely accepted that, at least at high Reynolds numbers, three-dimensionality is a key feature of wakes, irrespective of the end conditions. As was indicated in the previous chapter, numerous investigations have given sufficient evidence that an inherent instability causing three-dimensional effects would be present even if we could achieve a perfectly uniform flow around a perfect model with an infinite span. It is thus proposed that the main aim of this investigation be the achievement of a better understanding of this inherent three-dimensionality of bluff body wakes.

Turbulence is of course a very prominent feature of high Reynolds number flows, and by the nature of its most notable feature (vortex stretching) is heavily three-dimensional. The majority of the investigations into wake three-dimensionality has been for low Reynolds numbers (within the laminar flow regime), mainly due the ease of study of such flows. While these studies have illustrated many interesting wake flow structures, it is important to see to what extent high Reynolds number flows show similar properties and features under the influence of turbulence. A further intention of this study is thus to fill this gap, and investigate higher Reynolds number wakes.

As was mentioned in the previous chapter, Triantafyllou (1990) categorised the three-dimensional patterns in the context of "guided waves" (caused by body or flow inhomogeneities) and also in three-dimensional patterns due to what he termed "a secondary instability". Without wishing to contradict this grouping of three-dimensional patterns, it pays, perhaps, to categorise them into different groups, according more to their nature and less to their cause:

a) Mild three-dimensionality. Here we have continuous vortex filaments which may, however, not be parallel to the main axis of the body. The vortex filament lines may be oblique, "bowed" or wavy, but are continuous from the one end of the span to the other.

b) Strong three-dimensionality. Here the key effects are vortex splitting and vortex looping, mainly due to some spanwise variation in vortex strengths or in shedding frequency.

c) Smaller scale three-dimensionality as a result of a shear layer instability (e.g. Wei and Smith, 1986). The shear layer instability is of the convective type. Although it can also be purely two-dimensional, its small scale frequently results in three-dimensional turbulent structures.

d) Small scale three-dimensionality (turbulence). The distinction of this scale of irregularities from the ones mentioned above is basically a matter of convention. Whereas the scale of the previous examples is of the order of a characteristic model dimension (say, cylinder diameter), the scale of the turbulent structures may be considerably smaller.

It is worth noting that these types of three-dimensionality can occur separately or simultaneously, in any combination. The first two may be caused by end effects, by spanwise variations in flow conditions or they may be inherent

three-dimensional features of the flow. On the other hand, shear layer three-dimensionality and turbulence are caused (as a rule) by a secondary instability, in many cases accelerated by one of the first two types of three-dimensional patterns. Another aim of this work is thus a better understanding of the mechanics of the large-scale three-dimensionalities (types a and b) while chapter 8 will briefly move into the smaller scales of type (c). Throughout this investigation, the strong emphasis will be on such irregularities, and the effects of small-scale turbulence will only be considered from a macroscopic point of view, as opposed to a direct investigation of its fine structures.

There have been numerous publications throwing light on the dynamics of the two-dimensional near wake. If we combine works like that of Gerrard (1966b) with newer theories about the absolute/convective instability concepts we can obtain a fairly coherent appreciation (in both the physical and the mathematical sense) of the two-dimensional wake. However, although a number of researchers have identified key effects such as vortex splitting, our understanding of how some important three-dimensional wake parameters interact is still lacking. As such "important parameters", we could list (among others) the base pressure, the shedding frequency, the formation length, the wake width and the eventual strength of the Kármán vortices (related to the fraction of the original vorticity that survives vortex formation). Another important aim of this project is thus a better understanding of how these wake parameters interact and vary along the span.

Although the far wake can be of great importance in a variety of engineering applications (for example, in stratified water two dimensionality prevails and the vortex street of submarines can survive at a large downstream distance, thus making it detectable, generally an undesirable feature for an otherwise "quiet" submarine), it is not going to concern us in the present investigation. Due to the feedback characteristics of the near wake region (and the convective instability nature of the far wake), it is the near wake that interacts with the body and hence its dynamics determine the drag, the shedding frequency and the fluctuating lift (among other parameters). Hence, this project will concentrate on the near wake.

The majority of the absolute/convective instability investigations have concentrated on two-dimensional flows, but the term "absolute instability" has been used only in a qualitative manner in three-dimensions (although there can be no doubt that such stability characteristics play at least an equally important role in the three dimensions as they do in two). Similarly, there have been studies, such

as the mathematical models mentioned at the end of the previous chapter (Gaster 1969 and Noack et al 1991), that have considered three-dimensional flows to be a series of inter-linked and coupled quasi-two-dimensional flows. While it is obvious that such an approach can never achieve a perfect understanding of complex flow patterns, its attractions are also quite apparent. It would therefore be of much interest to see whether two-dimensional considerations can be of use in certain three-dimensional flows.

So, we have arrived at a summary of the main objectives of this research project:

a) The dominating feature will be the three-dimensionality of bluff body wakes. We will concentrate on the near wake, and on the larger-scale flow features (as opposed to small-scale turbulence).

b) It is aimed to achieve a better insight into key three-dimensional features (such as vortex splitting and vortex looping), as well as any other three-dimensional characteristics that may arise.

c) It is hoped to obtain a better understanding of the relations between wake parameters such as formation length, wake width, shedding frequency, base pressure and the eventual strength of the Kármán vortices, from a three-dimensional point of view (as the average or the instantaneous values of these parameters may change along the span). It would be nice to be able to link in some way the above to the concepts of absolute and convective instability.

d) Finally, this study aims to check the validity of quasi-two-dimensional considerations in bluff body flows.

It would be appropriate, after this summary of the project objectives, to stress, once again, areas which lie beyond the scope of this project. This project does not aim to study: (a) small-scale turbulence (other than a possible consideration of its macroscopic effects on the larger scale structures), (b) the far wake, and (c) means of "optimising" the flow (e.g. to reduce drag). Even though these areas would definitely present us with challenging problems, investigating such a diverse field would not allow us to give proper attention to the main target of this work, the understanding of the *physics* of the three-dimensionality of *near* wakes.

2.1.2 The approach to be used in this study

It is accepted that in the phenomena to de discussed in this study complexities abound. Obviously, it would be naive and over-ambitious to hope to put the issues outlined as project objectives in the previous section beyond further dispute. On the contrary, this project (and its expense) will be considered justified, even if its contribution is just a small step forward.

The nature of this study is fundamental. Its engineering applications are many steps away. Its purpose is to add to our "bank" of fluid mechanics understanding. The main advantage of a fundamental study is that there is no real risk: if the conclusions of this study are wrong, no building will collapse on its residents and no aeroplane will fall. In such cases conclusions have to be reached with certainty and safety.

Scientific progress thrives on dispute. Complacency and conservatism are tools often used to avoid any wrong statements: uncertain -but potentially good- arguments are often kept in the closet, purely to avoid the embarrassment of an error. This will not be in the nature of this project.

The concepts presented in later chapters, it is believed, are scientifically valid, possible explanations of the observed phenomena. Naturally, where possible, much effort has been put to make the suggestions watertight. However, as a result of the considerable flow complexity and the inadequate experimental apparatus (experimental apparatus, by definition, is never really adequate), in some cases plausible explanations could not be further verified. Ideas presented herein, may thus be overturned by other researchers, or they may be confirmed. In either case, they could, conceivably, be useful.

2.2 Three-dimensional, geometrically imposed disturbances

2.2.1 The significance of such disturbances in order to study wake irregularities

As was mentioned earlier, a measure of the three-dimensionality of the flow around a nominally two-dimensional body is the correlation length, the spanwise distance at which a certain fluctuating quantity remains correlated. For a sufficiently long cylinder at high Reynolds numbers, a typical value of the correlation length would be 4-5 diameters. One could explain this surprisingly low correlation length value by considering the shapes of vortex filaments. These have

to follow either some wavy pattern or there must be some form of vortex splitting/looping.

Experiments in the past have not identified any particular spanwise preference for these irregularities. By all indications, they seem to occur at random points in time and space. This erratic occurrence of three-dimensional effects makes them quite difficult to study in much detail and therefore our knowledge of their exact behaviour has been limited. In this investigation it is proposed to fix these three-dimensionalities in both time and space, in order to make them easier to study. A way to achieve that could be the imposition of some mild three-dimensional disturbance on the nominally two-dimensional geometry of the body.

Other researchers have used a similar approach, notably Nuzzi, Magness and Rockwell (1992) and Williamson (1992a). In the present work the disturbance to be used will be periodic in the spanwise direction. The logic of this periodicity (as opposed to a local and isolated disturbance used by other researchers) is two-fold. First, it is hoped that any end effects will be "filtered out" at the geometric disturbance wavelengths near the end-plates. Vortex splitting has been known, some times, to isolate end effects close to the end-plate (e.g. the end cylinders used by Eisenlohr and Eckelmann, 1989). In the present case, vortex splitting occurring close to the end-plates could limit their effects in that region, thus resulting in a purer three-dimensional effect at the wavelengths around the centre span. Second, the regular nature of the disturbance will hopefully eradicate most of the random type disturbances observed in nominally two-dimensional flows. Hence it is hoped that this periodic nature of the disturbance will achieve more regular three-dimensionalities, unaffected by the end effects.

2.2.2 Choice of the model

Most of the work on bluff body wakes has concentrated on the flow around circular cylinders. Despite the apparent geometrical simplicity of this shape, circular cylinders result in very complicated and interesting flow patterns, mainly due to the non-fixed point of separation and the wake interaction with boundary layer characteristics. Although the flow around circular cylinders is of big engineering importance (with applications in flows around pipes, cables, chimneys, etc.), the extra complications of the moving separation point would perhaps hinder our main purpose, the study of three-dimensional patterns.

As it was anticipated that the flow patterns that would emerge would be of considerable complexity, it was decided to reduce the number of irrelevant (to this study) unknowns. The most suitable model section for this would appear to be a shape with fixed separation points and minimum body-shear layer interaction. The most obvious shape for this is an aerofoil-type shape with a blunt trailing edge, similar to that used by Bearman (1965 and 1967a). The main section of the model used in the present investigation had a chord of 190mm. The front part was semi-elliptic (semi-major axis=120mm, minor axis=30mm), followed by a straight segment (parallel to the free-stream, 70mm long), leading to the blunt trailing edge of height, h=30mm. A trip-wire was used in all investigations at 40mm from the leading edge, measured along the chord.

Of the parameters listed above, the most important is the base height, h. It was thus decided that the mildest possible form of three-dimensional disturbance would be a model with constant height (and hence constant "expected, quasi-two-dimensional" shedding frequency and vortex strengths) along the span. A possible geometry to achieve this mild, periodic disturbance was a sinusoidal trailing edge shape. Figure 2.1 shows the main parameters of the model used for most of the experiments, and also the axis convention to be used throughout this study. It should be noted here that with this model geometry, each model section has the same main geometrical properties, with the only parameter varying along the span being the chord, whose variation was taken to be of negligible importance as far as the local, quasi-two-dimensional flow parameters are concerned.

Of, course we would expect the coupling of successive sections to cause some three-dimensionality. For example, if the formation length is the same everywhere, the vortex lines will follow the model trailing edge, and hence there will be some streamwise vorticity. Nevertheless, the shedding frequency *could* conceivably be the same everywhere and hence this imposed three-dimensionality initially appears to be milder than that of other studies, where the model geometry dictates shedding frequency variations along the span.

For the initial experiments, various models with the same basic parameters, but with different geometric disturbance wavelengths and waveheights were built. The geometric disturbance parameters of the models tested are listed in the table below:

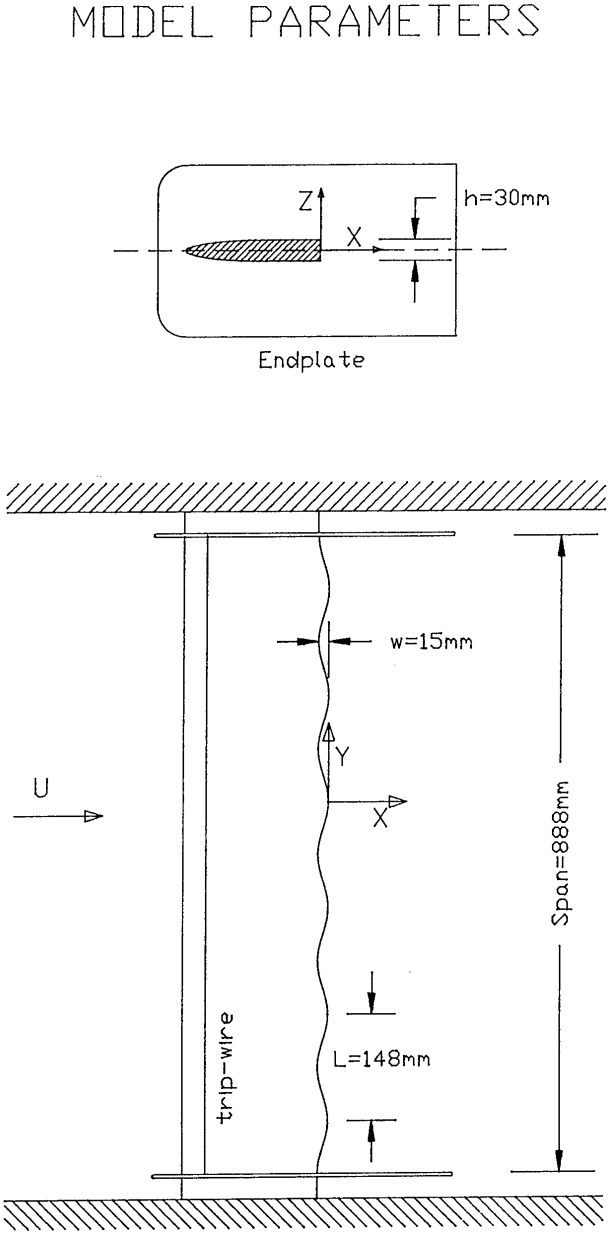

Figure 2.1 Diagram showing the general layout of the model and also the axis convention for this study.

wavelength, L (mm)	waveheight (peak-to-peak), w (mm)	steepness, w/L
Straight trailing edge		**0.000**
168	4	0.024
168	8	0.048
168	15	0.089
148	**15**	**0.101**
140	15	0.107
120	15	0.125
105	15	0.143

The models used in the more detailed experiments at a later stage are highlighted. They are the straight edge model (used for comparison purposes) and one of the sinusoidal trailing edge models (L=148mm, w=15mm).

3. EXPERIMENTAL SET-UP AND TECHNIQUE

3.1 Introduction

This chapter describes in detail the procedure used in the experiments of this study. Experiments were performed in a wind tunnel for quantitative measurements of velocities and pressures, and in a water flume for flow visualisation. The final experiments in the wind tunnel involved considerable complexity and sophistication. The processes described in this chapter were reached through continuous evolution and not instantaneously, and only represent the final state of the experimental procedure. The bulk of the results presented later stem from this experimental procedure.

After initial experiments with the models incorporating the various different parameters (wavelength and waveheight), a metallic model was constructed for the main series of experiments. The main feature of this model was its removable trailing edge (figure 3.1). This allowed the shape of the trailing edge to be easily changed (from sinusoidal with L=148mm, w=15mm, to straight), but also made an advantageous positioning of the pressure transducers possible, as will be discussed later.

3.2 Wind tunnel experiments

3.2.1 The 3' by 3' Wind Tunnel Laboratory

The quantitative part of this work was performed in the 3' × 3' Wind Tunnel of the Department of Aeronautics of Imperial College (figure 3.2a). This wind tunnel is of the closed-return type and has a working section of 0.92m by 0.92m wide and 4.9m long. The working section is preceded by a 2.7m × 2.7m settling chamber, followed by a honeycomb and three fine wire mesh screens, followed by a 9:1 contraction. The flow velocity in the working section can be varied up to a maximum speed of 50m/s approximately, and is uniform to within 0.5% with a turbulence level of less than 0.04%.

Although its air flow quality was very good, the wind tunnel initially lacked modern equipment which would make automatic experiment control possible. Furthermore, its air temperature would rise significantly after long running periods. Some of the experiments to be performed would require a large

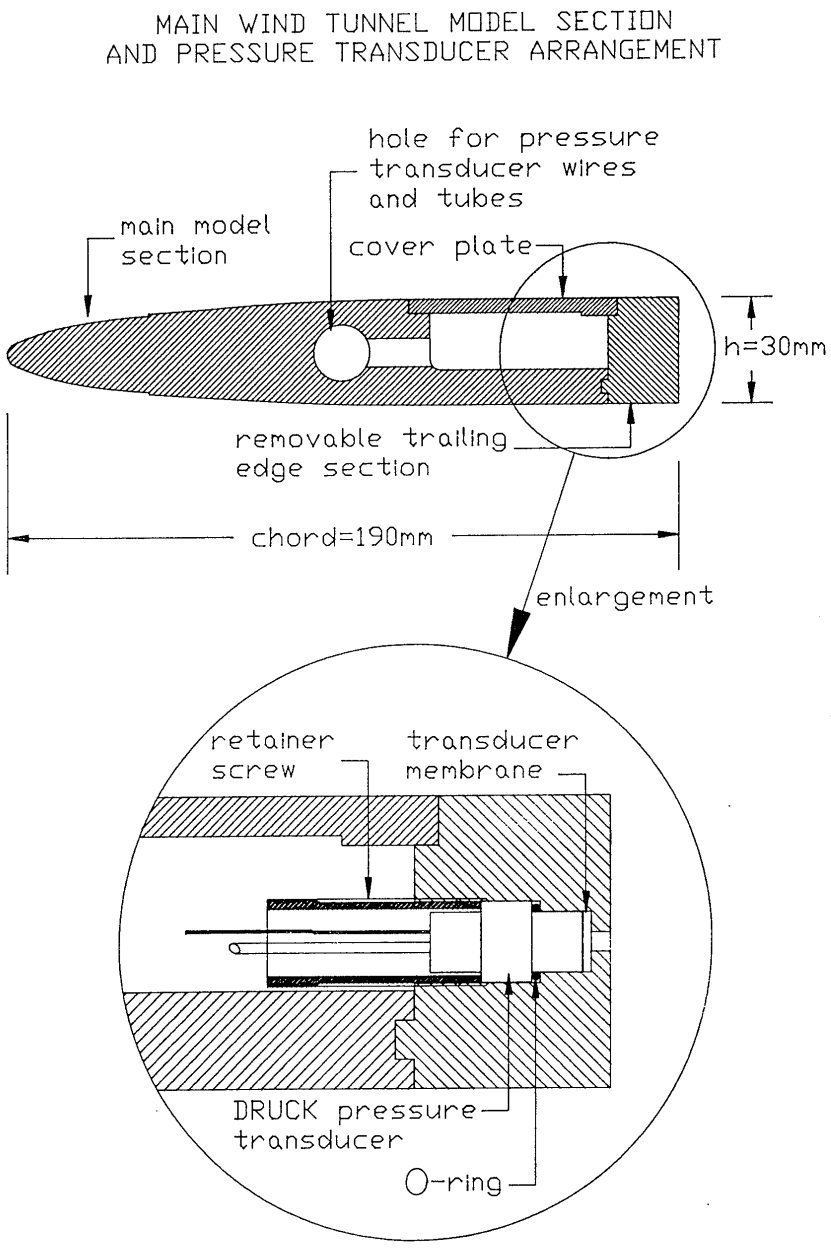

Figure 3.1 Cross section of the main model, featuring a removable trailing edge. The enlargement shows a Druck pressure transducer fitted within the model's trailing edge.

number of different (and hopefully accurately obtained) hot-wire probe positions, and continuous running times of 10-12 hours. Without a fully automated experiment, problems would arise in many areas: (a) with the increase of air temperature, the tunnel speed would tend to drop, in that way requiring frequent adjustment, (b) for long experiments, hot-wire probe calibrations would tend to drift, thus increasing experimental error, (c) hot-wire probe positions would have to be adjusted manually, thus reducing accuracy and increasing the chance of error, and (d) experiments would take a much larger amount of time (as an example, experiments that would have taken about two weeks to perform, only required one day after the automation was completed). Unfavourable aspects of an automated experiment include larger cost and long planning time, especially in this case when all the systems (to be described below) had to be developed more or less from scratch. Figure 3.3 is a schematic diagram showing the various components of the automated, experiment control layout (to be also described in detail in this chapter).

Control of all tunnel parameters by a 386 PC-compatible computer was achieved through a CIL interface system. A CIL A-Module multiplexer and 16-bit (high accuracy) A-D converter was used to monitor (among other quantities) temperature, free-stream velocity and atmospheric pressure. Temperature readings were obtained via a temperature-sensitive transistor. Tunnel speed was monitored from the output of an ultra-sensitive Honeywell mean pressure transducer, which measured the pressure difference between the beginning and the end of the 9:1 tunnel contraction. A Honeywell absolute pressure transducer was used to measure atmospheric pressure. A CIL O-Module D-A converter was used to control tunnel speed in accordance with the readings obtained by the A-D converter.

Considerable effort was put into developing a three-dimensional traverse (used to move a hot-wire probe). The traverse used eventually was a completely redesigned development of an old one that existed for that wind tunnel. The old traverse was inadequate in terms of position repeatability and its vertical arm was not stiff enough (and would hence vibrate). Furthermore, it could not be controlled digitally from the computer. The frame for the two horizontal axes of motion was kept unchanged, but had to be adapted for use with modern stepper motors. A new box holding the vertical arm was designed and built. All three stepper motors (and their controlling box) were supplied by Micromech Ltd. The controlling box for the motors was driven by three CIL S-Modules. The control of the traverse from the computer was open-loop, and therefore it was of paramount importance to ensure that position repeatability could be achieved, even after 500

(a)

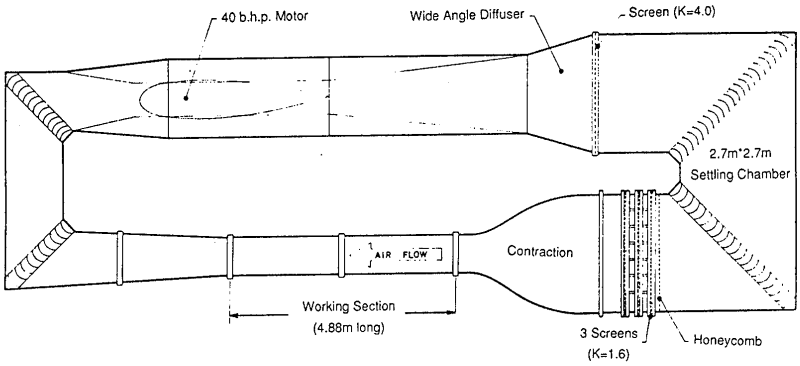

(b)

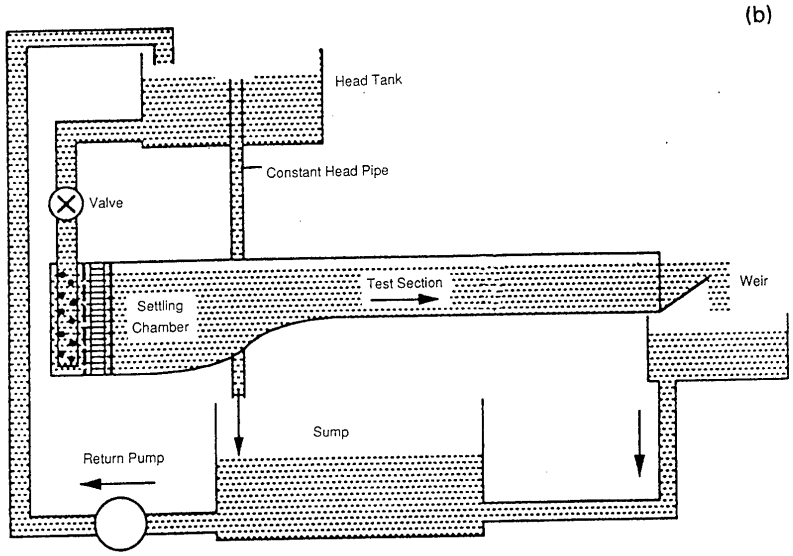

Figure 3.2 Laboratories used in the Department of Aeronautics, Imperial College of Science, Technology and Medicine: (a) the 3'×3' Wind Tunnel, and (b) schematic representation of the water flume.

movements that would occur in some of the experiments. In spite of many other precautions, the traverse was also programmed to move to a reference position (controlled by an accurate photo-diode) after a large number of movements, in order to check on its position accuracy and re-calibrate itself.

3.2.2 Hot-wire measurements

Hot-wire anemometry was the most important experimental tool of this investigation. The anemometers used were made by T.S.I., while the actual probes were made by Dantec, and were of the gold-plated type. Up to five channels were used at one time. All hot-wire probes were set to operate at a temperature of 250° C. Depending on their type (single or cross wire), and on their use (moving with the traverse or stationary) different calibration procedures were used. In all cases, calibration data would be fitted by a least squares algorithm to King's empirical cooling law:

$$\frac{E^2 R_s}{(R_s + R_L)} = \left[a + b(\rho V)^{\frac{1}{n}}\right](t_s - t_e)$$

where E is the bridge voltage, R_S is the sensor operating resistance, R_L is the resistance in series with the sensor, t_s is the sensor operating temperature, t_e is the environment temperature, ρ is the fluid density, V is the cooling velocity and a, b, n are constants ($n \approx 2$). Rearranging King's equation, we get:

$$V = \frac{t_e}{p_{atm}}\left[\frac{AE^2}{t_s - t_e} - B\right]^n$$

Thus the constants A,B and n would be used to convert voltages to velocities. Expected errors by using this empirical formula were of the order of 1%.

Frequently, single wires would be positioned at stationary positions in order to record phase or amplitude information, predominantly for comparison purposes (for example in conditional sampling). In these circumstances, the hot-wire probe would be calibrated against the free stream velocity (in an empty tunnel), to obtain the best values for A,B and n. Once the experiment was started, one could detect any drift in the values of the calibration constants by monitoring long period trends in the statistical properties of the signal (mean value, root mean square, and skewness). The values of the calibration constants could thus be

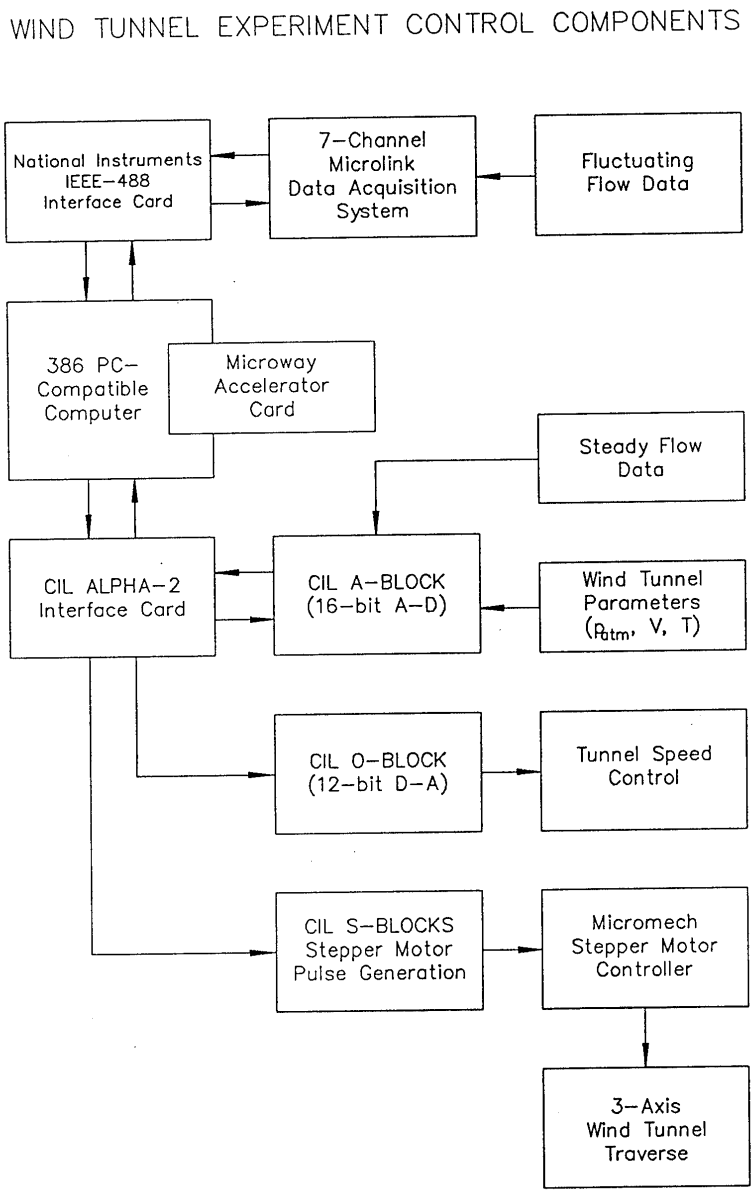

Figure 3.3 Block diagram showing the interconnection of the main, experiment-controlling devices. The whole experiment was automated.

corrected to compensate these trends. This process was necessary because of the long experiment duration and the need for great accuracy in comparing signals for the conditional sampling experiments to be described in a later chapter.

Single hot-wire probes were also used extensively in conjunction with the traverse. In this case the advantage was that they could be calibrated during the experiment. At regular intervals, the traverse would move the wire to a position close to a pitot-static tube (about 10h above the model) and the wire would be calibrated against a varying tunnel speed. The acquisition of wake flow data would then resume.

Cross wires (always moved by the traverse) followed more or less a similar procedure, a notable difference being that it was important to be able to evaluate the exact angles of the two probes towards the free stream. This was accomplished in the following way (a similar method having been used, among others, by Ho 1991). First, in the empty tunnel, the wire would be calibrated at different angles towards the free stream. Once the wire was positioned on the traverse for the experiment, the angles of the two probes towards the free stream could be obtained by re-calibrating them and matching the calibration curves to the ones obtained previously. All the cross wires used were conventional in that the two probes were nominally 90° apart (each one at 45° to the free stream). Considering that the aspect ratio of the sensors was large, the cooling velocity was taken as the velocity component normal to the sensor, any cooling effect of an axial velocity taken to be negligible.

3.2.3 Pressure measurements

Many of the experiments also involved measurement of the base pressure. All base pressure measurements were performed along the centre line of the model. Mean pressures were obtained in a fairly conventional way, using an ultra-sensitive Honeywell pressure transducer (positioned outside the tunnel) and simple pressure tappings.

As was briefly mentioned above, the model used eventually for the detailed experiments was designed in a way which permitted accurate fluctuating pressure measurement. The frequencies of interest could be of the order of 1000Hz, and therefore the dynamic response of the transducers was of importance. According to empirical formulae, and also to dynamic calibrations of the transducers by previous investigators in the Aeronautics Department of Imperial College, it was

apparent that the tube length to be used would have to be less than 25mm long. It was therefore decided to position the transducers as close as possible to the trailing edge (figure 3.1, bottom). As the transducer membranes were only 2mm from the flow, this arrangement was dynamically superior to a longer tube. The pressure transducers used were made by Druck, and in all cases were calibrated against the Honeywell transducer.

3.2.4 Data acquisition system

Fluctuating velocity and pressure signals would first pass through an amplifier and a low-pass filter. They were then recorded by a 12-bit Microlink A-D converter. Seven channels were available, permitting a simultaneous sampling of seven independent signals. Each channel had its own 16K-Sample memory, an adjustable voltage range and could sample at rates up to 100KHz. Data was transferred to the computer via an IEEE GPIB bus and stored on the hard disk for subsequent analysis.

3.2.5 General calibration procedures used

Although some indication was given above on how the hot-wire probes and the pressure transducers were calibrated, it is important to elaborate a bit more on some of the general calibration procedures used. The experiments performed involved a large number of voltage meters (e.g. the A-D converter), amplifiers, pressure transducers, velocity sensors etc., each contributing with its own, small or large, error. In order to keep the final error to a minimum, it was important to establish stable reference instruments. The instrument used as a pressure reference was a Betz manometer, while the voltage reference was chosen to be the ultra-accurate CIL 16-bit A-D converter.

The Honeywell pressure transducers were calibrated regularly against the Betz manometer and proved to be extremely stable. Subsequently, all Druck pressure transducers were calibrated against them. The velocity reference was a pitot-static tube connected to a Honeywell transducer. The tunnel (whose speed was evaluated by the pressure drop in the contraction) was calibrated against this pitot-static tube.

In all cases, the calibration would be automatically controlled by the computer, via the CIL 16-bit A-D converter. All calibration data would be stored in special-format files, in easy access by the experiment control or the experiment

analysis programmes. To cancel out any inaccuracies in the amplifiers or the filters, calibrations of pressure transducers or hot-wire probes were always performed through the amplifier-filter set that would be used with them in the subsequent experiments. Finally, all seven Microlink 12-bit channels were also calibrated (in all their voltage ranges) against the 16-bit CIL A-D converter.

Generally speaking, actual experiments tend to be more interesting than the calibration procedures of the apparatus. The procedures described above could have been performed manually. Considerable time was spent to completely standardise and automate the whole process and the total size of all the calibration program codes (written in QuickBasic) was about 60Kbytes. Once this had been accomplished, however, the logistical problems involved in keeping track of all the equipment was eliminated. Furthermore, the speed at which calibration could be obtained made it possible to perform this task more frequently.

3.2.6 Experimental procedure

In accordance with the calibration procedures described previously, all experiments were completely automated. The process to a completely trouble-free experiment was some times quite painful and evolved as time passed, but the final state of the programs permitted quick setting-up of each experiment, large flexibility and a compact and organised eventual storage of the data. Once all calibrations had been completed, an experiment consisted primarily of three phases. Source codes for these phases were of a total size of about 120Kbytes.

The first phase was the set-up of the experiment. Here the computer would obtain information about the nature of each signal to be sampled (pressure or velocity), the devices to be used (in order to access the correct calibration files), the path to be followed by the traverse, and the sampling parameters (number of cycles, sampling frequency, etc.). Special files would then be created to be used by the program controlling the experiment and by the data reduction program.

The second phase was the actual experiment. At each sampling cycle the following sequence would be followed:

a). Measurement of free-stream velocity, atmospheric pressure and temperature.

b). In the event that the speed had dropped below the acceptable limits, adjustment of the tunnel speed. Depending on the requirements of the experiment,

either the speed (in conditional sampling experiments) or the Reynolds number (in all other cases) could be kept constant.

c). Movement of the traverse to the next hot-wire position.

d). Sampling of data.

e). Storage of raw data on the hard disk.

As was mentioned before, the hot-wire probe would regularly move close to a pitot-static tube far from the model, in order to be calibrated. Much effort was put into reducing the time of each sampling cycle, as some experiments could last up to 12 hours. Both the first phase and the second phase programmes were written in QuickBasic.

In the third phase, the data was reduced to velocities and pressures and stored in a very compact, special binary format. Another file would contain all other information about experimental conditions, hot-wire positions and how to access the data of each sampling cycle. This phase looks quite simple but in reality was not quite so. In order to reduce all the data (some times up to 200Mbytes) much CPU time was needed. A Microway accelerator card running FORTRAN (about 10 times quicker than the 386-compatible PC) was used, but it still required up to 8 hours of data reduction for a long experiment. Also, considering the large amounts of data, it was of paramount importance to store it in a compact and easily accessible format. A FORTRAN subroutine was used in all analysis programmes, to access the data easily and reliably.

It should be noted, that after the third phase, data had still not started to be analysed. Analysing algorithms will be described at later stages, but were all written in accelerator card FORTRAN. A lot of the algorithms used were based on subroutines described in Press et al (1986, Numerical recipes).

3.2.7 Blockage correction

Although the tunnel blockage was less than 4%, a blockage correction was applied to all the data, following the principles described by Maskell (1963). That paper essentially recommends a first order, time-steady correction which removes the bulk of the blockage error. For a non-lifting body, it assumes a net increase of the free-stream velocity, obtained through various momentum considerations. Arguments were put forward in Bearman (1963) to take $C_D \approx Cp_b$, and the same

assumption was used here. As an indication, the maximum blockage correction was less than 2%.

3.3 Water flume experiments

3.3.1 The Water Flume Laboratory

Flow visualisation was carried out in a water flume in the hydraulics laboratory of the Department of Aeronautics of Imperial College (the flume is shown diagrammatically in figure 3.2b). The working section is 0.61m wide, 0.69m deep and 1.8m long. It is preceded by a settling chamber, followed by a honeycomb and wire screens, followed by a 4:1 contraction. The flow obtained in the working section can be varied up to a maximum speed of 0.30m/s approximately (a higher speed can be achieved by lowering the weir downstream of the working section, thus reducing its depth).

The main advantage of the water flume for flow visualisation was that, due to the lower speeds, the flow was easily observable. The Reynolds number, however, could only reach a value of 2500, about 16 times lower than that of the wind tunnel. Although quantitative data from the wind tunnel and from the water flume could not be compared, sufficient evidence emerged proving that the main characteristics of the two flows were the same. When comparing wind tunnel and water flume results, the reader should always keep in mind this Reynolds number discrepancy.

3.3.2 The flow visualisation technique

In a similar fashion to the wind tunnel techniques described previously, the flow visualisation technique to be discussed here was reached after many evolution stages. The pictures presented later were all obtained using these techniques.

The main element of the visualisation technique is a precipitate produced on the surface of the model. The advantage of producing the precipitate on the surface, as opposed to injecting it in the flow, is that in that way it gives a better indication of vorticity (also generated on the surface). Even though vorticity cancellation and diffusion can not be accurately indicated by the precipitate, this technique could highlight important aspects of the vortex dynamics of the wake. To produce the precipitate, a thin strip of pure tin was stuck on the model (usually on the semi-elliptic part, but some times also on the base). The strip was 0.107mm

thick, 30-40mm wide and would spread over the entire span of the model (the material was supplied by Goodfellow Metals; it is possible that other metals, e.g. lead, could produce a similar effect). An electrode was placed in the water, downstream of the model. When a voltage (about 30-40V, positive pole connected to the tin strip) was applied between the strip and the electrode, a thick white cloud (probably a tin oxide) would be produced from the tin strip, and convected downstream by the flow. The electrolytic precipitation method was described in detail by Honji et al (1980).

The flow was illuminated by a 5W laser sheet. By the use of mirrors, different sections of the flow could be highlighted and observed. The use of such a powerful light source was made necessary by the poor condition of the water. The pipes of the flume were predominantly made out of steel, and the water would quickly loose its clarity because of rust contamination.

A standard video camera was used in order to record the flow. Conventional photography could produce clearer images, but the video more than compensated its picture quality handicap by enabling the accurate selection of the most indicative frames. In order to achieve similar results by photography, tens of film rolls might have had to be wasted. The video was processed in the Olivetti Research Laboratory at Cambridge. Sequences of frames could be read by a workstation computer. After optimally adjusting contrast and brightness, a post-script file was produced and printed on a laser printer. The pictures presented later essentially are negatives of the video (hence vortex filaments appear to be dark).

The combination of unclear water, video resolution and a high Reynolds number, makes the final image much less clear than similar images presented in the works of Williamson or Rockwell. Nevertheless, flow visualisation presented us with numerous interesting phenomena.

4. RESULTS

4.1 Initial results

4.1.1 Mean Base Pressure

As an initial comparison between the various models, the mean base pressure was measured. To increase the effective span, all models were fitted with end-plates, as in Bearman (1965). For the straight edge model the result was a constant value of Cp_b in a spanwise region of 10h around the mid-span. The value of -0.585 obtained was in good agreement with previous results.

Tanner (1972) studied methods of reducing the drag of aerofoils with a blunt trailing edge (their section thus similar to the one in this work). He found that by "breaking" the separation line he could achieve significant drag reduction. In accordance with these results, it should thus come as no surprise that the wavy models had higher (less negative) values of Cp_b. The distribution of base pressure along a half wavelength of the various wavy models (all of them with w=15mm) is shown in figure 4.1. All models showed base pressure values that repeated themselves over many geometric wavelengths.

A notable feature in figure 4.1 is that in general, the steeper the wave (where steepness=w/L) the larger the drag reduction. Compared to the straight edge model, the drag reduction for the models with L=168,148,140,120 and 105mm was about 10%,16%,24%,25% and 34% respectively. It is unclear why the difference between the L=140 and the L=120 models is so small.

One more notable feature of figure 4.1 is the significant difference between the measured values of drag at a peak and a valley. All wavy models show a similar trend, with the peak exhibiting less negative values of Cp_b than the valley. For the L=148mm model, the value at the valley is about -0.48, smoothly increasing to a maximum of -0.44 at the peak. It should be noted that from y/L=0.2 to y/L=0.5 (valley) the base pressure remains quite constant, the main variations being observed for $y/L < 0.2$, i.e. close to the peak.

4.1.2 Velocity power spectra

Velocity power spectra were obtained from single hot wire signals, in order to determine the characteristic frequencies of the wake. The probes were

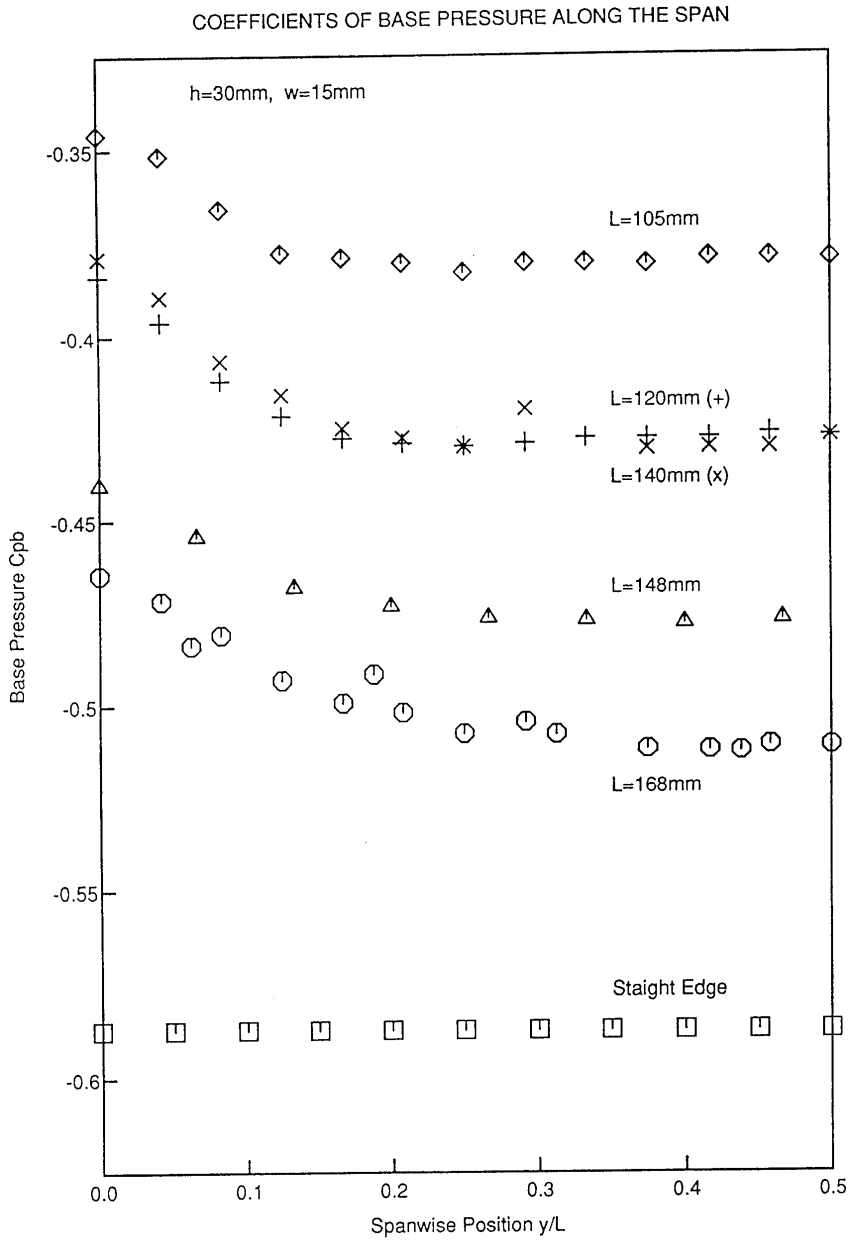

Figure 4.1 The variation of mean coefficient of base pressure along the centre-line of models with different wavelength, L. The spanwise position y=0 corresponds to a peak.

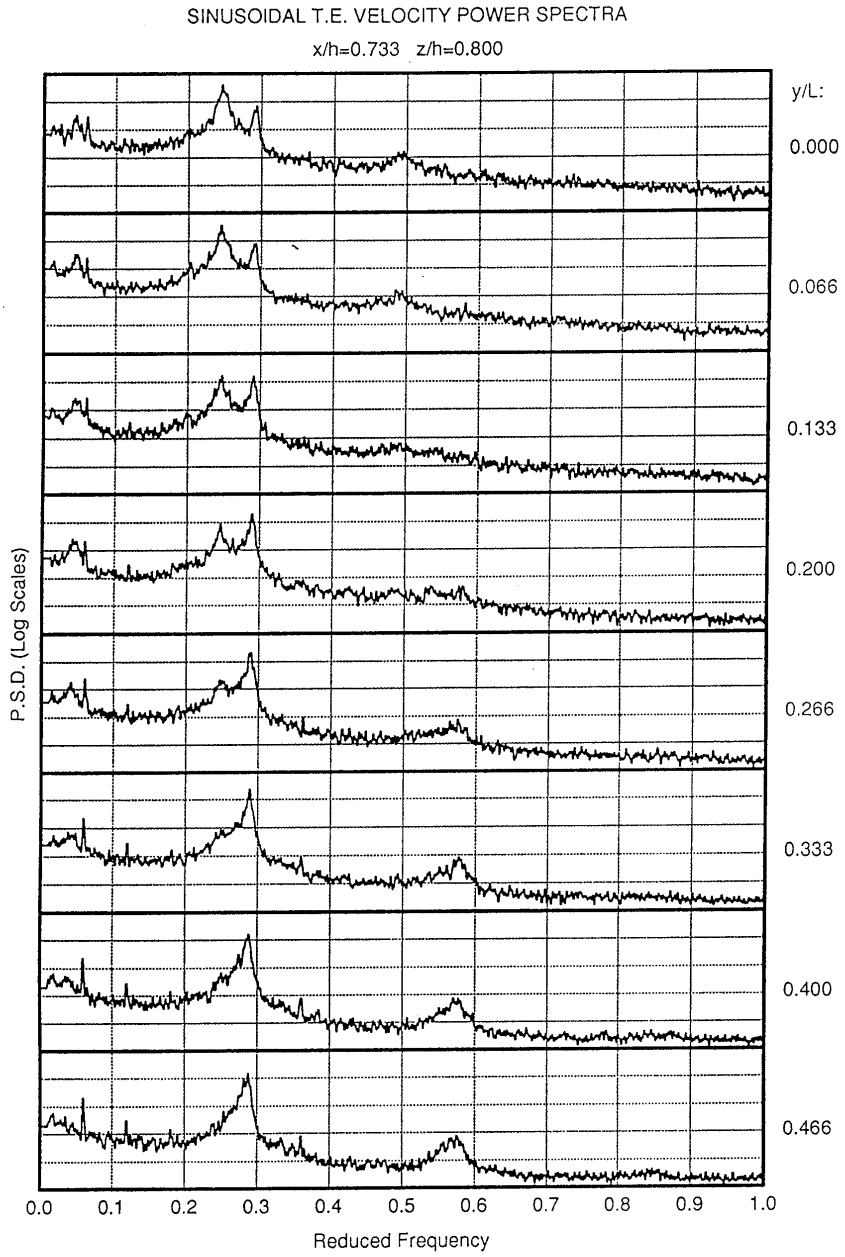

Figure 4.2 Velocity power spectra obtained from the sinusoidal model (w=15mm, L=148mm), at different spanwise positions.

positioned at approximately 0.7h downstream of the local trailing edge position and a distance 0.8h above the wake centre line (i.e. outside the shear layer). For the straight edge model the Strouhal number obtained (from the peak of the power spectrum) was 0.24, in agreement with values obtained by Bearman (1963).

Figure 4.2 shows spectra for the L=148mm, w=15mm model for different distances y from the peak of the wave. The main characteristic is the presence of two shedding frequencies (at S=0.24 and at S=0.29). Whereas at the peak the low frequency is stronger than the high one (note that in figure 4.2 the y-axis is a logarithmic scale), as we move towards the valley the low frequency dies off (becoming almost totally undetectable at y/L=0.333) and the high frequency component becomes stronger and stronger.

There are a few points one can make about these results at this prelminary stage. The presence of the two frequencies strongly suggests that at least at some times we have two cells (within this half-wavelength) shedding at different frequencies. At the peak there is the low frequency shedding and at the valley the high frequency. Further to that point, the high frequency cell seems to be stronger and some times spreads over the whole half-wavelength. The presence of these two cells indicates that there must be some vortex splitting occurring at the cell boundary. Most of the activity takes place at the peak, where we have maxima at both frequencies in the spectrum. In comparison, the valley spectra seem to be more like those for a straight-edged model. Interestingly, the double frequency characteristic appears in the region of the peak where, as was shown in the previous section, the base pressure showed the largest variation. Where we have both frequencies, a low frequency also appears at the difference of the two characteristic frequencies (like a beat frequency).

All wavy models again followed the same general pattern. It would be superfluous to include all the spectra. Figure 4.3 shows the spectra at the peaks of the various wavy models (and also the spectrum for the straight edge model). In a similar fashion that the drag reduction increased as the wave steepness, w/L increased (previous section), the level of disturbance also seems to increase with increasing steepness (which is not entirely surprising), with the two shedding frequencies becoming more and more distinct. Another point of interest is the apparent "memory" by which the flows retain the straight edge shedding frequency: all models seem to have a low shedding frequency of that order (S=0.24), while the high frequency varies.

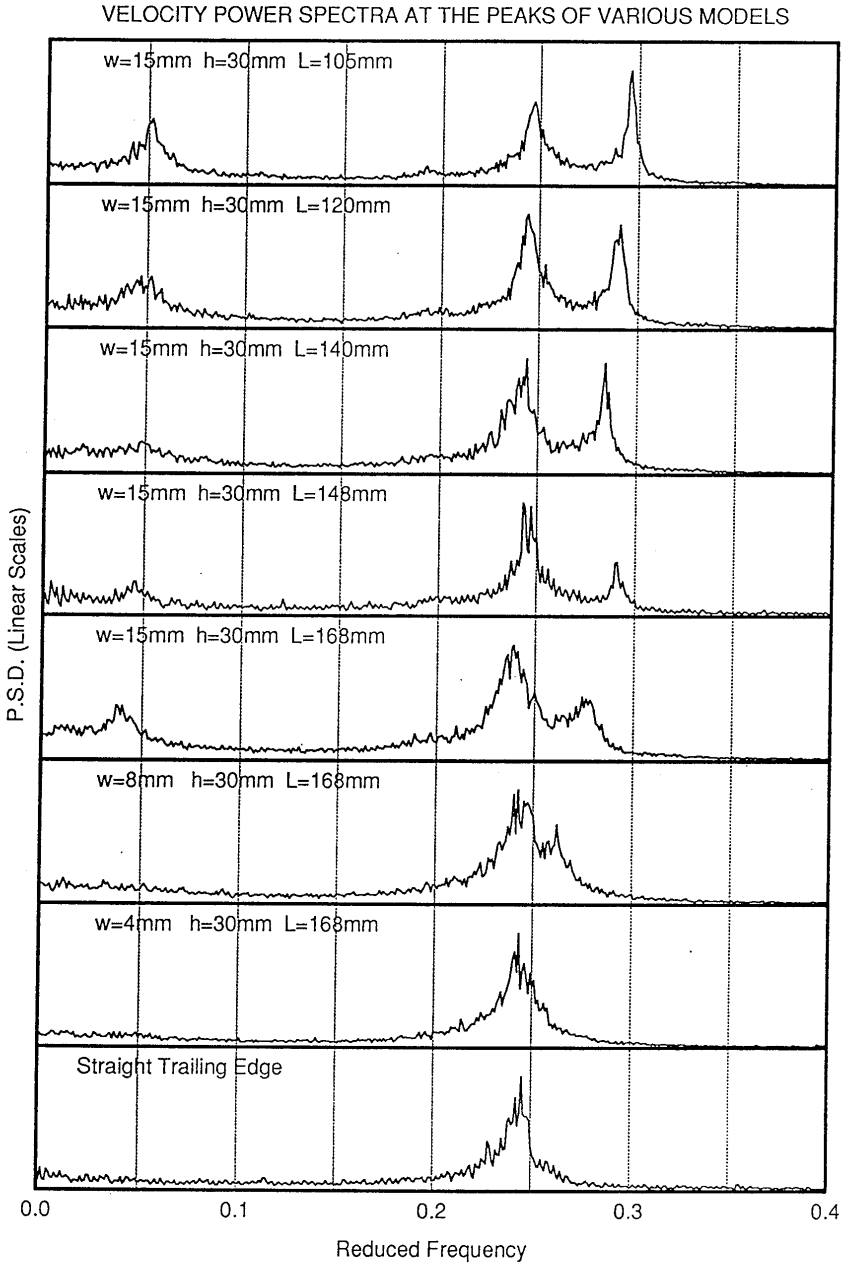

Figure 4.3 Velocity power spectra obtained at the peaks of models with different parameters.

4.1.3 Reynolds number dependence

The particular results presented above were all for Re=40000 (based on model height, h). Similar measurements were also performed for Re=20000 and for Re=60000. There was no detectable difference between the various Reynolds numbers. This is not surprising because all the models had trip-wires, with the point of boundary layer transition to turbulence thus being fixed. In any case, models with sharp edges and fixed separation points are known to be much less Reynolds number dependent than models where the point of separation can move (as, for example, happens with a circular cylinder).

Brief measurements were also performed at a Reynolds number of about 4000. The wind tunnel has not been designed to run at such low speeds and all the measuring instruments were not sensitive enough for accurate readings, but the purpose was to see whether the dual frequency characteristic still existed. Although the readings contained a large amount of noise, one could still see the dual shedding frequency. The reason this was of interest was that it confirmed that at the low, water flume Reynolds numbers the main flow characteristics would be the same.

4.1.4 Choice of parameters for detailed experiments

The results described above were all obtained at a very early point of this study. The main features are that:

a). All models show similar trends, the steeper the geometric disturbance wave, the larger the effects on base pressure and shedding frequency.

b). At least above Re=20000, the Reynolds number dependence appears to be negligible.

As the purpose of this work was to study aspects of three-dimensionality, it was decided to concentrate on one model and one Reynolds number. As was mentioned earlier, the model chosen was the one with L=148mm and w=15mm. It was chosen because it clearly displayed the various three-dimensional characteristics while, at the same time, its geometric disturbance was not too large. The chosen value for Reynolds number was 40000. Hence, all the wavy model results to be presented later will be for these parameters. Further detailed experiments will also be presented for the straight edge model (at the same Reynolds number).

4.2 Detailed results : sinusoidal trailing edge model

A few of the results to be discussed in this section were briefly mentioned earlier in this chapter. This section will present more detailed quantitative results for the chosen sinusoidal model, and also some flow visualisation pictures.

4.2.1 Discussion of velocity and pressure power spectra

The existence of a dual frequency characteristic was established in the previous section. For this model configuration, the two frequencies had the non-dimensionalised values of $f_1=0.24$ and $f_2=0.29$. What remains, of course, is to establish what these two frequencies represent from a physical point of view. A single hot-wire probe records velocities in the plane normal to the probe axis. Although it is easy to understand that at the hot-wire probe position there will be velocity fluctuations at the two observed frequencies (either simultaneously or at different time instants), two unclear points arise.

First, we cannot be sure whether each one of the two main peaks at a velocity spectrum necessarily reflects the frequency of vortex shedding (at some time instants, at least) at that spanwise position. For example, even though at a spanwise position A, say, we may observe noticeable peaks at both frequencies, f_1 and f_2, it may be that at that position A the vortex shedding is always at a frequency f_1, with the second peak at f_2 merely reflecting induced velocities from a spanwise position a bit further away from A, and not fluctuations of vorticity flux, which, strictly speaking, should be the real indication of the Strouhal number.

Second, does the dual frequency reflect a simultaneous presence of two frequencies, e.g. a signal like $C_1*\sin(2\pi f_1)+C_2*\sin(2\pi f_2)$, or does it represent a long interval of $C_1*\sin(2\pi f_1)$, followed by a long interval at $C_2*\sin(2\pi f_2)$?

It should be noted that both of these uncertainties are a result of one problem: we cannot be certain of the relation of the peak of a velocity spectrum to the shedding frequency when there is more than one frequency of interest. This uncertainty would not exist if we had only one clear peak in the spectrum. As a result of the fact that the signals are not pure signals, the peaks of the spectra are not delta function-like but have a noticeable bandwidth. Even though the two peaks are distinct, their bandwidths overlap. Hence it was not possible to measure

the period of shedding from the velocity signal and determine accurately the Strouhal number to which each shedding cycle belonged.

At each spanwise position, as far as the two peaks are concerned, spectra obtained from different hot wire positions in the near wake show similar patterns to figure 4.2 discussed earlier. Figure 4.4, for example was obtained closer to the centre-wake, and despite the increased noise level (the hot wire in figure 4.2 was outside the wake whereas in figure 4.4 it is not, and hence comes under the influence of wake turbulence), one can still see the dual frequency characteristic. The same applies for the spectra of figures 4.5-4.8: it is clear that the presence of the two frequencies, and their relative energies are mainly a function of the spanwise position, not the exact hot wire position in a y=constant plane (where y is the spanwise position).

Fluctuating base pressure power spectra were also obtained. The Druck pressure transducers used had a very low signal-to-noise ratio, and the spectra presented in figure 4.9 are averages of the spectra of 128 sets of data (each 4096 samples long). In general, base pressure fluctuations at the centre-wake tend to have a characteristic frequency of double the shedding frequency, as the centre-wake comes under the influence of vortices from both sides of the wake. In figure 4.9 we can see three main shedding-related frequencies: $2f_1$, $2f_2$ and (f_1+f_2). It should be noted that some times white noise seems to conceal those peaks. We have to relate the (f_1+f_2) component to the (f_2-f_1) component observed both in the velocity spectra and also in the pressure spectra.

The (f_2-f_1) component was observed in both the velocity spectra and the pressure spectra (where it actually is about 10 times more energetic than the high frequency fluctuations-a number that may have been amplified by the white noise characteristics of the pressure transducer). From a mathematical point of view, it has to be related to the simultaneous existence of both the f_1 and the f_2 components. Although it is reminiscent of a linear beat frequency, it should be noted that this does not seem to be the case in the present study. A linear beat frequency is the low frequency fluctuation of the *envelope* of the linear sum of two sine waves. If one were to take the Fourier transform of this linear sum, the (f_2-f_1) component would not appear. The presence of the two components, as can be seen in some of the spectra of figures 4.6 and 4.8, is not sufficient to cause the (f_2-f_1) component. It therefore seems that the (f_2-f_1) "beat" frequency is the result of a non-linear interaction of the two shedding frequencies of neighbouring cells.

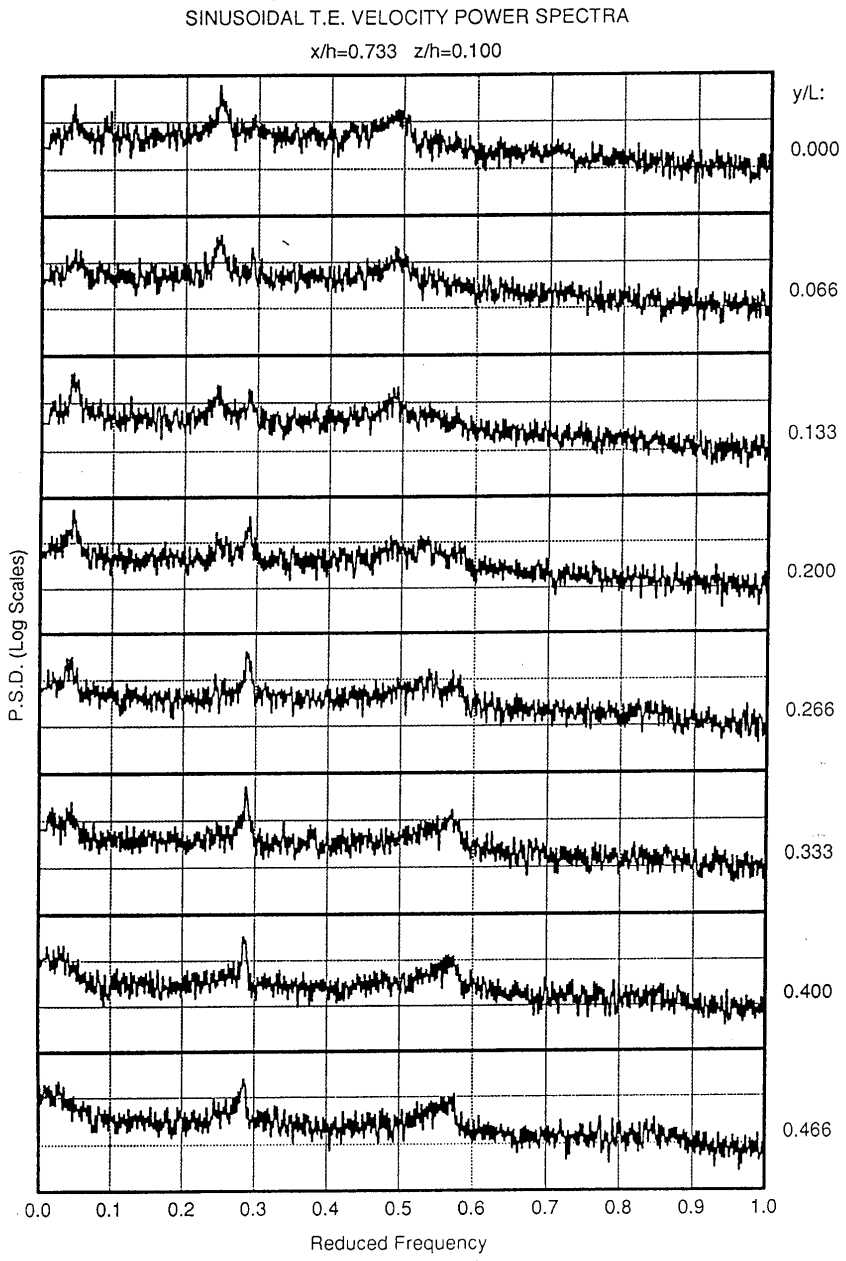

Figure 4.4 Sinusoidal trailing edge model: velocity power spectra for x/h=0.733, z/h=0.1 and y/L=0, 0.066, 0.133, 0.2, 0.266, 0.333, 0.4, 0.466.

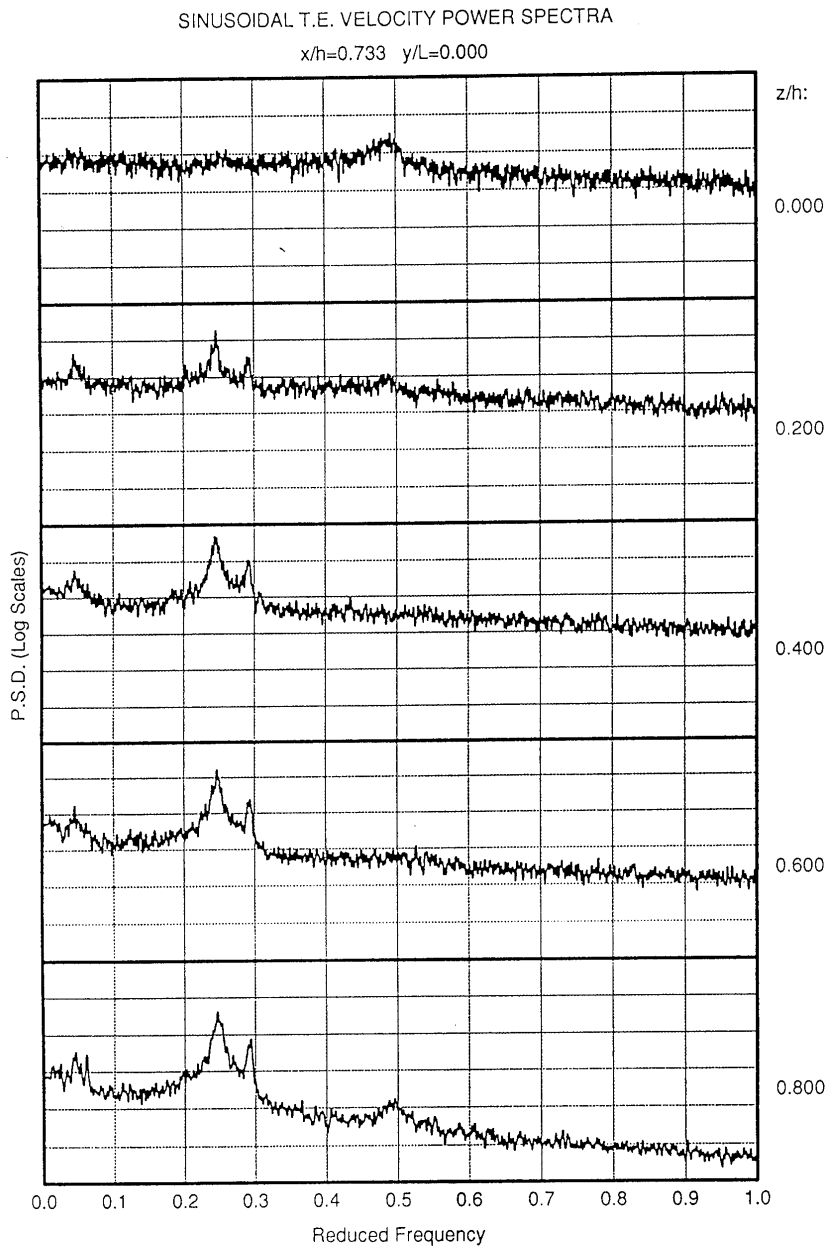

Figure 4.5 Sinusoidal trailing edge model: velocity power spectra for x/h=0.733, y/L=0 and z/h=0, 0.2, 0.4, 0.6, 0.8.

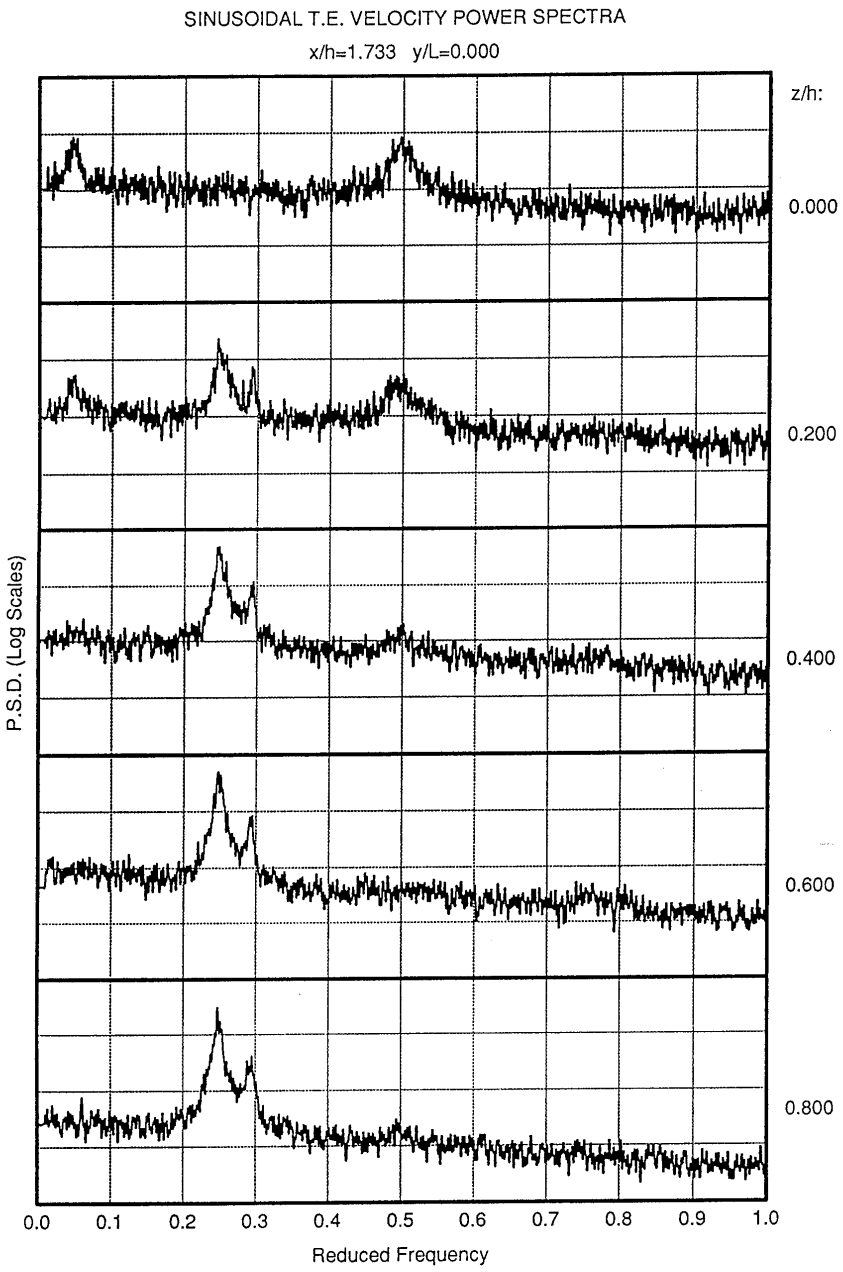

Figure 4.6 Sinusoidal trailing edge model: velocity power spectra for x/h=1.733, y/L=0 and z/h=0, 0.2, 0.4, 0.6, 0.8.

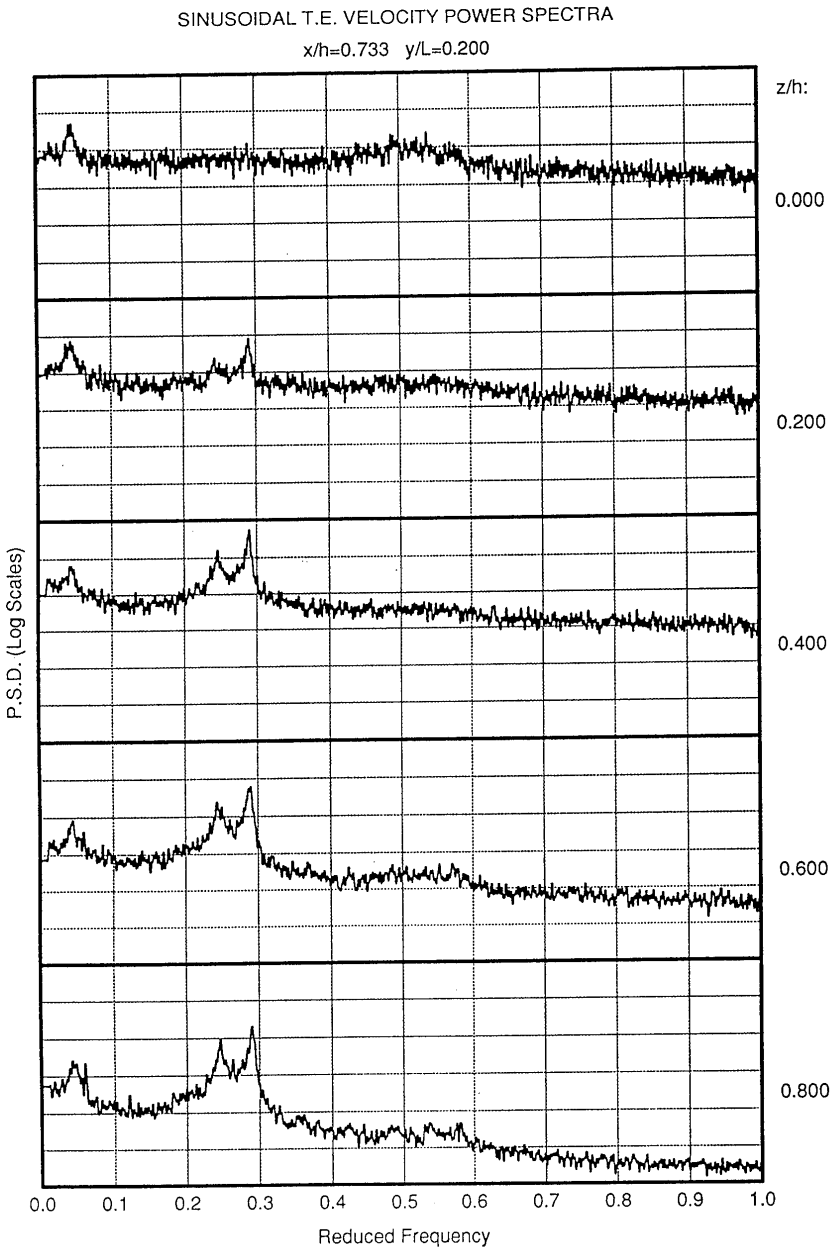

Figure 4.7 Sinusoidal trailing edge model: velocity power spectra for x/h=0.733, y/L=0.2 and z/h=0, 0.2, 0.4, 0.6, 0.8.

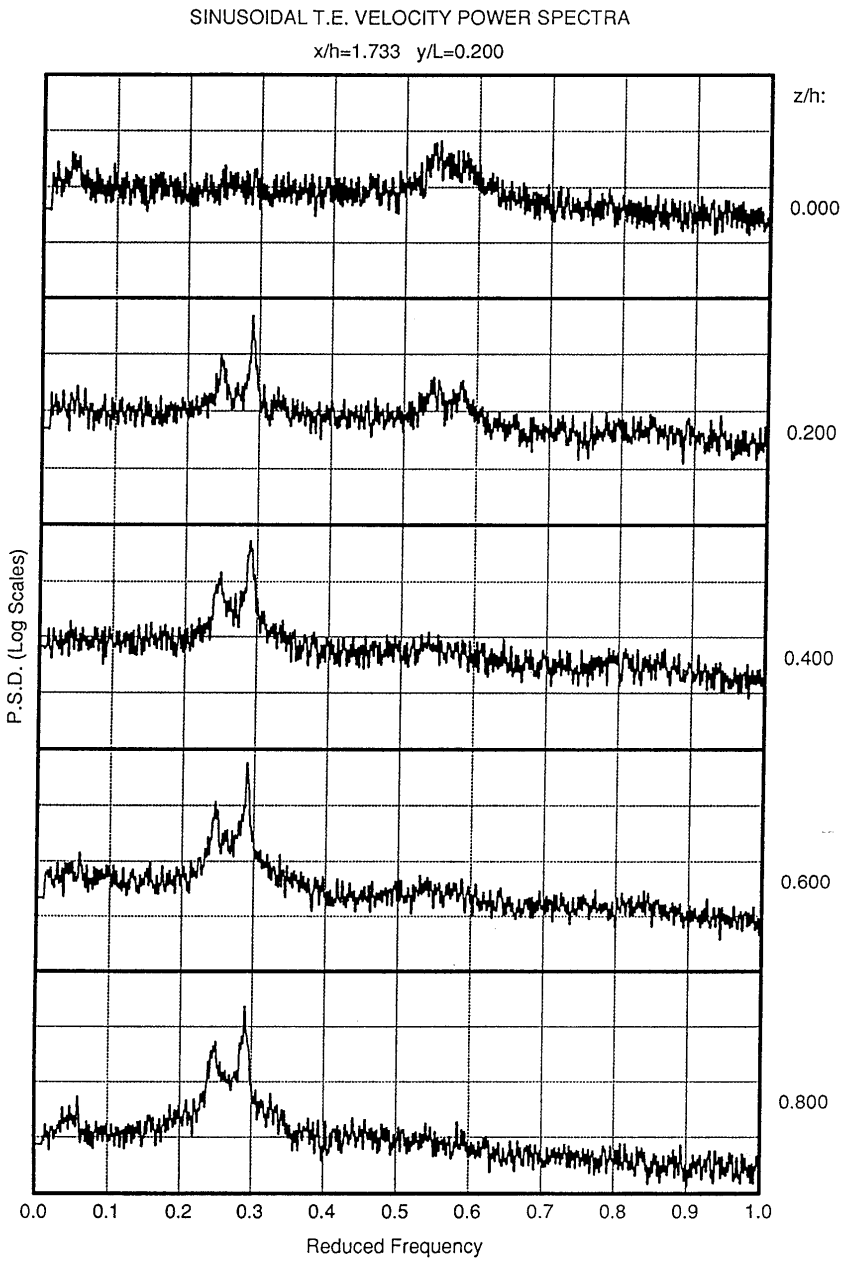

Figure 4.8 Sinusoidal trailing edge model: velocity power spectra for x/h=1.733, y/L=0.2 and z/h=0, 0.2, 0.4, 0.6, 0.8.

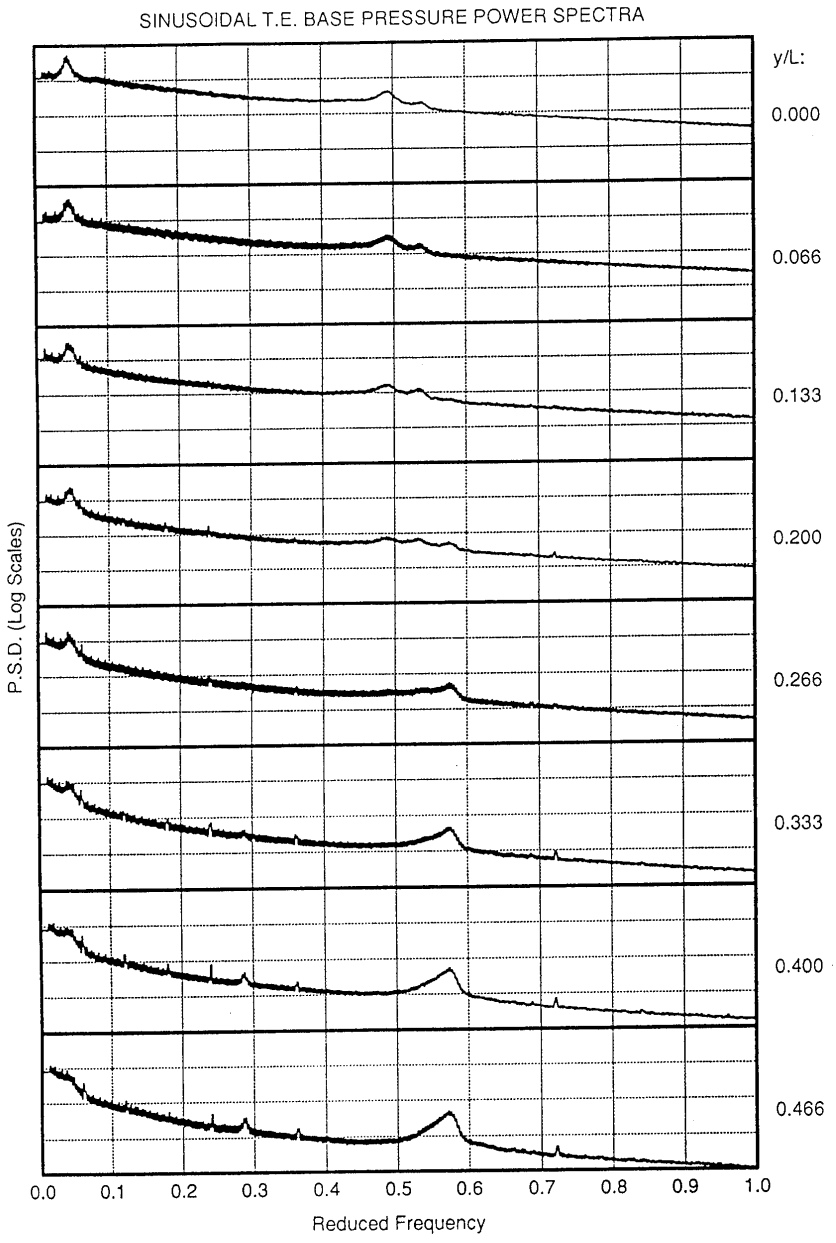

Figure 4.9 Base pressure power spectra along the span of the sinusoidal model.

The magnitude of this frequency in the pressure spectra, reflects significant low-frequency fluctuations in base pressure. Furthermore, we could note at this point that if we have two neighbouring cells shedding at frequencies f_1 and f_2, the frequency of vortex splitting (a non-linear phenomenon) will be (f_2-f_1). Hence, this low frequency must have important consequences on the physics of the wake. These will be discussed in more detail in a later chapter.

4.2.2 Flow visualisation: the different vortex shedding modes

Flow visualisation performed in the water flume confirmed the cellular nature of the wake of the sinusoidal model. The pictures to be presented in this section give a clear indication that vortex splitting occurs.

Figure 4.10 is a sequence which shows the low-frequency periodicity of vortex splitting. The photographs were extracted from a video sequence, with each shot being roughly one shedding cycle after its preceding shot. From (a) there is little to indicate the complicated three-dimensional nature of the flow. One shedding cycle later, at photo (b), the cell at the peak seems to have delayed its vortex shedding by a small amount. The vortices from the two neighbouring valleys have bowed backwards to accommodate this delay. At photo (c), one more cycle later, a further delay at the peak seems to have brought the two cells out of phase. The vortices from the valleys have bent further back. It appears that when this bowing angle becomes too large vortex splitting occurs: the vortex from the peak has linked-up with two vortices from each valley (Eisenlohr and Eckelmann, 1989, also identify the large oblique bowing angle as one of the reasons for vortex splitting). Photo (d) follows a similar pattern with vortex splitting once again being very pronounced, while from (e) to (h) the phase difference between the two cells starts to go down again, the vortex filaments then becoming straighter.

It is interesting to note the vortices further downstream of formation, which appear towards the right of each photograph. In each case these vortices show the downstream evolution of the vortex formed in the previous photograph. Where the previous photograph showed a fairly coherent, straight vortex, this vortex can still be clearly seen further downstream. On the other hand, in the cases when vortex splitting occurred, their evolution downstream seems to be much more disordered, as can be seen in photos (d), (e) and (f), which succeed photos (c), (d) and (e) respectively.

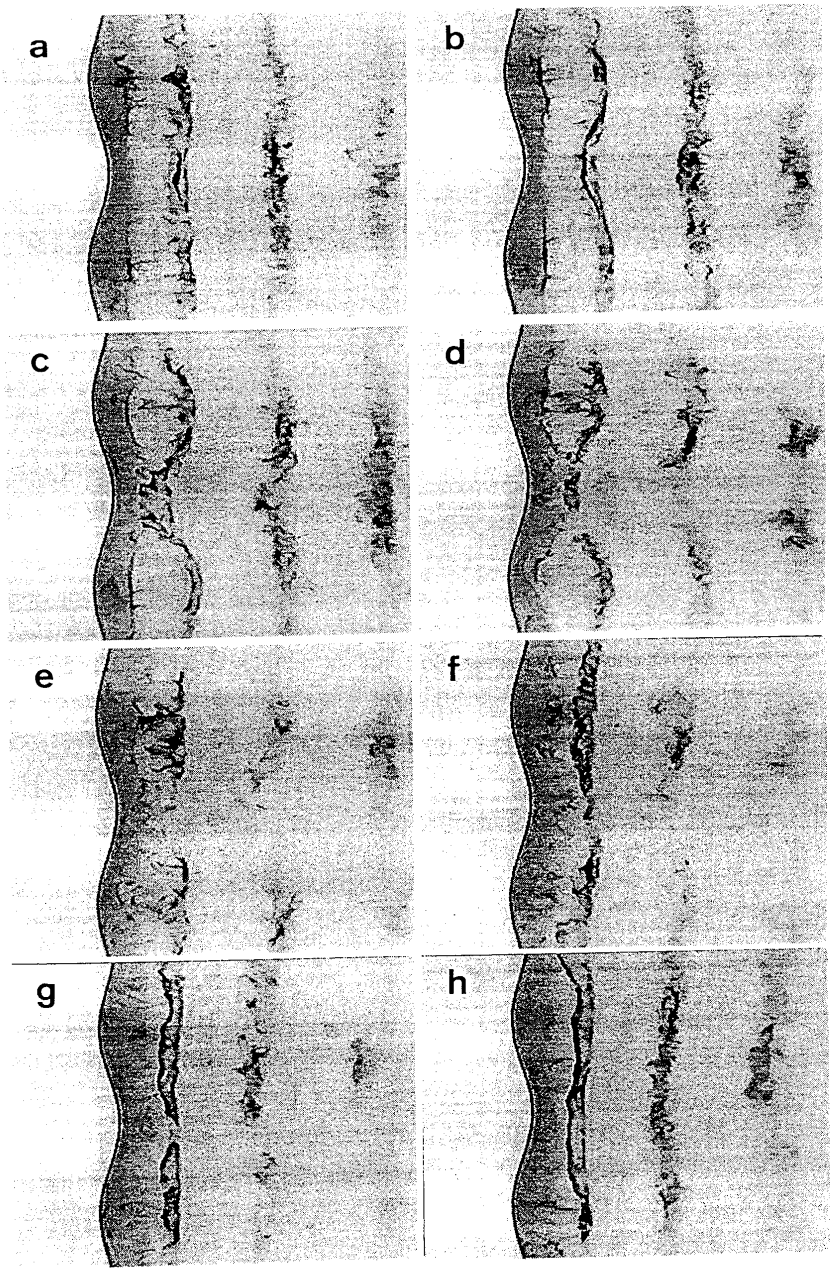

Figure 4.10 Flow visualisation for the sinusoidal model. Shots are from successive shedding cycles and demonstrate that the region of a peak sheds vortices at a lower frequency that the regions of its two adjacent valleys. Shedding mode is symmetric (w.r.t. peak). Vortex splitting is apparent in photos (c) and (d), when the phase difference between the f_1-cell and the f_2-cells is largest.

From this we can conclude that the complicated three-dimensional phenomena occurring in the near wake do not quickly relax to a two-dimensional state, but retain their three-dimensionality further downstream. In these highly turbulent phenomena, the tin oxide precipitate diffuses too quickly for us to be able to see the three-dimensional structure in the positions downstream of the near wake. Nevertheless, these observations seem to fit in well with Breidethal's suggestion (1980) that the asymptotic state of the two opposite strength shear layers (i.e. a wake) is three-dimensional.

Another interesting feature of figure 4.10 is the "stubbornness" by which each cell stays at its selected frequency. Even in photos (a) and (b), where the vortices appear to be fairly straight and undisturbed, the cell at the peak seems to "know" that it is shedding vortices at a slower rate. Each cell behaves thus like an oscillator, operating at its own characteristic frequency. Even though the flow may at times superficially seem (as in photos (a) and (b)) two-dimensional, the underlying physical mechanisms are in fact always three-dimensional.

In the sequence of figure 4.10, the flow is symmetric with respect to the peak. This symmetric mode is the mode where the characteristics described are at their clearest. Flow visualisation revealed a total of four modes, here termed *symmetric, antisymmetric (two types) and oblique*.

The oblique mode appears in photos (a)-(d) of figure 4.11. From these pictures one can see that these is no preferred oblique direction, i.e. the oblique mode is not due to an imperfection in the alignment of the model. During the oblique mode we could reasonably expect a uniform shedding frequency across the peak, which may explain the presence of the high shedding frequency (f_2) at the spectrum of the peak (as was seen for the wind tunnel results).

In the antisymmetric mode, shown in photos (e)-(h), the phenomena in the peak's two neighbouring valleys are in anti-phase. It is unclear exactly what happens in the region of the peak. One possibility involves two cells (each based of one valley and shedding at f_2) that extend up to the peak and link-up in that region. Another possibility involves three cells: f_2 at one valley, followed by f_1 at the peak, followed by f_2 at the other valley. The dislocations would then follow a pattern similar to that for the symmetric mode described earlier. We shall see that as a necessary mechanism of transition between the symmetric and the oblique modes, both kinds (two-cell and three-cell) of antisymmetric mode must exist.

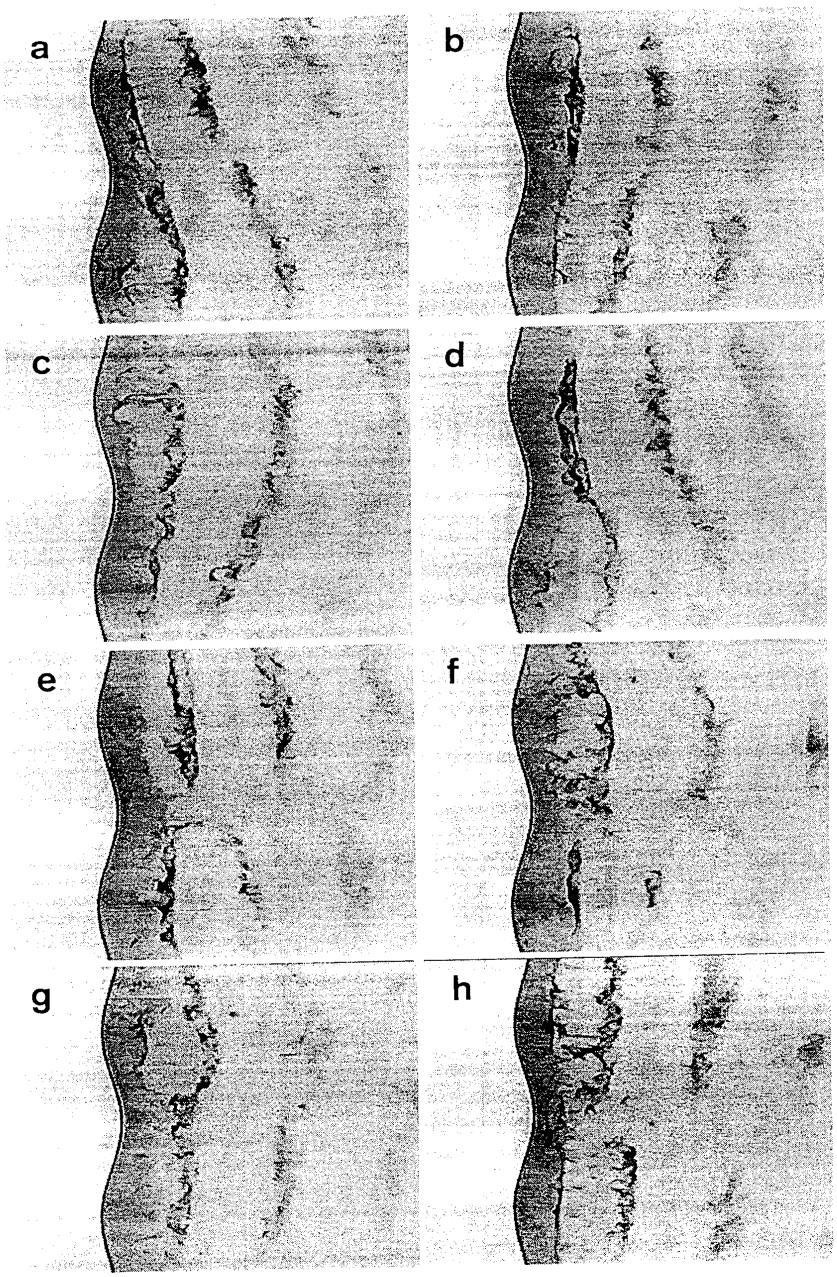

Figure 4.11 Flow visualisation for the sinusoidal model. Photos (a) to (d): oblique shedding mode. Photos (e) to (h): antisymmetric shedding mode.

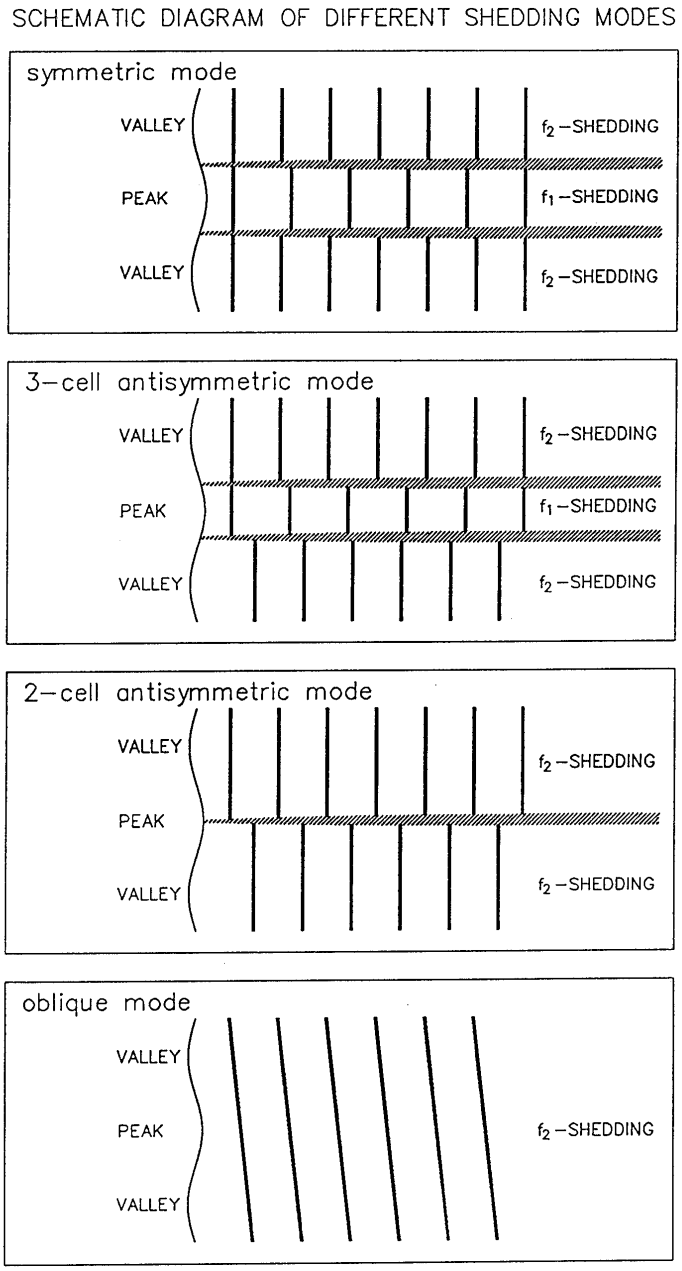

Figure 4.12 Schematic representation of the various shedding modes. Shaded areas represent dislocations. It is proposed that transition can only occur between adjacent boxes and also that in the wind tunnel (high Reynolds numbers) the two lower modes are either very weak or non-existent.

The flow alternates in seemingly irregular intervals from the one mode to the other. The transition between the modes does not, as a rule, occur instantaneously, but is gradual. Thus, in order to understand the flow we have to identify possible intermediate states that may aid the transition from one mode to the other. For example, too many parameters would have to change for a symmetric to oblique transition to happen. Figure 4.12 gives a possible explanation about the transition between modes. The various modes are ordered in such a way that each one is adjacent to the other modes which most closely resemble it. Thus, it is suggested here that the mode can only "jump" between two consecutive boxes of figure 4.12, either upwards or downwards.

A transition between the symmetric and the three-cell antisymmetric mode would involve the shedding in the two f_2 cells on either side of the f_1 cell gradually getting in or out of phase. It is debatable whether there is a preferred phase difference. These two modes are similar to the two-sided dislocations observed by Williamson (1992a). In that paper he suggests that the induced velocities from the one f_2 cell to the other serve as a means of synchronisation between these two cells. One could perhaps apply a similar consideration in the present case, but there is insufficient evidence. What is more likely is that the phase difference is fairly random, with the distinction of symmetric or antisymmetric being just a criterion to differentiate between broad features of the flow.

The transition between the two-cell and the three-cell antisymmetric modes basically depends on the size of the central (f_1) cell. If it fluctuates in spanwise size, it is possible that at certain times it will vanish completely (two-cell mode) while at other times it will reappear (three-cell mode). Once again, it should be stressed that this distinction between the two kinds of antisymmetric mode seems to be the best explanation in order to understand how the oblique mode comes about; concrete evidence is limited.

Finally, insight into the transition between the two-cell antisymmetric mode and the oblique mode is provided by photo (d) of figure 4.11. It is unclear which mode this shot really belongs to. One could imagine either of the two modes evolving from it. If we have a dislocation separating two cells of the same frequency but different phase, it is conceivable that in the vicinity of the dislocation the vortices straighten out, thus causing oblique vortex filaments.

It was mentioned earlier that the flow would switch between modes at seemingly random intervals. Although some logical mode-transition procedures were proposed above, the *mechanisms* of transition are unclear. Obviously, a number of questions regarding mode-transition arise.

We do not know if the four proposed modes are genuinely "self-contained" modes. They could each conceal a very low level instability that gradually forces a change of mode. If that is the case, in reality we then have only one mode, which is quite chaotic and has a very large time constant. An inherent feature of this one mode would then be the inevitable transitions between the various observed "modes". On the other hand, each of the observed modes could be a stable mode, in the sense that, in the absence of external de-stabilising factors, it could continue *ad infinitum*. In that case the transitions could be triggered by some irregularities in the flow. It should be noted that there is a very thin line separating these two concepts. At the moment one thing is clear: all modes would occur, irrespective of initial conditions and after sufficient time had been allowed for the flow to settle.

Another question concerns the Reynolds number. If the instability causing mode-transition is so small, it would seem possible that its nature could be Reynolds number dependent. We should therefore treat the existence of the four modes with caution, and not automatically assume their presence at the high Reynolds numbers of the wind tunnel.

In concluding this first flow visualisation discussion, we may say that the flow visualisation pictures fit in quite well with the explanations given when discussing the quantitative, wind tunnel spectral results.

4.2.3 The relation of the shedding frequency to the mode

The previous section included some speculation as to how the shedding frequency is related to the mode. An attempt was made in the wind tunnel to determine the mode of vortex shedding. Single hot wires were placed just outside the wakes of two consecutive valleys. The phase difference between the two signals would determine whether we had a symmetric or an antisymmetric/oblique mode. To be able to distinguish between the two kinds of antisymmetric modes and also to determine whether we had an oblique mode would have been very interesting, but it would require many more hot wires in the wake.

The following criterion was used, regarding the phase difference θ between the two hot wires:

$(-\pi/12) < \theta < (\pi/12)$:symmetric mode

$(\pi-\pi/12) < \theta < (\pi+\pi/12)$:antisymmetric/oblique modes (collectively referred to as "antisymmetric mode")

The flow would spend about 40% of the time in each mode and 20% in an intermediate condition. To obtain the power spectrum of a signal g(t) (velocity or pressure) at the symmetric mode, a window function w(t) was defined as follows:

symmetric mode not present : $w(t)=0$

symmetric mode present : $w(t)=k$ (a normalising constant)

The transition from 0 to k and from k to 0 would be a smooth cosine function (the continuity in value and first derivative ensuring minimum spurious spectral interference). Intervals where $w(t)=k$ lasted too little were removed (setting $w(t)=0$). The value of k was determined by solving the equation $r.m.s.(w(t))=1$. Hence the power spectrum of g(t) at the symmetric mode was taken as the power spectrum of $g(t)*w(t)$. Due to the fluctuations (at a low frequency) of w(t), the low frequency components of the resulting power spectrum were distorted. The higher frequencies, however, retained their main characteristics. An equivalent procedure was used to obtain spectra for the antisymmetric mode.

Not surprisingly, the most interesting effects were observed in the region of the peak. Figure 4.13 shows spectra obtained at $y/L=0$ (i.e. at the peak). The most significant feature is that for the symmetric mode the high frequency component (f_2) has disappeared. This appears to be conclusive evidence that the dual frequency characteristic of the spectra can, in fact, represent a (comparatively) long interval of $C_1*\sin(2\pi f_1)$, followed by a long interval at $C_2*\sin(2\pi f_2)$ (i.e. a flow switching between two frequencies), as opposed to a signal like $C_1*\sin(2\pi f_1)+C_2*\sin(2\pi f_2)$. For the particular mode in question (the symmetric mode) it effectively excludes the possibility of parallel shedding. If the shedding in two valleys is in phase, there must then definitely be a lower frequency cell in between.

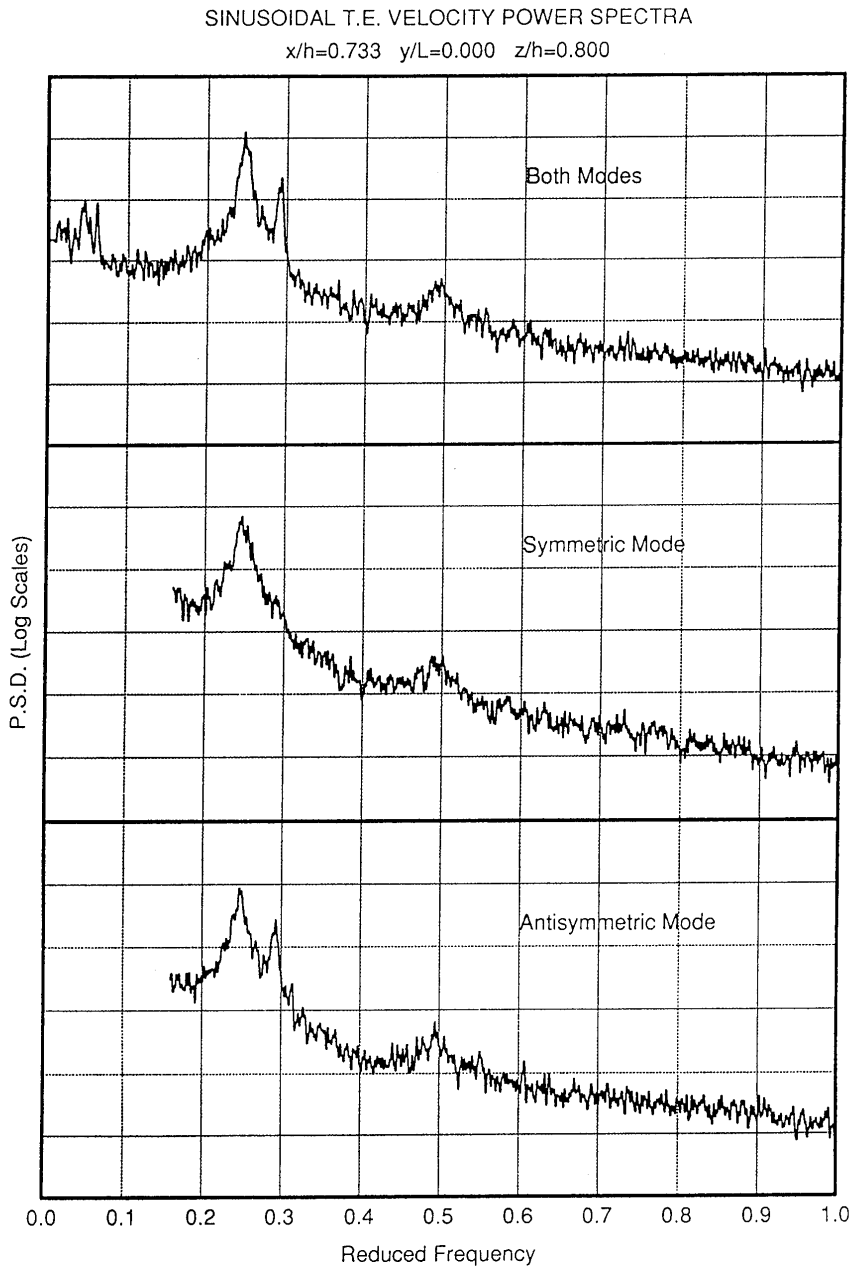

Figure 4.13 Velocity spectra obtained at the peak. Top is for the whole signal, while the lower two figures have been obtained by splitting the signal into its symmetric and antisymmetric mode parts. The symmetric mode spectrum shows no notable high shedding frequency (f_2) component.

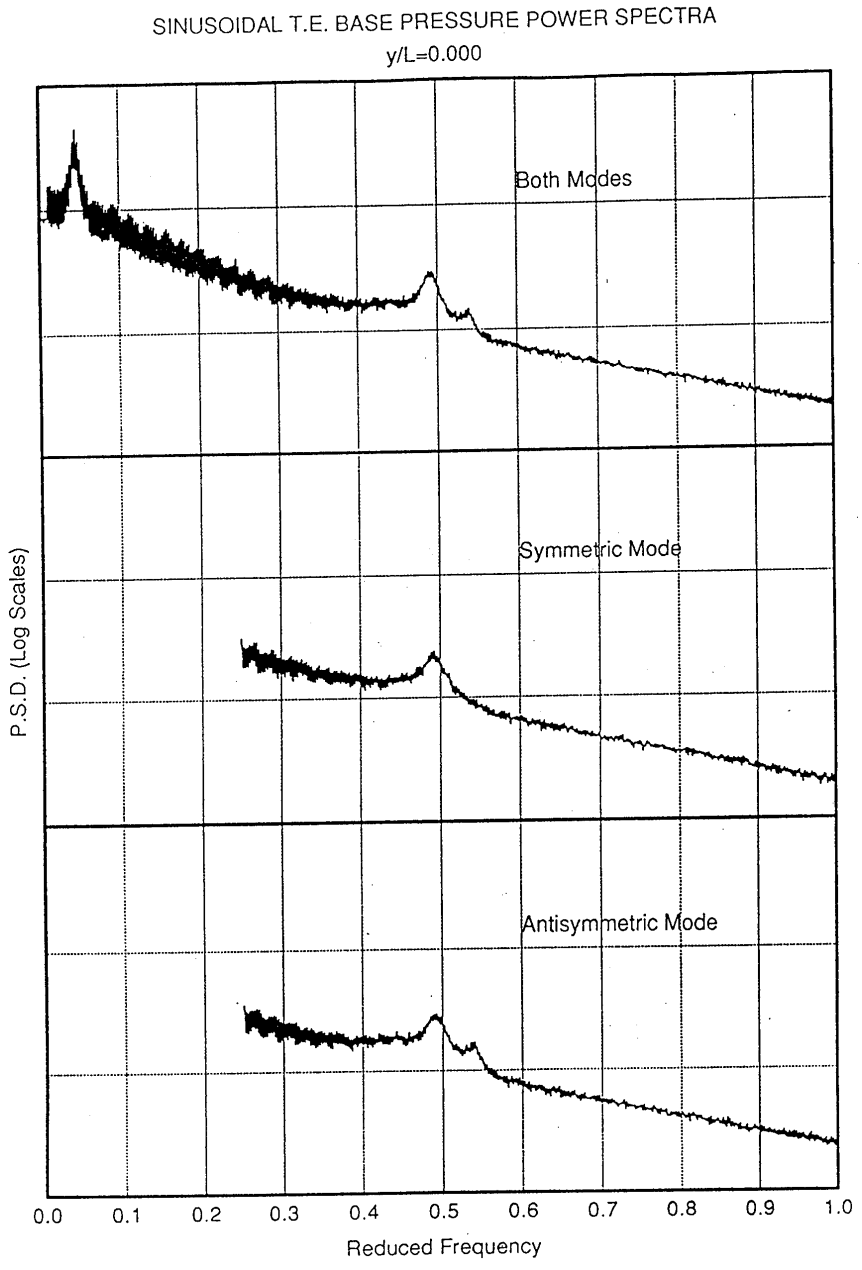

Figure 4.14 Pressure spectra obtained at the peak. Top is for the whole signal, while the lower two figures have been obtained by splitting the signal into its symmetric and antisymmetric mode parts. (f_1+f_2) component (present in the other spectra) is absent for the middle diagram, i.e. the symmetric mode.

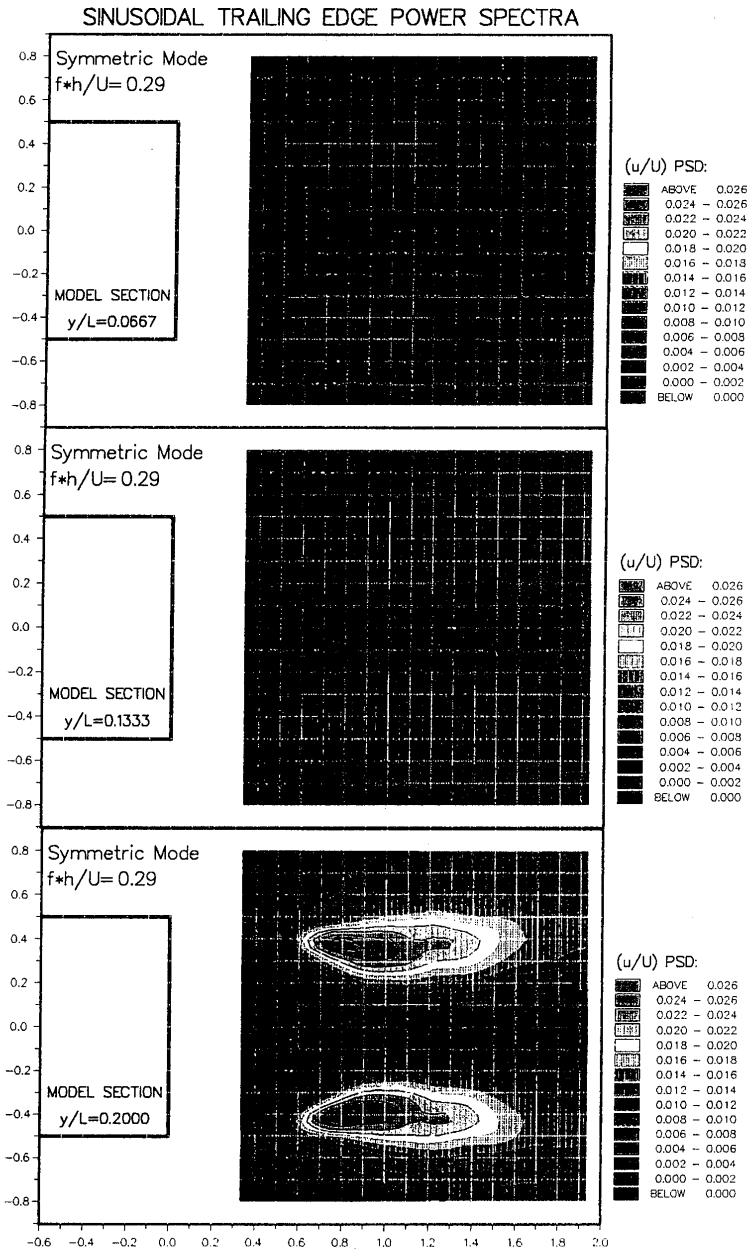

Figure 4.15 Contour plots showing the velocity f_2-fluctuation intensities at different spanwise positions for the symmetric mode. For y/L=0 (not shown here), no f_2 component appeared in the spectra, while it becomes stronger and stronger as we move towards the valley.

The antisymmetric mode spectrum is less spectacular. When compared to the spectrum of the whole signal, the only notable feature appears to be the relative increase of the f_2 component. It is not surprising that the antisymmetric mode still includes both peaks; we had already observed that the mode detection technique could not distinguish between the two antisymmetric modes and the oblique mode.

It is, of course, possible that the f_2 peak is mainly due to induced velocities from the high frequency cell nearby. Figure 4.14 is a plot of the base pressure spectrum, using the same mode-splitting analysis technique. It is interesting to note that for the antisymmetric mode the two peaks represent the $2f_1$ and the (f_1+f_2) components, while the $2f_2$ component is either missing or is very weak. The presence of the (f_1+f_2) component, in conjunction with the weakness or absence of the $2f_2$ component may indicate that actual f_2-shedding at the peak is very weak and that the f_2 component of figure 4.13 is in reality much more the result of an induced velocity and less an indication of a shedding frequency at the peak.

We conclude that the two-cell antisymmetric mode and the oblique mode are both very weak at the high Reynolds number of the wind tunnel, even if they regularly appear at the low Reynolds number water flume (the relation of the oblique mode to low Reynolds numbers having been observed by other investigators in the past, e.g. Gerrard, 1966a). Henceforth, if not otherwise specified, the term "antisymmetric mode" will mean the three-cell antisymmetric mode of the water flume. The f_2 component in the antisymmetric spectra of figures 4.12 and 4.13 is therefore mainly the result of an induced velocity. Its presence (and its absence from the symmetric spectra) could indicate that the f_1 cell is larger in the symmetric mode than it is in the antisymmetric mode.

The contour plots of figures 4.15 and 4.16 can give a clearer indication about the intensity of the f_2 component at the two modes (note that figure 4.15 does not include a plot for $y/L=0$; the f_2 energy there was zero for the symmetric mode). We can see that up to $y/L\approx0.1$ the fluctuation intensity patterns appear to be less well structured (than, say, at $y/L=0.1333$), and also weaker, which is what we expected, given that the f_2 component owes its presence predominantly to an induced velocity.

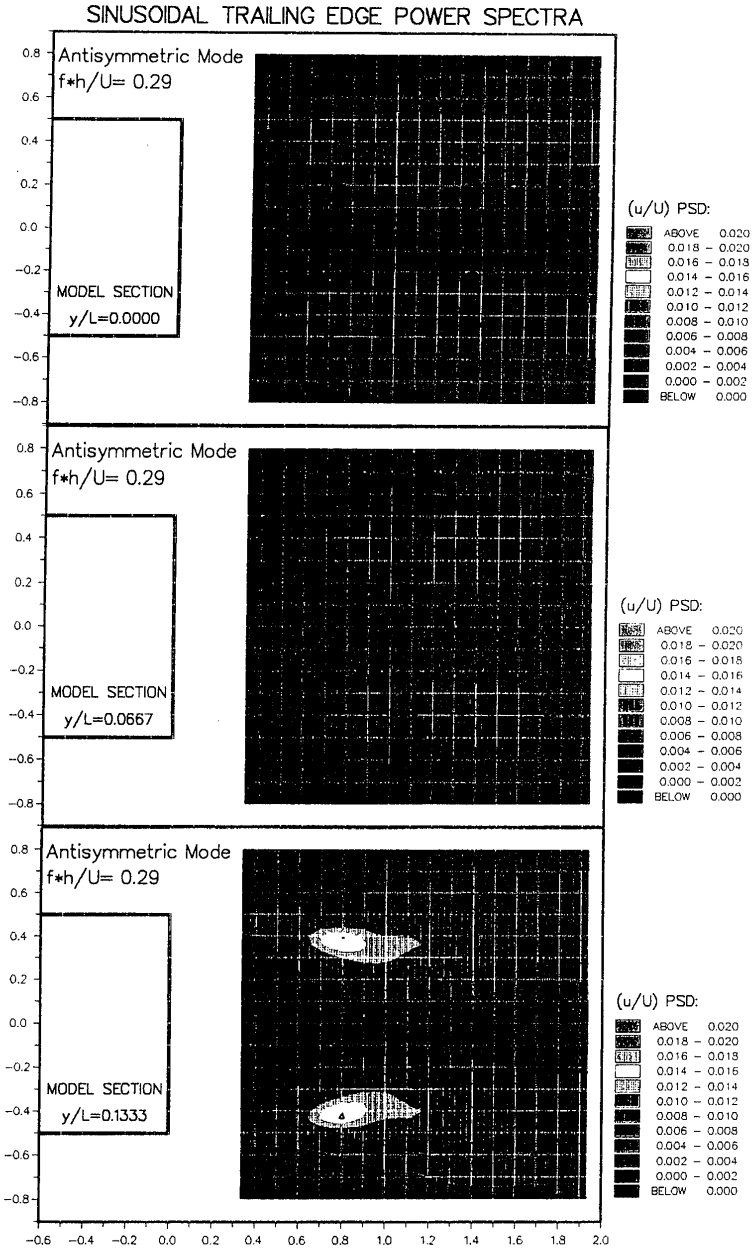

Figure 4.16 Contour plots showing the velocity f_2-fluctuation intensities at different spanwise positions for the antisymmetric mode. The f_2 component is now stronger than for the symmetric mode, but still quite weak in the region of the peak.

4.3 Detailed results : straight trailing edge model

The results presented in section 4.2 all concerned the sinusoidal trailing edge model. Separate experiments were conducted on a straight trailing edge model. As mentioned earlier, within a 10h spanwise region at centre-span the flow was found to be nominally two-dimensional. This means that statistical properties (e.g. Strouhal number and base pressure) do not vary along that portion of the span, although there may be plenty of irregularities in the flow, and the phase of vortex shedding may show spanwise variations. This section thus aims to identify some of these irregularities. Where appropriate, these identifications will be in the light of the observations made for the sinusoidal model.

4.3.1 Discussion of velocity power spectra

The power spectra of the velocity fluctuations in the wake of the straight model do not really present any new features. Some general comments will be made however, comparing these spectra to the ones obtained from the sinusoidal model. Figure 4.17 has five spectra obtained at different distances from the wake centre-line. The most noticeable feature is the single shedding frequency, at S=0.24. At z/h=0 the peak is (due to symmetry) at a value of 0.48. All this is quite standard.

Let us now consider what the effects of irregularities in the spectrum of a nominally two-dimensional wake would be. We can observe from figure 4.17 that the bandwidth of the S=0.24 peaks is quite large, which means that we could expect some shedding cycles to occur at reduced frequencies as low as 0.2 or as high as 0.3. It is suggested here that if we could obtain the same spectrum for a real two-dimensional flow (e.g. by a two-dimensional C.F.D. code) we would observe a narrower peak. The width of the spectrum peak could hence be a measure of the degree of three-dimensionality in nominally two-dimensional, but actually three-dimensional flows.

Taking this a step further, we can imagine an instant when two neighbouring spanwise positions A and B sandwich an irregularity, say a vortex split. This could have been caused by position A shedding at a frequency below 0.24 and position B at a frequency above 0.24. Instantaneously, we would have a "dual frequency characteristic" similar to that observed regularly for the sinusoidal model. At this instant we could also expect the base pressure to rise (towards the levels of the sinusoidal model), thus causing a fall in the average drag for the

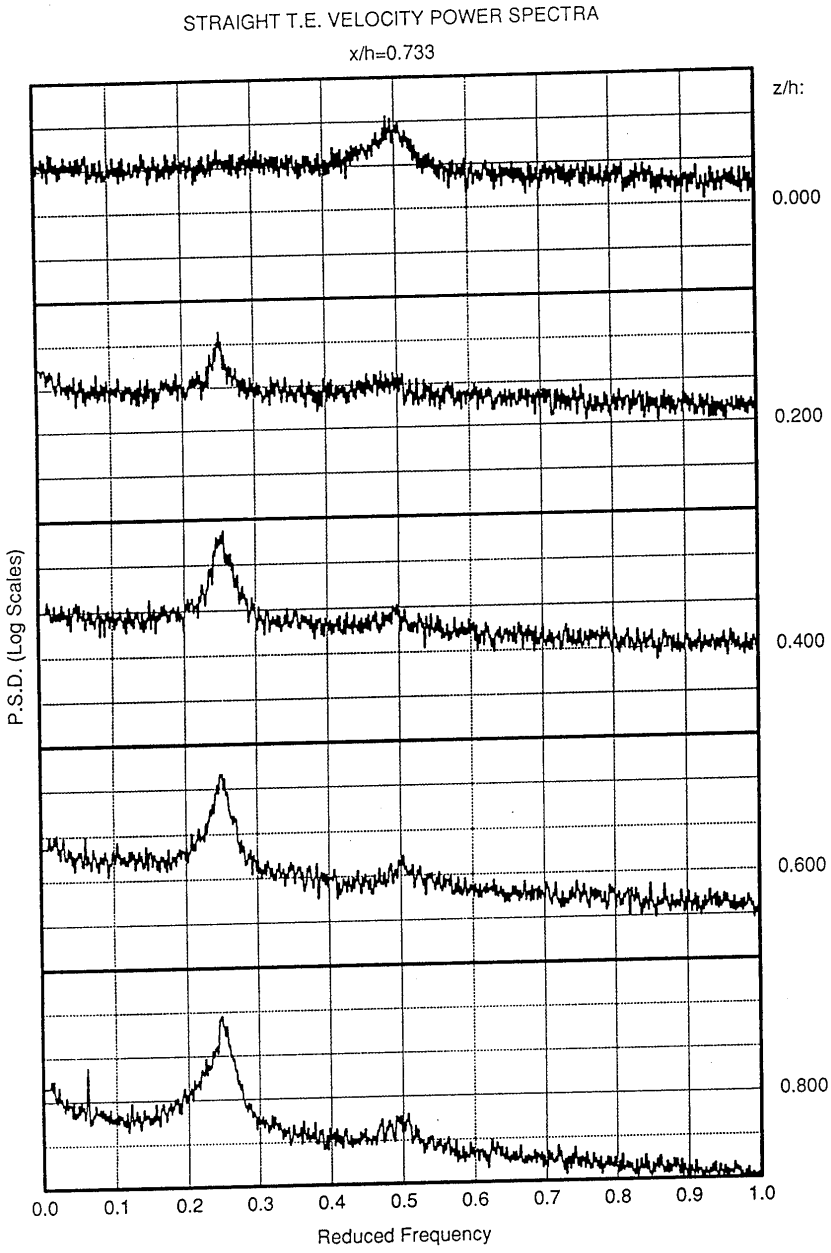

Figure 4.17 Straight trailing edge model: velocity power spectra for x/h=0.733 and z/h=0, 0.2, 0.4, 0.6, 0.8

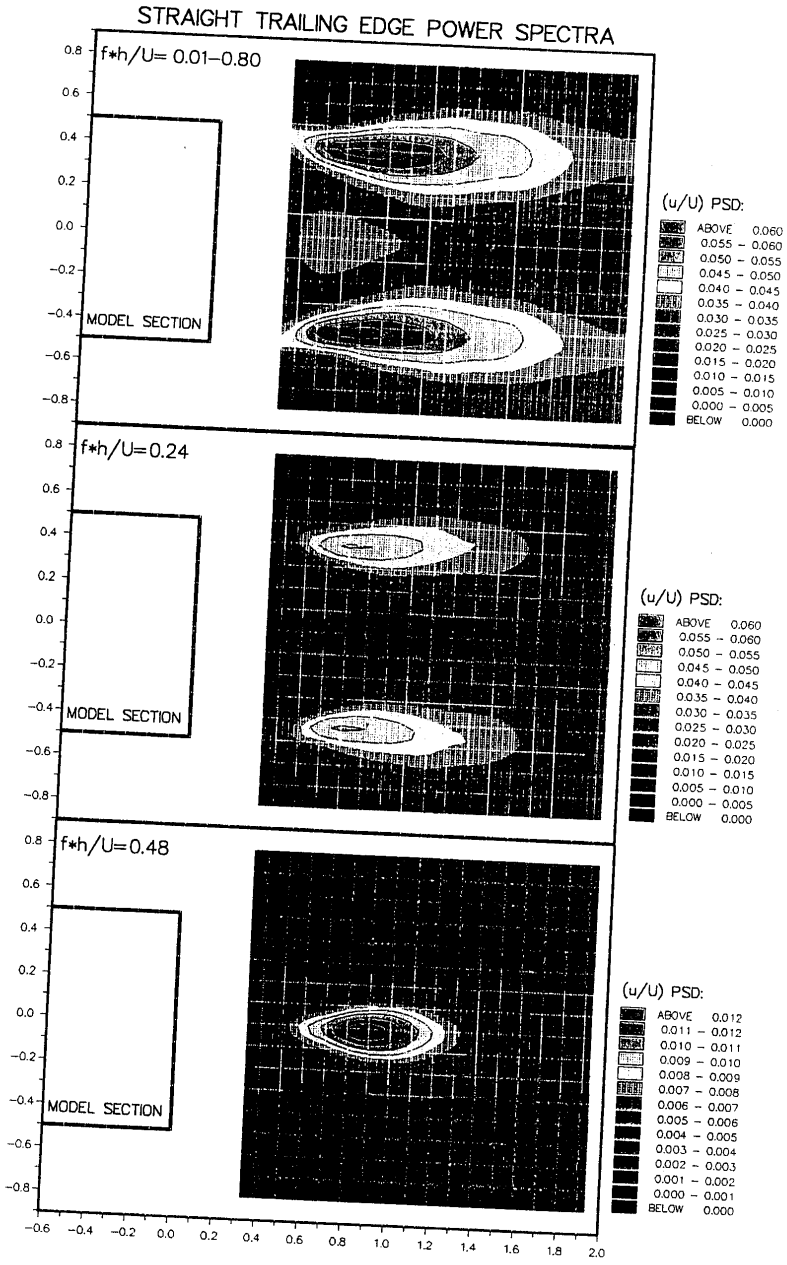

Figure 4.18 Contour plots showing the velocity fluctuation intensities within the near wake of the straight trailing edge model, for different frequency ranges.

straight edge model, when compared to its genuine, theoretical, two-dimensional value.

Figure 4.18 shows the distribution of spectral energies in the near wake. For the top two plots (total frequency range P.S.D. and shedding frequency-related P.S.D.) the maxima lie approximately where one would expect the vortex formation position to be. The bottom plot shows the 0.48 fluctuation energies, prominent close to the centre-wake. No noticeable low frequency component (similar to the (f_2-f_1)component for the sinusoidal model) was observed. Any such low frequency elements were probably too irregular to produce any prominent peak in the velocity spectra.

4.3.2 Spanwise correlation of signals

The correlation length has been used as a measure of the three-dimensionality of a nominally two-dimensional wake flow. The correlation coefficient $r(\Delta)$ between two signals $S_1(t)$ and $S_2(t)$ is defined as follows:

$$r(\Delta) = \frac{\overline{(S_1(t)-\overline{S_1})*(S_2(t-\Delta)-\overline{S_2})}}{\sqrt{\overline{(S_1(t)-\overline{S_1})^2}*\overline{(S_2(t)-\overline{S_2})^2}}}$$

where Δ is the time delay between these two signals (with a value of $r(0)=1$ indicating two perfectly correlated signals in phase). For the straight edge model, and for the signals to be discussed, the maximum value of correlation coefficient r was obtained for $\Delta=0$ (no delay). Thus, the correlation length, L_c was defined as:

$$L_c = \int_0^\infty r(0)\, dy$$

Spanwise correlations were measured for velocity and for base pressure signals. The correlation was computed for the original signals, and for digitally filtered versions of them (the filtering was accomplished by taking the Fourier transform of a signal, then selecting an appropriate frequency range and then transforming back to the time domain). The "appropriate frequency ranges" selected were centred on the shedding-related frequency of each signal (0.24 for the velocity, 0.48 for the base pressure) and included the whole bandwidths of these signals. To check on any low frequency characteristics, another range was

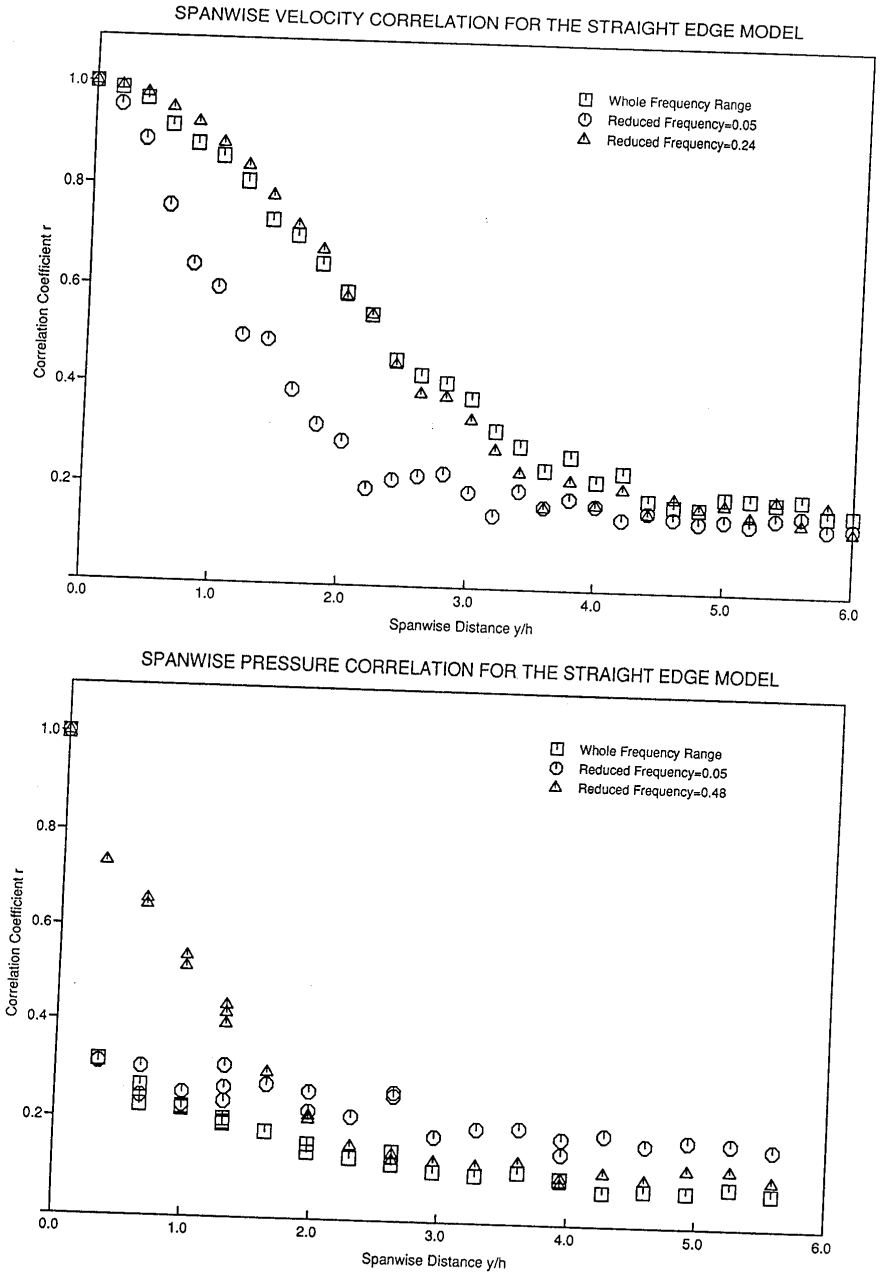

Figure 4.19 Spanwise decay of correlation coefficient for different frequency ranges. Top: velocity signals, bottom: base pressure signals.

also selected for both signals, centred at a reduced frequency of 0.05 (from 0.025 to 0.075).

Figure 4.19 shows the spanwise decay of correlation coefficient r for these signals. The corresponding values of correlation length are given below:

Signal	Reduced frequency	Lc/h
velocity	whole range	4.1
velocity	0.025-0.075	3.2
velocity	0.24 bandwidth	4.2
pressure	whole range	1.8
pressure	0.025-0.075	2.2
pressure	0.48 bandwidth	2.4

Not surprisingly, the velocity signal is best correlated when we select the shedding frequency range, which yields a correlation length of 4.2h. In comparison, the whole, unfiltered signal gives a value of 4.1h. This small difference is probably due to noise, which for the velocity signal is quite low (especially since the hot wire was placed a bit outside the wake). The essence of this is that the correlation length is about 4h.

For the pressure signal the noise level was much higher. An indication is given by the abrupt drop in correlation from $y/h=0$ to the first point of the graph. If we could have positioned two transducers at $y/h=0$ we would have not obtained $r=1$ but probably a significantly lower value, due to the contribution of the noise of each transducer (hence the value of 1 at $y/h=0$ is a bit artificial, as it does not take into account the noise of the transducers). The whole frequency range correlation length is a low 1.8h. For the shedding-related frequency of 0.48 the value is a bit higher, at 2.4h. It should be noted that due to the double frequency characteristic of the base pressure, if the shedding at two spanwise stations gets a bit out of phase, with the velocity signals having a phase difference of, say, φ, the pressure signals will have a phase difference of 2φ. Assuming a statistical, Gaussian-like distribution of φ, centred at $\varphi=0$, the lower correlation values for the pressure signal are then quite expected.

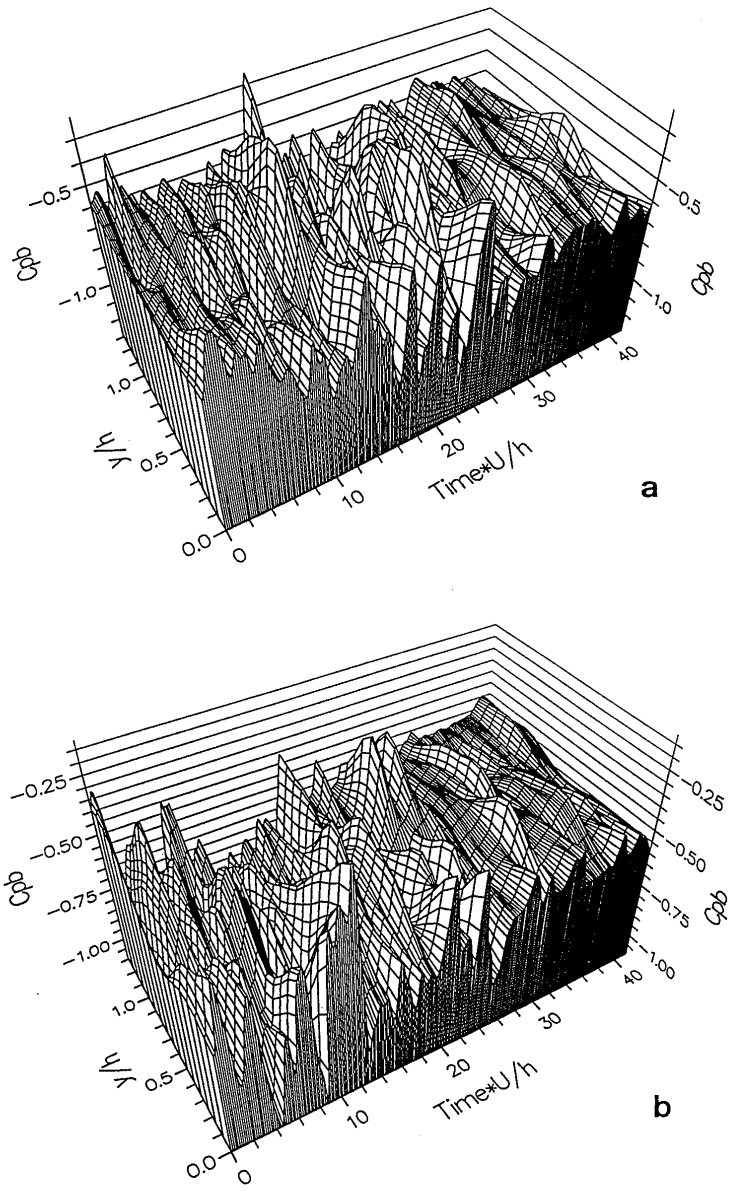

Figure 4.20 Two three-dimensional plots showing the irregularities (in both time and spanwise position) of the base pressure fluctuations.

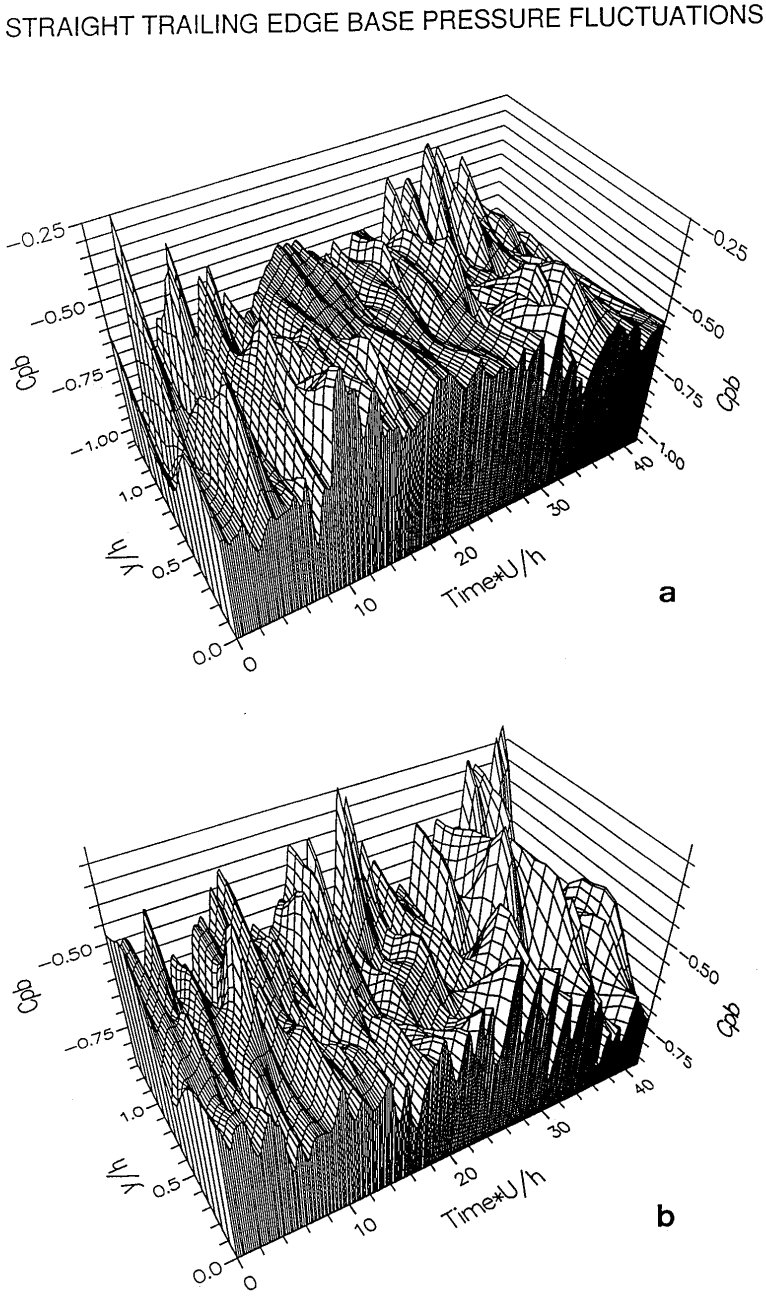

Figure 4.21 Two more three-dimensional plots showing the irregularities (in both time and spanwise position) of the base pressure fluctuations.

If the signals were much purer, we would expect most of their energy to accumulate around the shedding frequency. For ranges that do not include the shedding frequency, we would have basically random signals and zero correlation. That for the 0.025-0.075 frequency range (which does not include any peak), we get finite values of correlation length (again lower for the pressure signal), thus means that the low frequency fluctuations in the wake may have some physical significance, similar perhaps -if less well defined- to the (f_2-f_1) component of the sinusoidal model.

4.3.3 Pressure irregularities

The higher noise level of the pressure signals can not all be attributed to electrical interference. Estimates of the signal-to-noise ratios of the pressure transducers could not wholly explain the low correlation lengths. A large part of the pressure signal noise is due to "genuine" base pressure fluctuations. Figures 4.20 and 4.21 show four frozen time-histories of spanwise distributions in base pressure.

The high frequency oscillations in these plots correspond to the reduced frequency of 0.48. There are a few more noticeable features, apart from these oscillations. First, there are periods of relative peace (e.g. at the end of figure 4.20b and at the middle of figure 4.21a), in between periods of intense activity. Within these intense activity periods, we can observe large amplitude pressure fluctuations and also very large pressure gradients.

The plots of figures 4.20 and 4.21 give sufficient explanations on why the correlation length of the pressure signals is so much lower than that of the velocity signals. However, we have still not made any progress in understanding the cause of these large pressure gradients and pressure fluctuations. Suggestions about their cause are given in a later discussion chapter.

4.3.4 Flow visualisation: the presence of irregularities

Flow visualisation experiments were also conducted for the straight edge model, mainly in order to identify the nature of the spanwise irregularities. The extent to which the flow in water (Re=2500) was similar to the one in air (Re=40000) is unclear. The pattern of the observed irregularities (to be described later) could be what one would expect for L_c=4h, but since no quantitative

measurements were made, one cannot be entirely sure. Figure 4.22 includes photographs showing the main flow characteristics.

The correlation coefficients r(t) computed earlier all showed maxima at t=0, which probably suggests that the most usual state for the straight edge model is parallel shedding. Parallel shedding was also observed most frequently in the water flume and can be seen in photos (a) and (b). Although the vortex filaments in these two photos show smaller-scale irregularities and non-uniformities, their main axes are parallel to the model trailing edge. The flow could stay in this mode for a number of shedding cycles before irregularities appeared. An oblique mode was also observed, as can be seen in photos (c) and (d). In the light of observations made about the sinusoidal model, we should probably associate this oblique mode with the low Reynolds number of the water flume.

Photos (e) and (f) show instants when irregularities occur. In (e), the vortex filaments have become wavy and vortex splitting is occurring towards the top of the picture. Similar, if less clear, vortex splitting is occurring in (f). Vortex splitting was observed in many instants and could either happen continuously (for a number of cycles) to accommodate a phase change along the span, or could happen for a limited number of cycles in order to facilitate a mode transition (say from oblique to parallel).

Photos (g) and (h) are close-ups on the separated shear layer. The wide dark strip immediately after the trailing edge is the shear layer before vortex formation. The laser sheet was adjusted for these pictures in order to illuminate that plane, as opposed to the more central plane of the wake for the previous pictures. The pictures are not so clear because the shear layer has not yet rolled-up into a vortex and hence the precipitate density is not so high. In any case, one can still see irregularities in the separated shear layer. Where the colour is less dark, it has "dipped" behind the laser sheet and is hence less visible. This "pulling" of the shear layer towards the centre wake could be related to a momentary drop in base pressure, at these spanwise locations.

A transition from the oblique to the parallel mode has been captured by the sequence of figure 4.23. The period between two successive shots is approximately one shedding cycle. At (a) we can see oblique, slightly bowed vortices. As we progress through (b), (c) and (d), the top of the pictures seems to lag behind in vortex shedding, and thus a kink starts to develop in the vortex filaments, a bit above the centre of the picture. When the angle of the vortex becomes too large,

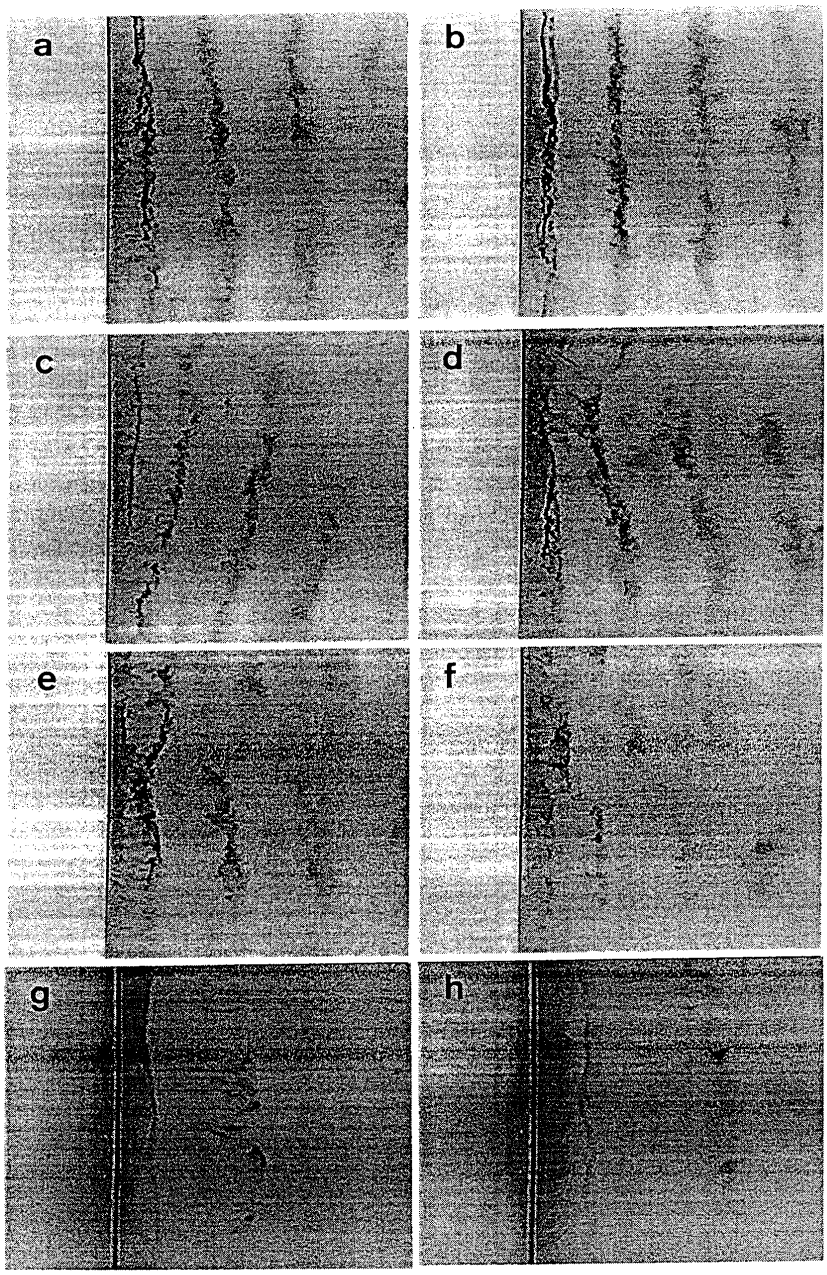

Figure 4.22 Flow visualisation for the straight model. For photos (a) to (f), the laser sheet illuminated the z=0 plane (centre wake). (a) and (b): parallel shedding, (c) and (d): oblique shedding, (e) and (f) vortex splitting-irregularities. For photos (g) and (h), the laser sheet illuminated the separated shear layer and some three-dimensionality can already be seen within it.

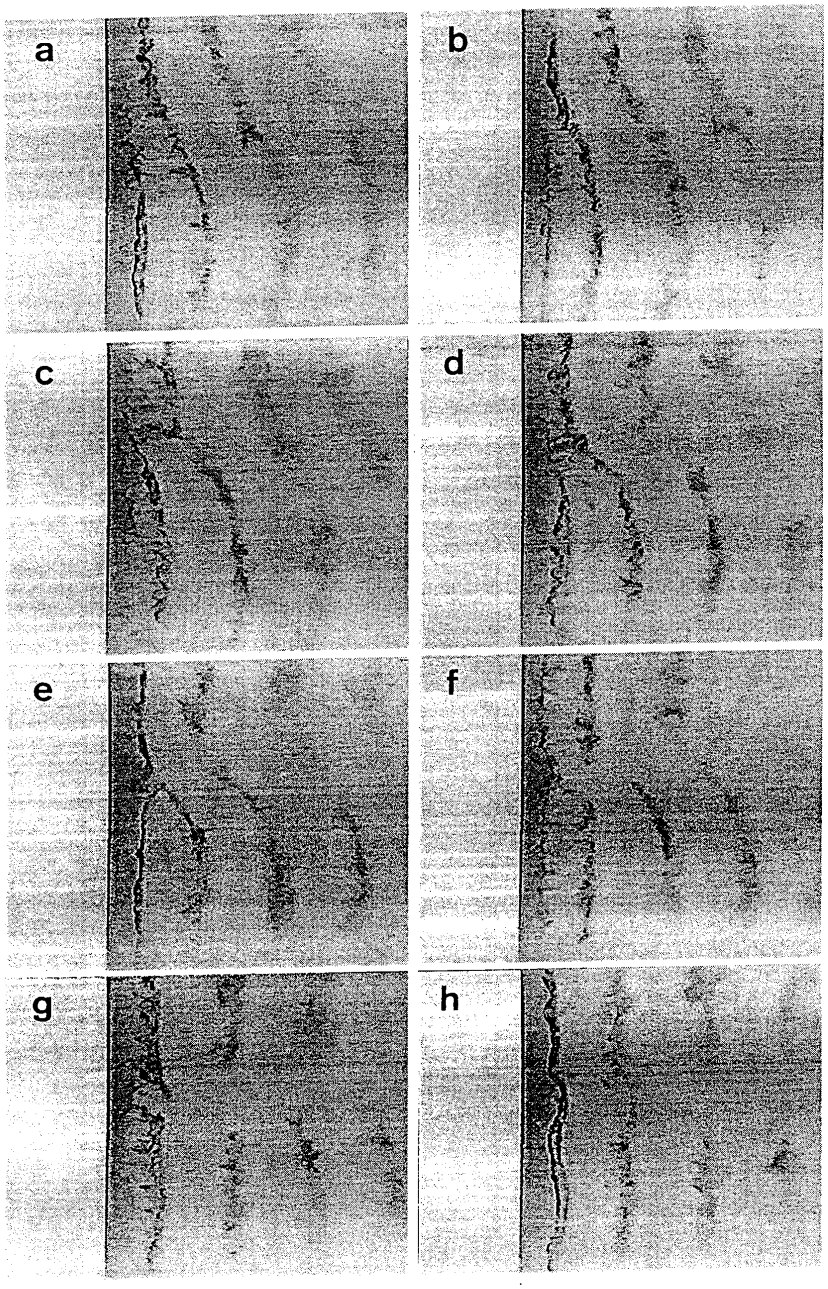

Figure 4.23 Flow visualisation for the straight model. Cycle-by-cycle capture of the transition from oblique shedding to parallel shedding. Vortex splitting can be seen (with different clarity) in photos (c) to (f).

vortex splitting occurs, the top of the picture effectively having missed one shedding cycle. The split can be seen in three photos (i.e. three consecutive cycles). Eventually, the shedding above and below the split gets in phase and the transition to parallel shedding has been completed, as is shown in (g) and (h).

Figure 4.24 is also a sequence (frame-by-frame this time) of an irregularity of some kind. The patterns observed most of the time would be of regular shedding, as have been recorded by numerous researchers in the past. In this sequence, however, we can see a direct interaction between the forming vortices in the upper and the lower side of the wake. At photo (a) and (b) a vortex is being fed with vorticity by the separated shear layer, very much according to Gerrard's model discussed in the first chapter. Before it has time to get cut off and shed downstream, vorticity has started gathering on the opposite side of the wake. The accumulation of this opposite-signed vorticity causes first, the flattening of the upper vortex, as can be seen in (c), and eventually tears it in half, as is shown in (d) and (e). In the remaining frames, the upper vortex (now considerably weaker), gets shed downstream, while the lower vortex (most probably also weaker), continues to form. The upstream half of the torn vortex is now propelled within the near wake towards the model. It is unclear to what extent its vorticity has been cancelled due to the influence of the lower vortex.

Patterns such as the one just described were not observed in such a clear form very frequently. However, similar irregularities were observed occasionally. These have to be related to the irregularities observed in figures 4.22 and 4.23. It is unclear what we would had seen had we been able to observe the irregularity of figure 4.24 from a different angle.

4.4 Similarities between the two models

The aim of this chapter was to present the general features of the wake flows for the two model configurations (sinusoidal and straight trailing edge). Although a plethora of interesting features were observed, explanations have not yet been given, and the aims of this project (section 2.1) have not yet been approached. The next four chapters will thus aim to draw more general conclusions on the dynamics of the near wake, based on the results presented in this chapter. This attempt for an improvement of our understanding of the near wake dynamics (irrespective of model geometry) would be more in line with the specific aims of this project. The models studied here (especially the sinusoidal model) do not have real practical applications, but are tools that will hopefully

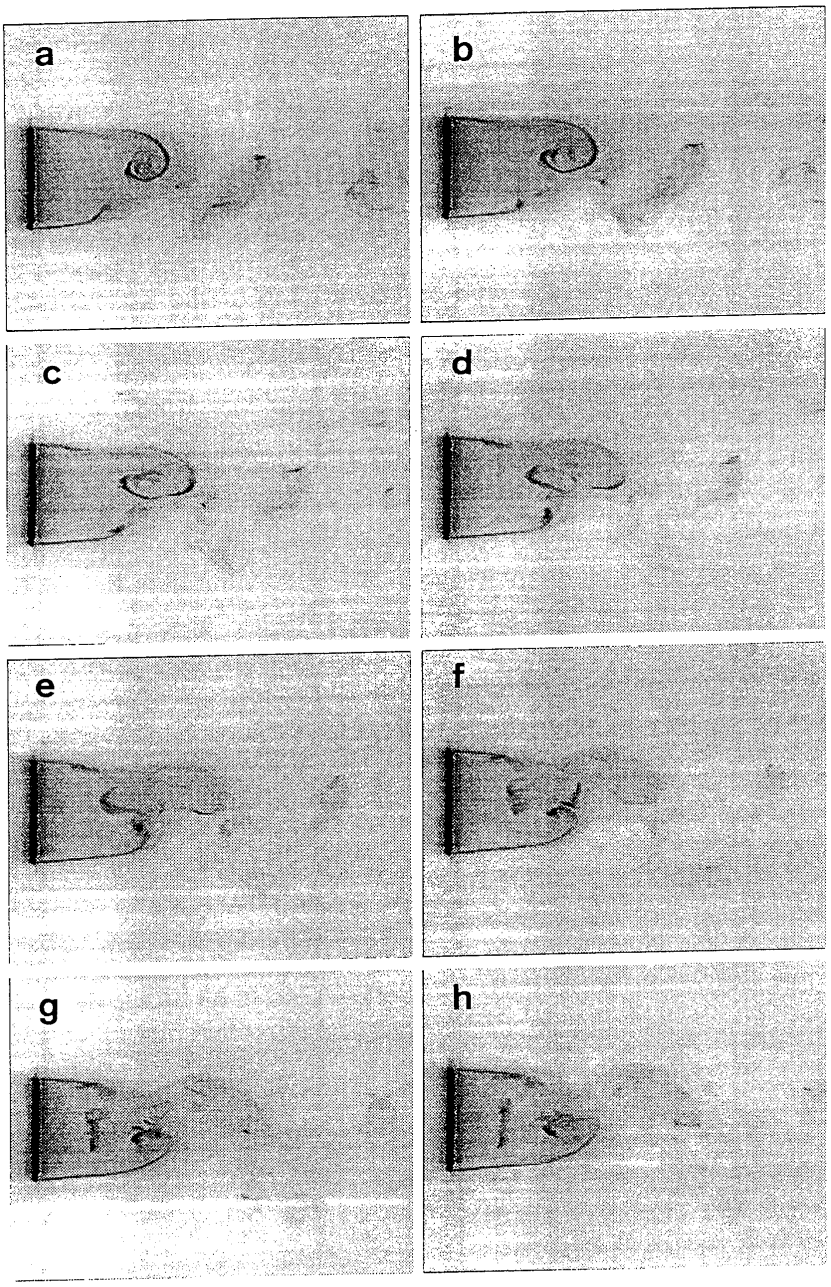

Figure 4.24 Flow visualisation for the straight model. Frame-by-frame sequence which shows a Kármán vortex being torn apart under the influence of strong vorticity at the other side of the wake.

enable us to understand wakes in a better way. Hence, if a further understanding of the specific flow details for the present models does not aid us in drawing general conclusions, it is then of little significance for this study.

A variety of broadly similar features were observed in the flows around both models, which justifies the particular choice of geometrical disturbance for the sinusoidal model. These are listed below:

a) The presence of large-scale irregularities (in particular vortex splitting). These were observed regularly in the sinusoidal model and less regularly in the straight model. As a consequence, one would expect dislocations to appear in the wake of the straight model, but for smaller durations, and in less well-defined positions.

b) A low frequency component was observed for the sinusoidal model. Evidence emerged that for the straight model similar low-frequency fluctuations exist, but not at a so well-defined frequency.

c) Large base pressure fluctuations and instantaneous pressure gradients. Although it was not mentioned in section 4.2, pressure fluctuations of exactly the same nature as described in section 4.3 for the straight model were observed for the sinusoidal model. These did not seem to be under any particular influence from the geometrical disturbance, and hence were presented only once, for the straight model.

The results of this chapter show that it is therefore scientifically valid to compare the flows around the two models. The next three chapters will split the problem in three parts:

Chapter 5 will concentrate on the dynamics of the dislocations. As these were more prominent for the sinusoidal model, they will be predominantly discussed under that prism.

Chapter 6 will present a theory on the dynamics of the formation region, and how the various three-dimensional wake parameters interact. Again the regularity of the sinusoidal model makes it attractive for the basis of discussion of that chapter.

Chapter 7 will present results related to chapters 5 and 6, but obtained by using a conditional sampling technique.

Chapter 8 will discuss the large, instantaneous base pressure gradients which featured in both flows. The emphasis of that chapter will be on the effects of non-Kármán vortices. As the pressure gradients did not seem to be affected by the sinusoidal model disturbance, their discussion will focus on the straight edge model.

These three aspects are, of course, not independent, and their separation into three main discussion areas is purely for practical reasons. Their inter-relation will be discussed at a later stage.

5. ON THE DYNAMICS OF VORTEX DISLOCATIONS

ABSTRACT : The dynamics of vortex dislocations at high Reynolds numbers are discussed. A mechanism is proposed which explains the significance of a characteristic dislocation frequency, f_d in the near wake dynamics. It is suggested that f_d is a result of the geometrical properties of the vortex filaments. It is proposed that a link exists between the dislocation frequency and fluctuations in base pressure, vortex strengths and spanwise dislocation position. The downstream evolution of the dislocation is also studied. The low frequency cell is found to expand in the spanwise direction.

5.1 Introduction

5.1.1 The term "vortex dislocation"

The term "vortex dislocation" has been used by Williamson (e.g. in 1992a) who borrowed it from solid mechanics, where a dislocation is a discontinuity in the ordered crystal structure of a solid. In fluid mechanics, the term is not yet widely used, but seems to be quite appropriate to describe discontinuities in vortex filaments, such as vortex splitting observed in wake flows. Williamson's work has mainly concentrated on low Reynolds numbers, and has given some fresh insight into a phenomenon that has been identified (as was mentioned in chapter 1) by numerous researchers in the past.

Williamson suggests that vortex dislocations may be a generic feature of transition to turbulence in all shear flows. In the present investigation, vortex dislocations were observed at high Reynolds number flows, where the shear layer is already turbulent even before separation. Thus the effects of the turbulent transport of momentum and vorticity would not allow the fine details (e.g. "vortex wisps") observed by Williamson for low Reynolds numbers to exist in such a well-defined way.

It is thus the purpose of this chapter to discuss the dislocation dynamics at higher Reynolds numbers. The experimental basis for the discussion will be the results obtained from the sinusoidal model. The regularity of vortex splitting in the wake of that model made the study of such complicated flow phenomena a bit easier.

5.1.2 The elementary causes of a vortex dislocation

The fluid dynamics of the dislocations are dominated by highly complicated effects. Nevertheless, a surprising number of studies dealing with dislocations (whether that specific term is used or not) ignore the elementary reasons for the existence of dislocations in wakes. This is, of course, not to imply that these reasons (to be identified below) are not known or appreciated by almost anyone involved in this field. Simply, their identification (even though it may seem a statement of the obvious) puts the problem into a proper context, with a simplifying effect.

The observations to be made below concern the near wake, i.e. a region extending from the body up to a short distance beyond the formation position. In the near wake the main phenomenon is the formation of a vortex. Vorticity cancellation can occur during formation through the process of entrainment. At the moment when a vortex is cut-off, however, its core still covers a fairly confined region in space, and for a while vorticity cancellation (due to the merging of Kármán vortices of opposite sign) is very limited. Thus it is a useful assumption to consider the formed vortex as discrete. The consequences of this are to be described below. We should, however, make a cautionary note: at high Reynolds numbers in particular, soon after formation, the turbulent vortices start to become more diffuse (they spread out) and soon start to interact with vorticity from the other side of the wake. Thus, for high Reynolds number flows one should be careful in treating vortices beyond the near wake as discrete. In the near wake, this assumption seems to be quite valid for the fully-formed vortices.

As was mentioned in chapter one, dislocations in the near wake mainly consist of two phenomena (or their combination). In *vortex splitting*, as the name implies, a vortex splits in order to get connected to two vortices on the other side of the dislocation. By its nature, vortex splitting accommodates abrupt spanwise variations in the phase of vortex shedding. It should be stressed once again that spanwise variations in the total circulation flux at each side of the near wake cannot be accommodated by vortex splitting. In vortex splitting, vorticity merely re-distributed in different "groups" (the vortex lines). On the other hand, spanwise variations in circulation flux (at each side of the wake) can be accommodated by *vortex looping*, where a vortex loops across the wake in order to join with one or more of its oppositely-signed counterparts on the other side of the wake (vortex

looping, of course, cannot deal with the previous problem, the spanwise variations in shedding phase).

Hence we should see both phenomena as consequences of the fact that vortex lines cannot end abruptly in the fluid. Each mechanism has its own topological characteristics that allow it to deal with a specific task in the near wake. Even though there may be flows where combinations of these two mechanisms prevail, these mechanisms are distinct and should not be confused.

Generally speaking, vortex looping is less likely to happen because it requires an interaction between the two sides of the wake. The times scales involved in the formation of vortices seem too brief for such interaction to take place across the wake, under normal circumstances. Hence, vortex looping can be found predominantly when very abrupt spanwise changes occur, such as a step change in cylinder diameter, a free end, or an end-plate.

On the other hand, in vortex splitting, the redistribution of vorticity happens on the same side of the wake, and could even be controlled at a very early stage within the separated shear layer, before vortex formation. Hence vortex splitting does not have the time scale problem that vortex looping has, and can occur with milder disturbances (or even, as was seen in the previous chapter, in nominally two-dimensional flows).

Throughout this study, there was no evidence of vortex looping, either in flow visualisation or in measurements. Hence, in this chapter (and in later ones), the term "vortex dislocation" will concern vortex splitting only, unless otherwise specified. The basic effect of a dislocation will then be the accommodation of abrupt spanwise changes of vortex shedding phase.

5.2 The existence of a characteristic dislocation frequency

5.2.1 The presence of the dislocation frequency in the wake

As was shown in the previous chapter, in the present investigation there are two neighbouring cells, each with its own, distinct shedding frequency (f_1 and f_2, where $f_1 < f_2$). In the vicinity of the cell boundary, a frequency component (f_2-f_1) was also observed. It was noted that this component must be the result of a non-linear interaction of the two shedding frequencies of the neighbouring cells. This fitted in well with the observation that (f_2-f_1) is in fact the frequency of vortex

splitting. We can therefore define the *dislocation frequency* f_d as the frequency difference (f_2-f_1).

It is easy to jump to the conclusion that the low frequency f_d peak in the spectra is a direct consequence of the coexistence of f_1 and f_2. However, this does not seem to be the case. Examining the spectra of figure 5.1 (for y/L=0) and figure 5.2 (for y/L=0.2), we can see that while in some cases the low frequency component is very prominent, in other cases it is virtually non-existent. In all graphs (except when z=0) we have both f_1 and f_2 present.

Figure 5.3 summarises, in effect the above, with the contour plots each showing the distribution of power spectral density (associated with the low frequency, f_d) in the near wake at different spanwise sections. The low frequency seems to be present mainly very close to the body (at x<h). Interestingly, there also appears a well-defined (if not so energetic) low frequency patch in the centre-wake, further away from the model.

5.2.2 The geometry of vortex filaments: fluctuations in formation region size

Let us now consider the two neighbouring cells, shedding at f_1 (in the region of the peak) and at f_2 (in the region of the valley). In order to accommodate the different numbers of vortices shed in the two cells, vortex splitting must occur at a rate of f_d, the characteristic frequency of the dislocation. In the immediate vicinity of the dislocation, we now have to consider what effect vortex splitting will have on the geometry of the vortices. On the two sides of the dislocation, vortices will some times be in phase and some times out of phase (the phase difference fluctuating, in fact at f_d). When they are in phase their interconnection will be quite simple, but when they are out of phase, vortices will have to bend in some way in order to meet their counterparts on the opposite side of the dislocation. Taking this argument a step further, if we now imagine these two cells gradually getting out of phase, the vortices will have to become more and more bowed. Thus the degree of vortex bowing will change, also at f_d.

The bowing of vortices is an effect that was observed also in the water flume. In the sequence of figure 4.10, we can see how the angle of bowing increases in photos (a) to (d), as the cell at the peak starts to lag behind its neighbours in its shedding of vortices, with the phase difference across the dislocation rising. When vortex splitting occurred, the cell at the peak found itself

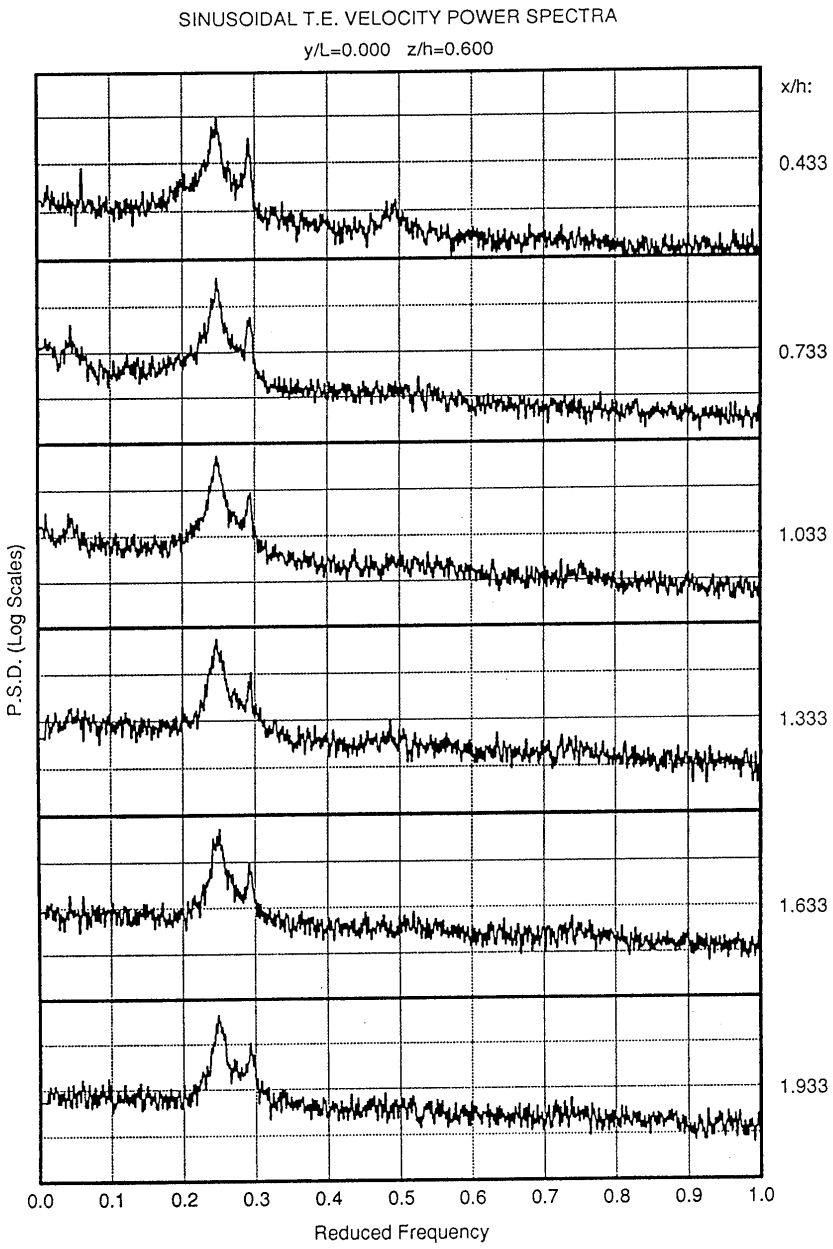

Figure 5.1 Sinusoidal trailing edge model: velocity power spectra for y/L=0, z/h=0.6 and x/h=0.433, 0.733, 1.033, 1.333, 1.633, 1.933.

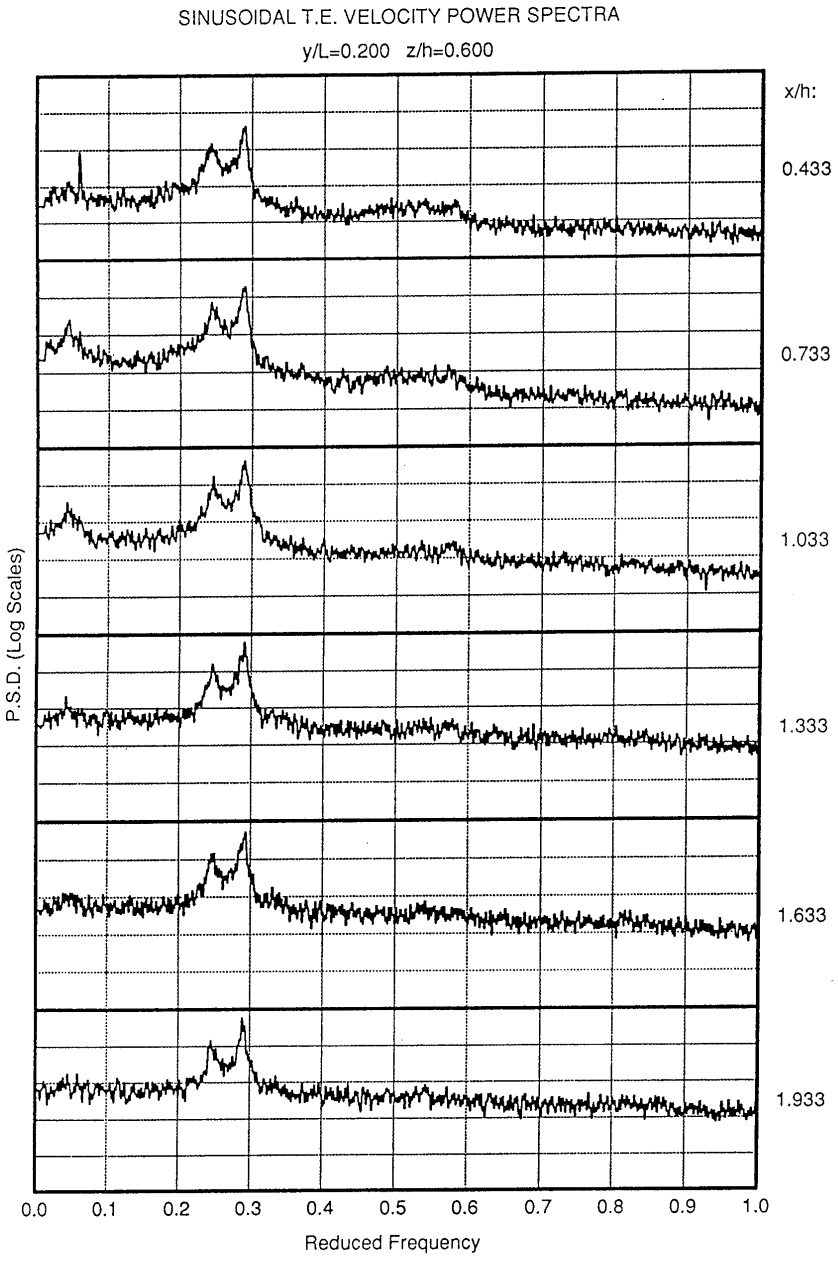

Figure 5.2 Sinusoidal trailing edge model: velocity power spectra for y/L=0.2, z/h=0.6 and x/h=0.433, 0.733, 1.033, 1.333, 1.633, 1.933.

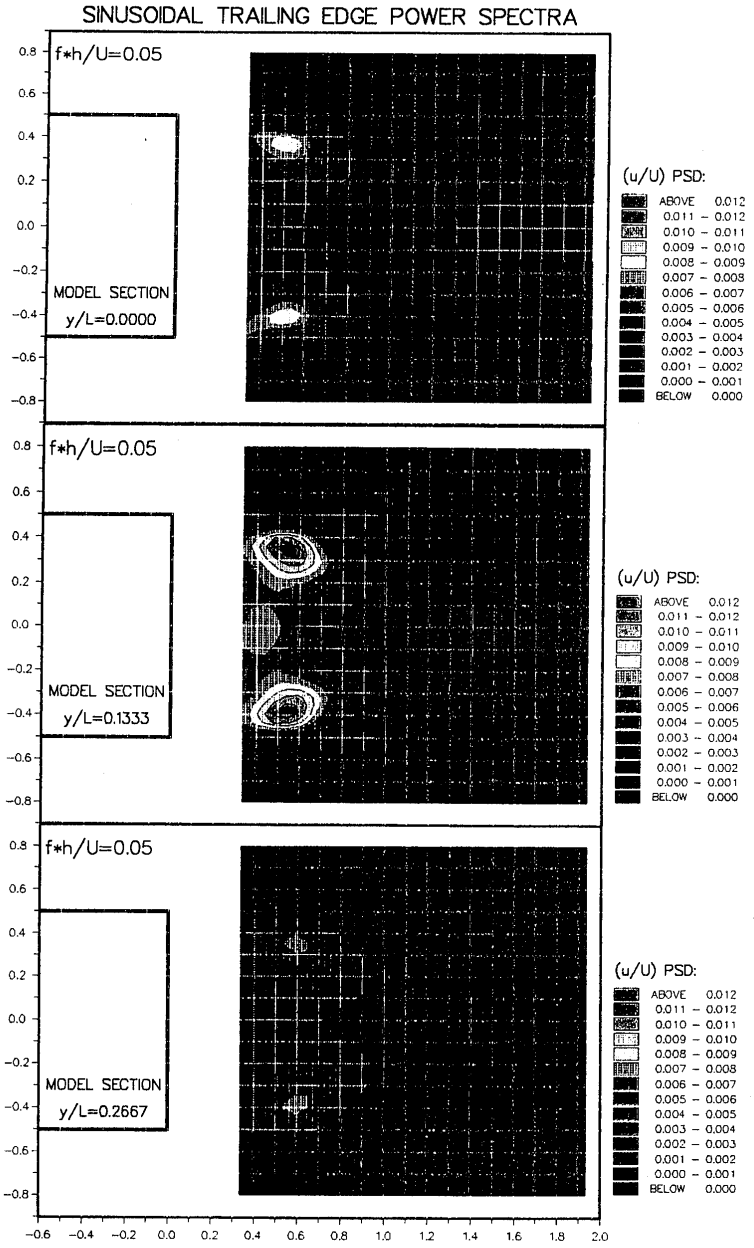

Figure 5.3 Contour plots showing the velocity f_d ($=f_2-f_1$) fluctuation intensities in the near wake of the sinusoidal model, at different spanwise positions. Note that the strongest f_d fluctuations appear away from the peak, around the region of the dislocation.

suddenly leading rather than lagging in phase. Thus, from (e) to (h), the shedding phase difference decreases, with the bowing getting less and less pronounced.

This "bowing" of the vortex filaments in the vicinity of the dislocation will have some effect on the size of the formation region: if at a certain spanwise position the forming vortex has to bend backwards, towards the model, the formation region will effectively shrink in size. Similarly, if the vortex bends away from the model, the formation region will grow. In the present case, we have shown why the "bowing" has to be periodic, from purely geometrical considerations. As a result, the formation region in the vicinity of the dislocation will have to fluctuate in size at the characteristic dislocation frequency f_d.

The periodic fluctuations of the formation region size seem to be reflected in figure 5.3. The most energetic parts of the contour plots seem to be close to the body, roughly where one would expect the re-circulating region to be. The peaks are close to the actual vortex formation positions. If we imagine the formation point changing position from one cycle to another, we may expect the points in the vicinity of this formation point to show the largest, low-frequency velocity fluctuations. It is interesting to point out that the most energetic plot is at $y/L=0.133$, not at the peak. This ties in well with observations made in flow visualisation and in measurements, regarding the position of the dislocation.

The formation region hence shrinks and grows at the dislocation frequency. In the few shedding cycles when the formation region is at its lowest size, the separated shear layers will have to bend inwards, towards the centre-wake, more steeply. This will have to be balanced by a decrease in base pressure. Thus, according to these considerations, the base pressure will have to fluctuate at the dislocation frequency, in order to balance the periodic shrinking of the formation region. These low-frequency base pressure fluctuations were the most notable feature of the base pressure spectra (figure 4.9).

We have thus seen how the presence of two cells shedding at different frequencies causes low frequency fluctuations in base pressure and near wake velocities. An important part in the described mechanisms has been played by the body. In its absence, this theory could not be supported and it is conceivable that we could have the dislocation separating the two cells without any noticeable peak in the spectrum at f_d, as was seen in the lower parts of figures 5.1 and 5.2. It is therefore proposed here that in trying to understand the physical reason of the f_d component in spectra we should look back to the effects of dislocations in the near

wake. Treating this spectral component as an inevitable feature once we have the simultaneous presence of two frequencies f_1 and f_2, puts us in danger of missing important physical explanations of the wake dynamics.

5.2.3 The strength of the formed vortices

We will now consider the strength of the vortices that have been created under the influence of the above theory. If we imagine a vortex that is being formed, its eventual strength will be related to the base pressure (as the circulation shed from the body is a function of the base pressure). Hence, if the base pressure fluctuates at an f_d frequency, the strength of the vortices being shed will also fluctuate in a similar way. This hypothesis may partly explain the presence of the low frequency "patch" which can be seen further away from the formation region, close to the centre-wake in figure 5.3 (the patch can be seen quite clearly in the top contour plot, but also exists -if in a less pronounced manner- in the lower two plots). Depending on their sign, vortices pass either just above or just below this region. If their strengths fluctuate at the dislocation frequency, their induced velocities on the centre-wake will also have an f_d frequency component. The effects of the oppositely-signed vortices of the two sides of the wake will be stronger in the region between them, but weaker further away from the centre-wake, an explanation that agrees well with the observed pattern in the contour plots.

As was discussed in the introduction of this chapter, the net effect of the dislocation in this flow is the re-distribution of vorticity of each sign into different groups. In the near wake, the flux of, say, positive circulation is preserved along the span. We therefore have to consider the mechanisms through which vortices link from this point of view: the total strength of the vortices on the one side of the dislocation must be equal to the total strength of the vortices on the other side.

In explaining this phenomenon, Williamson (1992a) considered two cells of vortices with a 9:10 frequency ratio. Figure 5.4 presents his ideas for vortex linking across a vortex dislocation. Diagram (a) is based on his flow visualisation pictures, while in diagram (b) an idealised sketch of his vortex connection pattern is given (similar sketches have been proposed in the past by a number of authors). Although the sketch is for a "two-sided" dislocation, it seems that his proposed pattern would be the same for a "one-sided" dislocation (we would just have to consider half the diagram). To preserve total circulation flux across the dislocation, vortex strengths are taken to be of the ratio 10:9 (low frequency

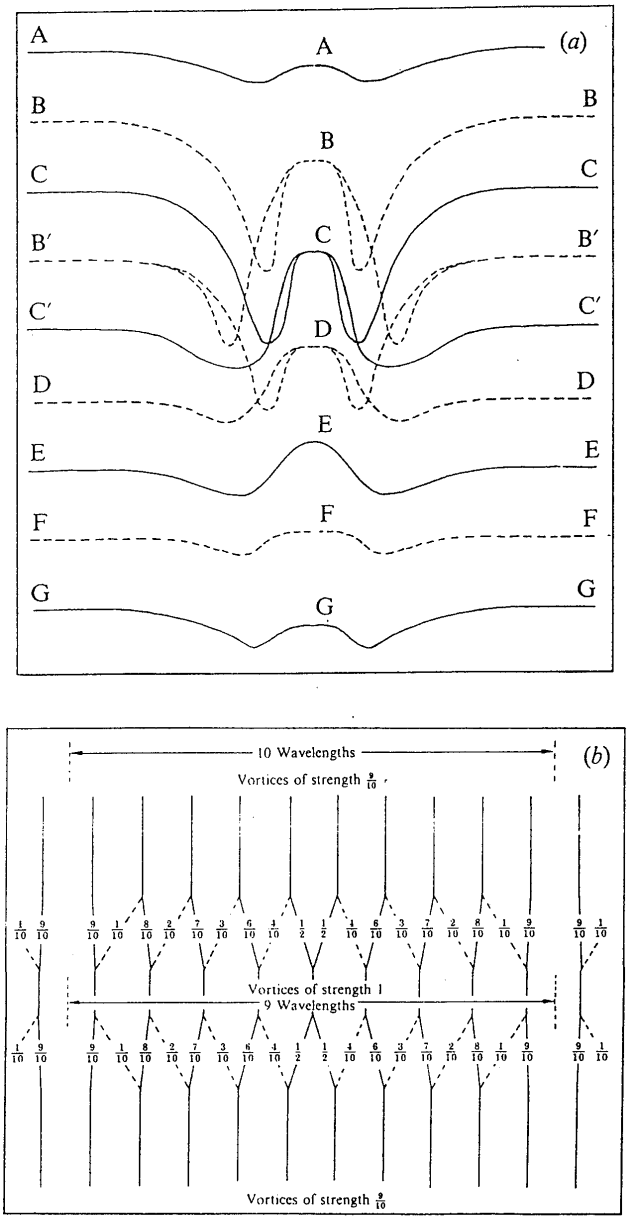

Figure 5.4 Williamson's proposal for vortex linking across a dislocation (from Williamson, 1992a).

vortex strength=Γ_0, high frequency vortex strength=$9\Gamma_0/10$). His proposal of the existence of "vortex links" is backed by his flow visualisation pictures, presented in the same paper. According to their strengths, he classifies the links into "primary links" (with strength$\geq\Gamma_0/2$), and "weak links" (with strength$<\Gamma_0/2$). The idealised diagram shows how the one cell could be connected to the other, through a series of such links of different strengths. Weak links do not, as a rule, appear in flow visualisation pictures, as their vorticity tends to be less intense.

In Williamson's proposed vortex connection scheme, one simplifying assumption is made: all vortices in each cell are considered to have the same strength. We have seen how, through the influence of the body and its near wake dynamics, this assumption is not necessarily correct. Earlier in this section, it was proposed that vortex strengths may fluctuate at the dislocation frequency. Williamson's dislocation model is for a far wake, and the influence of the body there is less apparent (but perhaps equally important).

A significant parameter in whether the vortex strengths fluctuate or not has to be the spanwise size of the cell. If the cell extends over a large portion of the span, the strength of the individual vortices would have to remain constant (from one cycle to another): the formation region fluctuations described earlier (resulting from the vortex dislocation) would be unable to spread over a large spanwise portion in order to have equal vortex strengths along the whole cell. On the other hand, however, if the cell size is small the influence of the dislocation could spread over its entire length, and vortex strengths could fluctuate. In Williamson's flow, the high frequency cell spreads over a large distance and hence his assumption for constant vortex strength seems reasonable. The same does not apply, however, for the low frequency cell. Its extent is limited and hence the dislocation could influence the whole cell.

Under the light of the observations made previously in this study, concerning the dislocation frequency, with the size of both cells (low and high frequency) being comparatively small, we would expect that vortex strengths could fluctuate at both sides of the dislocation. Considering that the f_l cell has the smaller size, maybe such fluctuations are more prominent there.

We have thus identified a possible source of "conflict" in the flow. On the one side, the presence of the dislocation (separating cells of two different frequencies) causes the vortices to bow in order to get inter-connected, thus causing f_d fluctuations in formation region size and hence base pressure, thus

causing a tendency of vortex strengths to fluctuate (also at f_d), with vortex strengths changing from cycle to cycle. The other side of the "conflict", stems from the spanwise size of each cell. The larger the cells, the more difficult they "find" it to readjust the strengths of their vortices according to the dislocation frequency.

One source of compromise in this conflict could again be found by considering the geometry of the vortex filaments. Let us consider an f_1 vortex having to connect to an out-of-phase f_2 vortex. Their connection depends on both vortices bending in order to meet each other. This could be achieved in a variety of possible bending combinations (f_1-vortex bending a lot, f_2-vortex not bending at all, or the other way round, or any intermediate "compromise"). Thus the degree to which vortices in each cell bend, could be determined by the flexibility of each cell to shed vortices of varying strengths, this flexibility itself being a function of the cell size.

So far we have not considered what the effects of vortex links (in particular the weak ones) may be. Vortex formation and vortex shedding tend to concentrate vorticity (that initially is spread in the shear layer) into discrete "lumps". The existence of weak vortex links thus appears to contradict that tendency, even though it appears necessary under Williamson's linking model. If, however, vortex strengths are allowed to fluctuate at the dislocation frequency, it is conceivable that they may adjust themselves in order for vortex interconnection to be achieved with the smallest possible number of weak vortex links. This possible tendency towards minimisation of weak vortex links could be yet one more factor that contributes to the determination of vortex strengths (in conjunction with cell size influence and dislocation frequency vortex strength oscillations).

It seems impossible, without considerably more sophisticated experimental technique, to determine the exact structure of vortex links. The occasional absence of weak links from flow visualisation pictures could either be attributed to the inadequacy of the visualising precipitate (smoke, dye, tin oxide, etc.), or could be due to the tendency of the flow to readjust the vortex strengths in the cells (possibly through the mechanisms described above, and only when such readjustment is possible) in order to make such (very weak) vortex links unnecessary.

Vortex links, of course, make it impossible to define the exact time of vortex splitting, as vortex splitting (of different degrees) may be occurring in

practically every shedding cycle. It thus seems more appropriate to define as the time of a vortex split the time when one cell has missed one complete shedding cycle. For example, when discussing figure 4.10, in the previous chapter, in the sequence of the eight photographs one vortex split occurred (the central cell missed only one shedding cycle), even though this split appeared in more than one shedding cycle (more prominently in photos (c) and (d)). The possible fluctuations in vortex strengths, as well as the existence of weak vortex links, are both unclear, judging from the flow visualisation photos and also from the quantitative measurements.

5.2.4 A *possible* mechanism for the spanwise motion of a dislocation

So far we have had clear indications that two cells of different frequencies exist, at least part of the time. The cellular nature of the flow is apparent both from flow visualisation and also from the study of the spectra of figures 4.2 and 4.4. Although the f_2 cell may (and probably does) induce f_2-frequency velocity fluctuations in the f_1 cell (and hence this could explain the gradual changes in the spectra of these figures, as we move from the peak to the valley) it seems more probable that in our problem the cell boundary (the dislocation) is not fixed in its spanwise position (in fact, one would only really expect "fixed" dislocations in bodies that have a spanwise step change in their geometry, not in the smooth periodic disturbance of our model). As the geometric disturbance of the model is quite mild, and the flow so irregular, it would be surprising if the dislocation chose a particular spanwise position.

Now let us consider, once again, the consequences of the bowed vortices. As was described previously, the vortices have to bend close to the dislocation for purely geometric reasons, in order to be linked to their counterparts on the other side of the dislocation. It seems reasonable to suggest, that on each side of the dislocation (at a given time) vortices will have to bend in opposite directions, i.e. while one will have to bend in the downstream direction, the other will have to bend towards the upstream direction. As a result, on the one side of the dislocation the formation region will tend to grow, while at the other side it will tend to shrink.

According to the mechanisms described earlier, this will result in an increase in base pressure on the one side, but a decrease on the other side. It is easy to see that all these phenomena will occur at the f_d frequency, and that there will therefore be a periodic component in the pressure gradient across the

dislocation, also at the dislocation frequency. If we assume a mean, spanwise dislocation position, sustained perhaps by some mean pressure drop across the dislocation, the periodic pressure gradient will act to "push" the dislocation back and forth relative to its mean position.

These ideas may give some insight into the physics behind the apparent unsteadiness in the dislocation position. They are not rigorously proven, and this mechanism may be either altogether wrong, or only partly responsible for the dislocation motion in the near wake.

5.3 The downstream evolution of the dislocation

The main aim of this work, as stated in chapter 2, is to study the dynamics of the near wake. This section will "stretch" the region of study a bit further downstream, up to positions 10h behind the model trailing edge, in order to observe the evolution of the dislocation created in the near wake. With this brief deviation from the near wake it is hoped that some interesting features of dislocations may emerge.

5.3.1 Experimental observations

The purpose of these measurements was to see whether the dislocation, once formed in the near wake, retained its spanwise position downstream or drifted in some way. Such a drift of the downstream dislocation position should not be confused with the movements in the spanwise position of the dislocation in the near wake, discussed previously. Those spanwise position fluctuations were not related to the motion of any fluid particles, but to the different position of the dislocation in successive shedding cycles. In the present case, we are interested in how inter-linked vortices evolve as they progress downstream.

The net effect of such a dislocation drift would be that as we progressed downstream spanwise cell sizes would vary, i.e. one of the two cells would spread into spanwise locations occupied by the other cell further upstream.

In the previous chapter, figure 4.2 showed the relative magnitudes of the two main frequency components (f_1 and f_2) at different spanwise positions in the near wake. Similar measurements were obtained at a downstream location of 10h and are presented in figure 5.5. Whereas in figure 4.2 the f_1 component was noticeable up to y/L=0.266, at the downstream position we can still see f_1 at

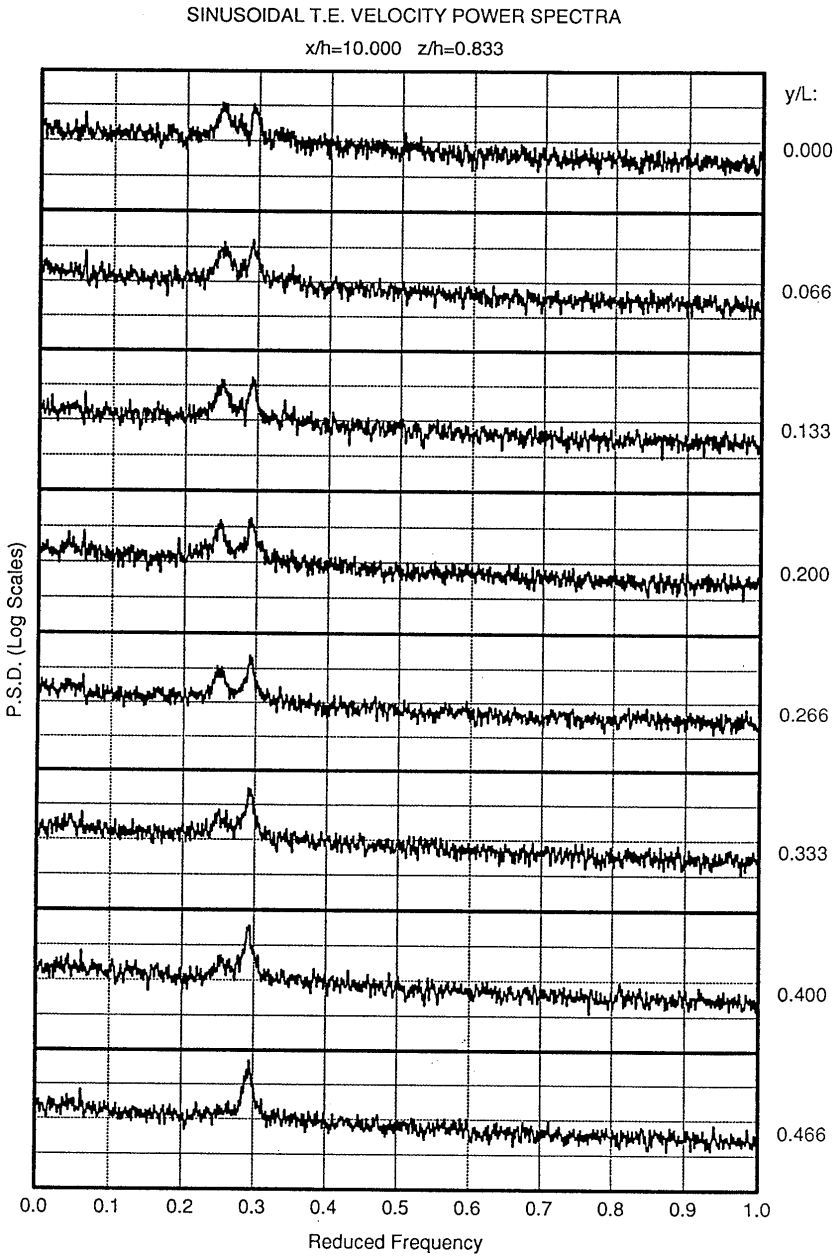

Figure 5.5 Sinusoidal trailing edge model: velocity power spectra for x/h=10, z/h=0.833 and y/L=0, 0.066, 0.133, 0.2, 0.266, 0.333, 0.4, 0.466. Comparison to figure 4.2 indicates that the low frequency cell has expanded in a spanwise sense.

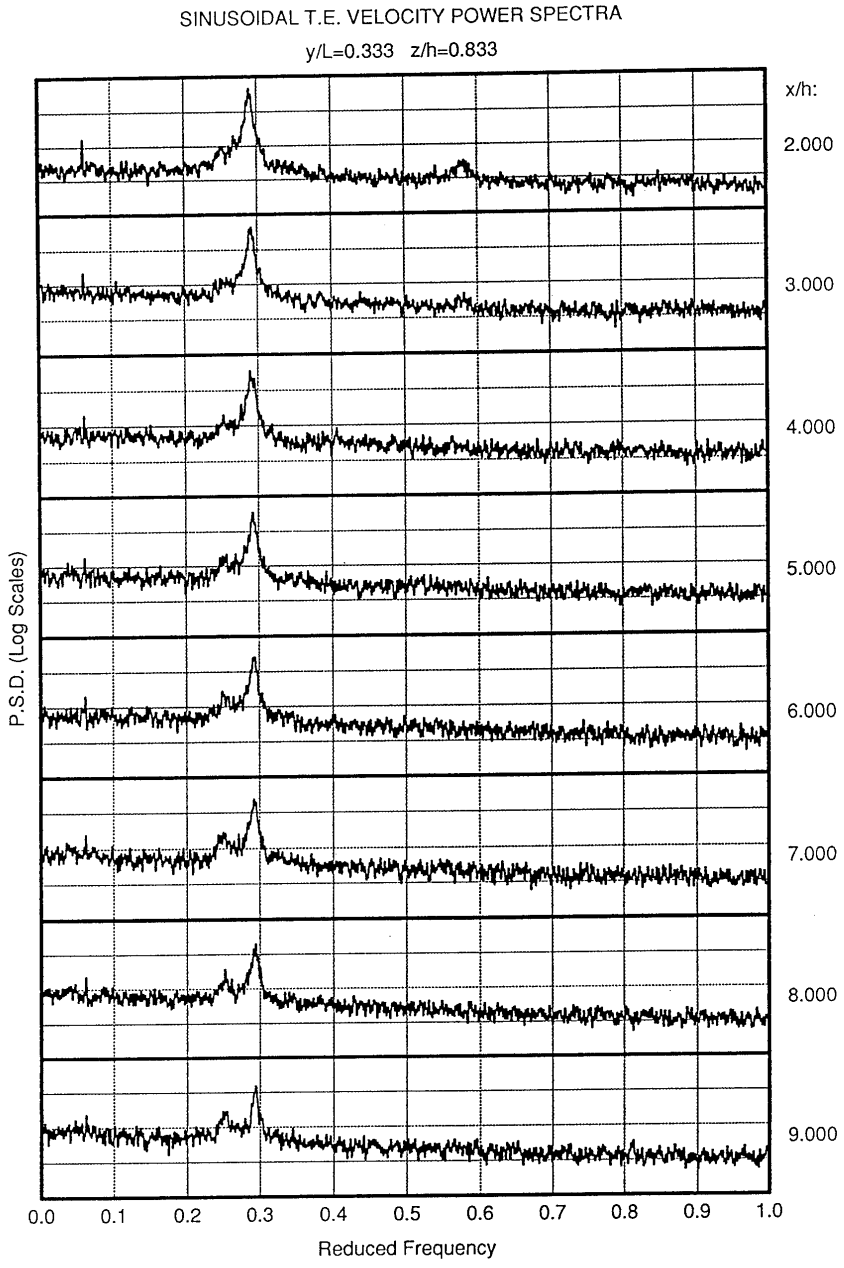

Figure 5.6 Sinusoidal trailing edge model: velocity power spectra for y/L=0.333, z/h=0.1 and x/h=2, 3, 4, 5, 6, 7, 8, 9. Note how the low (f_1) shedding frequency becomes more and more apparent as we move away from the model.

y/L=0.400. This implies that the f_1 cell has spread towards the valley. These effects are more striking in figure 5.6. In this plot, all spectra were obtained at the same spanwise position (y/L=0.333), but at different downstream locations. A noticeable feature is the gradual growth of the f_1 component, indicating an increase in the influence of the f_1 cell as we move away from the model.

We should also make a note on the total absence of a dislocation frequency component in both figures. This supports the discussion in the previous section which had identified the presence of the body as an amplifying factor for the dislocation frequency.

5.3.2 The expansion of the low frequency cell

Let us now consider the motion of a "vortex junction", the point in space where two vortices of the same sign join into a single vortex. We would expect such junctions to exist in a dislocation, where, for example, two high frequency vortices are linked to one low frequency vortex, through the process of vortex splitting. Thus, by considering the motion of a "vortex junction", we can gain some insight into the downstream evolution of the dislocation.

Towards the end of chapter 1, we had discussed Williamson's (1992a) proposals for the evolution of a vortex junction. Figure 1.12a, in particular, showed how the induced velocities due to a vortex branch would cause the junction to move axially, and the main vortex to split further. In the present study, however, we have observed the *low* frequency cell expanding. This appears to contradict with Williamson's proposed model: while in his proposals the tendency is for the main vortex to split further, in the present experiments the low frequency cell is expanding, which implies that the branch (high frequency) vortices are, in fact, merging.

Figure 5.7 is a sketch (influenced by Williamson's sketch of figure 1.12) which shows a possible, high Reynolds number mechanism whereby the branch vortices could merge, with the junction position thus moving in the opposite direction from that suggested by Williamson. We can see a strong vortex (strength=Γ) that has split into weaker vortices (strength=$\Gamma/2$) of the same sign, numbered (1) and (2). Let us now consider two planes, A and B, cutting the weaker vortices at the shaded areas, with plane A being closer to the vortex junction.

SCHEMATIC DIAGRAM OF A "VORTEX JUNCTION"

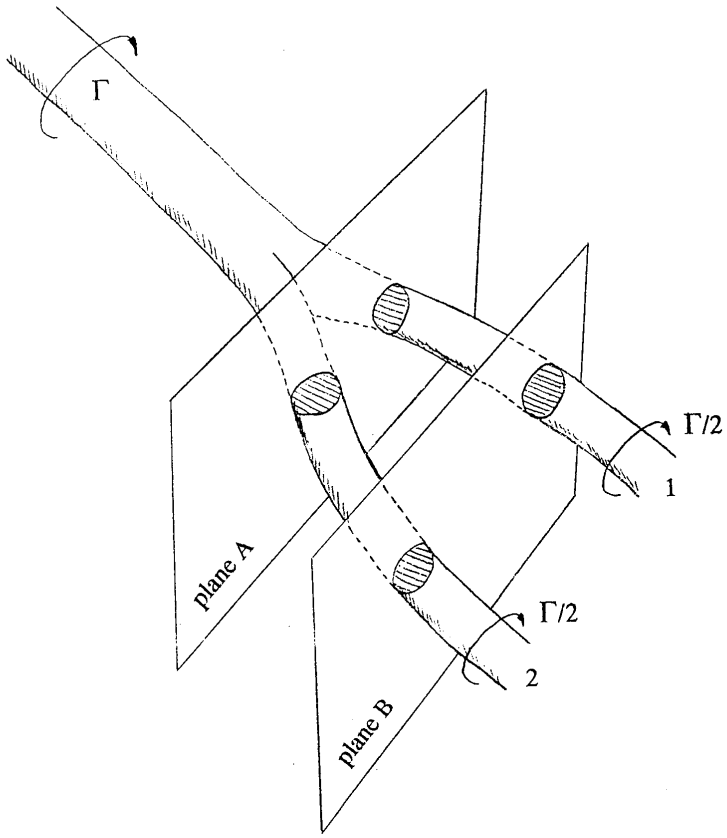

Figure 5.7 Definition diagram of a "vortex junction", showing the two planes (A and B) discussed in the text.

If we look, for reasons of simplification, at each one of the planes separately, we will see two vortex cores of strength $\Gamma/2$, that induce a velocity on each other. In plane A, the distance between these cores is smaller, so the vortex core pair will tend to rotate quicker than that of plane B. As a result, closer to the junction the two vortices (1) and (2) will tend to twist in a helical manner and hence, the two vortices will get stretched. Stretching will result in the two turbulent cores being pulled towards each other (because of the large strain rates) and also becoming much more energetic. It thus seems likely that, under the influence of turbulent diffusion, the two cores will merge, close to the vortex junction. The effect of this on the position of the junction will be that it will appear to move in the direction of the vortices (1) and (2).

An important role in this mechanism was apparently played by turbulence. It is uncertain whether a similar effect would be observed at lower Reynolds numbers. In any case, in the "rolling-up" mechanism suggested here could be the fundamental reason why the low frequency vortex cell seems to spread in the spanwise direction.

5.4 Concluding remarks on the dynamics of the dislocation

5.4.1 The interaction of unsteady wake parameters

This chapter mainly considered the consequences of the dual frequency characteristic in the wake of the sinusoidal model. It is widely accepted that a dislocation is the unavoidable result of a significant spanwise discontinuity in the phase of shedding. The dislocation examined in this study is of the vortex splitting type, i.e. there was no evidence for any looping across the wake (vortices would only link-up with similarly-signed vortices).

The source of the dislocation frequency, which was shown in this chapter to affect almost all parameters of the wake, is exactly the periodic variation of the shedding phase difference across the dislocation. If the two cells shed at f_1 and at f_2, the period of the phase difference will be the dislocation frequency f_d ($=f_2-f_1$). This chapter proposed numerous consequences of this simple fact:

a) When vortices on either side of the dislocation are out of phase, then in order to get linked to each other they will have to bend. The periodic bending of the vortices results in a periodic fluctuation of the size of the formation region.

The dislocation frequency fluctuations of the base pressure are probably a result of this fluctuation in the formation region size.

b) As a result of the f_d base pressure fluctuations, Kármán vortices should have strengths that also vary periodically, again at f_d.

c) The spanwise size of each of the two neighbouring cells must be an important parameter which determines the extent to which vortex strength fluctuations in the cell are permitted. A large cell will not be as "flexible" as a small one: formation region size and base pressure cannot fluctuate at f_d far away from the dislocation. The fluctuations in vortex strengths could also contribute in reducing the number of weak vortex links across the dislocation, which may explain why they have been difficult to observe in flow visualisation (they may, in fact, not be there).

d) A further suggestion concerns the probable spanwise motion of the dislocation. Vortices bend in order to meet their counterparts across the dislocation (as described in (a)). But to get linked, vortices on either side will have to bend in opposite directions and hence when the formation region on the one side shrinks, the formation region of the other side grows. It is proposed that a consequence of this must be a periodic (at f_d) pressure gradient across the dislocation, which may contribute in its spanwise motion.

As a separate observation, the f_1-cell was then found to expand downstream of the model, "eating into" the f_2-cell. It was proposed that the reason for this lies in the dynamics of "vortex junctions", the region where two vortices join into one (as happens in vortex splitting within a dislocation). The two vortices were said to roll-up (in a helical manner), with the strain and turbulent diffusion being the reason they merge.

5.4.2 Outstanding questions concerning the vortex dislocation

Model geometry was an important factor in the logical progression of the theories presented in this chapter. Key consequences of the model geometry were:

a) The dual frequency characteristic (to be discussed in more detail in chapter 6).

b) Vortex splitting *only*. No vortex looping due to mild geometrical disturbance.

c) Cell size.

d) Flexibility in dislocation position (no abrupt spanwise geometrical disturbance).

The theories presented in this chapter relied on these four points, and provided reasonable explanations for the specific phenomena observed in this flow. Outstanding questions fall into two groups: first, there are numerous uncertainties which concern the particular flow of this study, and second, other questions arise concerning the applicability of the proposals of this chapter to other flows. It is not possible to draw general conclusions from phenomena observed in the wake of just one particular model. Some of the unanswered questions about vortex dislocations in the near wake are:

a) To what extent do weak vortex links exist (especially in high Reynolds number flows)? Are they really suppressed by the fluctuations in the strength of the Kármán vortices?

b) Is the periodic pressure gradient across the dislocation the only reason for its spanwise motion?

c) What would be the effects of a fixed dislocation position, when fluctuating pressure gradients across it would not be balanced by its spanwise motion?

d) What would be the result if the two neighbouring cells were large in spanwise size (i.e. if the Kármán vortex strengths did not have the flexibility to fluctuate)?

e) What happens when there is vortex looping (and what exactly causes it)? (A small question which requires a very large answer.)

Thus the proposals of this chapter need to be confirmed for other flows satisfying similar conditions, and also need to be extended to flows showing significant differences from the present one, such as flows with stronger three-dimensionalities.

6. ON THE DYNAMICS OF THE FORMATION REGION

ABSTRACT : The dynamics of the formation region are discussed, by considering the interaction of mean, time-averaged quantities. It is suggested that forming vortices have a tendency to straighten-out. A concept is proposed which links the vortex formation length to other wake parameters, most notably wake width and base pressure. Wake similarity arguments are used in order to predict the distribution of mean shedding frequency along the span. A mechanism termed "spanwise lock-in" is proposed as the main cause for the discretisation of the mean shedding frequency into the two observed shedding frequencies. Fluctuations in the dislocation position are again said to play an important role in the wake dynamics.

6.1 Introduction

6.1.1 The mean wake parameters

A theory was proposed in the previous chapter that discussed the significance of the dislocation frequency f_d for the dynamics of the near wake. A large number of the near wake parameters (formation region size, base pressure, spanwise dislocation position, vortex strength) were found to fluctuate at that frequency. Although the theory explained the dynamics of the low frequency fluctuations of all the wake parameters, it did take, a priori, the presence of the two shedding frequencies for granted. Furthermore, the mean values of all these fluctuating parameters were not considered: the important issue of the previous chapter was the dislocation frequency fluctuations.

The theory to be presented in this chapter will try to establish the mechanisms that determine the mean values of the wake parameters. It is hoped to be able to adequately explain, for example, the fundamental cause of the dual frequency feature, the mean base pressure distribution, and other important mean wake characteristics.

6.1.2 The two-dimensional formation region

Two-dimensional near wakes have been the object of a large number of previous studies. In chapter 1 there was a description of Gerrard's (1966b) formation region dynamics model. Two characteristic lengths were suggested in

that paper: the distance from the body to the forming vortex (the formation length, l_f) and the thickness of the shear layer just before the point of vortex formation (the diffusion length). These two characteristic lengths were judged to play an important role in the balance of the vortex formation flows, diagrammatically illustrated in figure 1.1.

A main issue that has attracted a lot of attention is the selection of the shedding frequency. It is interesting to note the similarity between older and more recent studies. Roshko (1954), Gerrard (1966b) and others have discussed the possible existence of a "universal" Strouhal number that would depend on characteristic length scales of the *wake*, not the model. More recent studies (e.g. by Karniadakis and Triantafyllou, 1989) have relied on the stability characteristics of wake velocity profiles to predict the Strouhal number. Conceptually, both approaches are based on the assumption that some kind of wake instability must determine the wake oscillation frequency.

The theories mentioned above and also in chapter 1 highlight the level of complexity even of the two-dimensional near wake. In closing this very brief detour into two dimensions, a few important concepts should be emphasised.

a) The role of the wake (and in particular the interacting shear layers) as a feedback mechanism is important for the sustaining of vortex shedding.

b) The emphasis for the selection of the shedding frequency is more on the instability characteristics of the actual flow pattern of the wake, which in turn should be viewed as a consequence of the body geometry.

c) A number of characteristic length scales (formation length, wake width, diffusion length) are important in order to predict the resulting flow pattern.

6.1.3 The present study: the three-dimensional formation region

Let us now consider the three-dimensional wake again. We expect the same concepts outlined above to apply, but with the addition of a few complicating factors:

a) As was also discussed in the previous chapter, when there is no vortex looping in the wake, the total strength of the vortices that are formed and shed downstream, on each side of the wake, must be constant along the span. Again we should note that, for a high Reynolds number, this assumption holds for the instant

when vorticity from the shear layer is cut off (and the vortex shed downstream). When vortices from the two sides of the wake become more diffuse and start to interact further downstream, we should not use the above condition.

b) In a similar way that lock-in occurs in many cases when some kind of periodic forcing is applied to the wake, in the three-dimensional wake we may have a spanwise form of forcing from one flow section to its neighbouring section. This could be significant should there arise a case of two (or more) shedding frequencies in the wake.

c) Apart from the coupling of shedding frequencies along the span, there must also be some form of spanwise coupling in quantities like base pressure, formation length, etc.

d) In the three dimensions we should also consider two more vortex effects: vorticity in the x and the z directions and also vortex stretching, both of which can not occur in two dimensions.

For this chapter, the fact that key wake features like base pressure and shedding frequency were not constant along its span, made the sinusoidal model results more attractive for such a study. As a simplification, the diffusion length (a parameter considered by Gerrard to be a significant characteristic length of the wake) will not enter the considerations of the model to be presented. As it is mainly a function of the Reynolds number and the free stream turbulence level, and as the Reynolds number of this investigation is constant (Re=40000), the diffusion length will also be taken to be a constant, and hence not significant for any proposed model considering spanwise variations of wake quantities.

An important feature that will enter our considerations will be the relation of vorticity destruction in the near wake (through entrainment and vortex cancellation) to the formation length. Generally speaking, the level of entrainment is expected to rise as the formation length becomes longer.

6.2 A model for the determination of the mean wake properties

6.2.1 The measurement of the mean formation length and mean wake width

According to Gerrard's model (1966b), a vortex grows while it is being fed with vorticity from the separated shear layer. During its formation the position of its centre remains more or less at a fixed point relative to the body. When the

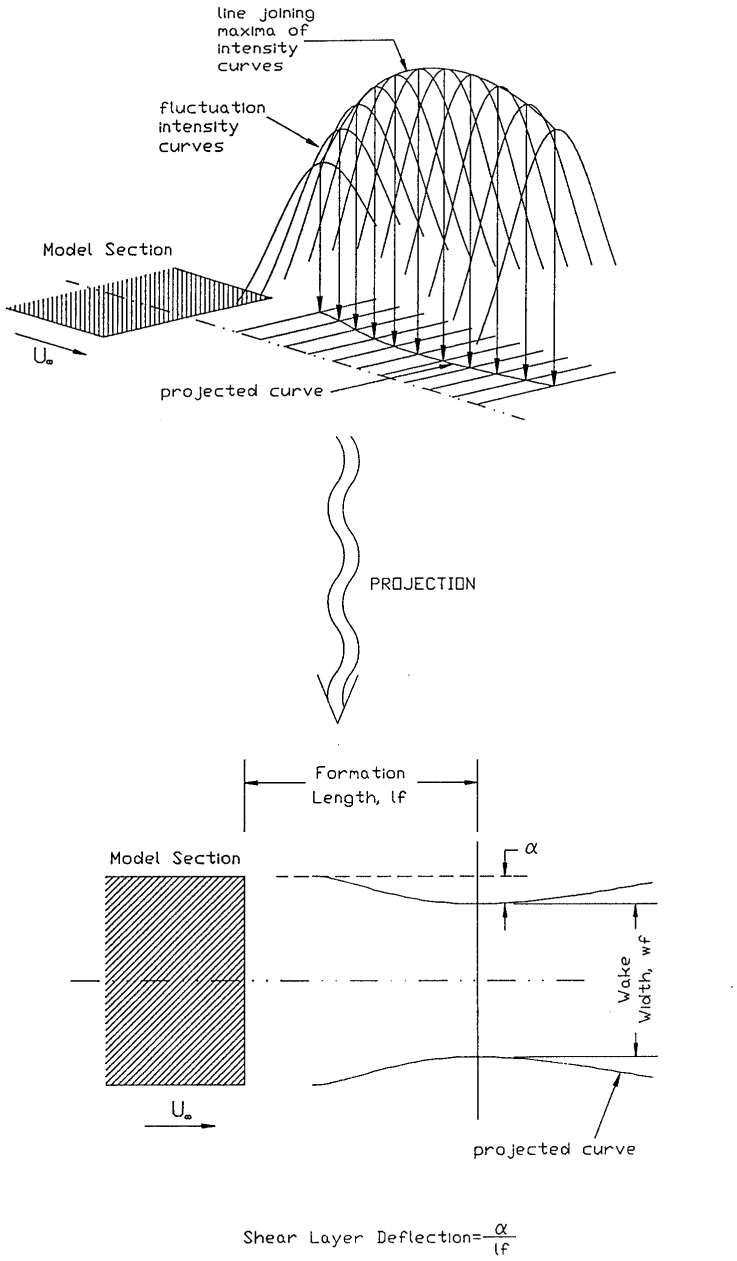

Figure 6.1 Definition diagram showing the criterion for the determination of the formation position (whence the formation length, the wake width and the shear layer deflection can be derived).

vortex becomes strong enough to draw the opposite shear layer across the wake, entrainment of oppositely-signed vorticity into the shear layer interrupts the feeding of vorticity to the growing vortex. It is at that instant when we can say that the formation process has finished and the vortex has been shed downstream.

There now arises the question how to determine the formation position experimentally, for each spanwise position. A hot wire was made to traverse the wake covering a dense grid (cell size=0.1h×0.1h, local x_{min}=0.33h, local x_{max}=1.93h, z_{min}=0, z_{max}=0.8h) for different values of y (spanwise position). The probe axis was parallel to the y-axis, so that it would record velocities induced by the predominantly y-oriented Kármán vortices. With this set-up it is not possible to determine rigorously the formation position and hence some assumptions need to be made.

If, for a given spanwise section, we imagine the circulation flux (instead of discrete vortices) through a vertical line, we may say that the point of maximum flux is related to the point along this vertical axis where the velocity fluctuations are at their maximum. For the time being, let us assume that these two points coincide. Thus, for each spanwise section and for each streamwise position we can determine the point along the z-axis where there is the maximum flux of circulation. Now, after their formation is completed, vortices are convected downstream, but also move slowly away from the centre-wake. Before the formation region, the vorticity-carrying shear layer is being pulled inwards by the suction in the near wake. We can thus conclude that the formation point is the point where the maximum circulation flux z co-ordinate is a minimum. This procedure of determining the formation point (also used by Bearman, 1965) is shown schematically in figure 6.1. In the top diagram, the maxima of the velocity fluctuation intensity curves are joined in order to determine the curve of maximum circulation flux. Once this has been obtained, the position of vortex formation is taken to be at the closest point of this curve to the centre-wake (bottom diagram).

The measured formation position was used to determine the formation length, l_f (the values presented later always using the local trailing edge as the reference) and the wake width at formation, w_f. As the analysis of the signals used spectral techniques, it was considered advantageous to select appropriate frequency ranges in order to determine the velocity fluctuation intensity curves. In that way we can detect the mean formation position for each of the two shedding frequencies and also we can eliminate the irrelevant interference of noise and any other non-shedding frequencies. All evaluations of maxima or minima of curves

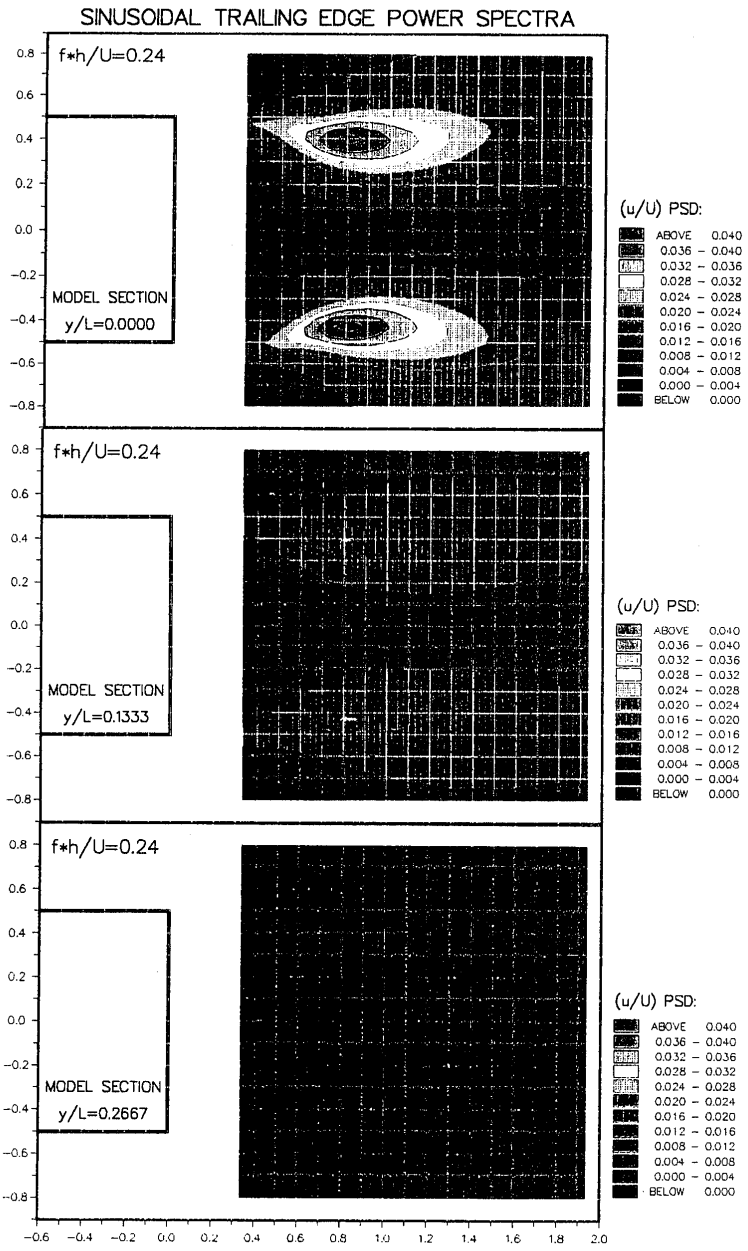

Figure 6.3 Contour plots showing the velocity f_1 (=0.24) fluctuation intensities in the near wake of the sinusoidal model, at different spanwise positions. Note the decay as we move towards the valley.

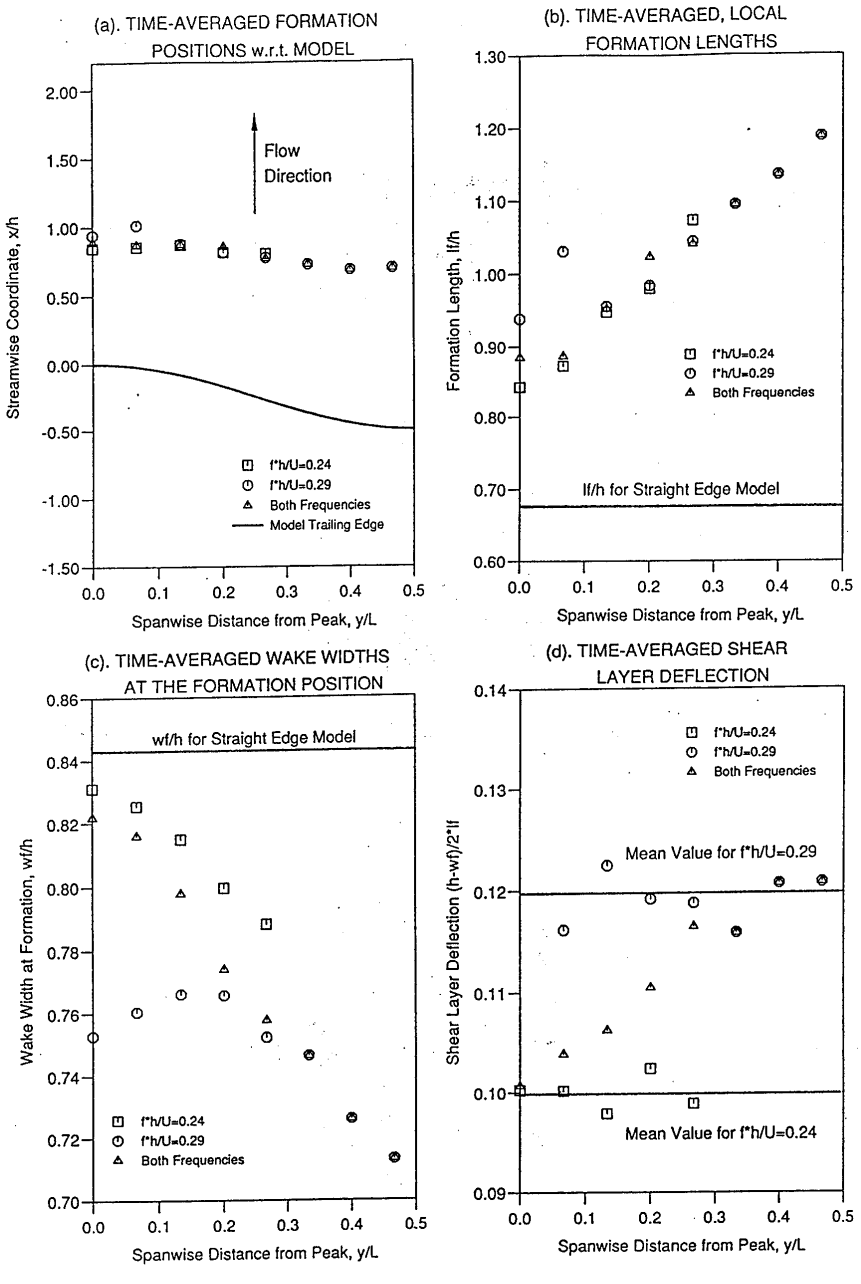

Figure 6.2 Spanwise variations of: (a) time-averaged formation positions w.r.t. model (note the straightening of the vortices), (b) time-averaged local formation lengths, (c) time-averaged wake widths (note the difference between the two frequencies, f_1 and f_2), and (d) time-averaged shear layer deflection.

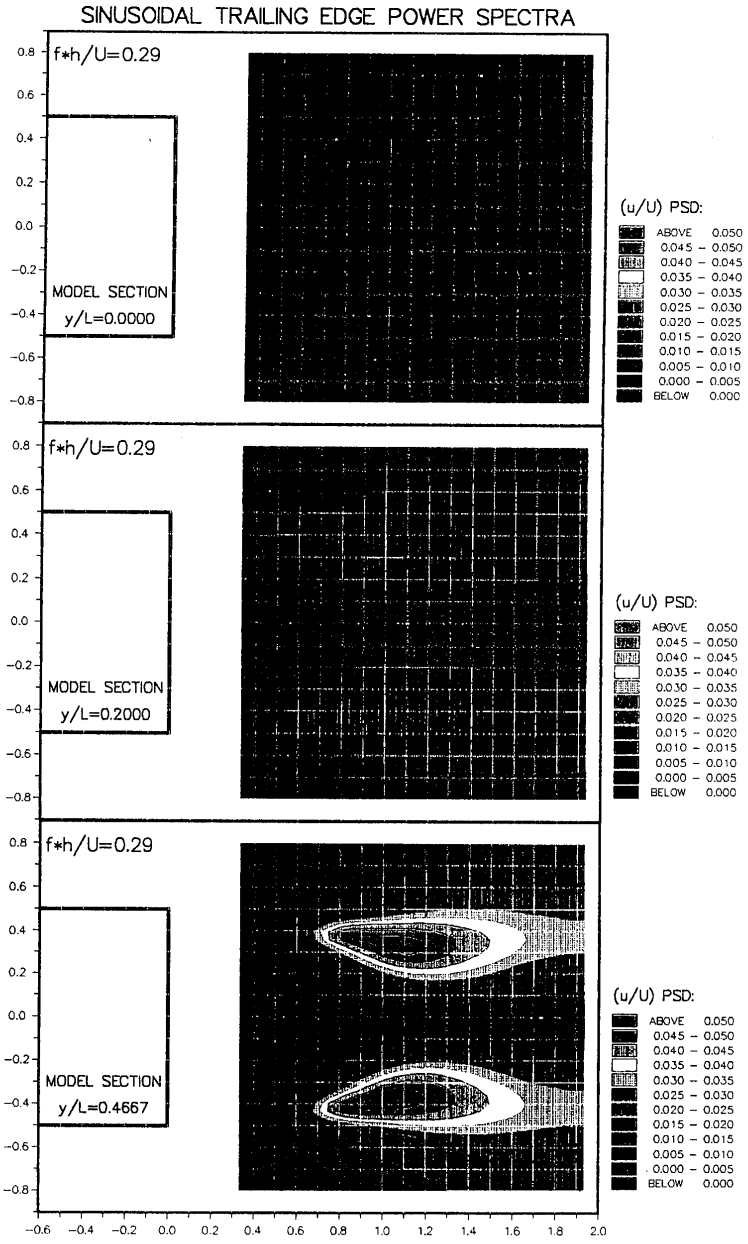

Figure 6.4 Contour plots showing the velocity f_2 (=0.29) fluctuation intensities in the near wake of the sinusoidal model, at different spanwise positions. Note the weakness of the f_2 fluctuations in the region of the peak.

used a polynomial fitting technique to detect a maximum (or minimum) lying between two node points of the grid traversed by the hot-wire probe.

Schaefer and Eskinazi (1959) used a simple viscous core model for the wake and showed analytically that the actual maximum circulation flux is not exactly at the point stated above, but a bit closer to the wake centre. The maximum velocity fluctuations were found to be approximately at the immediate neighbourhood of the core edge, farthest from the centre-wake. This effectively means that the actual wake width is smaller than the values to be obtained by the method described above. No estimate was made for the vortex core diameter, and therefore the suggestions of Schaefer and Eskinazi will not affect the results presented later, but should nevertheless be kept in mind.

6.2.2 The formation length

The formation length was measured for three frequency ranges: f_1 (S=0.24), f_2 (S=0.29) and the combination of these two shedding frequencies.

Figure 6.2a shows the formation position relative to the model trailing edge. We can see that the forming vortex has the tendency to straighten out and not follow the exact shape of the model trailing edge. This is reminiscent of the vortex volume minimisation tendency observed also by Breidenthal (1980). Generally, the total induced kinetic energy of the forming vortex would be larger if that vortex followed the model trailing edge. We can therefore perhaps attribute this straightening out of the forming vortex to the inherent tendency of the flow to minimise its energy.

Figure 6.2b shows the result of the vortex straightening. The formation length (always measured from the local model trailing edge) is longer at the valley than at the peak. The two shedding frequencies seem to show similar trends and from the diagram we cannot really distinguish between them. The first two points for the high shedding frequency (S=0.29) should not be taken very seriously. We have observed earlier that this frequency is very weak at the peak, its signal there owed to a large extent to induced velocity fluctuations.

Figure 6.3 shows the distribution of velocity power spectral density for S=0.24. It is clear that this frequency dies off quickly as we move towards the valley. Therefore points for that frequency were obtained only up to y/L=0.266. The contrast between the two shedding frequencies is shown in the similar plots of figure 6.4. Here the fluctuation intensity is much smaller at the peak, but quickly

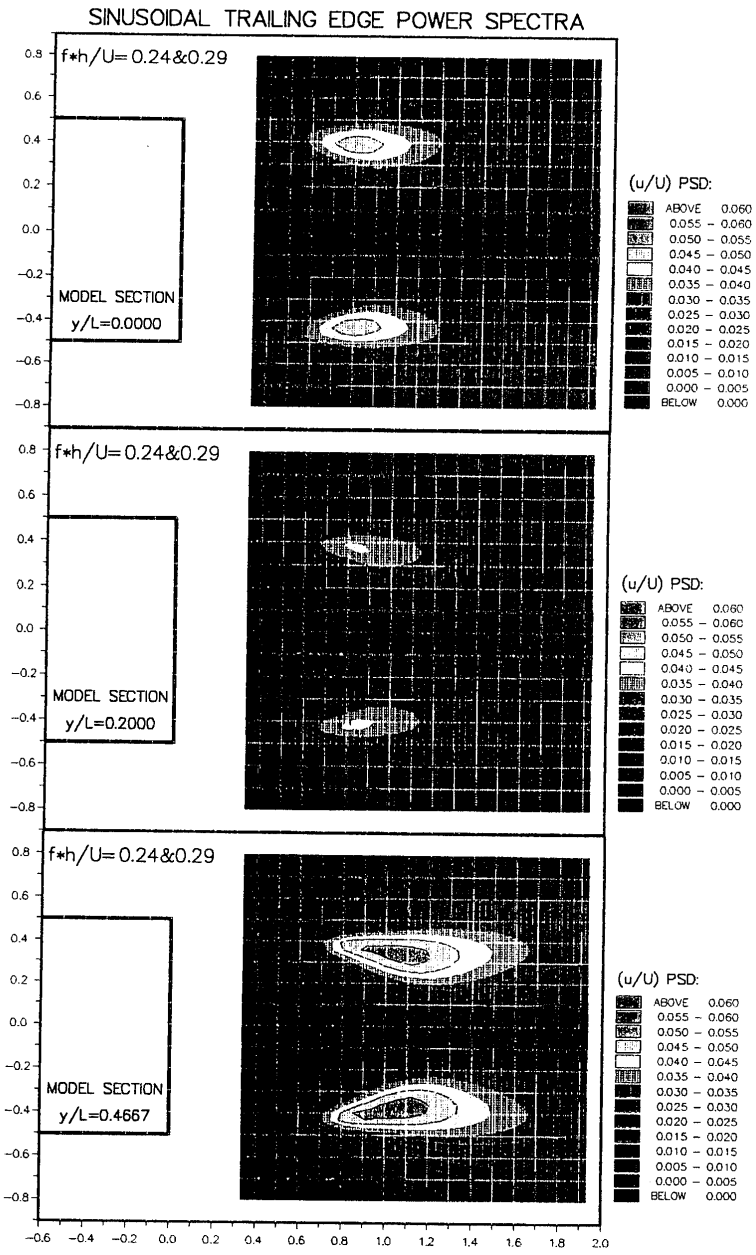

Figure 6.5 Contour plots showing the velocity shedding frequency (f_1 and f_2) fluctuation intensities in the near wake of the sinusoidal model, at different spanwise positions. Note how the high fluctuation intensities occur further away from the model at the valley than at the peak.

increases towards the valley. Of course we had observed the same trends when discussing the power spectra in earlier chapters, but as the scales there were logarithmic, it was perhaps not so easy to detect, for example, how weak the f_2 fluctuations really are at the peak.

Figure 6.5 shows the contours of the fluctuation intensities for the combination of the two frequencies. The results displayed in these last three figures were analysed according to the procedure of figure 6.1 in order to obtain values for the formation length and the wake width. That the vortex formation position is further away from the valley than from the peak is visibly obvious from figure 6.5.

In the past, increase in the formation length has been generally linked to a reduction in base drag. This was observed by many investigators, e.g. by Bearman (in 1965 by the use of splitter plates and in 1967a by applying base bleed - see also figure 1.4). The thinking behind this idea is basically that an increased formation length means increased entrainment, i.e. weaker vortices, and hence less base drag. This trend is also obeyed in the present case when we compare the straight edge formation length (solid line in figure 6.2b) to the mean formation length for the sinusoidal model. The straight edge model had a higher base drag, which is complemented by a much shorter formation length.

Let us now consider the sinusoidal model in detail. Previous measurements of the base pressure had revealed lower local base drag at the peak (see figure 4.1). Presently, we have also observed (in figure 6.2b) a significantly smaller formation length at the peak. This seems to contradict the trend discussed above, linking the drag to the formation length.

Closer study will reveal that this phenomenon is not a contradiction to the previous theories but their extension into the third dimension. The base pressure Cp_b can be related to the velocity at separation by the equation $Cp_b=1-(u_s/U)^2$, where u_s is the velocity outside the boundary layer at the separation point. Davies (1976) discussed the second order effect of the fluctuation of u_s and concluded that it was negligible. This was also checked in the present study reaching the same conclusion. The mean rate of vorticity shed from, say, the top edge of the model is given by $d\Gamma/dt=(1/2)u_s^2$, as all the circulation shed lies within the boundary layer. Now some of this vorticity is cancelled in the formation region, while a fraction α survives and contributes to the strength of the formed vortex of that sign. An expression for α is:

$$\alpha = \frac{S\,\Gamma_v}{(1/2)Uh(1-Cp_b)} \qquad (1)$$

where Γ_V is the mean vortex strength just after formation. Note that the nominator here represents the circulation flux carried by, say, positive, Kármán vortices, while the denominator is based on combining the two previous equations, and represents the vorticity shed from the one side of the trailing edge. Effectively, the three-dimensional condition mentioned in the introduction of this chapter (resulting from the continuity of vortex lines and provided that there is no vortex looping), is that $d(S\Gamma_V)/dy=0$. Now the relation of the fraction α to the formation length l_f was also explained earlier. As entrainment (and hence vorticity cancellation) increases with l_f, we would expect α to decrease as l_f increases (i.e. $d\alpha/dl_f<0$). If we satisfy $d(S\Gamma_V)/dy=0$ then from (1) we get $d\alpha/dCp_b>0$. Hence, from these two inequalities and taking $C_D=-Cp_b$, we get $dC_D/dl_f>0$, i.e. local base drag increases with formation length.

To explain this qualitatively, when we have a larger formation length, there will be more vorticity cancellation, and hence, if we want to satisfy the condition that the total vorticity shed per unit time in the formed vortices does not vary along the span, we must have a higher rate of circulation shed at the trailing edge. This in turn implies higher separation velocity and hence higher drag. It should be stressed, once again, that the use of this concept is solely to be applied in order to compare local wake properties of different spanwise locations of a particular model.

The explanation above thus agrees well with the observed trends in formation length and base pressure for the sinusoidal model. We should perhaps make a note here for the applicability of this concept to models of other shapes. If there is no vortex looping, it should be possible to apply some similar concept. However, in each case the particular relation between vorticity cancellation and the local spanwise conditions should be established. In the present case vorticity cancellation (due to the geometrical simplicity of the model) was directly related to the formation length. In some geometries we may have some spanwise variable (e.g. a splitter plate with a spanwise geometrical disturbance) which affects the level of entrainment. In such cases the application of the above concept is more complicated, as the relation between formation length and entrainment is not as clear cut as it is for the present investigation.

6.2.3 The wake width and the deflection of the separated shear layer

The theory described in the previous section provided us with a good explanation on why the base drag is higher at the valley of the sinusoidal model. There is another issue, however, that is still unaddressed. Traditionally, the decrease of base drag with an increase of formation length had been also explained from the point of view of the curvature of the separated shear layer. A shorter formation length usually implied a shear layer curving more rapidly towards the centre-wake. This increased streamline curvature would have to be balanced (or even caused) by a larger pressure drop across the shear layer (as we move from the undisturbed stream towards the centre-wake). This factor thus seemed to fit in well with the traditional relation between formation length and base pressure.

The curvature of the shear layer does not, however, depend only on the formation length but also on the wake width at formation. If the vortices form closer to the centre wake, the curvature of the shear layer will be larger. If we now compare the peak and the valley, at the valley we have longer formation length and higher local base drag. Therefore, in order to balance the larger drag by a higher shear layer curvature, we may expect a narrower wake. This agrees well with the trends of figure 6.2c (the triangular markers representing the mean wake width for both shedding frequencies - the variation between the two shedding frequencies will be discussed later).

The curvature of the shear layer is a difficult quantity to measure accurately. Conceptually we could approximate it by the *shear layer deflection* δ. The definition of this quantity can be seen also from the lower part of figure 6.1, where α is taken to be the vertical distance between the formation position and the point of separation. Now $\alpha \ll l_f$, and hence the shear layer deflection can be taken as $\delta=\alpha/l_f$ (since $\alpha=(h-w_f)/2$, we also get $\delta=(h-w_f)/2l_f$). Shear layer deflection is thus an easy quantity to measure, but we should not forget that it not quite the same as the shear layer curvature. We should therefore be cautious when thinking in terms of a direct Cp_b-δ relationship.

Shear layer deflection has been plotted against spanwise position in figure 6.2d. Again the trend of the mean value seems to fit in well with the base pressure trend. Figure 6.2d also presents us with a somewhat surprising fact: if we plot values of δ obtained for the two shedding frequencies separately, we can clearly see that the shear layer deflection at each of these two frequencies lies approximately on a δ=constant line. The difference between the two levels is

about 20%. Shear layer deflection is then found to be a function of shedding frequency, at least along the span of one particular model.

The value of δ for the straight edge model was found to be about 0.115. This initially seems surprising, as we would expect it to be larger than that observed for the sinusoidal model at f_2. We should remember, however, our previous observation on the wake width, w_f. From Schaefer and Eskinazi (1959) we had concluded that the actual wake width is probably narrower than that which we measure by about two core radii. Our inability to measure the core diameter forced us to use this distorted value for w_f. If we assume the core diameter to be about 0.1h (probably a conservative estimate), the sinusoidal model values for δ get shifted up (to about 0.157 for f_1 and 0.166 for f_2), while (due to its much shorter formation length) the straight edge would yield a value of 0.19. The above consideration should just serve to emphasise the pitfalls in interpreting the plots of δ. The qualitative conclusions of figure 6.2d should be (a) that the combination of longer formation length and higher drag leads to a narrower wake, and (b) that there is a significant difference between the mean values of shear layer curvature at the two shedding frequencies (indicated perhaps by the 20% difference in the value of δ).

6.2.4 The relation of the base pressure to the shedding frequency

Given the conceptual connection between shear layer deflection and base pressure, it is tempting to say that the base pressure may also be a function of the shedding frequency, thus implying that base pressure may be fairly constant within each cell and that there may be a steady pressure gradient across the dislocation (this, of course, should not be confused with the fluctuating pressure gradient suggested in the previous chapter). Should this be the case, the smoothly varying base pressure distribution of figure 4.1 could be the result of a pressure gradient "step" (the theoretical discontinuity being the instantaneous position of the dislocation), moving back and forth with the dislocation. The mean base pressure at each point would depend directly on how much time that point spent at each of the two shedding frequencies.

The latter could be obtained by measuring the mean shedding frequency. This was accomplished by counting velocity signal zero-crossings for large lengths of data. The resulting "time-averaged" Strouhal number is plotted against the span in figure 6.6b (square markers). The continuous lines show the two Strouhal numbers (f_1=0.24 and f_2=0.29). We can see how the time-averaged Strouhal

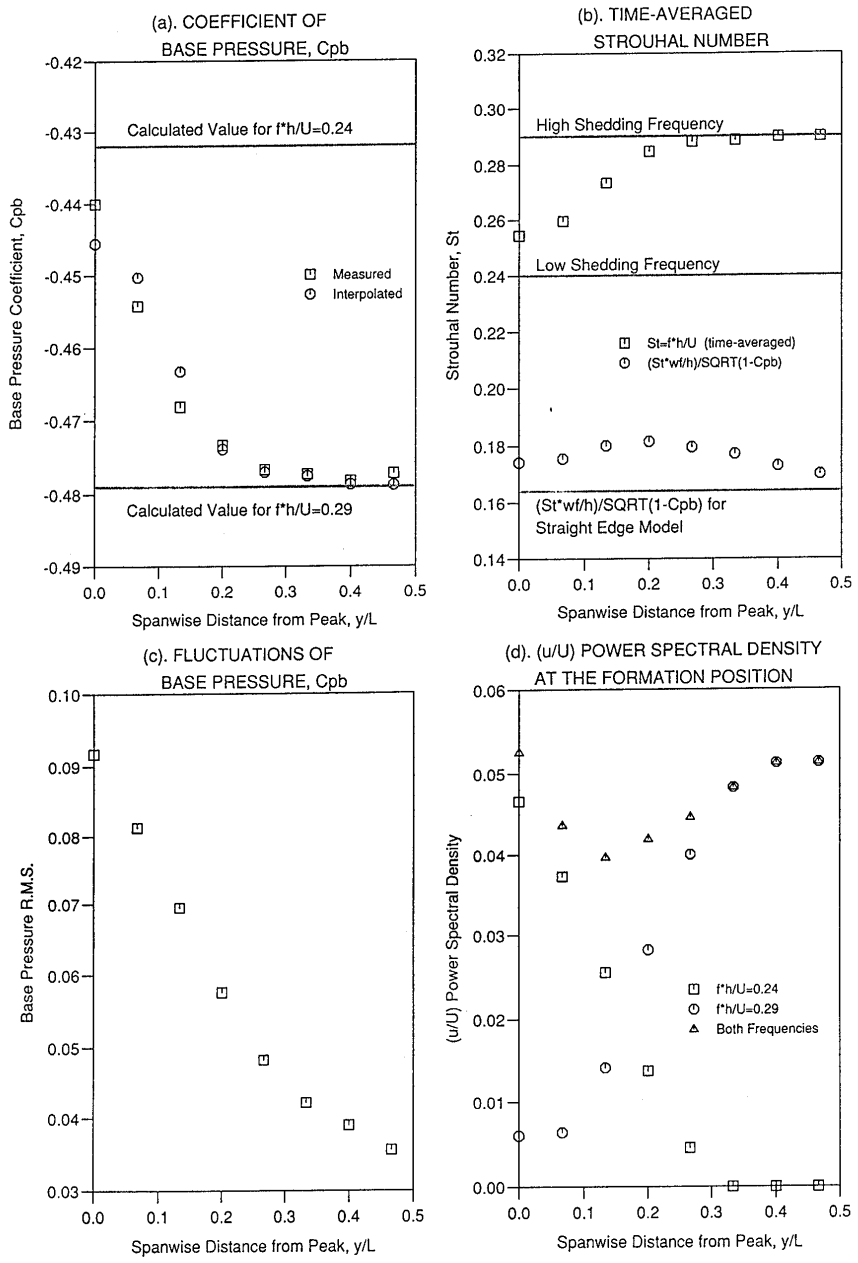

Figure 6.6 Spanwise variations of: (a) base pressure coefficient, (b) time-averaged Strouhal number (based on both the model and the wake parameters), (c) base pressure fluctuations, and (d) velocity fluctuations at the formation position.

number lies between those two levels. By interpolation we can also deduce the proportion of time spent at each frequency. Note that from figure 6.6b, f_2-shedding has to happen some times at the peak (but not very much), while f_1-shedding never happens at the valley, in agreement with previous observations.

We can now check the simplistic model that for any spanwise point, the base pressure fluctuates between two main levels, depending on the side of the dislocation the point lies on. Let us define the two levels to be Cp_{b1} and Cp_{b2}. Values for Cp_{b1} and Cp_{b2} were estimated using a least-squares approximation to the known, mean base pressure distribution ($Cp_{b1}\approx$-0.432, $Cp_{b2}\approx$-0.479). The interpolated, time-averaged base pressure distribution is plotted together with the measured distribution in figure 6.6a. The agreement between the two seems to be quite good, perhaps justifying the simple model based on a 1:1 base pressure-shedding frequency relation. Note that the agreement is, admittedly, enhanced by the least squares calculation. The proposed base pressure model is quite crude, and reality is undoubtedly more complicated. Thus figure 6.6a serves to illustrate and prove a general tendency of the flow; to suggest that reality follows such a simple rule would be quite naive.

We should pause to understand the physical significance of these observations. Clearly there is no universal relation between the base pressure and the Strouhal number: for the straight edge model the Strouhal number is equal to the low frequency Strouhal number of the sinusoidal model. As we have seen, the base drag is much higher. Thus emphasis should be put not on the S-Cp_b relationship, but on the probable near-constant base pressure within each shedding cell. Now within each cell vortices are fairly parallel, apart from the edges, close to the dislocation. The tilting and bending of vortices close to the dislocation (for vortex splitting to occur) results in a strong streamwise component of vorticity, which may act to sustain a steep base pressure gradient at that spanwise dislocation position. We would not expect to observe similar levels of streamwise vorticity in the middle of a cell, and therefore the mean base pressure may not show any such step changes within that cell.

If there was indeed a certain, constant mean base pressure value for each cell, we would arrive at a dead-end: the value of $d\Gamma/dt$ would also have to fluctuate between two near-constant values (arising from Cp_{b1} and Cp_{b2}). Then the link between formation length and base pressure would collapse, because in figure 6.2b the formation lengths for f_1 and f_2 would each have to have a certain,

constant value. By the nature of vortex inter-linking, the formation length must not show any large discontinuities along the span (and indeed it does not).

Based on the simplistic model linking base pressure to the shedding frequency, we may therefore suggest a more realistic one. In each cell base drag would still show a gradually increasing trend moving towards the valley. A steep change would occur across the dislocation. Given that the formation length does not show any equivalent discontinuities (figure 6.2b), it is possible that the discrepancy between the wake widths at the two frequencies (figure 6.2c) could compensate for the step change that would also occur for $d\Gamma/dt$ (resulting from the step change of the base drag across the dislocation). The wake is a bit narrower at the high shedding frequency. The closer proximity of the two shear layers could increase entrainment, thus compensating this step change in $d\Gamma/dt$ across the dislocation.

Hence we can conclude that there will be a strong base pressure gradient across the dislocation. The pressure gradient is thought to be sustained by streamwise vorticity that arises through the bending of vortex filaments in the vicinity of the dislocation. This pressure gradient is distinct from the one observed in the previous chapter that fluctuated at the dislocation frequency.

6.2.5 The determination of time-averaged Strouhal number

In our passage towards understanding the selection of the two shedding frequencies, we will first consider how the time-averaged Strouhal number could arise. The use of time-averaged quantities is valid as an approximation in this case because we want to establish general trends in the wake. Of course it would be nice to be able to explain the following phenomena in terms of the two shedding frequencies separately but, as will be discussed later, some complications arise in that case.

The concept of a "universal" Strouhal number which was outlined in the introduction of this chapter has been appreciated since 1954 (Roshko). Very simply, it considers near wake properties to be the relevant parameters for the selection of frequency, as opposed to global properties. The Strouhal number, by its conventional definition, is given by $S=f^*h/U$. Both the model height h and the free stream velocity U should not be considered as totally relevant parameters. In the near wake region where the vortex shedding instability arises, the flow cannot directly "know" what the values of U and h are. Hence, more relevant would be the local parameters, the wake width at formation (w_f) and the velocity outside the

wake at that formation position. The latter wake parameter can be taken to be directly related to u_S (the velocity at the separation point, defined previously, where $u_S/U=\sqrt{(1-Cp_b)}$). For the present study, we can thus define a "wake Strouhal number" S_*, given by:

$$S_* = \frac{S(w_f / h)}{\sqrt{1 - Cp_b}}$$

The circular markers in figure 6.6b show the variation of this quantity along the span. A good collapsing of the shedding frequency has been achieved ($S_* \approx 0.17$ along he span), especially when the S_* curve is compared to that of the time-averaged S (in the latter there is a much larger variation of the Strouhal number along the span). The value obtained for the straight edge model is also quite close.

In terms of significance, the wake Strouhal number in the present study is less ambitious than the universal number suggested in the past by other investigators. It has not been attempted to predict the actual magnitude of the Strouhal number, but to explain how this number has to vary along the span of the sinusoidal model. The advantage of the present body geometry is that the second important characteristic length suggested by Gerrard (1966b), the diffusion length, does not vary along the span (variations due to formation length changes along the span can only be thought of as a second order effect). As a result, we are left with only one characteristic length (taken here to be the wake width) and we can thus apply similarity arguments to understand the selection of the time-averaged shedding frequency along the model span. Hence we have been able to explain why different spanwise positions have to shed vortices at different rates.

6.2.6 The discretisation of the shedding frequencies

The similarity arguments applied in the previous section established that there cannot be a single shedding frequency along the span of the sinusoidal model. In this particular case the flow has chosen two shedding frequencies (f_1 and f_2) and alternates between them, with f_1 dominating at the peak (but not completely) and f_2 becoming gradually more prominent and eventually totally dominant as we progress towards the valley.

There is no obvious explanation why the flow has chosen two frequencies, instead of each spanwise section shedding constantly at the predicted time-

averaged frequency. We could conceivably have such a phenomenon, with vortices gradually getting out of phase and vortex splitting occurring at various different spanwise positions (this flow perhaps resembling the patterns observed by Gaster, 1969, for the flow around slender cones). One reason this does not happen could be due to the tendency of the flow to reduce the volume of its vortices (a kinetic energy minimisation consideration). If the flow followed such a pattern, the vortices would probably tilt at fairly large angles and it is possible that this would be "uneconomic" in terms of vortex-induced kinetic energy. Obviously, no certain claim can be made for the scientific validity of the above argument.

Perhaps a more plausible explanation could lie in some sort of spanwise flow "lock-in". We can observe from the spanwise distribution of time-averaged shedding frequency shown in figure 6.6b, that over a considerable portion of the half-wavelength (ca $0.27<y/L<0.5$) the time-averaged shedding frequency is constant at $S=0.29$. It would then seem reasonable to expect that frequency to be chosen as one of the characteristic frequencies of the wake. Consequently, we will have a strong cell shedding at a uniform frequency. It is possible that under the influence of the induced velocities of that cell other spanwise sections occasionally get "locked-in" and shed at that frequency (note that we have established that the whole wake cannot get permanently locked-in at that single, strong frequency). The selection of the second characteristic frequency could then be forced in order to achieve the required value of time-averaged shedding rate for each spanwise position. Once a certain frequency (<0.29) has been established over a small portion of the span, it could (under the mechanism of the spanwise lock-in) spread out until the wake is dominated by these two characteristic frequencies.

There is no evidence to support these suggestions, apart from the fact that the flow does indeed select two such frequencies. It seems possible that if a balance could not be reached with any two frequencies, one (or more) extra characteristic frequencies would emerge, and we would then have a considerably more complex flow pattern, with three (or more) shedding frequencies and multiple combinations of cells. In two-dimensional experiments, lock-in has been achieved under a multitude of different forcing conditions (in-line oscillation, transverse oscillation, oscillatory rotation, sound waves, etc.). It then seems quite reasonable to expect a spanwise form of lock-in (under the influence of velocities induced by the more dominant frequencies) and a consequent discretisation of the shedding frequencies.

It is not easy to examine wake similarity when using the two discrete shedding frequencies (as opposed to the time-averaged frequency), because we cannot be sure of the value for base pressure. Let us consider the two values obtained by the least squares approximation of the simplistic base pressure-shedding frequency model (for need of more accurate Cp_b values). The wake Strouhal numbers obtained at the peak and the valley (respectively the "strongholds" of the f_1 and the f_2 characteristic frequencies) are both very close to the "universal" value of 0.17, but considerable deviations would occur at spanwise positions in-between the peak and the valley. It is uncertain whether these deviations are predominantly due to the unquestioned inaccuracy of the Cp_b estimates. We should note, however, that while for a section left free to oscillate at its own preferred frequency we expect it to obey the wake similarity arguments, this should not necessarily be the case for a section temporarily locked-in to one of the two characteristic frequencies.

6.2.7 Further observed phenomena

A few more observations fitted in well with the proposals of this chapter:

a) The fluctuation intensity of base pressure (R.M.S. of Cp_b) is plotted against spanwise position y/L in figure 6.6c. The significantly larger values obtained at the peak are attributable to the closer proximity of the forming vortex and also to the larger mean vortex strength Γ_v at the peak (as $S*\Gamma_v$=constant, and S is smaller at the peak, Γ_v must be larger at the peak).

b) Figure 6.6d shows the power spectral density of velocity fluctuations at the formation position. The predominance of f_1 at the peak and the total dominance of f_2 at the valley have been discussed many times. It is interesting to observe the dip in the total power (for the two frequencies combined) at $y/L \approx 0.1\text{-}0.2$. This spanwise position is the most frequent position of the dislocation. In its vicinity vortex filaments tend to be bowed, which may cause lower induced velocities for the particular orientation of the single hot wire.

c) Figure 6.7 is a series of side views of vortex formation (a, b, c and d: y/L=0; e and f: y/L=0.25; g and h: y/L=0.5). The wider wake is noticeable for y/L=0. Note also that for the valley we can see the trailing edge of the peak, with the formation length mistakenly appearing to be shorter in that region. Photos (d) and (f) are indications of the less regular shedding observed towards the peak. Suppression of vortex shedding (even momentary) was never observed when

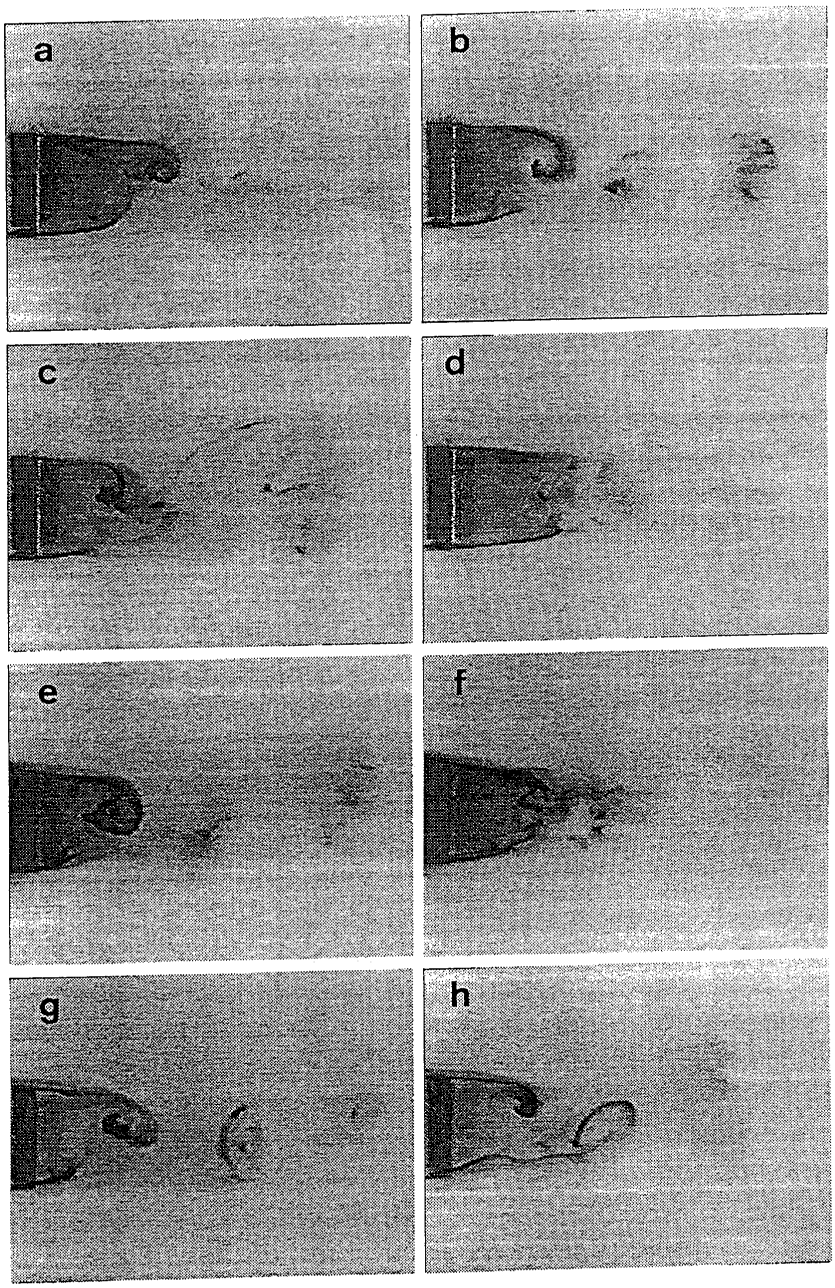

Figure 6.7 Flow visualisation for the sinusoidal model (side view). Photos (a) to (d): y/L=0 (peak), photos (e) and (f): y/L=0.25, and photos (g) and (h): y/L=0.5 (valley). Note how the wake appears to be narrower at the valley than at the peak.

looking at the plan view of the wake. Therefore we have to associate photos (d) and (f) with local instantaneous phenomena, the most probable of which seems to be vortex splitting.

d) By using the mode-detection criterion described in detail in section 4.2.3, formation lengths and wake widths were measured for the two shedding modes (symmetric and antisymmetric). These results are plotted in figure 6.8. Both modes seem to follow the patterns of the average flow (i.e. the measured values without the use of any mode criterion). The largest discrepancies are found towards the edges of the cells, where we expect vortices to be weak and also to bend, under the influence of vortex splitting. It is also at the cell edges where the vortices are susceptible to the peculiarities of the shedding modes. We thus conclude that as far as the mean wake dynamics discussed above are concerned, the particular shedding mode is only of secondary importance.

6.3 Concluding remarks on the dynamics of the formation region

6.3.1 The interaction of steady wake parameters

This chapter mainly concerned the mechanisms that determine the mean parameters of the near wake of the sinusoidal model. Purely in terms of time-averaged quantities, the following suggestions were made, concerning the near wake:

a) Forming vortices have the tendency to straighten out, possibly in order to minimise their volume (an energy consideration). Due to the model geometry, this results in a longer formation length at the valley than at the peak.

b) As a result of the $d(S\Gamma_V)/dy=0$ assumption, and the fact that the fraction of surviving vorticity, α, decreases with an increase in formation length ($d\alpha/dl_f<0$), there must be a larger amount of circulation shed at the trailing edge (due to the longer formation length), and hence the local drag at the valley is larger than the local drag at the peak.

c) High local drag implies high suction in the formation region, which in turn has to be balanced by an increased curvature of the separated shear layer. Therefore the combination of higher drag and longer formation length at the valley has to be balanced by a narrower wake (in comparison to the peak).

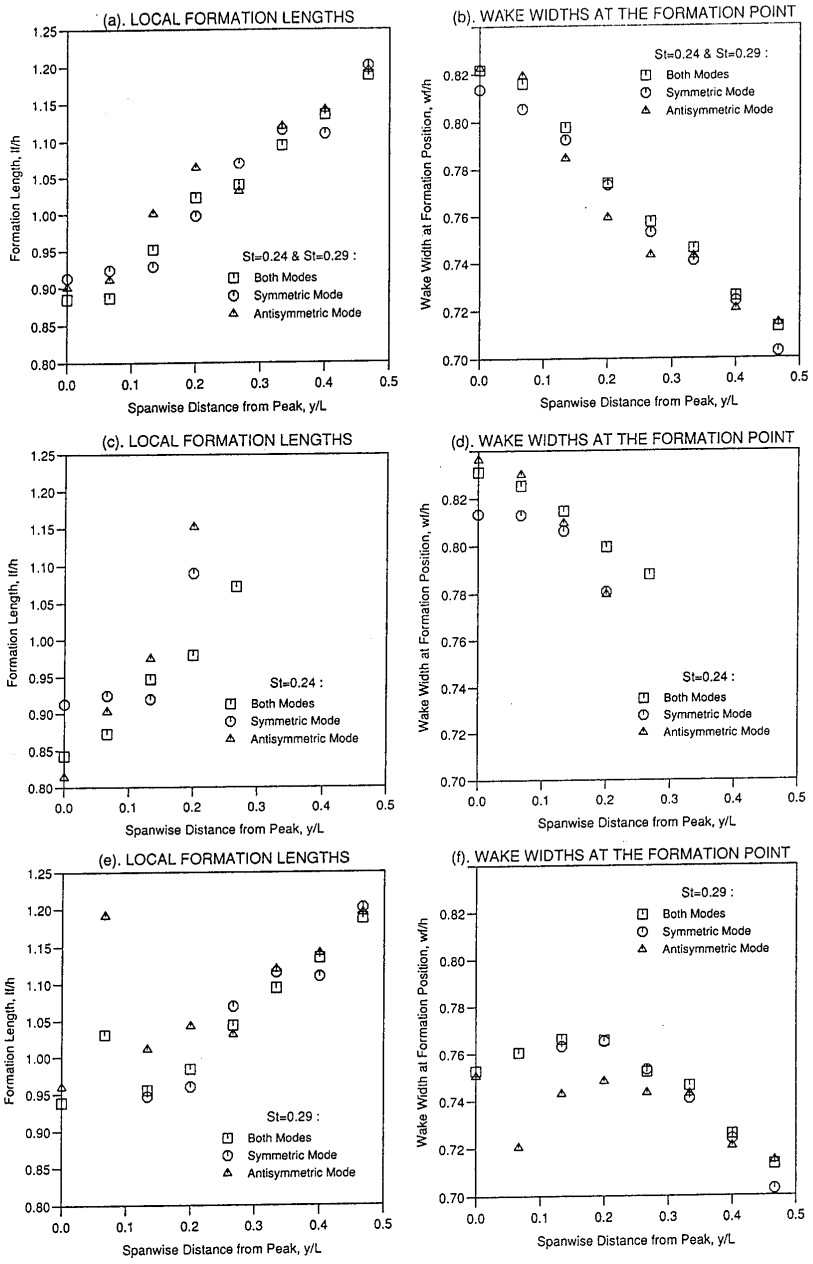

Figure 6.8 A comparison for the values of formation length and wake width (at the different shedding frequencies) for the two shedding modes (symmetric-antisymmetric). The two modes appear to follow a similar pattern.

d) Wake similarity arguments suggest that the underlying mechanism for the selection of shedding frequency must be related to wake properties (i.e. wake width and velocity at separation, not model base height and free stream velocity). Applying these arguments, a higher time-averaged Strouhal number has to prevail at the valley, in order to balance the narrower wake and the higher separation velocity.

It was further proposed that "spanwise lock-in" must be an important mechanism in the discretisation of the shedding frequency to the two distinct observed values. Through this mechanism, the most dominant frequency components could spread along the span. The dual frequency characteristic would then generate a dislocation.

Wake properties at the two distinct shedding frequencies suggested that there must be a steady pressure drop across the dislocation. This pressure drop could be sustained by streamwise vorticity within the dislocation. Its periodic spanwise motion (as described in chapter 5), would then ensure (a) that the mean base pressure distribution does not show any steep drop across the mean dislocation position, and (b) that the time-averaged Strouhal number prediction is satisfied.

The above proposals have been drawn from the flow around the sinusoidal model. It is probably appropriate to note at this point that the choice of a relatively simple geometry for the model (i.e. fixed separation point, minimal base area-shear layer interaction, etc.) has been fully justified by these results. Nevertheless, the proposals of this chapter need to be tested, confirmed and extended for different geometries, where important relations (such as the relation between the fraction of surviving vorticity and the formation position) follow different patterns.

6.3.2 Quasi-two-dimensional flow considerations

This chapter aimed to give a physical insight into the mechanisms that determine the parameters of the near wake. Obviously the flow is strongly three-dimensional. It is interesting to note, however, that for a large number of the arguments of this chapter quasi-two-dimensional considerations were used, with results that appear to be satisfactory.

This is, of course, not to suggest that in each section the flow behaves as if it were two-dimensional, nor that the spanwise velocity component is negligible.

What emerges from this chapter is that some of the near wake phenomena are nearly two-dimensional:

a) The predominant axis of the Kármán vortices has remained parallel to the spanwise direction.

b) Vorticity within the separated shear layer is also mainly in the y-direction, especially considering that the flow just outside it is almost aligned to the free stream.

c) We have found the fluctuation spectra to be heavily dependent on the actual spanwise position, but to show no noticeable variation (regarding the relative magnitude of the two frequency components) between different points of the same spanwise section.

It is therefore suggested that for a first order appreciation of the interaction of the main flow parameters, quasi-two-dimensional considerations can provide us with significant insight into three-dimensional wakes of mildly three-dimensional bodies. Such considerations should be always used with caution, however, and without forgetting the real, three-dimensional nature of the flow.

7. CONDITIONAL SAMPLING

ABSTRACT : Conditional sampling is used as a tool to obtain further information about the near wake. A detailed account is given of the conditional sampling technique used and also on considerable improvements that could be made to it. On the fluid dynamics front, indications emerge in favour of various assumptions or suggestions of previous chapters. The vorticity flux at each side of the wake after formation is found to be constant along the span (i.e. $d(S\Gamma_V)/dy=0$). Vortex strengths are found to vary from cycle to cycle (in particular for the cell situated at the peak) and the spanwise position of the dislocation is found to move.

7.1 Introduction

7.1.1 The concept of conditional sampling

In any unsteady fluid flow the experimentalist encounters a well-known problem: in quantitative experiments, the entire flow cannot be studied simultaneously. Usually, financial constraints confine us to measuring certain properties (in the present case, pressure or velocity) at a limited number of positions. Intrusive sensors (such as a hot-wire probe) can not be used in large numbers, as the flow disturbance would then become too large. Laser-Doppler Anemometry (L.D.A.), a non-intrusive method, is still too expensive for us to be able to measure more than a few flow "spots" at the same time. Particle Image Velocimetry (P.I.V.) obviously has a lot of potential, but is still expensive and limited to a single plane of the flow at a time (not to mention the considerable development that still has to go in that technique). Flow visualisation, on the other hand, can give a broader qualitative picture of the flow but lacks the quantitative element.

In this study, the largest number of sensors used simultaneously was seven (five pressure transducers and two single hot-wire probes). The deductions and theories presented in the previous chapters are based on an appreciation of fluid mechanics laws and a general knowledge of the nature of unsteady, Kármán wakes. It is quite clear, however, that while a lot of useful information can be obtained by studying such confined regions of the flow, theories on the actual topology of the flow and the instantaneous vortex dynamics can only be based on a series of assumptions.

Conditional sampling is based on the repeatability of certain flow patterns of the wake in order to obtain wider information on its topology and properties. Literature reviews have been published by Van Atta (1974) and Antonia (1981). In general, the basis of conditional sampling is one or more indicator functions, which are compared to data obtained at different times in order to detect similar flow patterns. A further discussion on the various techniques of conditional sampling will follow later, but initially we must separate the general approach in two categories, related to the selection of the indicator function(s):

a) The indicator functions can be obtained from the actual signals that have to be analysed. In such an approach the predominant purpose is to detect repeatable patterns, obtain their ensemble average and determine their statistical significance. Such a method has been used, among others, by Blackwelder and Kaplan (1976), introducing the V.I.T.A. (Variable Interval Time Averaging) algorithm for turbulent boundary layers, Browne et al (1986), using a modified V.I.T.A. technique for the far wake, Bisset et al (1990a and 1990b), comparing different algorithms for the far wake of a cylinder, and Ferré and Giralt (1989), who used a pattern-recognition analysis -strictly speaking not a conditional sampling technique- to detect coherent structures in the far wake. We will not go into the details of the various different methods here, as they are of no consequence for the present investigation (at least an array of cross-wire probes is needed in order to obtain any meaningful results, which was not available for this study).

b) The indicator function(s) can be used as a trigger (when certain conditions are met) for the sampling of the signal from an independent sensor to start. Depending on the level of sophistication and the nature of the experiment, the triggering can be done in real time (triggering the operation of an A-D converter) or can be done in the computer analysis phase by selecting the suitable portions of the sampled data. The independent sensor(s) can move around the flow volume of interest, while stationary sensors obtain the signal to be compared to the indicator functions in order to perform the triggering. Such a technique has been used by numerous researchers, notably for the near wake by Cantwell and Coles (1983).

In the present investigation, the technique used (to be described in full later) was based on the second approach.

7.1.2 The aims of this part of the investigation

Ideally the results of this chapter should not be presented separately from those of earlier chapters. The aim of this study, after all, is to achieve a better understanding of the dynamics of the three-dimensional near wake, not the development of a new experimental technique. The main aim of the conditional sampling experiments was to measure the strength of the Kármán vortices for the sinusoidal model. The findings are presented later.

The next sections will highlight some of the drawbacks of the conditional sampling experiments performed here. They include the assumptions about the spanwise velocity component v ($v \ll \sqrt{(u^2+w^2)}$), the approximations for the measurement of reversed flow and errors related to the conditional sampling procedure. Later, one more important source of error will emerge, the use of Taylor's hypothesis for the calculation of vorticity. Therefore, unfortunate as it is, the results of this chapter should be considered in the light of the errors arising from these over-simplifications. Hence, although results will be shown later to agree well with the theories of the previous chapters, no claim can be made about their accuracy.

A secondary aim of these experiments was to explore the potential of such experiments for the study of the near wake. Some proposals for a better experimental technique (using equipment not available in this study) are included towards the end of this chapter.

7.2 Description of the conditional sampling technique used

7.2.1 Fundamental conditional sampling assumptions

In the present study, the indicator functions were used as triggers, while a cross-wire probe collected data in the flow region of interest. The main limiting factor that confined us to the second technique was the number of available hot-wire anemometers. We will see later, however, that this approach also has some advantages and a lot of potential.

The main assumption of this type of conditional sampling concerns the repeatability of flow patterns and the uniqueness of their influence at the points of the stationary sensors (the ones that obtain the signal to be compared to the indicator functions). To put this in proper perspective, let us consider a flow

region of interest R (which, in fact, may not have a finite volume but just be a plane or even a line). We now assume that there exists a repeatable flow pattern p of interest with duration Δ. We now consider a series of stationary comparison points of the flow $S_1,S_2,\ldots,S_n$, at each of which we measure a flow property q (this property may be a velocity signal, a pressure signal, another flow property, or any function that may arise from such signals). For each of the comparison points S_n, we somehow determine an indicator function F_n, which corresponds to the flow property q_n and is of duration Δ. There are then two theoretical conditions necessary (but not sufficient) for the success of the conditional sampling procedure:

a) Excluding any random contributions (e.g. turbulence, noise, measurement inaccuracies, etc.), if we have a time interval [t, t+Δ] such that:

$$q_n(t+\delta) \equiv F_n(\delta) \quad \forall\, S_n,\ \delta \in [0,\Delta]$$

then we must have:

$$\forall\, a \in R \ : p_a \text{ is unique}$$

Of course, if there exists a small number of possible flow patterns (say, two or three) we may still be able to separate them by considering the patterns at adjacent points within R.

b) The second condition relates to the intrusion of the sensor that traverses R. In simple terms, the flow distortion due to the sensor must be negligible for all points within the volume of interest R and also for all comparison points S_n.

It should be stressed that the comparison signals q_n were obtained from the stationary sensors at the points S_n. The actual flow pattern p would be obtained once the best time t (for $q_n(t+\delta)\equiv F_n(\delta)$) was determined. The *moving* sensor within the region R would obtain the flow pattern p for one point within R (sampling of the moving sensor signal and the signals from S_n would, of course be simultaneous). The whole process would be repeated for all the points of interest within R, each time obtaining p for one more point. Compliance with the two fundamental conditions (a) and (b) would then allow us to combine selected data from all the points in order to obtain the flow field within the region R.

7.2.2 The selection of the indicator functions

The selection of the appropriate indicator function is very much dependent on the complexity of the flow. In the simplest case we have an accurately repeatable two-dimensional flow with a well-defined "time pulse". Such flows may be low Reynolds number Kármán flows. If there is no frequency of amplitude modulation in the shedding, a sensor can simply detect the phase of vortex shedding and accordingly trigger the sampling. This is an ideal situation, as the final ensemble average could stem from a large number of consecutive cycles. Other simple flows (purely in terms of selecting a suitable indicator function) include cases when an abrupt change is forced on a previously steady flow. An example here is the rapidly-deployed spoiler, used by Ho (1991) on an unstalled two-dimensional wing section.

The very interesting work reported in Cantwell and Coles (1983) falls in a similar case as far as the selection of indicator function is concerned: they assumed a basic repeatability of each shedding cycle and used a triple decomposition technique to split the flow into the steady component, the shedding-frequency periodic component and the random component. No information was obtained, however, about the *instantaneous* flow.

The flow around the sinusoidal model is strongly modulated (with all vortices not being of equal strength). It is clear from this that the use of a simple phase criterion would not be sufficient. The modulation of the flow has to be taken into account. Furthermore, we have seen that vortex splitting occurs, which means that the shedding is not in phase along the span. The consequence of this is that a single comparison sensor would not be sufficient, as it would be primarily affected by the phase of shedding at its particular spanwise position. It was thus decided to use three indicator functions. All three were velocity fluctuations from stationary, single hot-wire probes positioned just outside the wake. The possibility of using a fourth signal from a pressure transducer was also examined. Its highly irregular fluctuations made it unsuitable for the conditional sampling experiments.

As the comparison signals were obtained from intrusive sensors, their positions had to be outside volume R. Common sense suggests that the closer they are to R the easier it will be to satisfy fundamental condition (a). As a result of the observations reported in previous chapters, concerning the two shedding modes (symmetric-antisymmetric), two of the probes were positioned at adjacent valleys,

mainly as a means of mode-detection. The third hot-wire probe was positioned at different locations, depending on the experiment.

The time duration Δ of the indicator function was selected to correspond to about five shedding cycles, in order to capture a full cycle of the dislocation frequency. For each experiment thirty sets of indicator functions were selected to be compared to the sampled data (i.e. eventually we would have thirty flow "pictures", each one being about five shedding cycles long). The selection of the best indicator functions was done digitally, by selecting the most repetitive trends of duration Δ, but also taking into account the shedding mode (symmetric-antisymmetric). As will be seen later, the comparison of the sampled data to the indicator function was based on correlation analysis, and therefore a similar procedure was applied to determine the most repetitive trends (in order to select the best indicator functions). To be more specific, the algorithm would consider all possible indicator signal intervals of duration Δ, and compare them to the rest of the signal of that stationary sensor. The intervals that were found to have the highest degree of repeatability were selected to be used in subsequent experiments as indicator functions.

It should be stressed here that the above process is non-critical. The whole idea was just to select the most suitable sets of data to be compared subsequently with the sampled signal in order to obtain the flow field. Any comparison inaccuracies would not arise at this point. Analysis of the repeatability of the flow patterns revealed that some would not be repeated frequently enough (to a sufficient accuracy) within the length of the A-D converter memory (16384 samples). Typically, following the application of various techniques to be presented later, the flow conditions for each point within R would be the average of three independent measurements. In other investigations, ensemble averages are usually obtained from thousands of shedding cycles (e.g. Cantwell and Coles 1983). It should be emphasised once again that the purpose here was to obtain instantaneous flow fields, not averages.

However, the above considerations highlight one important limitation of the present experimental set-up. The flow had a poor degree of repeatability. Simply collecting more and more data could help solve the problem but was not permitted by the computational power and memory (more of which later). Towards the end of this chapter a technique to perform on-line data comparison will be suggested, which would enable us to obtain averages of a larger number of data sets.

7.2.3 The comparison process

For each position of the moving sensor (traversing *R*), apart from its signal, the signals of the three stationary comparison sensors (positioned at points S_1, S_2 and S_3) would also be sampled at the same time. Comparison of the signals q_1, q_2 and q_3 to the indicator functions F_1, F_2 and F_3 would enable us to determine the best intervals (each of duration Δ) to be selected from the moving sensor signal. This section describes this comparison and selection procedure.

The basic tool used was comparison by linear correlation analysis. For each possible Δ-interval (starting at $q_n(t)$ and finishing at $q_n(t+\Delta)$) the correlation coefficient $r_n(t)$ would be computed between the sampled data q_n and the indicator function F_n (for zero delay). The correlation coefficient only considered the fluctuating part of the signals. A value of +1 shows perfectly correlated signals in phase, but there may still be a difference in the r.m.s. value (e.g. $f_1(t)=A\sin(\omega t)$ and $f_2(t)=B\sin(\omega t)$ are perfectly correlated but clearly not the same). To compensate for this a normalising factor $c_n(t)$ was computed, defined as:

$$c_n(t) = \frac{2 * \sqrt{\left[\overline{q_n^2}\right]_t^{t+\Delta} * \overline{F_n^2}}}{\left[\overline{q_n^2}\right]_t^{t+\Delta} + \overline{F_n^2}}$$

whence $c_n(t)$ will take a maximum value of +1 if the two signals have an equal r.m.s. Thus, for each interval of length Δ starting at time t, we can define the degree of similarity to the indicator functions, Q(t):

$$Q(t)=[c_1(t)*r_1(t)][c_2(t)*r_2(t)][c_3(t)*r_3(t)]$$

Perfect similarity for an interval starting at time t would yield a value of $Q(t)=1$. To avoid two negative r_n signs giving a positive Q(t), values of r_n less than zero were set equal to zero. The most efficient way to compute the correlation for all possible Δ-intervals was a spectral method. The FFT of the signal q_n would be multiplied by the complex conjugate of the FFT of the F_n signal (padded with a large number of zeros to be of the same length as the q_n signal). The inverse FFT would then give the correlation.

Typically Q(t) values of about 0.7 were considered satisfactory and would be selected for the ensemble average ($Q(t)=0.7$ corresponds to three correlation

coefficient values of about 0.9). Usually, for one set of data there would be an average of three instants satisfying this condition. As was said in the previous section, this is not a satisfactory number. If there was no interval [t, t+Δ] satisfying the condition $Q(t)>0.7$ the interval with the highest value of Q(t) would be selected.

One of the problems of this type of conditional sampling is known as "phase jitter". This results because the sampling points within the selected Δ-interval will not exactly match the sampling points from the indicator functions, i.e. the selected signals within the region of interest *R* will be shifted by up to half a sampling period with respect to one another. Of course, a sampling rate much higher than that necessary for the satisfaction of the Nyquist criterion does solve the phase jitter problem but reduces our available length of data considerably. The solution to this problem was based on the recommendations found in Wills (1991). For band-limited signals sampled according to Nyquist's criterion, Wills reminds us of the often forgotten implications of the sampling theorem:

$$h(t) = \Delta t \sum_{n=-\infty}^{\infty} h_n \frac{\sin[\pi(t - n\Delta t) / \Delta t]}{\pi(t - n\Delta t)},$$

where h(t) is the original signal and h_n the sequence sampled at equal intervals of Δt. Effectively, this formula means that, provided the sampling rate is high enough and a large number of samples is available, the whole original signal can be reconstructed to as close a spacing and as high an accuracy as desired. The above formula was first used to double the length of the data. For each pair of consecutive samples, the intermediate sample would be obtained. Thus the effective memory of each A-D converter channel was doubled to 32768 samples. The actual sampling rate (2500Hz), was effectively also doubled to 5000Hz. The spectral correlation analysis would be performed on this enlarged set of data (the R.A.M. and the speed of the Microway accelerator card were essential for the required number of 32768-sample FFT's).

The indicator function signals had been obtained at a much higher sampling rate, at 20000Hz. Each comparison signal was 500 samples long. Of those, 125 samples (1, 5, 9,...) were used for the initial correlation comparison described above, in order to select the best 125-sample interval of the 32768-sample array. Once that interval had been determined, it would be compared to other 125-sample sets of the indicator function data (set (2, 6, 10,...), set (3, 7, 11,...), and set (4, 8, 12,...)). From that comparison the phase jitter would be determined and

reduced, as the sampling theorem would be used to project the moving sensor signal back on to time instants corresponding to set (1, 5, 9,...). By the above technique, phase jitter can practically be eliminated. In the present experiment the phase matching would be to within 1% of a shedding period.

Another concern was whether fundamental conditions (a) and (b) were satisfied. Condition (a), concerning the uniqueness of the flow pattern, was checked extensively by comparing the appropriate intervals from the moving probe signal. Deviations were more attributable to random contributions rather than to an altogether different flow pattern, and hence the condition was considered to be satisfied. Condition (b), concerning the intrusion of the moving sensor, could not be checked easily. One cannot say that the hot-wire probe intrusion is completely unimportant but, given the available facilities, not much else could be done.

7.2.4 The analysis of the moving sensor data

So far we have reached the point where we are able to select the best part of the moving sensor data in order to put together the flow field within *R*. The data reduction from the moving sensor is another complicated area, mainly due to the nature of the flow within a near wake. The moving sensor was a cross-wire probe, oriented in such way as to record velocities in the x-z plane. The inadequacy of a hot-wire probe in the near wake is well known, and basically results from the reversed flow (a problem which does not occur in far wake flows). The advantages (for the present experiment in particular) of using a laser-Doppler system is quite apparent.

It is probable that the bulk of the experimental error in the measurements presented in this chapter results from the use of hot-wire probes. Unfortunately, once again, not much else could be done. An assumption was made in that the spanwise velocity component was negligible ($v \ll \sqrt{(u^2+w^2)}$). Obviously, in a strongly three-dimensional flow this is not true, but it was felt that the benefits in attempting to measure the spanwise component would not justify the added complication and error. The symmetric shedding mode probably has smaller magnitudes of spanwise velocity, and therefore was judged to comply best with the $v \ll \sqrt{(u^2+w^2)}$ assumption. Hence, the indicator functions chosen (and the results presented later) are all for the symmetric mode.

Further approximations were made in order to be able to estimate the reversed flow. Cross-wire sensors in reversed flow have three main drawbacks (added to the standard cross-wire drawbacks such as wire separation, etc.):

a) The intrusion of the probe holder becomes larger, as in a reversed flow the actual sensor lies in the "wake" of the probe holder. This error is probably reduced by the unsteady nature of the reversed flow. Due to the unsteadiness of the flow the probe holder can probably not develop a steady wake pattern, which would increase the error.

b) In the present experiment the axes of the two wires of the cross-wire sensor had nominal direction cosines of ($\sqrt{2}/2$, 0, $\sqrt{2}/2$) and ($\sqrt{2}/2$, 0, $-\sqrt{2}/2$). For straightforward, plane velocity measurements the instantaneous velocity vector would have to lie within a 90° envelope, a condition obviously not satisfied in unsteady, reversed flow. Thus some further criteria would have to be applied to determine the direction of the flow. Conceptually similar criteria to the ones to be described below have also been used by Sokolov and Ginat (1992) to measure reversed flow using a hot-wire rake ("ladder probe").

c) Contrary to the ladder probe used by Sokolov and Ginat (1992), the cross-wire probe cannot be calibrated in reversed flow, mainly because of its unsteady nature (the unsteady reversed flow conditions would be impossible to simulate in a steady calibration process). As a result, the same calibration parameters had to be used for all the flow directions.

The method used to determine flow direction was based on detecting the zero crossings of the velocity signal for each of the two wires. Hot-wire signals, in general, never show a zero velocity for three main reasons: (a) the zero velocity instant is unlikely to be matched by the exact sampling instant of the A-D converter, (b) calibration at low velocities is affected by natural convection effects, and (c) the low-pass filtering of the signal (necessary in order to apply the sampling theorem) may smoothen the abrupt velocity signal gradient change that would accompany a zero crossing. Thus a threshold in the velocity signal had to be established, more or less by trial and error: when the velocity signal of one sensor dropped below that value, a zero crossing was assumed to have happened. The threshold used was 0.08U.

Each of the two signals of the cross-wire probe was analysed separately. At the centre wake, where reversed flow occurs more regularly, we have seen the

predominant frequency to be twice that of shedding. If we assume that the maximum zero crossing frequency can be that double frequency, then up to four zero crossings can occur within one shedding cycle. Hence, if this limit was exceeded, a secondary procedure would select the four most likely zero crossings and neglect the other ones. Furthermore, we would only expect an even number of zero crossings within one shedding cycle. If the detected zero crossings were of an odd number, the least likely one would be dropped.

Once the zero crossing instants had been determined for the whole length (duration Δ) of the hot-wire signal, the sign of the signal would be changed for each zero crossing (see figure 7.1a). A smoothing function would be applied at the position of the zero crossing in order to prevent the abrupt change in value. The most frequent pattern observed was of the type shown in figure 7.1b, where two zero crossings would occur very close to one another. It should be noted, for both figures 7.1a and 7.1b, that the abrupt change in slope of the velocity signal confirms that this is indeed a zero crossing, as the reflection of the signal (shown in the two figures) subsequently yields a much smoother function.

What of course remains is the actual determination of the sign at $t=0$ of the Δ-interval. That was accomplished by first computing the magnitude of the average value of the velocity signal at each point within the region R. Depending on the experiment, a different criterion was then used to determine the sign of each mean value. Where the measurements were along a straight vertical line (the experiments described in section 7.3), the values chosen were such that the u and w mean velocity components had the smallest second derivatives w.r.t. z. As a boundary condition, mean velocity in the outer wake was taken to be in the direction of the free stream. Where the measurements covered an entire plane (as described in section 7.4) continuity in that plane was applied. The points furthest from the model and from the centre wake were taken again to have a velocity direction similar to the free stream (and used as a boundary condition to determine the directions in the rest of the near wake).

The methods described in this section, it should be stressed once again, are not claimed to record accurately the velocity fluctuations. They were developed not as an ideal solution to the problem, but as an engineering solution to the limitations of the available apparatus. The errors involved, apart from the ones presented earlier, should also include the possibility that the above direction-determining criteria fail completely at some times.

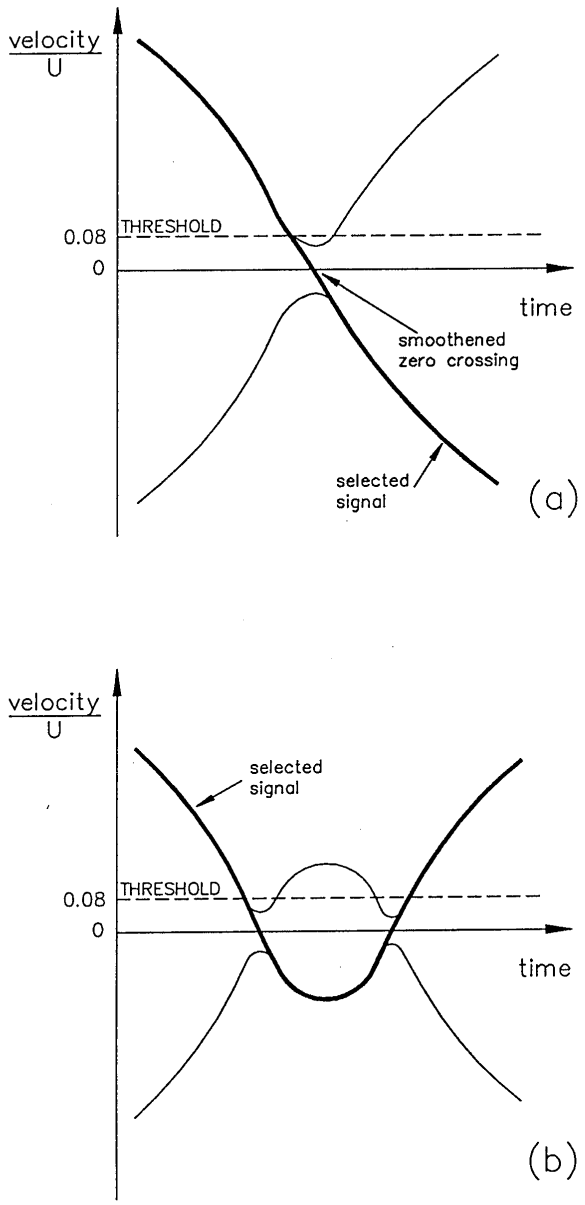

Figure 7.1 Schematic diagram showing the treatment of zero crossings of hot-wire signals.

7.3 The use of Taylor's hypothesis

7.3.1 Errors involved in Taylor's hypothesis

The present experiments aim to measure ω_y (spanwise) vorticity. This is given by:

$$\omega_y = \frac{\partial w}{\partial x} - \frac{\partial u}{\partial z}$$

Taylor's hypothesis is frequently used to transform the x-axis derivative into a time derivative. Thus, by using,

$$\frac{\partial}{\partial x} = -\frac{1}{U_c} * \frac{\partial}{\partial t}$$

(where U_c is the mean convection velocity in the x-direction), vorticity can now be expressed as:

$$\omega_y = -\frac{1}{U_c} * \frac{\partial w}{\partial t} - \frac{\partial u}{\partial z}$$

The obvious advantage of using this transformation is that one may now measure the two velocity components along a vertical line only (e.g. with an array of hot wire x-probes), and still be able to determine the vorticity. The disadvantage is that it is not a rigorous transformation and therefore includes some error.

Hinze (1975, p.46) gives a useful discussion of Taylor's hypothesis. The hypothesis holds if the mean flow field is parallel and constant (in the direction of the x-axis), and if:

$$\sqrt{\overline{(u - \bar{u})^2}} << \bar{u},$$

i.e. if the x-velocity fluctuations are very small compared to the mean velocity. The physical significance of Taylor's hypothesis is that at any fixed point we imagine the velocity fluctuations to be caused by the passing of a "frozen" flow field.

In the present case, neither of the two main conditions is fully satisfied. In our favour, however, is that we may be able to assume that vorticity gets

concentrated in discrete "lumps", and thus, within those confined lumps we may say that the mean velocity shows a relatively small variation. The velocity U_c will then be the velocity at which the formed Kármán vortices get convected. The instantaneous velocity of the vortex centres was used by Takamoto (1986), who also used a numerical, viscous core vortex model to estimate the error involved in Taylor's hypothesis, concluding that the error was small.

For the present experiment, at first sight, we could do away with Taylor's hypothesis. The cross-wire probe could traverse two (instead of one) vertical lines, adjacent to each other, in which case x-derivatives could also be determined. However, it was decided that the use of a dubious (for the present flow) hypothesis would be better than to double the number of necessary readings using dubious apparatus (again, for the present flow).

7.3.2 Experimental set-up

The cross-wire probe was made to traverse along various vertical lines in order to determine the strengths of the Kármán vortices crossing those lines. These lines were at distances from the local trailing edge of h, 1.5h, 2h, 2.5h and 3h. The spanwise locations examined were for y/L=0.1 (peak) to 0.5 (valley), in steps of 0.1.

As was mentioned earlier, two of the three hot-wire comparison sensors were located at two adjacent valleys, mainly for mode-detection purposes. The third sensor was fixed on the vertical arm of the traverse, and lay on the extension of each vertical line that was to be examined. The cross-wire sensor moved from z/h=-0.333 to z/h=0.75, in steps of 0.0833 (2.5mm). This asymmetry with respect to the centre wake (i.e. $z_{min} \neq -z_{max}$) was so that one of the comparison sensors could be as close as possible to the wake, in order to detect fluctuation modulations. In any case, the vortex strengths could be calculated from the one side of the wake, which was covered by the range of the cross-wire probe.

7.3.3 Estimation of the convection velocity

Having decided to use Taylor's Hypothesis, a valid method had to be used in order to estimate the vortex convection velocity U_c. An investigation into this matter was published by Zhou and Antonia (1992), who compared different techniques and criteria but obtained similar results. It is apparent that the most

suitable technique for the present investigation would use the data obtained from the same experiments.

Zhou and Antonia used an initial estimate of $U_c=0.8U$, applied Taylor's hypothesis and thus obtained the position of the vortex centres. U_c was then taken to be the velocity at the vortex centres. The technique used here was based on the same philosophy, i.e. taking U_c=(velocity of vortex centre). Again an initial estimate $U_c=0.8U$ was taken, but the process now involved an iteration: apply Taylor's hypothesis, obtain a new estimate for U_c, use the new value for Taylor's hypothesis, and so on.

The vortex centre was determined by fitting (using least squares) a second order function (w.r.t. z-co-ordinate and time) to the nine points with the highest vorticity for each shedding cycle. U_c was then taken as the weighed average of the x-velocities of the four points surrounding the vortex centre. As was mentioned earlier, thirty flow field pictures were obtained for each vertical line. The final value of convection velocity would then the average obtained from all the vortices of these thirty sets, i.e. the average of about 150 vortices.

7.3.4 Discussion of vorticity contour plots

All the contour plots presented in this chapter have been obtained by the methods outlined above. Apart from the symmetry reasons stated earlier, the reason the symmetric shedding mode was chosen for all the measurements was that in that mode we had previously observed a clear-cut S=0.24 at the peak and S=0.29 at the valley. As a result of using Taylor's hypothesis, the ordinate of these graphs is time. If we imagined the transformation $x=-U_c*time$, and transformed the ordinate of the graphs accordingly, the free stream would be from right to left. Furthermore, it should be noted that the time-axis and the z/h-axis are not to scale (i.e. $[z]\neq[U_c*time]$), and thus the vortices appear much more elongated in the z-direction.

Figures 7.2 and 7.3 show the flux of vorticity at different downstream stations for the peak (y/L=0) and the valley (y/L=0.5) respectively. The period of the vorticity fluctuations corresponds to the observed Strouhal number both for the peak (0.24) and for the valley (0.29), and the signs of vorticity are as one would expect. Both observations show nothing new, but are reassuring. The two sets of plots show some similarities and some differences.

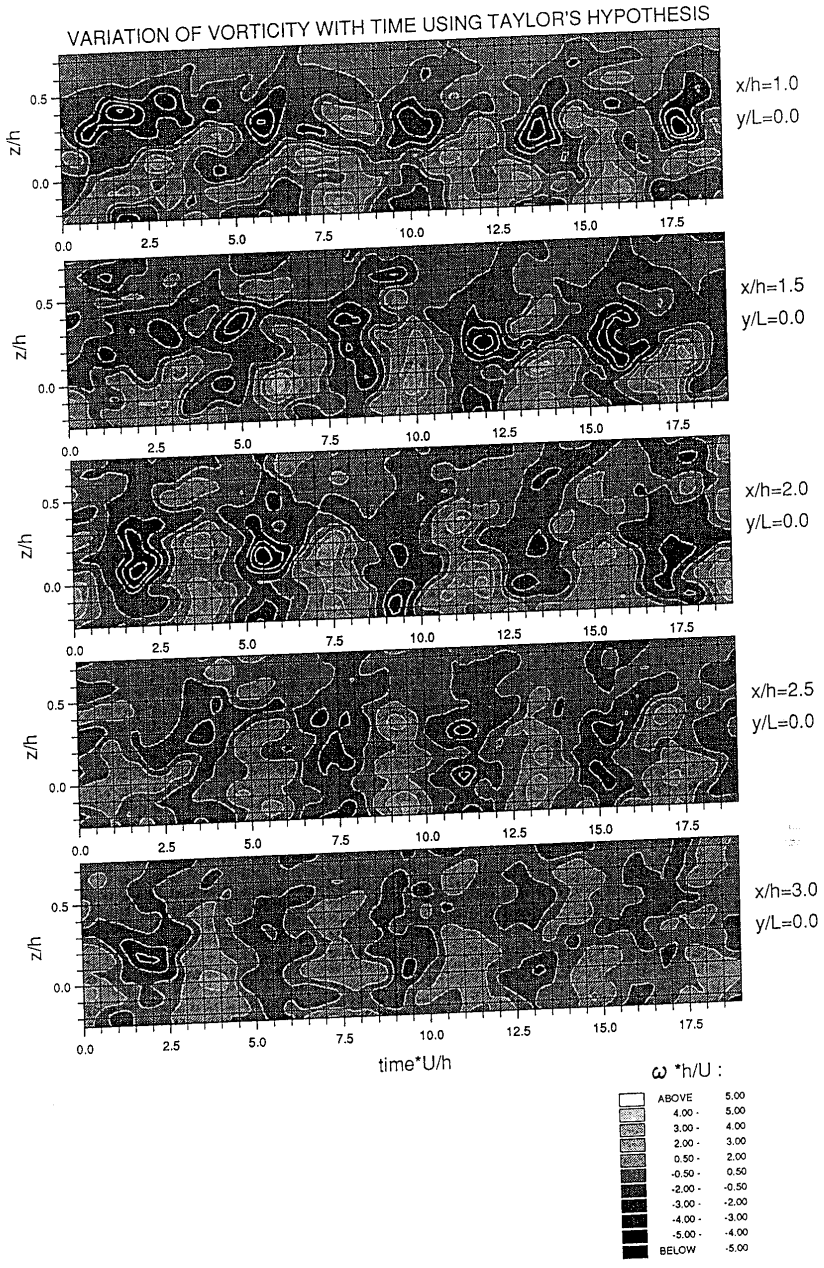

Figure 7.2 Variation of vorticity with time, for the sinusoidal model, using Taylor's hypothesis. These plots were obtained at the peak. Note how vortices become more spread-out as we move downstream (lower plots), and also the apparent variation in the vortex strength, from one vortex to the other.

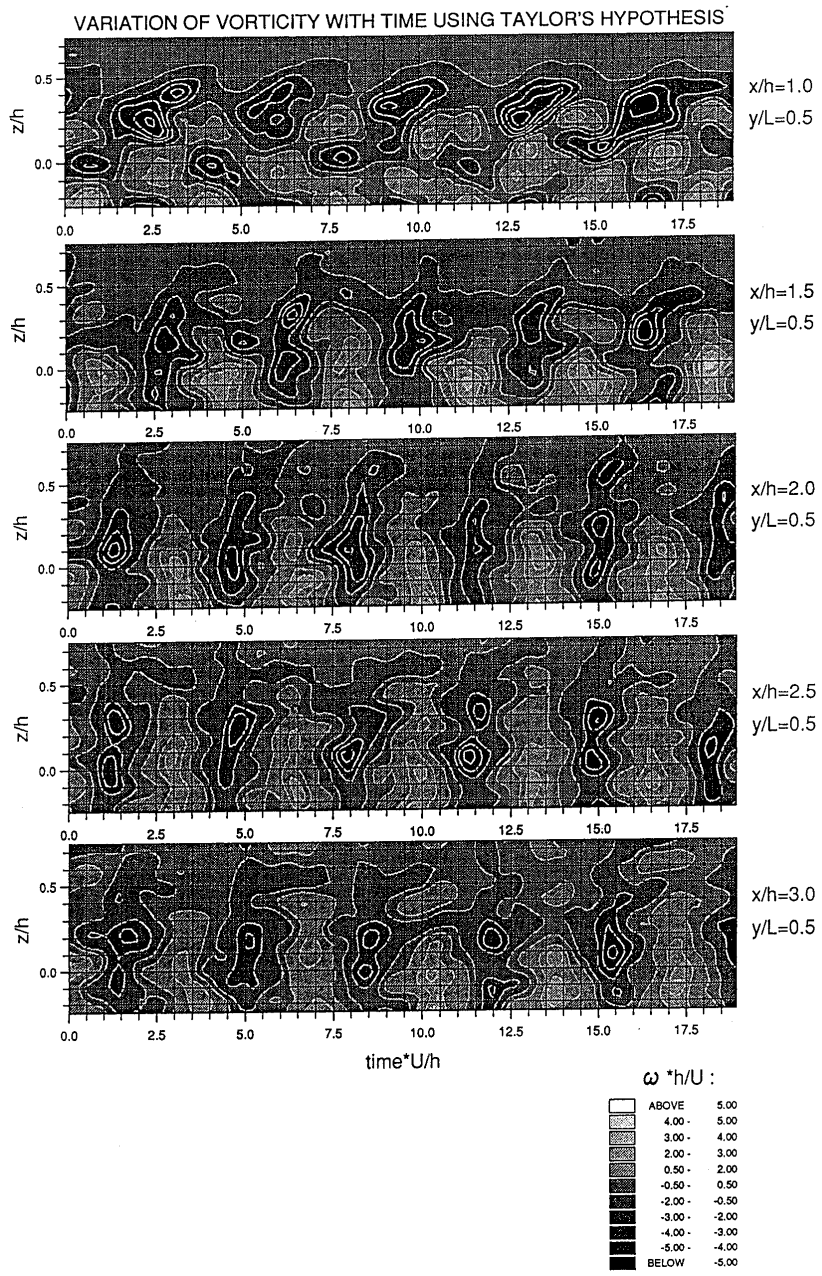

Figure 7.3 Variation of vorticity with time, for the sinusoidal model, using Taylor's hypothesis. These plots were obtained at the valley. Note the small (in comparison to figure 7.3) fluctuations in vortex strength, from one vortex to the other.

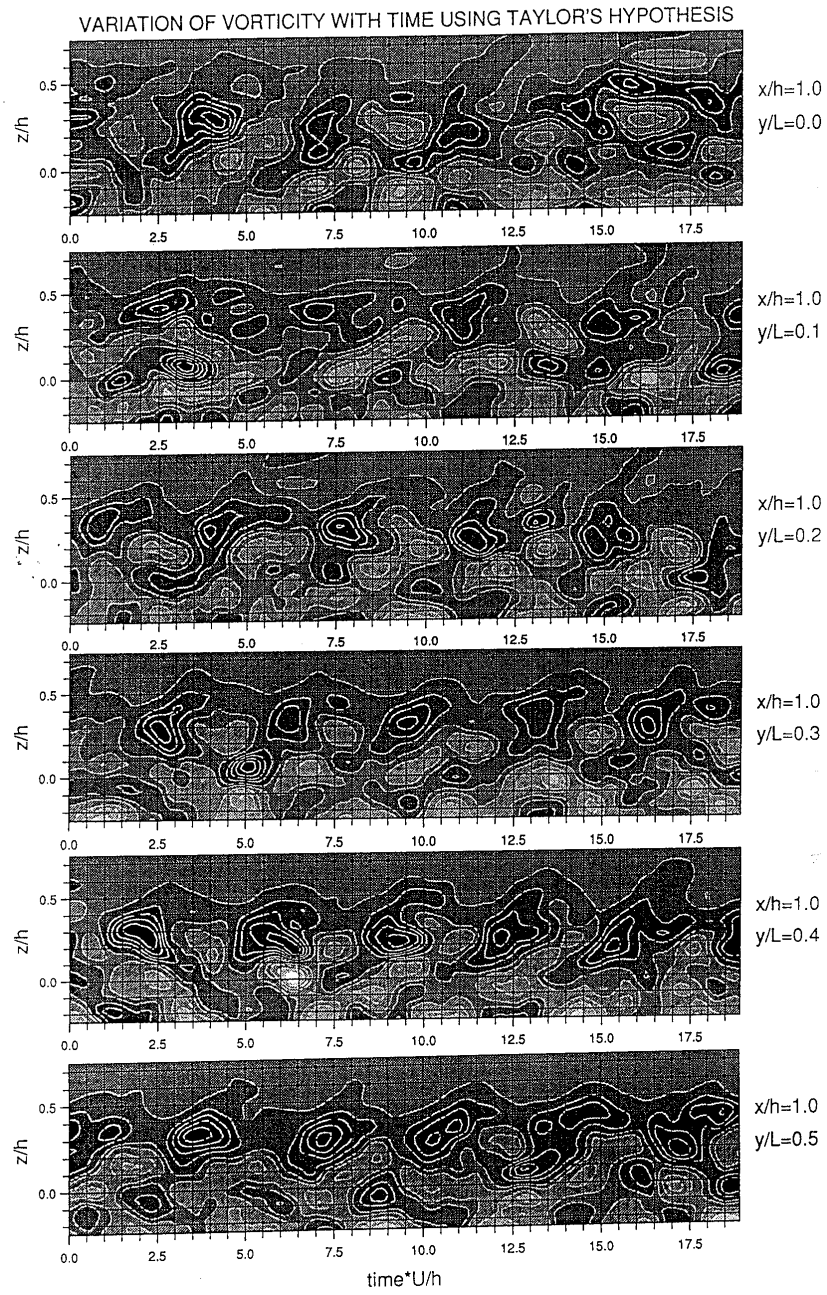

Figure 7.4 Variation of vorticity with time, for the sinusoidal model, using Taylor's hypothesis. These plots were obtained at x/h=1, for different spanwise positions. Note how the shedding becomes a little more frequent and much more ordered in the region of the valley.

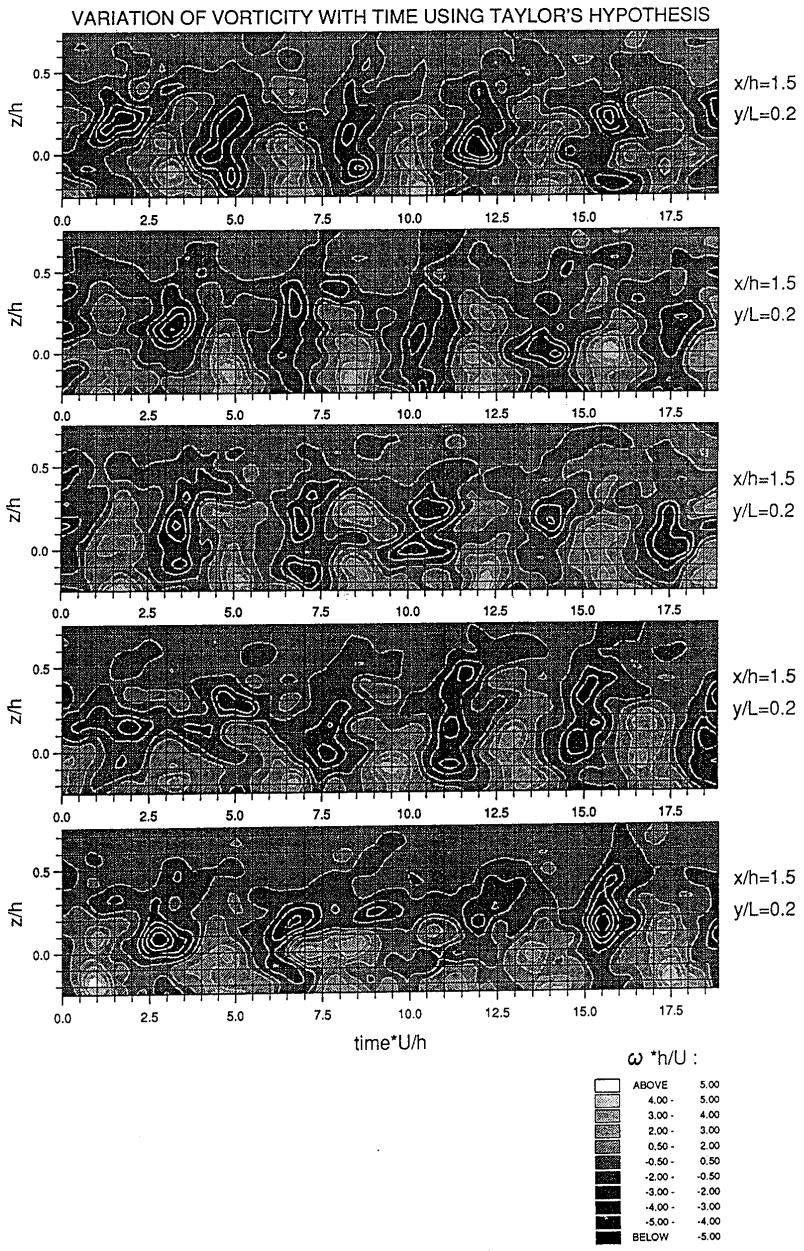

Figure 7.5 Variation of vorticity with time, for the sinusoidal model, using Taylor's hypothesis. These plots were all obtained at the same position (in the vicinity of the dislocation). Note the inconsistency in the shedding period, indicating a spanwise motion of the dislocation.

A common feature of both graphs is the layout of the vortices. Close to the body, at x/h=1, the vortices are quite flat and more well-defined. As they move downstream the vortices soon get stretched in the vertical direction and become more round (it should not be forgotten that the two axes are not to scale). The main vorticity on the upper side of the wake is negative. Smaller but also negative vortical structures appear for x/h=1 close to the centre wake and in anti phase to the main, Kármán vortices (especially apparent for the valley). The origin for these structures is unclear, but it should be pointed out that this is the region of heavily reversed flow where the experimental method is most likely to fail. It is possible that the cross-wire method over-predicts vorticity at the centre of the wake with the vortices thus appearing to be closer than expected to the wake centre.

There are, however, some notable differences between figures 7.2 and 7.3, other than the shedding frequency. At the peak (7.2), closer study of the contour plots reveals that there are significant fluctuations in the strengths of the Kármán vortices, while at the valley (7.3), even though we could not expect the vortices to have exactly equal strengths, any variations in the vortex strength appear to be much less noticeable. This seems to agree well with the hypothesis presented in section 5.2.3. In that section it was suggested that vortex strengths vary from one cycle to the next, in balance with both the fluctuating size of the formation region and also with the possible tendency of the flow to reduce the number of weak vortex links (their existence having been suggested by Williamson, 1992a). The spanwise size of each cell was cited as an important parameter for the ability of its vortex strengths to fluctuate from cycle to cycle. The low frequency cell of the peak has been repeatedly found to be of smaller size than that of the valley, and it was speculated that vortex strengths may fluctuate more in the peak than at the valley, which seems to fit with the present observations. It should also be noted that a conditional sampling method based solely on shedding phase (and not signal modulation) could not possibly detect the vortex strength fluctuations. Vortices in figure 7.2 appear also to be much less regular (more chaotic) than their counterparts of figure 7.3, a fact most probably related to the fluctuation of their strength.

Figure 7.4 shows a series of contour plots (all obtained for a distance from the local trailing edge of x/h=1) moving from the peak to the valley. The gradual transition from the relatively disordered state of the peak to the ordered state of the valley is apparent. Less obvious is that the wake is wider at the peak than at the valley.

Figure 7.5 presents different plots obtained from the same flow location, close to the estimated position of the dislocation. In chapter 5, a main issue had been the spanwise, periodic motion of the dislocation, probably at a frequency f_d ($=f_2-f_1$). If this is indeed the case then, most of the time, we would expect a spanwise position to exist where the shedding alternates between f_1 and f_2. This is confirmed by figure 7.5. The lower two plots have noticeable regions where the time between successive vortices is smaller than is usual in the other plots. For example, the reduced time between the second and the fifth vortices of the top plot is about 12.2 (corresponding to S=0.25), while between the first and the fourth vortices of the bottom plot it is approximately 10.0 (corresponding to S=0.3). Of course we should remember that the bandwidth of the spectra was wide to allow deviations of that order ($\approx$0.01) from the two Strouhal numbers of 0.24 and 0.29.

7.3.5 Estimation of vortex strengths

The average strengths of the vortices were obtained from numerous results such as those presented in figures 7.2 to 7.5. Of more relevance, of course, to the results presented in earlier chapters was the mean flux of vorticity (of one sign, negative in this case). In that way we would be able to see what fraction of the circulation shed from the model's trailing edge survived vortex formation. The results presented later are averaged for about 150 shedding cycles for each location of the flow studied.

Two criteria have to be established: (a) there has to be a criterion to decide whether a certain flow particle (containing some vorticity) belongs to a Kármán vortex or not, and (b) once the first criterion has been established, there also has to be an accurate determination of the time interval over which a certain whole number of Kármán vortices pass the line of the sensors (for example, if we look at figure 7.5 top, the number of whole vortices does not spread over the length of the plot, and to find the correct total vorticity *flux*, total vorticity would have to be calculated for a whole number of shedding cycles). Although the Taylor's hypothesis time-distance transformation has no real physical relevance for the present study (in the sense that although vortices are assumed to pass our reference line in a "frozen" state, we can obviously not expect them to be in the same state further upstream or downstream), the time co-ordinate was transformed into distance in order to compute the vortex strengths.

The first criterion (used to determine the extents of the vortices) first starts by detecting the peaks of the Kármán vortices. To determine the extent of the

vortices, we start to move radially outwards from each peak, until a certain threshold value of vorticity is reached (0.2 of the maximum level of vorticity). This is then taken to be the limit of the Kármán vortex. This is repeated for many radial directions, in order to establish the complete Kármán vortex boundary. The threshold value unavoidably had to be determined by trial and error but was chosen so that the vortices would have a fairly round shape (i.e. would not extend into the random, non-Kármán vortical structures of the wake).

The second criterion depended on determining vortex centres. The method used was described in section 7.3.3 (used there for the determination of the convection velocity). Once the peaks had been established, the total Kármán circulation between the leftmost and the rightmost peak for each Δ-interval would be divided by the appropriate time elapsed between those two peaks.

7.3.6 Discussion of wake parameter results

The results of this section would fit better in chapter 6 (the dynamics of the three-dimensional formation region). As was stated earlier in this chapter, the reason they are presented separately is the uncertainty concerning their accuracy.

Flux of spanwise vorticity was calculated as described in the previous section and is plotted in figure 7.6a. The most prominent feature is the significant decay of vorticity flux (and hence vortex strengths) as we move downstream. As Kármán vortices move downstream, they become more diffuse and start to interact with their counterparts from the other side of the wake. The rate of decay does, however seem a bit excessive. The possible cause could lie in the criterion used to determine the boundary of the vortices. Although for similar conditions we could, perhaps, expect the percentage error resulting from this criterion to be of the same order, it is probable that different percentage errors arise for different "kinds" of vortices.

We have postulated previously that an important parameter is the strength of the Kármán vortices just after vortex formation is completed. At that stage vortices will not yet be so diffuse as to interact with the opposite side of the wake, but will also have to link-up in some plausible way. Vortex strengths were thus evaluated by interpolation from graph 7.6a at $x=l_f+0.1h$, i.e. just after formation (the constant of 0.1h was not used to "adjust" the results, but to bring the value of x within the range of figure 7.6a, for all the spanwise positions). The dotted line of graph 7.6b shows the variation of vorticity flux along the span. For

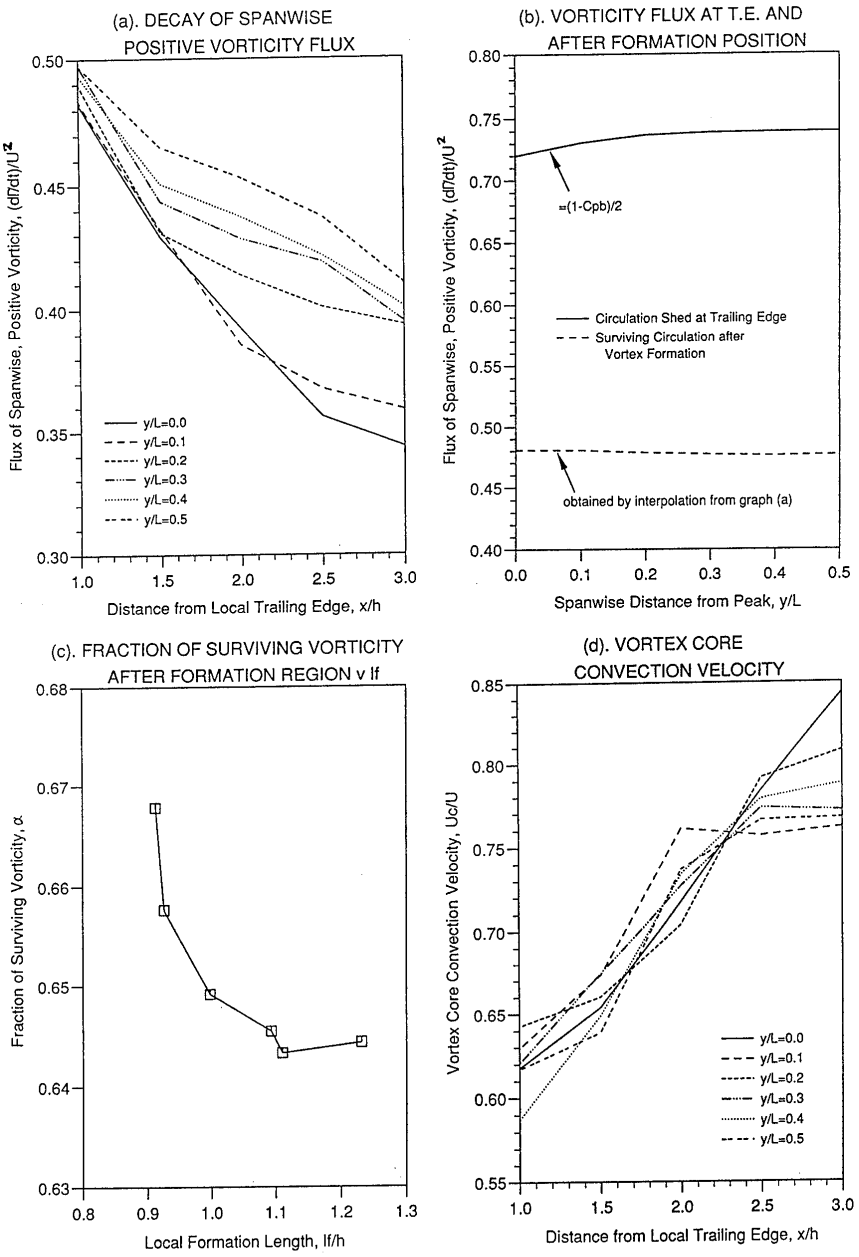

Figure 7.6 (a) Downstream decay of positive vorticity flux, (b) comparison of the vorticity flux at the model's trailing edge and at the formation position, (c) fraction of vorticity surviving the vortex formation process as a function of the formation length, and (d) vortex core convection velocity, as a function of downstream distance.

comparison, the continuous line represents the vorticity shed at the trailing edge, evaluated from the base pressure. Clearly, the amount of surviving vorticity appears to be much more constant (along the span) than the vorticity at the trailing edge. This result justifies the main assumption of chapters 5 and 6, that vortex looping does not occur and that $d(S\Gamma_V)/dy=0$.

A cautionary note should be made here about graph 7.6b. Obviously the results agree fully with suggestions and assumptions of previous chapters, a rather surprising fact, considering the errors that accumulate in the determination of the vortex strengths. It is proposed here that the suggestions of the previous chapters are reasonable and can stand without the results of this chapter. The fact that errors (unavoidable, given the available facilities) are involved in this chapter does not disprove figure 7.6b, nor does it disprove the main assumptions concerning vortex looping and vortex strengths ($d(S\Gamma_V)/dy=0$). Now the good agreement (despite the plethora of errors) between figure 7.6b and the $d(S\Gamma_V)/dy=0$ assumption could be due to the fact that the percentage error (overprediction or underprediction) is of a similar order for all spanwise locations.

The fraction α of surviving vorticity (as defined in chapter 6) can be deduced from figure 7.6b. The relation of fraction α to the formation length (l_f) is shown in figure 7.6c. Quite simply, when the formation length increases, we have increased entrainment and thus more vorticity destruction (as was suggested in chapter 6). It should be pointed out that the relationship shown in figure 7.6c is probably not unique. We have seen that the wake width (w_f) is also an important parameter related to the fraction α, perhaps a bit less significant than the formation length.

The convection velocity of the vortices was determined by using the methods described previously (in section7.3.3, mainly to be used for Taylor's hypothesis). Its downstream evolution, for the different spanwise locations, is shown in figure 7.6d. The general trend here seems to be the same for the different spanwise positions, with the convection velocity increasing as the vortices move away from the model. At a distance $x/h=1$ from the trailing edge the convection velocity is about 0.63U, gradually increasing to about 0.79U at $x/h=3$. Generally speaking, the convection velocity has been known to increase with downstream distance from the body, in theory starting from very small values during formation and then gradually tending towards the free stream velocity, far downstream. Bearman (1967b) reported on measurements obtained for a similar

model (with a blunt trailing edge, but without the sinusoidal disturbance) and the results were of a similar order to those of this chapter.

The downstream increase of the convection velocity could also be partly related to the downstream decay of the vortex strength. If we consider an ideal, infinite Kármán vortex street, the velocity induced on each vortex opposes the free stream. When the vortices become weaker (downstream of the model, as shown in figure 7.6a) they will tend to induce lower velocities on each other, and hence their convection velocity will tend towards the free stream.

7.4 Near wake instantaneous vorticity

7.4.1 Experimental set-up

An experiment was also performed which aimed to obtain the flow field in an entire plane. In that way Taylor's hypothesis would not have to be used for the determination of vorticity. Considering all the limitations of using hot-wire sensors in the near wake, this experiment was conducted mainly in order to see the potential of conditional sampling to obtain complicated, three-dimensional flow fields.

The three comparison hot-wire probes were located at valley-peak-valley, while the only plane studied was the vertical plane passing through the peak. The choice of that plane was for symmetry reasons, in order to assume that the spanwise velocity component is negligible ($v \ll \sqrt{(u^2+w^2)}$) when the shedding mode is symmetric. The size of the plane covered by the cross-wire probe was quite small (x/h=0.4 to 1.8, z/h=-0.5 to 0.5). Even for this small region, the amount of data that had to be sampled and analysed was quite large, of the order of 150Mbytes.

7.4.2 "Visualisation" of a complete shedding cycle

The calculated vorticity data had to be smoothened for the vortical structures to appear more coherent. A complete shedding cycle is shown in the sequence of figure 7.7.

At t*U/h=0 we can see a forming vortex at the upper side of the wake, which starts to break away and seems to have been fully shed by t*U/h=1. Meanwhile, vorticity has started to roll-up on the other side of the wake, gradually

INSTANTANEOUS SPANWISE VORTICITY CONTOURS

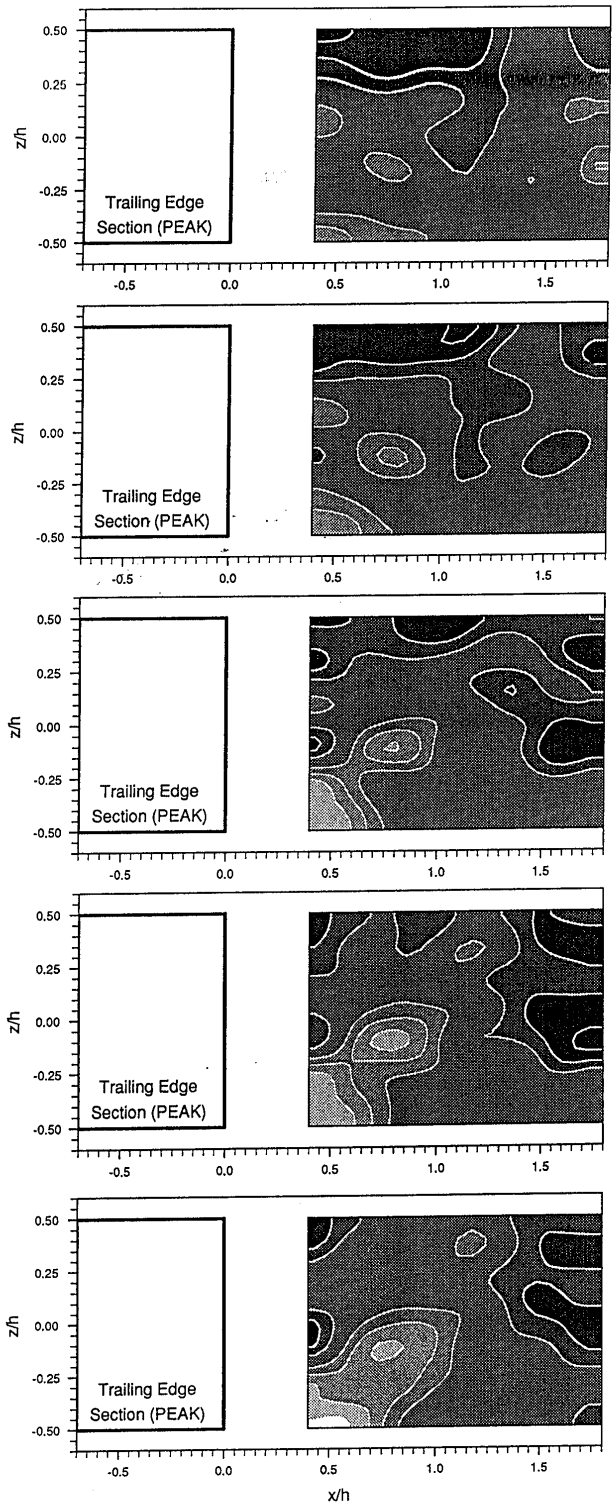

t*U/h= 0.000

t*U/h= 0.333

t*U/h= 0.667

t*U/h= 1.000

t*U/h= 1.333

INSTANTANEOUS SPANWISE VORTICITY CONTOURS (cont.)

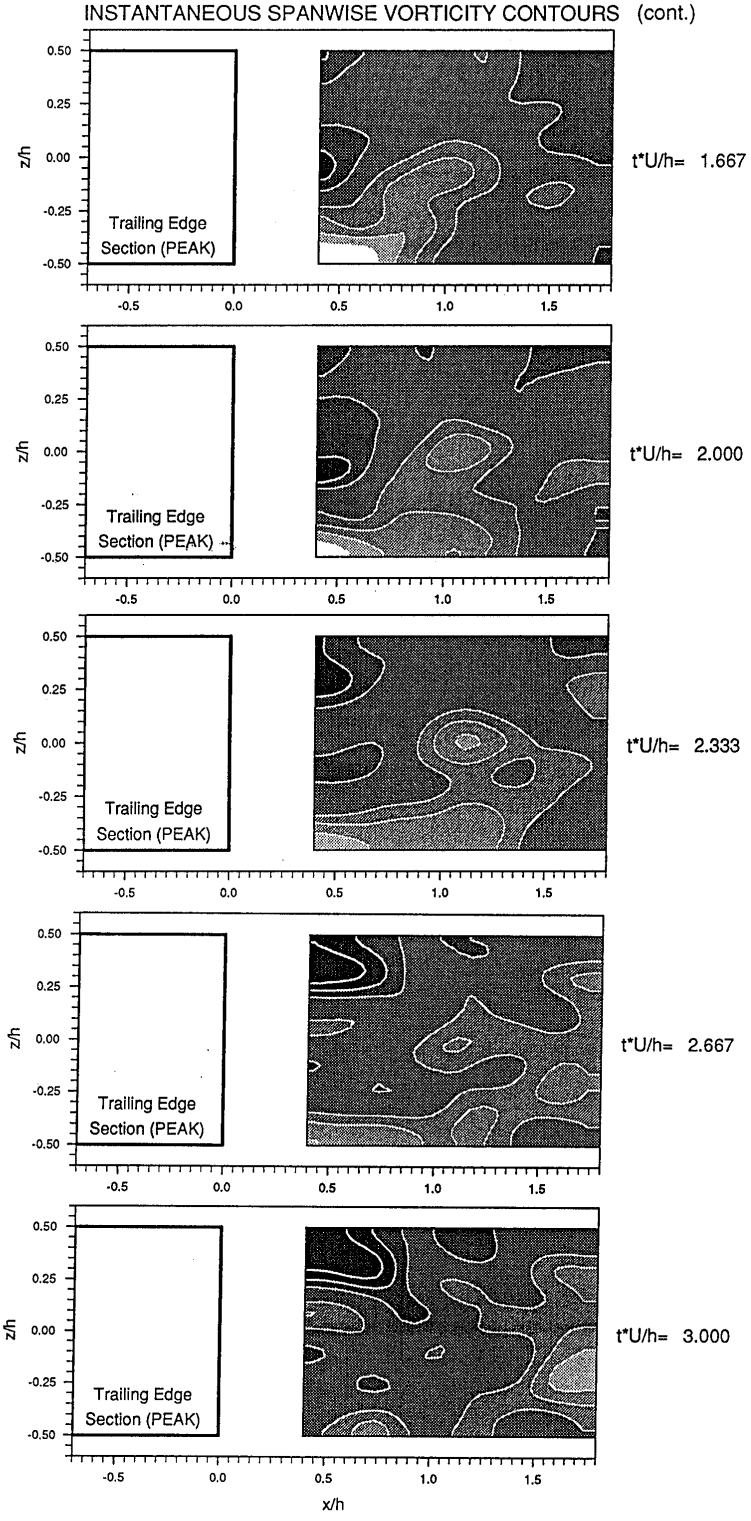

t*U/h= 1.667

t*U/h= 2.000

t*U/h= 2.333

t*U/h= 2.667

t*U/h= 3.000

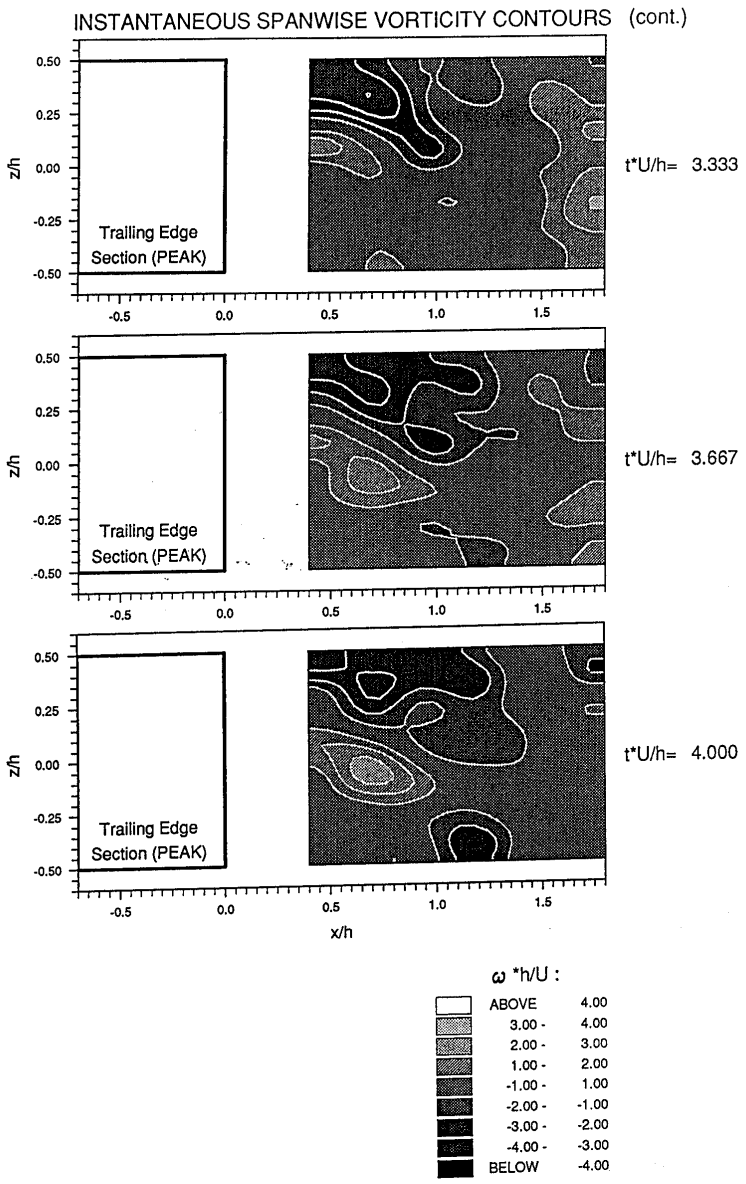

Figure 7.7 Step-by-step capture of one complete shedding cycle: the vorticity distribution in the near wake of the peak of the sinusoidal model.

becoming more apparent from t*U/h=0.667 to t*U/h=1.333. This vortex continues to grow until t*U/h=2.667, when it appears to have broken away (and thus we arrive again at the beginning of the cycle at about t*U/h=3.667.

Vortices also appear at the centre wake, close to the body (very noticeable at t*U/h=4, for example). They probably arise due to the limitations of the experimental technique in the near wake. Furthermore, it should be pointed out that, although vorticity appears to be roughly where we would expect it to be (i.e. in the forming vortices that then break away), we can by no means be certain of the geometrical properties of the vortices, which appear to have an irregular shape.

7.5 Conclusions

7.5.1 The near wake parameters

From the fluid mechanics point of view, the main purpose of this part of our investigation was to measure the strength of Kármán vortices. This was performed using conditional sampling, hot-wire anemometry and Taylor's hypothesis, each one of those factors by itself being able to undermine the validity of the results for the present application. Therefore the results of this chapter have been presented as "indications", not "proofs". The main *indications* stemming from part of the investigation were:

a) $d(S\Gamma_V)/dy=0$. The vorticity flux at each side of the wake after formation was found to be constant along the span. This was in agreement with the main assumption of both chapters 5 and 6. As a result, a larger proportion of the circulation shed at the trailing edge was found to have survived at the peak than at the valley, which yielded figure 7.6c, a relation between surviving vorticity and formation length.

b) Vortex strengths were found to vary from cycle to cycle (contradicting Williamson's 1992a hypothesis that all Kármán vortices within a cell have the same strength). This was observed more at the peak than at the valley (where the cell is larger and stronger). This was in agreement with the theories presented in chapter 5, concerning vortex linking across the dislocation and the fluctuation of vortex strengths at the dislocation frequency.

c) Indications emerged that the dislocation does indeed move in the spanwise direction. At y/L=0.2, there were instants where the shedding was at the low frequency and other instants when it was at the high frequency.

d) Vortex strengths were found to decay significantly as we moved away from the model.

e) Vortex convection velocity was found to rise as we moved away from the model.

7.5.2 Conditional sampling potential

In spite of experimental errors that were unavoidable given the available equipment, the present chapter gave some indications of the possible potential of conditional sampling for three-dimensional near wake studies. This section will not reiterate the shortcomings of the available apparatus, but make a few suggestions for well set-up future conditional sampling experiments.

The most important addition in terms of equipment would be a three-dimensional Laser-Doppler Anemometer. This would have the advantage of not being intrusive and also have the ability to measure reversed flow accurately. For the comparison signals hot-wire probes are adequate in terms of performance, as they can lie outside of the wake. A larger number of signals could have advantages.

The importance of comparing not only phase but also modulation cannot be emphasised strongly enough. The memory requirements of conditional sampling experiments where the comparison is performed after the experiment are huge. Similarly, on-line comparison within the computer would make experiments unreasonably long. A large step forward would be achieved if the comparison could be achieved on line at the A-D converter stage. For example a device could have in its memory the indicator functions and would perform continuous correlation with the incoming comparison signals. When all comparison signals recorded a certain level of correlation, data acquisition would be triggered (modern A-D converters can record data before the trigger, a feature necessary for the above procedure). The characteristic frequencies of the flow (up to a few kHz) are low enough to allow such an experiment. One more advantage of on-line correlation comparison would be that a higher degree of similarity between the indicator function and the incoming signal could be attained.

It is believed that with these two main additions (and with an experimental layout conceptually similar to the one used in the present experiment), fine details of three-dimensional near wake dynamics could be measured with accuracy.

8. NON-KÁRMÁN VORTICAL STRUCTURES

ABSTRACT : Vortical structures in the x- and z- directions have been observed. ω_z vortices are present in the near wake. It is suggested that they first get entrained into the shear layer (with the creation of ω_x vorticity) and then roll-up around the Kármán vortices. It is further proposed that the observed vortices are responsible for the intense base pressure fluctuations and gradients, and also for thin "wisps" appearing between Kármán vortices in flow visualisation.

8.1 Introduction

8.1.1 Observations in other investigations

When the flow around a bluff body separates, vorticity created on the body surface is shed downstream. We have seen how an instability causes this vorticity, initially contained within the separated shear layers, to reorganise itself into coherent structures. For bodies with a base (the area bounded by the separation line) of larger aspect ratio than about 2-3, the reorganisation of vorticity can take the form of the Kármán vortex street. In the simplest case, a Kármán vortex has all its vorticity in the y-direction but there can be also components in the x- and z-directions when three-dimensionality prevails. All the vortical structures we have discussed so far are Kármán vortices, irrespective of any vortex splitting that may take place. Even though the most dominant wake structure is the vortex street, other types of vortices have also been observed in wake flows. Some examples are:

a) Turbulence, the most obvious and common example, present in all but the very low Reynolds number cases.

b) Transition waves within the separated shear layer. These are caused by a Kelvin-Helmholtz instability within the shear layer and have been observed in a number of studies. Figure 1.2 showed flow visualisation pictures from Gerrard (1978).

c) ω_z vortices in the near wake, observed by Rockwell (1992 and private communication). These are shown in figure 8.1. Vorticity contours were obtained by P.I.V. (Particle Image Velocimetry) in water at a Reynolds number of about 2000. Note the alternating sign, spanwise organisation of the ω_z vortices. More details about the structure of these vortices were not known at the time of

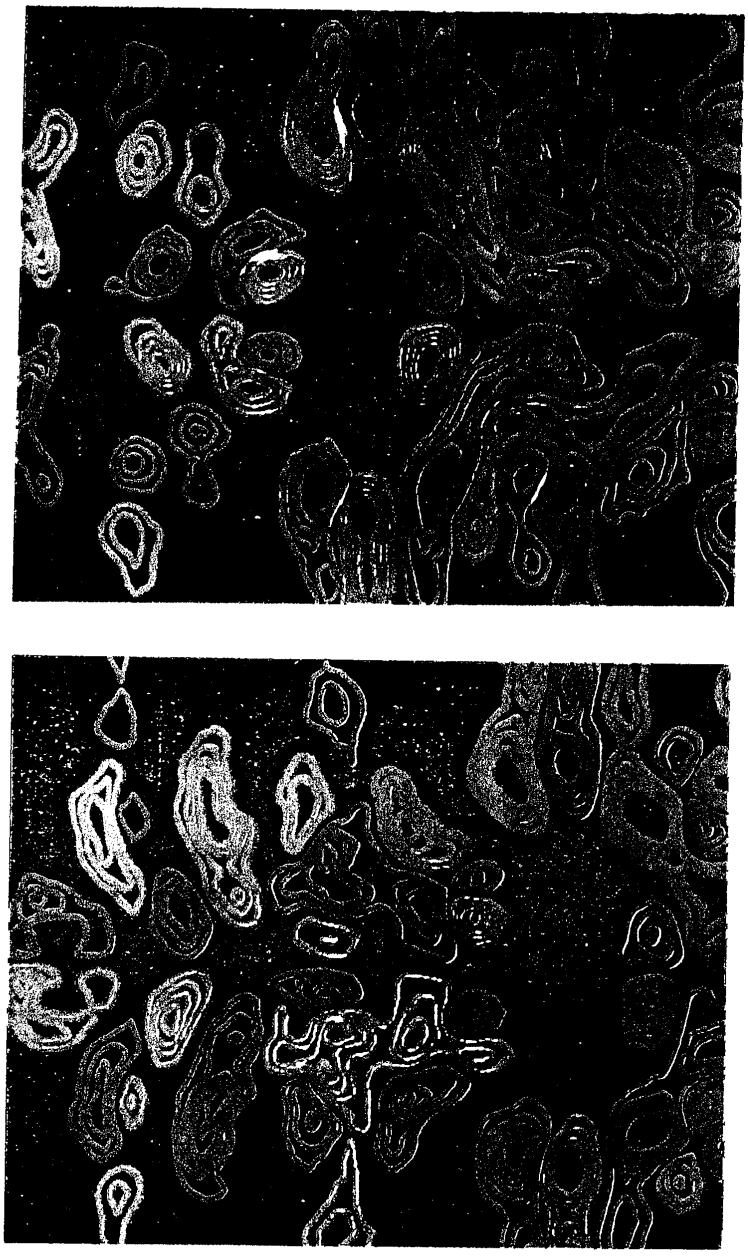

Figure 8.1 ω_z vorticity measured in Lehigh University, using a P.I.V. technique. These pictures show the centre-wake planes for the flow behind a non-uniform cylinder (flow is from left to right). Similar patterns were observed by Rockwell for uniform cylinders (Rockwell, 1992).

communication. The strength of the vortices was not necessarily constant from one shedding cycle to the other. Somewhat surprisingly, these vortices were said to have strengths comparable to those of the Kármán vortices.

8.1.2 The present study

Figures 4.20 and 4.21 illustrated large base pressure irregularities that were said to be one of the reasons for the low base pressure correlation length (in comparison with the velocity signal correlation length). In these graphs we can see periods of intense activity in the base pressure fluctuations when large instantaneous base pressure gradients would also arise. The existence of ω_z vortices in the near wake (similar to those observed by Rockwell) could neatly explain this phenomenon.

P.I.V. facilities such as those used by Rockwell to observe the near wake ω_z vortices were not available in this study, and so flow visualisation experiments were performed. Both types of experiment (base pressure fluctuation measurements and flow visualisation) were carried out for both the straight and the sinusoidal model. There was no noticeable influence of the body shape on the observations, and so only the straight trailing edge results are presented in this chapter.

It was thus the purpose of this part of the investigation to search for near wake ω_z vortices and any other related vortical structures. Understanding their structure, apart from explaining the base pressure fluctuations, could have certain implications on the formation region vortex dynamics discussed in chapters 5 and 6. As will be seen, near wake ω_z vortices are smaller structures than the Kármán vortices. It is difficult to say whether they should be classified as "turbulence". As was stated in chapter 1, the dividing line between turbulence and larger structures is very thin and not well-defined. No attempt will be made in this chapter to give an answer to that question.

As a final cautionary note, it should be stressed that the investigations presented in this chapter are of a very preliminary nature. To draw more certain conclusions about such smaller scale structures would require a considerably more complicated and expensive experimental set-up.

8.2 The structure of non-Kármán vortices

8.2.1 Observation of z-axis vorticity

The flow visualisation technique used was described in section 3.3.2. In this particular experiment, the tin strip was positioned on the model base. Creating the precipitate in the unseparated boundary layer would have confined the precipitate within the separated shear layer which has vorticity that predominantly reorganises into Kármán vortices, thus concealing the lower vorticity structures of the near wake. In the present arrangement, however, the precipitate would first diffuse from the base into the near wake and then get carried away by the Kármán vortex street.

The laser sheet was deflected by a mirror located far downstream of the model (50h). It was adjusted to illuminate z=constant planes (e.g. z=0 is the centre wake). The fluid motion predominantly highlighted by the laser sheet would be within those planes, thus giving an impression of ω_z vorticity, when the camera looked down along the z-axis. Note also that due to the unclear water and the remoteness of the laser source the illuminated "plane" was about 2-3mm thick.

Figure 8.2 shows a series of photographs obtained using the above arrangement (as always the pictures were processed from a video). At the centre wake (photos a and b) we can see tin precipitate that has diffused from the model and been distorted by the complex velocity patterns in the near wake. We should always remember that there is no direct link between precipitate concentration and vorticity (especially in this case when the precipitate does not necessarily get created in the same location as vorticity). Nevertheless, from photos (a) and (b) we can see how the precipitate has been twisted by near wake vorticity. This twisting was even more apparent when studying the video.

Similar patterns can be seen in photos (c) and (d) which represent a z=(1/6)h section of the wake. We can thus conclude that these structures are, in fact, similar to those observed by Rockwell. Photos (e) and (f) represent a z=(1/3)h section. Again at this plane similar structures could be observed. We should make a note about photo (f), where very little seems to be happening. At the other planes there would also be prolonged intervals when there was no apparent near wake ω_z vorticity. This could possibly fit in with the periods of low

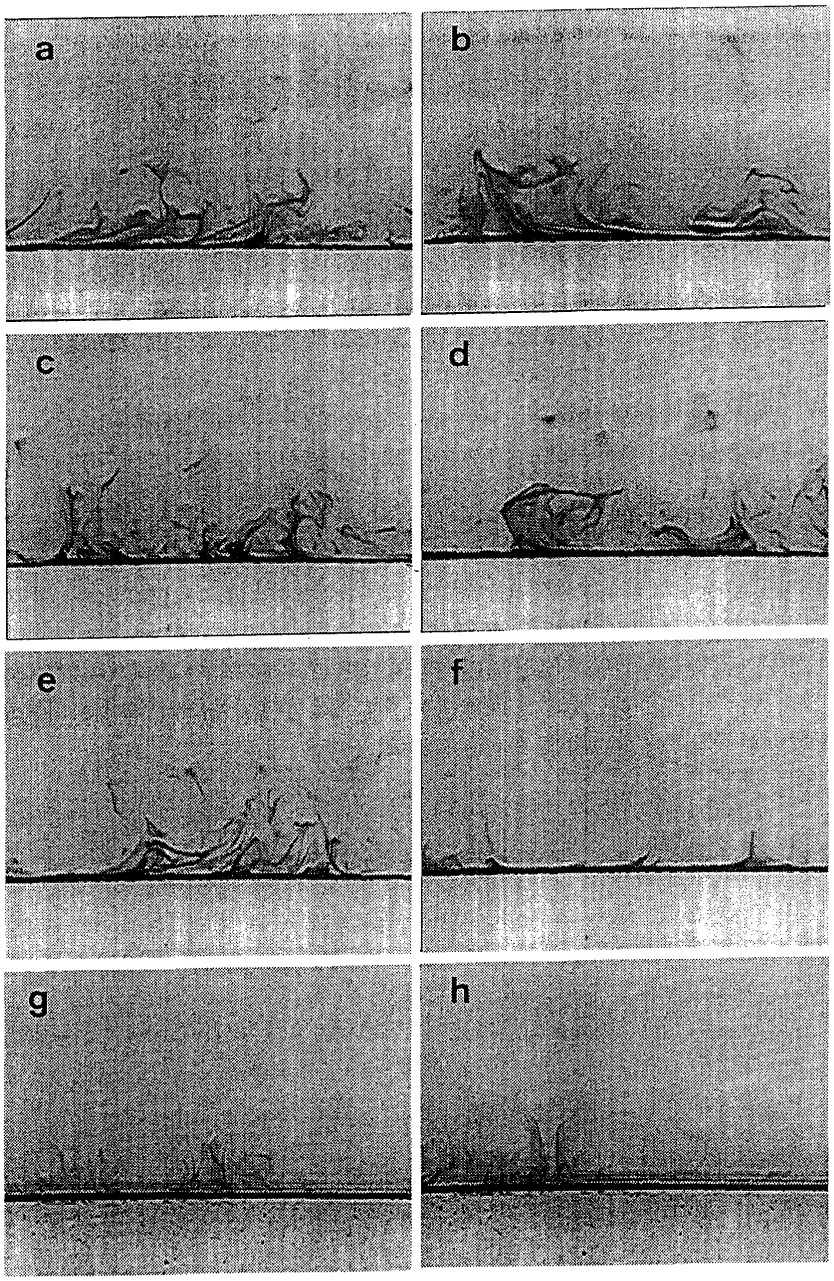

Figure 8.2 Flow visualisation for the straight model (plan view, precipitate produced at model base, flow is going upwards). Laser sheet illuminates z=constant planes. Photos (a) and (b): z/h=0, photos (c) and (d): z/h=0.167, photos (e) and (f): z/h=0.333, and photos (g) and (h): z/h=0.5.

base pressure fluctuations and pressure gradients observed at some parts of figures 4.20 and 4.21.

Photos (g) and (h) have been taken for z=(1/2)h, i.e. at the level of the separated shear layer. Obviously we would not expect the near wake ω_z vortices to extend that far and this can also be seen in the photographs. What probably happens is that the vortices, under the influence of the shear layer, bend around and get entrained in it, thus getting convected downstream. At the centre of photo (g) and at about 2/5 from the left of photo (h) we can see what could be the entrainment of the near wake ω_z vortices into the shear layer.

8.2.2 Observation of streamwise vorticity

If we are to assume that vorticity gets bent around from the shear layer, we then have a shear layer which carries not only y-vorticity but also x-vorticity, even though we would expect x-vorticity to be less uniformly distributed that y-vorticity. An experiment was set-up to observe such streamwise vorticity, other than the component which invariably arises during vortex splitting. Tin precipitate was created in both of the unseparated boundary layers of the model. The laser sheet was adjusted to be parallel to the model base, and different x=constant planes were studied. The video was shot looking upstream, through the mirror positioned 50h downstream of the model. The major disadvantage of this arrangement was the long path of unclear water between the laser sheet and the camera. Photographs obtained using the above procedure are shown in figure 8.3.

For illuminated planes with $x<h$, the shear layers could be seen, and although they had the occasional ripple and waviness, no clear vortical structures could be observed. Clearer ω_x vortical structures were observed for $x\geq h$, i.e. after the vortex formation position. From the photographs we can see the ω_x vortices becoming larger and clearer as we progress downstream (a&b: x=h, c&d: x=(4/3)h, e&f: x=(5/3)h, g&h: x=2h). Again there are periods with much reduced activity. Even though there are isolated vortices (e.g. in photo f), the predominant feature seems to be pairs of vortices of opposite signs. This can be seen in (b), (d), (e) and (h), and could be related to the array of oppositely-signed ω_z vortices observed by Rockwell in the near wake (if these vortices are entrained by the shear layer, as suggested earlier, we could then also expect ω_x vortices of opposite signs to be adjacent to each other.

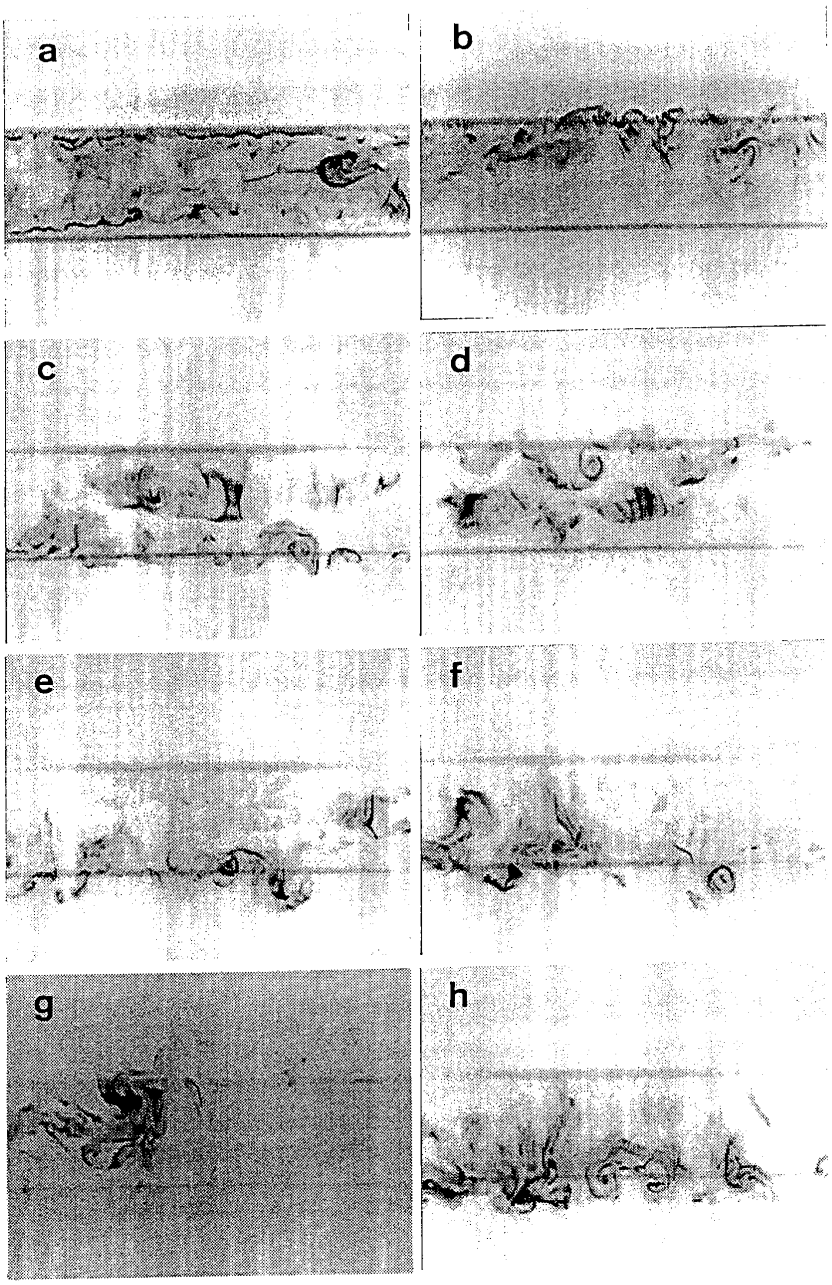

Figure 8.3 Flow visualisation for the straight model (rear view, looking upstream). Laser sheet illuminates x=constant planes. Photos (a) and (b): x/h=1, photos (c) and (d): x/h=1.333, photos (e) and (f): x/h=1.667, and photos (g) and (h): x/h=2.

There was also the impression that the streamwise vorticity would get entrained together with the shear layer into the forming vortex. The inhomogeneities observed along the length of Kármán vortices could then be partly due to the x-vorticity found in the shear layer.

8.3 Closing remarks on non-Kármán vortices

8.3.1 Some brief thoughts on the possible structure of non-Kármán vortices

So far we have observed ω_z vortices in the near wake and ω_x vortices downstream from about x=h onwards. We have also observed these vortices to have a higher degree of irregularity and also to be of smaller scale than the Kármán vortices, facts that make them considerably more complicated in their experimental study. It is apparent that the observations of this chapter are incomplete. Not enough evidence has emerged about the structure and the origin of the non-Kármán vortices that were observed.

There are indications, however, that the near wake ω_z vortices and the ω_x vortices are related. Photo 8.2h probably shows an ω_z vortex getting entrained into the separated shear layer. In that way the shear layer will also contain ω_x vorticity, which could then form the ω_x vortices observed in flow visualisation. If we now imagine the shear layer rolling-up into a Kármán vortex, we would then expect the ω_x vortices to follow suit. At the time when the forming vortex gets cut-off from the shear layer, there must also be some consequences on the ω_x vortices. Now vortices cannot get cut in half along their axis and so, if we are to assume that something like that happens to the ω_x vortices, we must adequately explain how ω_x vortex lines link to other vortices, in order not to violate fundamental fluid mechanics laws. There are probably various different and possible accommodating mechanisms but one process seems to be the most probable.

ω_x vortices could roll-up around the Kármán vortex, but not actually break-up. In that case the Kármán vortex would get shed in the normal way but leave behind it thin "wisps" of ω_x vorticity. These would roll-up in one of the next forming Kármán vortices, either the next one (of opposite sign) or the next one of similar sign. Looking back to flow visualisation pictures of earlier chapters, thin links between Kármán vortices have been observed. They can be seen in most plan views of the wake (for both models) but most notably in photos 4.10d, 4.10e, 4.22d and 4.23c. In the previous section we saw that, in general, ω_x vortices tend to form pairs of opposite signs. This could be quite significant in terms of their

influence on the strengths of the Kármán vortices: the effects of two (paired) ω_X vortices could effectively cancel each other out.

We have thus seen a possible geometrical structure of the ω_X-ω_Z vortices, but even if the above suggestion is correct, we still have to explain the origin of this vorticity. Batchelor (pages 277-282) gives a theoretical account on the generation of vorticity. The main conclusion is that for a uniform fluid where motion has started from rest, vorticity has to diffuse into the fluid from a solid boundary. In the present case flow visualisation and fluctuating base pressure observations showed that the presence of the near wake ω_Z vortices is intermittent. We saw how periods of intense ω_Z activity could be superseded by relatively "quiet" periods. This means that ω_Z vorticity does not only get generated at the initiation of the flow, but can also arise in a fully-developed flow and also possibly vanishes when the conditions allow.

8.3.2 Outstanding questions

As was stated at the beginning, this chapter presented work that was of a very preliminary and speculative nature. Some ideas were presented concerning their structure, but considerably more effort has to go into this area for certain conclusions to be reached. Perhaps the most important consequence of the non-Kármán vortices to the present study is that their presence can account for the large spanwise base pressure gradients observed in the wind tunnel. Many more questions have been left unanswered, however:

a) What is the exact geometry of the ω_Z and the ω_X vortices and how are they related?

b) What are the strengths of these vortices?

c) What is the significance of the pairing patterns observed?

d) Which model surface is the source of this vorticity, and what instability causes it?

e) What is the reason for the apparent intermittency in the "activity" of the non Kármán vortices?

We could think of many more questions that are still far from answered concerning the non-Kármán vortices. It is apparent that much more comprehensive investigations into that subject are needed. The present study merely scratched the

surface of that potentially large subject. Many thanks are also due to Professor D. Rockwell, of Lehigh University, for his invaluable discussions on the subject.

9. THE INTERACTION OF NEAR WAKE PARAMETERS

ABSTRACT : In summarising the proposals of previous chapters, a systematic method is proposed in order to sub-divide the near wake problem into smaller modules. The various significant frequency ranges of the flow are considered to represent different levels of hierarchy. By neglecting weak interactions of wake parameters, it is possible to view the flow as a system controlled by instructions and feedback fed between the different wake parameters and the various levels of hierarchy.

9.1 Modular sub-division of the flow

9.1.1 The frequency scales of wake flows

Looking back to the theories of the previous chapters, we can see that chapters 5, 6 and 8 each concerned a particular frequency range. In chapter 5, wake dynamics were studied from the point of view of fluctuations at the dislocation frequency, in chapter 6, mean wake characteristics were considered, while chapter 8 looked into smaller scales of fluid motion. Each of these chapters thus looked at the flow from a different perspective, taking certain facts for granted and not elaborating on the consequences of some other features.

It is, of course, an undeniable fact that for a strongly non-linear physical system such as a wake flow, one must consider all effects together. It is difficult to think of two wake features that do not depend on each other. For a complete understanding (both qualitative and quantitative) of the dynamics of the flow we would need to solve the Navier-Stokes equation down to its smaller scales. Chapters 5 and 6 (and to a much lesser extent, chapter 8), however, have given what appear to be satisfactory explanations of various flow phenomena despite considering limited aspects of the flow at any one time.

The purpose of this study is to understand some of the *physics* of the wake. Although this approach will not be considered to be very rigorous from a mathematical point of view, we will attempt to assess the influences of the frequency ranges separately. In the model to be proposed in the present chapter, the interaction between the various frequency scales will be macroscopic, but not negligible. To illustrate this approach, let us consider how it would attempt to deal with the two-dimensional flow around a circular cylinder at a very low super-

critical (Re≈50-60) Reynolds number (this example not aiming to explain that particular flow). Such a flow would have mainly two characteristic frequencies: f=0 and the shedding frequency. The shedding frequency characteristics would be controlled by a series of steady, unchanging parameters, such as base pressure, formation length, wake width and vortex strength. The mechanisms which actually prevail at the shedding frequency would have to move within this framework, and are reasonably understood. Some form of feedback could readjust the steady wake parameters should an imbalance arise.

In the flow around the sinusoidal model, we have more or less identified the various important frequency ranges:

a) The dynamics of the *mean flow* parameters were discussed in chapter 6. Perhaps the biggest contribution of this chapter was the realisation that, given the geometry, the dual frequency characteristic has to exist.

b) Fluctuations at the *dislocation frequency* (presented in chapter 5). In this chapter the emphasis was on the mechanisms that spread the dislocation frequency disturbance to practically all the near wake parameters.

c) Fluctuations at the actual *shedding frequency*. Perhaps ironically, for a Kármán wake flow study, these effects are only considered macroscopically and not in much detail in the present study.

d) *Smaller scale vortical structures* (briefly presented in chapter 8).

e) *Turbulence* (not necessarily very distinct from (d)).

It should be noted that considering the effects of the various frequency ranges separately does not imply some kind of spectral solution to the Navier-Stokes equation. For example, let us consider the mean characteristics of a flow, where vortex shedding would still be taken into consideration. In a solution to the steady Navier-Stokes equation, the main assumption would be that shedding frequency fluctuations do not exist. Under the proposed approach to the flow, vortex shedding is seen as the consequence of the equilibrium between mean flow properties (such as formation length, wake width, base pressure, etc.). The assumption here is that one shedding cycle does not depend much on the previous one, but rather its parameters are set by slower varying factors.

The aims of such an approach are to give a qualitative explanation of the dynamics of the wake, the main advantage being that it helps put the flow

parameter interactions into a proper perspective. In order to simplify the considerations, parameters that are not judged to have a direct and pronounced effect on each other are simply "uncoupled" from each other.

9.1.2 A systematic approach to the interaction of wake parameters

So, it is generally accepted that almost all wake parameters are interrelated and linked to each other. In order to gain a better understanding of the fundamental mechanisms of the near wake, we will discard all weak links and dependencies, and only consider dependencies of primary importance. A convenient way to do that is by considering the separate frequency ranges.

An approach like this allows us to view the flow as a system of interacting parameters and to draw relevant block diagrams that outline the important dependencies within the near wake. The attraction of a block diagram is that it makes it easier to appreciate the various fundamental relations between all the relevant parameters. This chapter is, in effect, a summary of the theories and suggestions of the present study, in the context of the proposed systematic approach to the near wake problem.

We can perhaps view the various frequency ranges as different levels of hierarchy. Not all of them are of the same importance for the eventual overall flow pattern. Let us imagine a periodic pattern within one of the frequency ranges. In relation to patterns of much smaller time scales, it is difficult to imagine that it depends on the exact instantaneous state of the smaller time scale pattern; at best, it will feel the time-averaged effect of the smaller time scale pattern. On the other hand, if we consider the influence of a slower-varying pattern, the exact instantaneous state of this slow pattern will be influential. Hence, the different hierarchy levels are in the order of the time scales of the various frequency ranges (i.e. the mean flow is the highest level of hierarchy).

The whole approach is similar to the dynamics of a large organisation where instructions circulate between the various levels of the hierarchy. Not all levels have access to all the information. "Instructions" are fed downwards and are influenced by feedback going upwards. Similarly, other "decisions" have to be taken in order to balance two (or more) conflicting trends within the company.

9.2 A model for the interaction of wake parameters in the present flow

9.2.1 High hierarchy level: mean flow parameters

The block diagram of figure 9.1 is effectively a summary of chapter 6, showing the interaction of the mean flow characteristics. In the main section of the diagram, angular, "property" boxes represent various wake parameters, and rounded boxes represent explanations justifying the relation between some of the property boxes. Note also the significance of the arrows, outlined in the key at the bottom of the diagram. The main features of the diagram are outlined below.

As a result of (a) the tendency of the forming vortices to straighten out, and (b) the model geometry, the formation length will have to be larger at the valley. To satisfy $S^*\Gamma_V$=constant along the span, and as a result of the higher level of entrainment (because of the longer formation length), the vorticity shed from the separation point at the valley must be larger, and similarly then we will expect the base drag to be higher at the valley. As the wake curvature of the separated shear layer is related to the base pressure, the wake will have to be wider at the peak than at the valley.

Now wake similarity arguments can be used to predict the mean shedding frequency along the span. It is proposed that the selection of the two shedding frequencies is due to a spanwise lock-in, which results in the domination of two frequencies. A natural progression then is vortex splitting, as is a streamwise component of vorticity, said to be vital to sustain a steep pressure gradient across the dislocation.

The main "instruction" passed on from this hierarchy level to the dislocation frequency dynamics is the magnitude of the two shedding frequencies. A variety of other instructions (combined with others arising from the dislocation frequency hierarchy level) also get passed on to the shedding frequency hierarchy level.

A feedback is received from the dislocation frequency hierarchy level, which determines the spanwise motion of the dislocation. In that way, mean value distributions of quantities like base pressure, shedding frequency and wake width can be predicted by considering the time spent by each spanwise position at each shedding frequency. Not shown in figure 9.1, are numerous feedbacks received from the shedding frequency level: in a way, a large number of the general rules

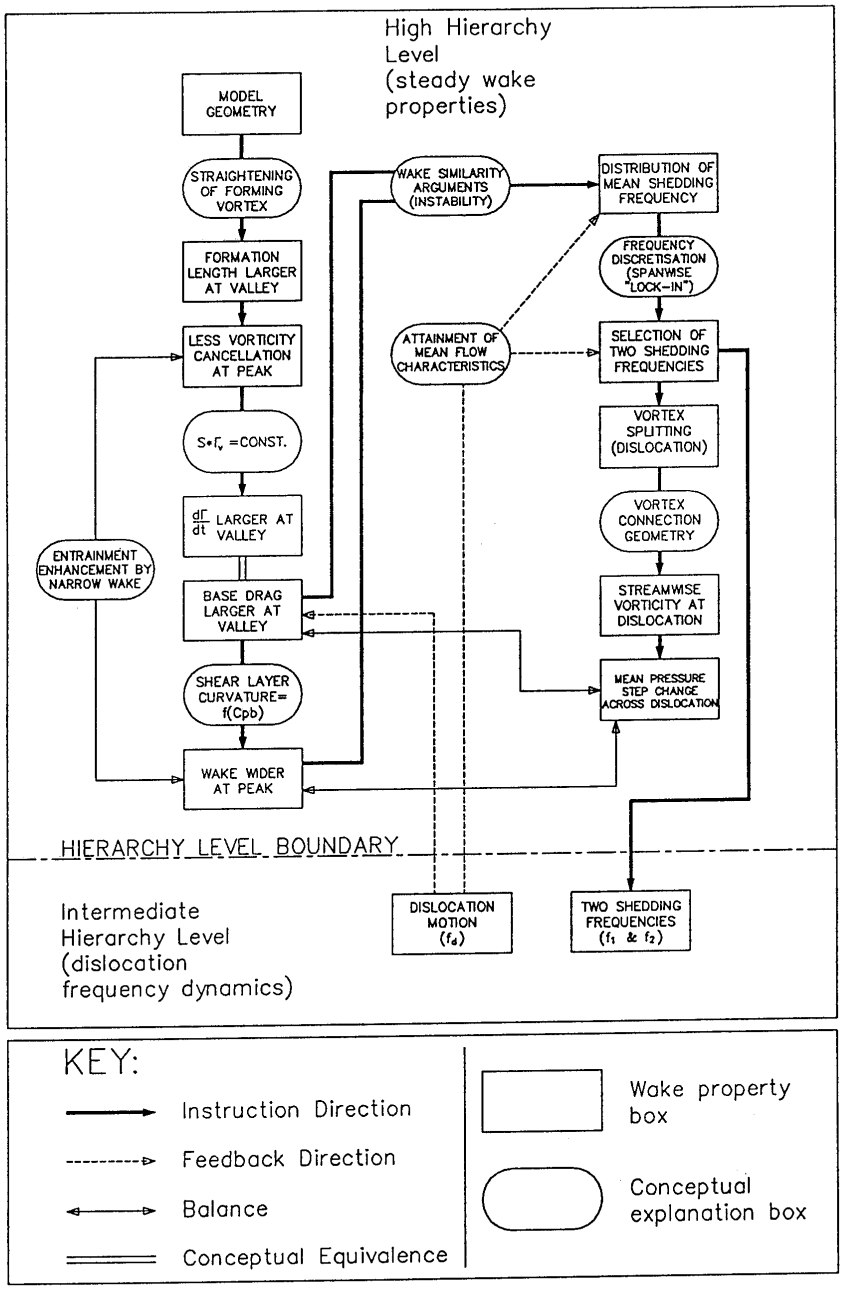

Figure 9.1 Block diagram showing the interaction of wake parameters at the high hierarchy level (steady wake properties).

used for the logical progression from the one box to the other are some kind of feedback from the shedding frequency dynamics (e.g. the relation between the formation length and the fraction of surviving vorticity). It is interesting to note the macroscopic nature of this feedback: the exact dynamics that determine this particular relation (or other relations) are of no interest or consequence.

Obviously, a lot of over-simplifications exist in the proposals outlined by the block diagram of figure 9.1. If we thought more about it, good reasons could perhaps emerge to add a lot more boxes and arrows linking all the possible combinations of boxes. The diagram is not intended as a "solution" to the myriads of simultaneous equations that need to solved in the wake, but a framework that helps explain the main interactions and influences between some of the wake quantities.

9.2.2 Intermediate hierarchy level: dislocation frequency parameters

This section will, in effect, be a summary of the mechanisms described in chapter 5 in the context of the considerations outlined just above. Figure 9.2 is a block diagram showing a possible way that the dislocation frequency parameters interact. The emphasis is not on the exact relation between two parameters, but on the physical reasons behind that interaction.

On the top of the figure we have parameters that belong to the higher hierarchy level and arrive in the form of "instructions". For example, the reason why there are two shedding frequencies is not the issue, but is taken for granted in this diagram. The middle section of the diagram (and also the largest) is a block representation outlining the routes of interaction of the parameters that are affected by the dislocation frequency f_d. More "instructions" emerge from this section and are passed to the lower section of the diagram, which represents the shedding frequency hierarchy level dynamics.

We will briefly go through the logical stages of the central portion of the diagram. All the quantities fluctuate at the dislocation frequency. As a result of the two shedding frequencies, vortex splitting occurs. Geometrical considerations on how the vortices link across the dislocation mean that vortices have to bow in its vicinity, which is conceptually equivalent to the formation region fluctuating in size. In turn this results in dislocation frequency base pressure fluctuations, and consequently, in unequal vortex strengths from cycle to cycle.

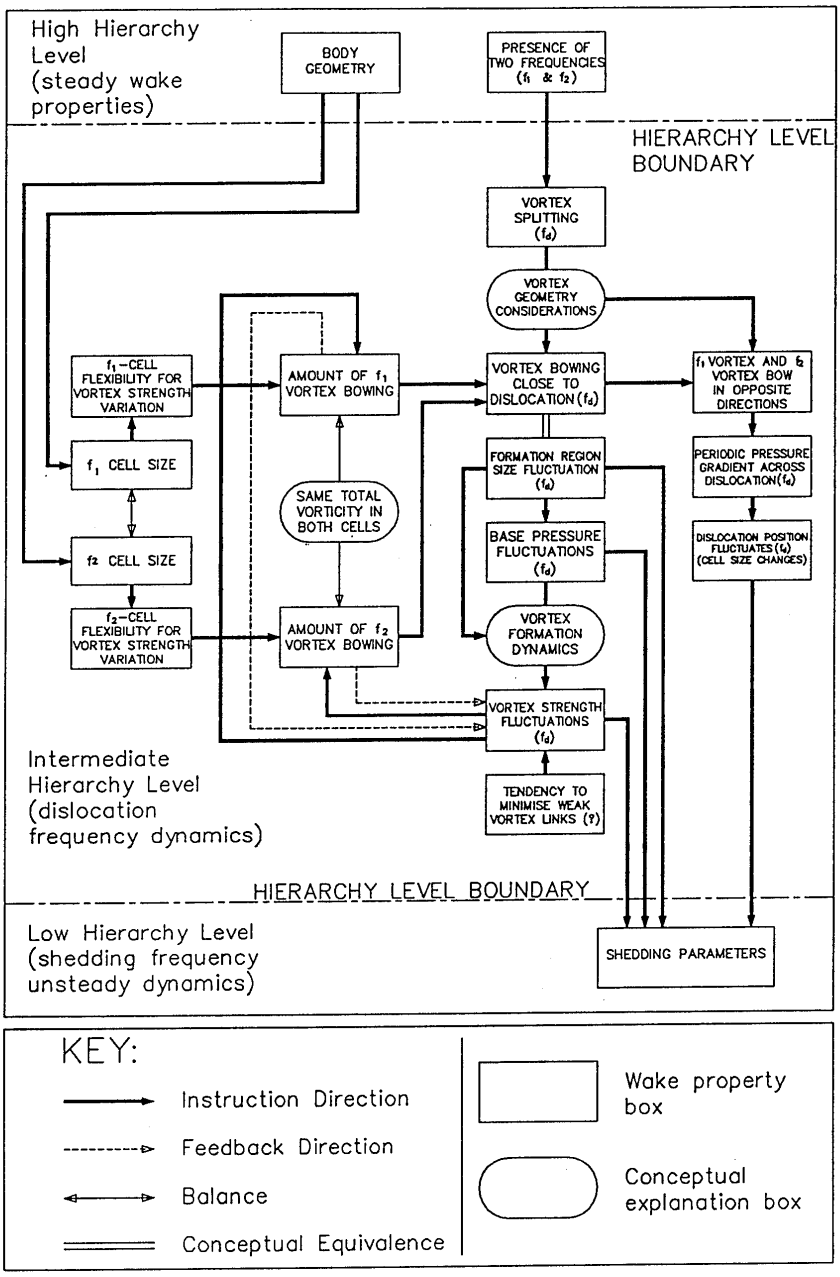

Figure 9.2 Block diagram showing the interaction of wake parameters at the intermediate hierarchy level (dislocation frequency dynamics).

In order for two vortices (on either side of the dislocation) to meet, they both have to bow. The quantity of bowing that goes to each cell depends on the flexibility of each cell to change its vortex strengths from cycle to cycle, which, in turn, depends on the mean cell size (which was information received from the higher hierarchy level). A balance has to exist between these parameters in order to obey a fundamental rule, that the sum of the vortex strengths on either side of the dislocation is the same (given that no vortex looping occurs). A further parameter that may influence the vortex strengths is a possible tendency of the flow to adjust in such a way so to minimise the weak vortex links.

The fact that the bowing of vortices on each side of the dislocation tends to be in the opposite direction (again for geometrical reasons) means that a periodic spanwise pressure gradient could arise across the dislocation, again fluctuating at the dislocation frequency. This could be the reason the dislocation seems to move back and forth in the spanwise direction.

9.2.3 Lower hierarchy levels

It is clear from section 2.1 ("Aims of the project") that a detailed study of the lower hierarchy levels was not one of the primary aims of this investigation. Too many studies in the past have described (in much detail) the shedding frequency fluctuations, for this study to have something to add. The small deviation into smaller time-scales (the non-Kármán vortical structures of chapter 8) did not yield sufficient information for a systematic approach to the dynamics of that frequency scale. Within the framework of the systematic approach of this chapter, we can speculate on how some of the lower hierarchy levels *may* function.

At the shedding frequency level, a significant assumption is that one shedding cycle is only influenced very lightly from its immediate predecessor. Its main parameters are controlled by the two higher hierarchy levels: depending on the spanwise position and the instantaneous position of the dislocation, the shedding frequency is decided. Further steady and unsteady (f_d) interactions determine parameters such as the formation length, wake width and vortex strength. From a fluid mechanic point of view, we could expect, in the event of some imbalance (e.g. if the level of entrainment, base pressure and vortex strength do not balance out), the present shedding cycle to influence its successor. Within the context of the proposed approach, this matter could be dealt with in the following way: the imbalance would be fed upwards by some feedback

mechanism, adjusted in the high hierarchy level, and then fed back to the next shedding cycle (with an "instruction").

Moving down one more level, it was suggested in chapter 8 that the non-Kármán vortical structures arise from an instability either within the near wake region of within the separated shear layer. Cross flow due to a pressure gradient could also play an important role. If we had a better idea of these mechanisms we could, perhaps, use a similar, systematic model to show the dependence of the non-Kármán structures on the higher hierarchy levels. Similar arguments should also apply for the generation of turbulence. Again, the influence of these effects on higher hierarchy levels would be macroscopic.

9.2.4 Limitations of the proposed "systematic" approach

The very brief entry into the lower hierarchy levels highlighted one major drawback of the proposed systematic approach. There seems to be a general inability to deal with chaotic effects (that invariably appear in the small scales of fluid motion). The block diagrams of figures 9.1 and 9.2 almost seem to suggest that a deterministic model can solve the three-dimensional near wake problem.

It is quite clear that this is not the case. If we forget the actual interactions illustrated in figures 9.1 and 9.2, it becomes apparent (simply by the sheer number of parameters that need to be balanced) that some form of chaos should prevail: the number of interacting parameters makes it improbable that a non-chaotic, repeatable trend would emerge. The degree to which a repeatable trend can be found is in a way an indication of the level of chaos.

At low Reynolds numbers (say, $Re < 150$), where turbulence is not present, a balance between the various wake parameters seems to be obtained with relative ease, and thus the shedding cycles are highly repetitive. If we now imagine that (through the addition of extra parameters, e.g. turbulence) more conditions have to be satisfied, it is possible that the overall balance will not be achievable within one shedding cycle. At this stage there may arise a modulation in the vortex shedding, and the flow will have made a step towards less repeatability and more chaos. It is thus clear that the proposed "systematic" approach cannot (through its deterministic nature) extend into a detailed description of chaos and irregularity. However, it is hoped that it can help for a better (and more important, clearer) understanding of some of the physics of the wake.

This inability to describe flow irregularities would also be demonstrated if we were to construct a similar diagram for the straight trailing edge model. Ironically, the straight trailing edge model seems to produce the more irregular flow of the two, mainly because of the intermittent nature of its three-dimensional irregularities (three-dimensional patterns are more regular for the sinusoidal model where the trailing edge shape fixes them in both time and space, as we have seen previously). Hence, the systematic approach of this chapter would show weaknesses if it were to tackle the straight trailing edge problem.

Interestingly, the degree of irregularity and unrepeatability of complex three-dimensional flows is yet one more important handicap of CFD for such flows. Compared to low Reynolds number, two-dimensional flow simulations, simulations of flows such as the one of the present study would not only need solution of a much larger number of simultaneous equations (arising from the three-dimensional grid): For results to have any significance, much longer simulation times would also be needed.

10. CONCLUSIONS AND RECOMMENDATIONS FOR FURTHER WORK

10.1 Overview of the results of this investigation

10.1.1 The approach used in the present study

This work set out to investigate the three-dimensionality of near wakes at high Reynolds numbers. A blunt trailing edge model was used for the experimental investigation. Two main configurations were studied, a straight trailing edge model (i.e. a two-dimensional geometry) and a sinusoidal trailing edge model, with the trailing edge shape serving as a geometric disturbance in order to induce and control three-dimensionality in the wake.

In the light of the results presented throughout the previous chapters (to be summarised in the present chapter), a significant conclusion is that the choice of the model was justified. With the points of separation not moving, one complicating factor that is present for the circular cylinder (which would be of secondary importance for this investigation) was eliminated. A further important element of this work was the level of entrainment within the separated shear layer. The physics of that was also kept as simple as possible because of the model section shape: the interaction of the part of the model submerged into the wake with the separated shear layers was as small as possible. Therefore, even though the chosen model shape has fewer engineering applications than, say, a circular cylinder, it showed significant advantages when it came to meeting the initial aims of this project.

Using this model, numerous experiments were conducted and theories put forward. The emphasis was on drawing general conclusions about the physics of the near wake, not specific details of the particular flow around the model, although some interesting features were observed and are outlined below.

10.1.2 General flow pattern characteristics

Most of these results were presented in chapters 4 and 8. The most notable feature of the flow around the sinusoidal model was the dual vortex shedding frequency characteristic. Two frequencies (f_1 and f_2, where $f_2 > f_1$) were observed by using spectral analysis. The higher frequency dominated at the valley

while at the peak there was a "coexistence" of the two frequencies (and the conditions would change gradually when moving from the peak to the valley). This observation suggested that vortex splitting must occur in the wake of the sinusoidal model (and hence the flow was strongly three-dimensional).

Measurement of base pressure revealed that for the sinusoidal model there was a significant drop in base drag along the whole span of the model (compared to the straight edge model). This feature was more apparent at the peaks than at the valleys. An important observation was that the stronger the three-dimensional disturbance was, the larger the decrease of drag. This could fit in well with the fact that drag is over predicted by two-dimensional computational codes (the inherent three-dimensionality of real flows could cause a decrease of the drag).

Flow visualisation in the water flume showed that more than one shedding mode exists for the sinusoidal model. Vortex splitting would occur regularly in the region of the peak, but at the two neighbouring valleys vortex shedding could be in phase (symmetric mode), or out of phase (three-cell antisymmetric mode). A two-cell antisymmetric mode and an oblique mode were also observed in the water flume experiments, but there was no evidence of their existence in the wind tunnel. No conclusions could be drawn concerning the lifespan of each of the modes, but it is believed that transition from one mode to another has to follow gradual changes, and hence cannot happen between any combination of modes.

Further flow visualisation experiments indicated the existence of smaller, non-Kármán vortical structures. ω_Z vortices were observed very close to the model base. It is possible that they get entrained into the separated shear layer to form the ω_X vortices that were also observed. The thin wisps linking successive Kármán vortices could then have their origin in the ω_Z vortices of the near wake. There were also indications that both the ω_X and the ω_Z vortices tend to occur in alternating sign patterns, or in pairs (of opposite signs). The complexity of the non-Kármán vortical structures did not permit this study to approach this subject in more than a fairly superficial way. Their observation could not be complemented by more than vague hypotheses concerning their structure.

Nevertheless, for the present study, the observation of non-Kármán vortices served to provide a possible explanation for the very irregular base pressure fluctuations measured in the wind tunnel. Spanwise correlation of the base pressure fluctuations had been found to be much lower than that for the velocity fluctuations. This was caused by large and irregular base pressure gradients which,

in turn, could be due to the near wake ω_z vortices. Correlation lengths of about 4h for the straight edge model (measured using two hot-wire probes), suggested that three-dimensionality was a key feature despite its two-dimensional geometry (and three-dimensional features were also observed for the straight edge model in the water flume).

10.1.3 Near wake dynamics for the sinusoidal trailing edge model

In chapters 5 and 6 (both based on the observations for the sinusoidal model) general ideas about the dynamics of the near wake were proposed. Due to the nature of these chapters (discussion of the *physics* of wake flows) they are of primary significance for this work.

It was proposed that the presence of the dislocation frequency f_d in the spectra (where $f_d=f_2-f_1$) is primarily the consequence of the interaction of the body with the near wake. The dislocation in the present flow appears because of the two different shedding frequencies at the peak and at the valley. In general, for vortices to join with similarly-signed vortices on the other side of the dislocation (which at times may be 180° out of phase), they have to bend. It was proposed that this bending causes f_d fluctuations in the formation region size, which in turn results in the observed base pressure f_d fluctuations. A result of this would be the varying strength of the Kármán vortices from one cycle to the next. These simple suggestions have a few significant implications.

First, the spanwise size of each of the two neighbouring cells must influence the extent to which vortex strengths can vary from cycle to cycle (i.e. for a large cell, formation region size and base pressure fluctuations cannot spread over a large spanwise distance from the dislocation). This would imply that the smaller cell is the one that changes the strengths of its vortices most easily. It is conceivable that the vortex strength fluctuations may contribute to the reduction (or, sometimes, elimination) of the weak vortex links.

Second, the fact that, in order to meet across the dislocation, vortices from the two sides have to bend in opposite directions, implies that the shrinking and growing of the formation region size may be in anti phase across the dislocation. We would expect to find a similar pattern for the base pressure, and hence we arrive at the conclusion that there will be a base pressure gradient across the dislocation, fluctuating at the dislocation frequency.

Further suggestions were made in chapter 6 that eventually explained why there had to be more than one shedding frequency. The starting point of that discussion was the tendency for the vortices to straighten out. That meant that at the valley the formation length would be larger than at the peak. As a result, the level of entrainment at the valley would be larger, and hence the fraction of the surviving vorticity would be smaller. In order for the circulation within the Kármán vortices to be constant along the span (a result of no vortex looping), more vorticity would have to be shed from the trailing edge at the valley. Thus we arrived at an explanation for the higher base drag of the valley (when compared to the peak).

It was further proposed that suction within the formation region causes the shear layer to deflect inwards. Thus, the high suction (high drag) of the valley, in combination with the long formation length would imply a narrower wake at the formation point for the valley than for the peak (also observed in experiments).

Wake similarity arguments were also used to predict the mean shedding frequency along the model's span. By using the wake width (instead of the base height) and also the separation velocity (instead of the free stream), a good collapse of Strouhal number was achieved along the span of the model. With these considerations it was shown that a single frequency could not exist along the model's span. It was suggested that a form of spanwise "lock-in" could cause the discretisation of the shedding frequencies.

Evidence also emerged that there must be a constant, strong base pressure gradient across the dislocation. This could be sustained by the streamwise vorticity lying within the dislocation. The periodic fluctuation of the dislocation position (at the dislocation frequency-described previously) would then serve to smoothen out any steep wake property changes across the dislocation, in order to produce the measured time-averaged values.

10.1.4 Further notes

Further conclusions also emerged in the following areas:

a) Quasi-two-dimensionality. Most of the theories outlined above used quasi-two-dimensional considerations. In spite of the obvious fact that strong three-dimensionality prevails, these theories seemed to produce quite good results and explanations. We should never forget that the flow is three-dimensional; however,

using quasi-two-dimensional arguments to obtain a qualitative understanding of some flow features has been demonstrated by this study to be quite valid.

b) Systematic approach to the wake problem. In chapter 9 a model was proposed in order to subdivide the wake problem into smaller "modules". It was suggested that we can consider different levels of hierarchy that determine the nature of the flow. The hierarchy levels corresponded to the important frequency ranges. The main philosophy of this approach is that the high frequency/small scale features receive detailed instructions from the higher ranks (e.g. each shedding cycle has to "see" how strong the Kármán vortex has to be, depending on the phase of the dislocation frequency fluctuations, and react accordingly). On the other hand, higher ranks (low frequency/larger scales) only perceive the smaller scales macroscopically. The advantage of this approach is that it eliminates weak interactions between unrelated wake parameters and thus allows us to concentrate on the important features of the wake.

c) Conditional sampling technique. Experiments performed using conditional sampling were not accurate enough for the results to be included in the main discussion of this work. However, given proper apparatus, conditional sampling seems to be an important technique if we are to understand the fine structure of wake flows.

10.2 Recommendations for further work

No research program can claim to produce definitive answers to all problems, and the present study is no exception. A number of questions were left unanswered and also new questions emerged from the proposed theories of this study.

We should perhaps view the particular flows of this study as tools that aided us in our understanding of the near wake dynamics. Numerous questions directly concerning these flows were left unanswered. Unless it is judged that significant information could still be extracted from these flows, it seems more reasonable to diversify, rather than to elaborate too much on understanding "all" the details of this particular flow. After all, the important thing is our better understanding of the general laws governing wake flows; flow details around models with no direct engineering application are only of secondary importance. We will therefore not discuss unanswered questions about the particular flows, but

put them in a proper context for more general research projects. Possible research areas of interest that emerged are:

a) The proposals of chapters 5 and 6 were based on the sinusoidal model but should hopefully be adaptable to other body geometries. It would be interesting to check their validity for other flows, and also to expand them to cover a larger number of flow parameters. Interesting examples include non-periodic mild geometric disturbances, isolated disturbances, free ends, etc.

b) The approach of this study to the non-Kármán vortical structures was very superficial. A better understanding of their structure would be vital in order for us to obtain a more complete picture of the three-dimensionality of wakes. This area seems to be very fruitful and demanding, as it has not been the subject of many studies.

c) The detailed structure of vortices linking within the dislocation has not yet been understood (especially at high Reynolds numbers). More advanced experimental facilities could help us appreciate many more dislocation features and hopefully incorporate them into the theories proposed in this study.

d) The alternative form of dislocation (vortex looping) has not been considered in the present investigation. It was demonstrated how a simple constraint of vortex splitting ($d(S*\Gamma_V)/dy=0$) can have such large consequences on the wake dynamics. It would be of great interest to see how a similar constraint of vortex looping could affect the wake.

REFERENCES

ANTONIA, R.A. 1981 Conditional sampling in turbulence measurement. *Ann. Rev. Fluid Mech.*, 131-156

BATCHELOR, G.K. 1967 An introduction to fluid dynamics. *Cambridge University Press*

BEARMAN, P.W. 1963 A theory of unsteady base flows. *PhD Thesis, Cambridge University Engineering Department*

BEARMAN, P.W. 1965 Investigation of the flow behind a two-dimensional model with a blunt trailing edge and fitted with splitter plates. *J. Fluid Mech.* 21, part 2, 241-255

BEARMAN, P.W. 1967 The effect of base bleed on the flow behind a two-dimensional model with a blunt trailing edge. *Aero. Quart.* 18, 207-224

BEARMAN, P.W. 1967 On vortex street wakes. *J. Fluid Mech.* 28, part 4, 625-641

BEARMAN, P.W. 1984 Vortex shedding from oscillating bluff bodies. *Ann. Rev. Fluid Mech.*, 195-222

BERS, A. 1983 Space-time evolution of plasma instabilities-absolute and convective. *Basic Plasma Physics* Vol. 1, ed. A.A. Galeev and R.Z. Sudan, 451-517

BISSET, D.K., ANTONIA, R.A. & BROWNE, L.W.B. 1990 Spatial organisation of large structures in the turbulent far wake of a cylinder. *J. Fluid Mech.* 218, 439-461

BISSET, D.K., ANTONIA, R.A. & BRITZ, D. 1990 Structure of large-scale vorticity in a turbulent far wake. *J. Fluid Mech.* 218, 463-482

BLACKWELDER, R.F. & KAPLAN, R.E. 1976 On the wall structure of the turbulent boundary layer. *J. Fluid Mech.* 76, 89-112

BRAZA, M., CHASSAING, P. & HA MINH, H. 1986 Numerical study and physical analysis of the pressure and velocity fields in the near wake of a circular cylinder. *J. Fluid Mech.* 165, 79-130

BREIDENTHAL, R. 1980 Response of plane shear layers and wakes to strong three-dimensional disturbances. *Phys. Fluids* 23 (10), 1929-1933

BROWNE, L.W.B., ANTONIA, R.A. & BISSET, D.K. 1986 Coherent structures in the far-field of a turbulent wake. *Phys. Fluids* 29, 3612-3617

BROWNE, L.W.B., ANTONIA, R.A. & SHAH, D.A. 1989 On the origin of the organised motion in the turbulent far-wake of a cylinder. *Exp. in Fluids* 7, 475-480

CANTWELL, B. & COLES, D. 1983 An experimental study of entrainment and transport in the turbulent near wake of a circular cylinder. *J. Fluid Mech.* 136, 321-374

CHOMAZ, J.M., HUERRE, P. & REDEKOPP, L.T. 1988 Bifurcations to local and global modes in spatially developing flows. *Phys. Rev. Let.* 190,25-28

CORKE, T.C., KRULL, J.D. & GHASSEMI, M. 1992 Three-dimensional-mode resonance in far wakes. *J. Fluid Mech.* 239, 99-132

COUTANCEAU, M. & DEFAYE, J.R. 1991 Circular cylinder wake configurations: a flow visualisation survey. *Appl. Mech. Rev.* 44, no 6, 255-305

DAVIES, M.E. 1976 A comparison of the wake structure of a stationary and oscillating bluff body, using a conditional averaging technique. *J. Fluid Mech.* 75, part 2, 209-231

EISENLOHR, H. & ECKELMANN, H. 1989 Vortex splitting and its consequences in the vortex street wake of cylinders at low Reynolds numbers. *Phys. Fluids* A1 (2), 189-192

FERRÉ, J.A. & GIRALT, F. 1989 Pattern-recognition analysis of the velocity field in plane turbulent wakes. *J. Fluid Mech.* 198, 27-64

GASTER, M. 1969 Vortex shedding from slender cones at low Reynolds numbers. *J. Fluid Mech.* 38, 565-576

GASTER, M. 1971 Vortex shedding from circular cylinders at low Reynolds numbers. *J. Fluid Mech.* 46, 749-756

GERICH, D. & ECKELMANN, H. 1982 Influence of end plates and free ends on the shedding frequency of circular cylinders. *J. Fluid Mech.* 122, 109-121

GERRARD, J.H. 1966 The three-dimensional structure of the wake of a circular cylinder. *J. Fluid Mech.* 25, part 1, 143-164

GERRARD, J.H. 1966 The mechanics of the formation region of vortices behind bluff bodies. *J. Fluid Mech.* 25, part 2, 401-413

GERRARD, J.H. 1978 The wakes of cylindrical bluff bodies at low Reynolds number. *Phil. Trans. Royal Soc.* A288, 351-382

GRAHAM, J.M.R. 1969 The effect of end-plates on the two-dimensionality of a vortex wake. *Aero. Quart.* 20, 237-247

GRIFFIN, O.M. & HALL, M.S. 1991 Review-Vortex shedding lock-on and flow control in bluff body wakes. *J. Fluids Eng.* 113, 526-537

HANNEMANN, K. & OERTEL, H. Jr 1989 Numerical simulation of the absolutely and convectively unstable wake. *J. Fluid Mech.* 199, 55-88

HINZE, J.O. 1975 Turbulence. *McGraw-Hill* Second Edition

HO, Q.W. 1991 Experimental investigation of the aerodynamics of fixed and rapidly-activated spoilers. *PhD Thesis, Imperial College, London.*

HONJI, H., TANEDA, S. & TATSUNO, M., 1980 Some practical details of the electrolytic precipitation method of flow visualisation. *Rep. Res. Inst. Appl. Mech. Kyushu Univ. Japan* 28, 83

HUERRE, P. & MONKEWITZ, P.A. 1985 Absolute and convective instabilities in free shear layers. *J. Fluid Mech.* 159, 151-168

KARNIADAKIS, G.E. & TRIANTAFYLLOU, G.S. 1989 Frequency selection and asymptotic states in laminar wakes. *J. Fluid Mech.* 199, 441-469

KARNIADAKIS, G.E. & TRIANTAFYLLOU, G.S. 1992 Three-dimensional dynamics and transition to turbulence in the wake of bluff objects. *J. Fluid Mech.* 238, 1-30

MANSINGH, V. & OOSTHUIZEN, P.H. 1990 Effects of splitter plates on the wake flow behind a bluff body. *AIAA Journal*, May 1990, 778-783

MASKELL, E.C. 1963 A theory of the blockage effects on bluff bodies and stalled wings in a closed wind tunnel. *ARC R&M* 3400

MONKEWITZ, P.A. and NGUYEN, L.N. 1987 Absolute instability in the near-wake of two-dimensional bluff bodies. *J. Fluids & Struct.* 1, 165-184

NOACK, B.R., OHLE, F. & ECKELMANN, H. 1991 On cell formation in vortex streets. *J. Fluid Mech.* 227, 293-308

NUZZI, F., MAGNESS, C. & ROCKWELL, D. 1992 Three-dimensional vortex formation from an oscillating, non-uniform cylinder. *J. Fluid Mech.* 238, 31-54

PRESS, W.H., FLANNERY, B.P., TEUKOLSKY, S.A. & VETTERLING, W.T. 1986 Numerical Recipes: the Art of Scientific Computing. *Cambridge University Press*

ROCKWELL, D. 1992 Control of 2- and 3-dimensional wake instabilities from bluff bodies. *Presentation at O.N.R. Workshop on Bluff Body Wake Dynamics, Columbia, Ohio.*

ROSHKO, A. 1953 On the development of turbulent wakes from vortex streets. *NACA report* 1191

ROSHKO, A. 1954 On the drag and shedding frequency of two-dimensional bluff bodies. *NACA Technical note* 3169

SCHAEFER, J.W. & ESKINAZI, S. 1959 An analysis of the vortex street generated in a viscous fluid. *J. Fluid Mech.* 6, 241-260

SOKOLOV, M. & GINAT, Z. 1992 The ladder probe: reverse flow measurements with a hot-wire rake. 1992 *Exp. in Fluids* 12, 307-318

SZEPESSY, S. & BEARMAN, P.W. 1992 Aspect ratio and end plate effects on vortex shedding from a circular cylinder. *J. Fluid Mech.* 234, 191-218

TAKAMOTO, M. 1986 A study of the wake structure behind bluff rings. *PhD Thesis, Imperial College, London.*

TANNER, M. 1972 A method of reducing the base drag of wings with blunt trailing edge. *Aero. Quart.* 23, 15-23

TRIANTAFYLLOU, G.S. 1990 Three-dimensional flow patterns in two-dimensional wakes. *ASME Symp. on Non-Steady Fluid Mechanics*, FED Vol. 92, 395-402

TRIANTAFYLLOU, G.S., KUPFER, K. & BERS, A. 1987 Absolute instabilities and self-sustained oscillations in the wakes of circular cylinders. *Phys. Review Letters* 59, 1914-1917

TRIANTAFYLLOU,G.S.,TRIANTAFYLLOU,M.S.&CHRYSSOSTOMIDIS,C. 1986 On the formation of vortex streets behind stationary cylinders. *J. Fluid Mech.* 170, 461-477

TRIANTAFYLLOU,G.S.,TRIANTAFYLLOU,M.S.&CHRYSSOSTOMIDIS, C. 1987 Stability analysis to predict vortex street characteristics and forces on circular cylinders. *J. Offshore Mech. & Arctic Eng.* 109, 148-154

TRITTON, D.J. 1959 Experiments on the flow past a circular cylinder at low Reynolds numbers. *J. Fluid Mech.* 6, 547-567

UNAL, M.F. & ROCKWELL, D. 1988 On vortex formation from a cylinder. Part 1. The initial instability. *J. Fluid Mech.* 190, 491-512

UNAL, M.F. & ROCKWELL, D. 1988 On vortex formation from a cylinder. Part 2. Control by splitter-plate interference. *J. Fluid Mech.* 190, 513-529

VAN ATTA, C.W. 1974 Sampling techniques in turbulence measurements. *Ann. Rev. Fluid Mech.*, 75-91

WEI, T. & SMITH, C.R. 1986 Secondary vortices in the wake of a circular cylinder. *J. Fluid Mech.* 169, 513-533

WILLIAMS, D.R., MANSY, H. & AMATO, C. 1992 The response and symmetry properties of a cylinder wake subjected to localised surface excitation. *J. Fluid Mech.* 234, 71-96

WILLIAMSON, C.H.K. 1988 Defining a universal and continuous Strouhal-Reynolds number relationship for the laminar vortex shedding of a circular cylinder. *Phys. Fluids* 31 (10), 2742-2744

WILLIAMSON, C.H.K. 1989 Oblique and parallel modes of vortex shedding in the wake of a circular cylinder at low Reynolds numbers. *J. Fluid Mech.* 206, 579-627

WILLIAMSON, C.H.K. 1991 The natural and forced formation of spot-like lambda-structures caused by vortex dislocations in a wake. *Eighth Sympos. Turb. Shear Flows* 1991

WILLIAMSON, C.H.K. 1992 The natural and forced formation of spot-like "vortex dislocations" in the transition of a wake. *J. Fluid Mech.* 243, 393-441

WILLIAMSON, C.H.K. 1992 3-D aspects of nominally 2-D and 3-D bluff body wakes. *Presentation at O.N.R. Workshop on Bluff Body Wake Dynamics, Columbia, Ohio.*

WILLS, J.A.B. 1991 Data sampling and data recovery. *Exp. in Fluids* 12, 23-28

ZDRAVKOVICH, M.M., BRAND, V.P., MATHEW, G. & WESTON, A. 1989 Flow past short circular cylinders with two free ends. *J. Fluid Mech.* 203, 557-575

ZHOU, Y. & ANTONIA, R.A. 1992 Convection velocity measurements in a cylinder wake. 1992 *Exp. in Fluids* 13, 63-70